Imperial College London

Department of Bioengineering

Mathematical design of optimal treatment schedules for atopic dermatitis based on a mechanistic modelling approach

Thesis by

Panayiotis Christodoulides

Supervisor: Dr Reiko Tanaka

March 2018

Submitted in partial fulfilment of the requirements for the degree of Doctor of Philosophy in Bioengineering of Imperial College London and the Diploma of Imperial College London

Declaration of Originality

I hereby declare that all material provided in this thesis is a product of my own work. Any ideas from the work of other people are fully acknowledged and appropriately referenced.

Panayiotis Christodoulides

4^{th} March 2018, London

Copyright Declaration

The copyright of this thesis rests with the author and is made available under a Creative Commons Attribution Non - Commercial No Derivatives licence. Researchers are free to copy, distribute or transmit the thesis on the condition that they attribute it, that they do not use it for commercial purposes and that they do not alter, transform or build upon it. For any reuse or redistribution, researchers must make clear to others the licence terms of this work.

To my dear grandparents
Panayiotis and Niovi,
Omiros and Lito.

Abstract

Atopic dermatitis (AD) is a highly pruritic, chronically relapsing, inflammatory skin disease and is characterised by acute flares and eczematous lesions with dry skin. Despite efforts by the research community to uncover its pathophysiological mechanisms, they remain elusive. Furthermore, effective guidelines of treatment are not well established with a lack of consensus about the best and safest way to apply treatments. Failure to understand the pathogenetic mechanisms and establish effective treatment guidelines will continue to affect the quality of life of existing patients and increase prevalence of the disease.

In our group, there has been a concentrated effort to study AD using a systems-biology approach, through the synthesis of mathematical modelling frameworks that integrate experimental and clinical data. Our models describe regulatory networks of key biochemical and cellular interactions related to the pathology and pathogenesis of AD. Previous models, explored the onset mechanisms of the disease, as well as, the genetic or environmental factors that trigger it, however they did not consider late stages of AD characterised by impaired adaptive immune responses.

In this thesis, we use a systems-level approach, by constructing and analysing mathematical models, to investigate AD with the aim of uncovering the mechanisms of its onset and progression, and to develop computational treatment regimens. We first develop a mathematical model of the late stages of AD, by including adaptive immune responses. The model reproduces several clinical phenotypes and suggests a qualitative pathogenic mechanism of disease progression, from early to late stages, via allergic sensitisation. By incorporating the effects of treatments in our model, we propose a theoretical framework for the computational design of patient-specific preventive and symptom management treatments. Our approach stratified patient phenotypes based on the success and effectiveness of treatment. Finally, since the process of allergic sensitisation can be mediated by a defective epidermal barrier, we propose a model of the de-novo synthesis of epidermal barrier components. With this model, we explore how the dysregulation of the networks controlling epidermal homeostasis can lead to a pathophysiologic state. This work provides a theoretical framework for the study of AD and the design of optimised patient-specific treatment protocols.

Acknowledgements

This thesis has been a long and torturous, but at the same time enlightening and rewarding journey. As with all journeys, it is when one reaches the final destination, when one has had enough time to reflect on the past events, hardships, and experiences that one truly values the journey.

I would first like to express my appreciation towards my supervisor Dr Reiko J. Tanaka for giving me the opportunity to complete this next step in my life at a time when I believed that it was impossible. Her teachings, support, and motivation have brought this thesis to fruition and have helped to shape me as a person. With her ethics and character she created a stable environment to flourish in.

I would like personally thank two friends and colleagues, Dr Elisa Domínguez-Hüttinger and Dr Mark van Logtestijn. The late nights at the h-bar will never be forgotten, as well as, the suffering and laughs we experienced together. Elisa thank you for introducing me to biological modelling and for providing a "listening ear" to all my worries and complaints. Mark thank you for introducing me to classical music and all of the million discussions related to MATLAB (no one gets bored of those!); I hope one day we play that golf game. Your feedback and recommendations has improved the contents of this thesis tremendously.

The work in this thesis would not have been possible without the contribution from my collaborators: Dr Yoshito Hirata, Dr Kirsten McEwen, Professor Hywel C. Williams, Professor Michael J. Cork, Dr Simon G. Danby, Professor Kazuyuki Aihara, Dr Kosuke Miyauchi, Professor Alan D. Irvine, Dr Mariko Okada-Hatakeyama, and Dr Masato Kubo.

I would like to express my gratitude to my examiners Dr Becca Asquith (Department of Medicine, Imperial College London) and Dr Marcus Tindall (Institute of Cardiovascular and Metabolic Research, University of Reading) for the fruitful and insightful discussion during my viva and their comments on the material presented in this Thesis. Their advice has served to improve the contents of this Thesis.

To my other fellow group members (past and present): Dr Sang Y Lee, Dr Neville Boon, Dr Alejandro Granados, Scott Lovell, Andrea Fiorentino, Matthias Malago, Harley Day, thank you for your insightful comments and discussions.

For taking a keen interest in my research project I would like to thank Anastasia Giannari, Riccardo Barbano, Weng Foo, William Lin, and Peter Sarvari. Also, special thanks go to Miroslav Gasparek for his dedication, interest, motivation, and inputs.

I am also grateful to Professor Emmanuel Drakakis who has been a mentor throughout all the years of my PhD and for being available at any time to lend his support and advice. The words "a good thesis never ends" will stay with me for ever. During my undergraduate years at Imperial we would always engage in intellectual conversations about the taught material (which most certainly was a catalyst for pursuing a PhD), but also about real life.

I want to express my appreciation towards Alexandros Houssein, Ilias Pagkalos, Ermis Koutsos, George Zafeiropoulos, and Christian Marton; thank you for being true friends. Your words, input, and ideas, both in and outside the work environment, have contributed to the completion of this thesis. Your company and friendship has kept me sane during the years of the PhD.

Many thanks for the insights and help of Professor Drakakis group members (past and present): Dr Kostas Papadimitriou, Dr Andreas Prokopiou, Dr Panayiotis Georgiou, and Kostis Petkos. Both Kostas and Andreas helped me profoundly during the first years of my PhD.

I am eternally grateful to my family: my father Andreas, for being the pillar of our family and for setting the examples and standards with which to live by; my mother Annita, for raising me virtually and always being next to me providing unconditional love; and my brother Omiros who has suffered me throughout the years and for reading my thesis; your drive, virtue, and ethics are unparalleled. All of you are the most important people in my life, thank you for giving me your love and support.

To my second family, my uncle Demeteris and auntie Nana Spyridaki, thank you for being there in all the moments and brightening my day. Your support, motivation, and love have been essential for the completion of this thesis. To two extremely special people in my life my cousins Niovi and Savvas Spyridaki: we grew up together and the bond that unites us is unbreakable. Thank you for sharing your lives with me and for being the people you are. I cannot wait to see what the future hold for us as we grow older together.

My life would not have been the same without my grandparents Panayiotis and Niovi, Omiros and Lito. You have always stood by my side, encouraging me to be better.

I truly treasure and treasured our moments together. Pappou Panayioti your stories and anecdotes made my childhood a happy one, Giagia Niovi your kindness knows no bounds. Pappou Omire and Giagia Lito your memory will be eternal.

Special thanks go to my auntie Lenia Christodoulidou, for providing her baking and cooking expertise to nourish everyone (literally) and for being a constant reminder of how important family is.

To all my friends back in Cyprus: Stephanos Englezoudis, Antria (Papisi) Englezoudis, Paris Charalambous, Claire Charalambous, Paraskevas Lordos, Marina (Tsangari) Lordou, George Phylactou, Nicolas Georgiades, Emilios Frangos, Xenios Antoniou, Doros Jeropoulos and Panos Jeropoulos (the craziest brothers I know), Nicolas Erotokritou, Aristos Potamitis, George Economides. Your friendship and brotherhood is dear to me and has allowed me to evolve into the person I am. Thank you for being a constant help during tough times and the people to share my experiences with. You are my third family.

Special thanks go to my house mate Andreas Christodoulou for reading parts of this thesis, Nikolas Kylilis, Sarah Jeyaprakash, and Juan Kuntz for their support in the final months of the thesis.

I am very grateful to Daisy Petevis, for taking part in some duration of this journey.

"*Excellence is an art won by training and habituation. We do not act rightly because we have virtue or excellence, but we rather have those because we have acted rightly. We are what we repeatedly do. Excellence, then, is not an act but a habit.*"

Aristotle

Symbols and Abbreviations

AD	**A**topic **D**ermatitis
AMP	**A**nti-**M**icrobial **P**eptide
DC	**D**endritic **C**ell
DDE	**D**elay **D**ifferential **E**quation
DE	**D**ifferential **E**volution
EA	**E**volutionary **A**lgorithm
FLG	**F**ilaggrin
GWAS	**G**enome-**W**ide-**A**ssociation-**S**tudy
IL	**I**nter**L**eukin
KLK	**K**allikrein
LEKTI	**L**ympho-**E**pithelial **K**azal-**T**ype *I*nhibitor
LMS	**L**inear **M**ultistep-**S**tep
MPC	**M**odel **P**redicitve **C**ontrol

ODE	**O**rdinary **D**ifferential **E**quation
OVA	**O**valbumin
PAR	**P**rotease **A**ctivated **R**eceptor
SN	**S**addle-**N**ode
TC	**T**rans**C**ritical
TEWL	**T**rans-**E**pidermal-**W**ater-**L**oss
TLR	**T**oll-**L**ike **R**eceptor
TSLP	**T**hymic **S**tromal **L**ympho-**P**oietin

Contents

Abstract **iv**

Contents **xi**

List of Tables **xvi**

List of Figures **xvii**

1 Introduction **1**

1.1 Motivation 1

1.2 Aims and objectives 2

1.3 Thesis overview 3

1.4 Publications 4

2 Literature review **6**

2.1 AD background 6

2.1.1 Epidemiology and socioeconomic burden 7

2.1.2 Genetic and environmental risk factors 8

2.1.3 Treatments for AD 10

2.1.4 Skin barrier function 11
2.2 Systems-biology approach 12
2.3 Previous mathematical models of AD 14
2.3.1 KLK Model 14
2.3.2 A multi-scale model of AD 18
2.4 A toy hybrid model 22

3 A hybrid model of atopic dermatitis 25
3.1 Introduction 27
3.2 Methods 28
3.3 Results 33
3.4 Discussion 45

4 Computational design of corticosteroid and emollient treatment 48
4.1 Introduction 49
4.2 Mathematical model of treatment effects on AD pathogenesis 50
4.3 Optimal control problem formulation 53
4.4 Methods 56
4.5 Computational identification of optimal treatment schedules 57
4.6 Discussion 64

5 Computational design of corticosteroid and coal tar treatment 67
5.1 Introduction 67
5.2 Mathematical model of treatment effects: corticosteroids and coal tar application 68

5.3 Optimal control problem formulation 69
5.4 Methods 72
5.5 Results 72
5.5.1 Identification of constant potency of coal tar treatment 73
5.5.2 Treatment design based on target level 74
5.5.3 Genetic risk factor-dependent treatment design 82
5.5.4 Treatment design under non-adherence to treatments 88
5.6 Discussion 91

6 Dual feedback structures with delay for epidermal homeostasis 97
6.1 Biological background 98
6.2 Methods 102
6.3 Self-recovery model 102
6.3.1 System description 102
6.3.2 A unique stable steady-state 103
6.3.3 System dynamics 104
6.4 Skin barrier homeostasis model 107
6.4.1 System description 107
6.4.2 Bistable behaviour 109
6.4.3 System dynamics 112
6.5 Discussion 120

7 Conclusion and Future work 123
7.1 Summary 123

7.2 Future work 126

Bibliography **129**

Appendix A Supplementary Methods for Chapter 2 **155**

A.1 LPS challenges and histological evaluation of epidermis-specific *Stat3* knockout mice 155

A.2 Minimum flare time and minimum relaxation time 156

A.3 OVA patch challenges and measurement of IgE levels in *Stat3* knockout mice 158

Appendix B Supplementary Methods for Chapter 3 **160**

B.1 Sensitivity to risk factors ($\kappa_{\mathrm{P}}, \alpha_{\mathrm{I}}$) 161

B.2 Sensitivity to weights of objective functions (k_{r}^1, k_{r}^2, k_{r}^3, k_{r}^4, k_{m}^1, k_{m}^3, k_{m}^4) 161

B.3 Sensitivity to model parameters (γ_{B}, δ_{P}, κ_{B}, γ_{R}, γ_{G}, δ_{B}, β_1, β_2, β_3) . . . 163

Appendix C Differential evolution **164**

C.1 Introduction 164

C.2 DE description 164

Appendix D Delay-Differential Equations **167**

D.1 Introduction 167

D.2 System definition 167

D.3 Stability considerations 168

Appendix E Linear stability analysis of the self-recovery model 173

E.1 Positivity of solutions 173

E.2 Linear stability analysis 174

E.2.1 Non-delayed system 175

E.2.2 Delayed system 176

Appendix F Computational investigation of the stability of the self-recovery and skin barrier homeostasis models 181

F.1 Introduction 181

F.2 Stability considerations 182

F.2.1 Self-recovery model 182

F.2.2 Skin barrier homeostasis model 185

List of Tables

2.1 Definition of parameters and their nominal values for the *KLK Model* (Eq. 2.1). 16

2.2 Definition of parameters and their nominal values for the multi-scale model of AD (Eq. 2.2). 20

3.1 Definition of model parameters and their nominal values for Eq. 3.1. . . 31

4.1 Description of simulation parameters and their nominal values for Eq. 4.1. 52

5.1 Treatment amount used during the induction and maintenance phases for risk factors conditions shown in Figs. 5.8, 5.9, and 5.10. 88

6.1 Description of the *self-recovery model* and *skin barrier homeostasis model* parameters and their nominal values. 100

List of Figures

2.1 Pathogenic mechanisms of AD. 9

2.2 Schematic representation of the structure and functions of the skin barrier. 12

2.3 Regulatory network of the biochemical interactions controlling protease activity and PAR2-mediated inflammation (*KLK Model*). 17

2.4 The *KLK Model* displays bistable behaviour with respect to the stimulus. 18

2.5 Regulatory network of the biochemical and tissue-level interactions controlling epidermal permeability function (mutli-scale model). 21

2.6 Oscillatory behaviour of the toy hybrid model defined by Eq. (2.4). . . . 23

3.1 Mechanistic model of AD pathogenesis with a double-switch motif. . . . 26

3.2 Computationally predicted effects of the 2 main genetic risk factors on the dynamic response to environmental stressors. 36

3.3 Proposed mechanisms of AD progression through a double switch. . . . 38

3.4 Four AD phenotypes described by the status of the double switch. . . . 40

3.5 Genetic risk factors increase the susceptibility to environmental stressors in developing systemic T_H2 sensitisation. 43

3.6 Emollient treatments prevent the progression to severe AD 45

3.7 "Double-switch" mechanism for onset and progression of AD. 47

4.1 Mathematical model of treatment effects on AD pathogenesis. 51

4.2 Optimal control problem formulation to design treatment strategies for proactive therapy for AD. 55

4.3 Effects of the choice of the maintenance target level (blue dotted lines) on the optimal treatment strategies calculated and the resulting dynamics of the system. 59

4.4 Calculated optimal treatment strategies for different patient cohorts . . 61

4.5 Effects of poor adherence to the calculated optimal treatment strategies during the induction phase. 63

5.1 Steady-state value of pathogen (P_{ss})with respect to constant application of corticosteroids ($\bar{C}$) and coal tar ($\bar{CT}$). 74

5.2 Optimally calculated treatment strategies for corticosteroids and the resulting dynamics of the model for different induction target levels (red dotted line) 76

5.3 Convergence of the optimisation of the induction and maintenance phases, showing only the first 10 generations, with induction target levels set to (a) $\hat{P}_{\text{r}} = 22$ mg/ml, (b) $\hat{P}_{\text{r}} = 24$ mg/ml, and (c) $\hat{P}_{\text{r}} = 26$ mg/ml. In the legend I stands for induction, while M_{i} stands for the i^{th} maintenance cycle. 77

5.4 Optimally calculated treatment strategies for corticosteroids and the resulting dynamics of the model for different maintenance target levels (blue dotted line) 78

5.5 Optimally calculated treatment strategies for corticosteroids and the resulting dynamics of the model for different maintenance target levels (blue dotted line) 79

5.7 Total normalisied corticosteroid treatment amount for induction and maintenance phases. 82

5.8 Optimally calculated treatment strategies for corticosteroids and the resulting dynamics of the model for different patient cohorts with compromised barrier integrity. 84

5.9 Optimally calculated treatment strategies for corticosteroids and the resulting dynamics of the model for different patient cohorts with dysregulated innate immune responses. 85

5.10 Optimally calculated treatment strategies for corticosteroids and the resulting dynamics of the model resulting from synergistic effects of the risk factors. 87

5.11 Dynamics of the model and disease progression when not adhering to the optimally calculated induction treatment protocol 94

5.12 Dynamics of the model and disease progression when not adhering to the optimally calculated maintenance treatment protocol. 95

5.13 Dynamics of the model and disease progression when not adhering to the optimally calculated maintenance treatment protocol. 96

6.1 (a) Epidermal homeostasis regulatory network. (b) Schematic of the *self-recovery model*. (c) Schematic of the *skin barrier homeostasis model*. . . 101

6.2 Schematic representation of the dynamics of the *self-recovery model*. . . 105

6.3 *self-recovery model* recovery dynamics with respect to instantaneous barrier damage. 106

6.4 Schematic of the regulatory network of filaggrin processing (*skin barrier homeostasis model*) and fitted response. 108

6.5 Eigenvalues associated to the equilibria of the *skin barrier homeostasis model* for the nominal parameters (Table 6.1), plotted in the complex plane. 111

6.6 Characterisation of the bistable behaviour of the *skin barrier homeostasis model*. 111

6.7 Effect of different stimuli strengths and durations on the dynamics of the *skin barrier homeostasis model* 113

6.8 Effect of different stimuli strengths and durations on the convergence and recovery time (Δt_r) of the *skin barrier homeostasis model*. 114

6.9 Stimulus-induced ($t_{\bar{u},\bar{u}}$)-manifolds of the *skin barrier homeostasis model* with respect to changes in the model parameters. 115

6.10 Calculated recovery time (Δt_r) for convergence to the *healthy state* for different parameter values. 116

6.11 Calculated recovery time (Δt_r) for convergence to the *healthy state* for different parameter values. 117

A.1 Induction of AD symptoms by environmental triggers (LPS) in *Stat3* knockout mouse model of AD. 158

A.2 Constitutive environmental challenges with OVA result in an increase in IgE levels in *Stat3* knockout mice ($n = 3$) but not in WT ($n = 1$) mice. 159

B.1 Schematic for the procedure used to complete the sensitivity analysis. . 161

B.2 The calculated optimal treatment strategies for the induction phase for 1600 different combinations of $(\kappa_{\mathrm{P}}, \alpha_{\mathrm{I}})$. 162

B.3 Sensitivity of the calculated optimal treatment strategies with respect to the changes in $(\kappa_{\mathrm{P}}, \alpha_{\mathrm{I}})$, weights for the objective function terms ($k_{\mathrm{r}}^{\mathrm{i}}$ and $k_{\mathrm{m}}^{\mathrm{i}}$), and model parameters. 162

C.1 Differential Evolution flowchart with mutation strategy DE/rand-to-best and binomial crossover rate. 166

F.1 Eigenvalues with minimal real part $\alpha = -5$ in the complex plane for the system of Eq. (6.1a) and (6.1b). Simulation parameters are shown in Table 6.1. 182

F.2 Stability diagram: Trajectory of the real part of the eigenvalues as the parameter δ_x is varied (blue lines). Cyan line is the trajectory of the dominant eigenvalue. Dashed line is the imaginary axis. 183

F.3 Stability diagram: Trajectory of the real part of the eigenvalues as the parameter k_x is varied (blue lines). Cyan line is the trajectory of the dominant eigenvalue. Dashed line is the imaginary. 184

F.4 Stability diagram: Trajectory of the real part of the eigenvalues as the parameter f_y is varied (blue lines). Cyan line is the trajectory of the dominant eigenvalue. Dashed line is the imaginary axis. 184

F.5 Stability diagram: Trajectory of the real part of the eigenvalues as the parameter τ_d is varied (blue lines). Cyan line is the trajectory of the dominant eigenvalue. Dashed line is the imaginary axis. 185

F.6 Stability diagram: Trajectory of the real part of the eigenvalues as the parameter f_x is varied in $[1, 1000]$ (blue lines). Cyan line is the trajectory of the dominant eigenvalue. Dashed line is the imaginary axis. 186

F.7 Stability diagram: Trajectory of the real part of the eigenvalues for all equilibria as the parameter f_x is varied in $[0.001, 1]$ (blue lines). Cyan line is the trajectory of the dominant eigenvalue. Dashes lines are the imaginary axes. 187

Chapter 1

Introduction

1.1 Motivation

Atopic dermatitis (AD) is a highly pruritic [1], chronically relapsing [2], inflammatory skin disease [3], with a high socioeconomic burden [4]. The motivational factor to study AD in this thesis, lies in the yet undiscovered underlying pathogenic mechanisms [5–7] and lack of individualised effective treatment strategies [8]. The unknown etiopathogenesis prevents the development of effective treatments which, in turn, increase disease prevalence and further escalates the socioeconomic burden.

Current understanding of the pathogenic mechanisms involve defective epidermal function [9–11] and aberrant immune responses [5, 12, 13]. Although, genetic factors have been identified as the main pathogenic contributors [14–16], increased incidence rates [17] and the disease association to allergen sensitisation [18], suggest an environmental component involved in the development of AD [19]. Therefore, the gene-environment interactions [20] result in the multifactorial pathogenesis of AD [21]. This renders AD a complex disease, contributing to the undeciphered pathogenic mechanisms and lack of effective treatments. Current treatments target the symptoms of AD [22] instead of the underlying causes, which could possibly explain why only 24% of patients and caregivers believe that symptoms are adequately managed by these treatments [23]. Topical emollients and corticosteroids form the cornerstone treatments for AD [24–27], however, as suggested in [28] there is "limited evidence to recommend an optimal dosing or frequency of topical corticosteroids". In [29] a similar sentiment is expressed concerning

emollients, while other research is still focused on improving their efficacy [30,31]. Possible reasons for the lack of effective treatment strategies and the unknown pathogenic mechanisms include the heterogeneity of severity [32], the varied clinical phenotypes of AD [33–35], genetic variability in world-wide populations [36], and the relatively recent standardised outcome measures established for treatment in clinical trials [37,38].

The complex multifactorial nature of AD implies that seldom only one factor results in the development of the disease [35]. Therefore, disruption of the regulatory networks of biochemical and cellular interactions that control epidermal barrier function [9,19,39–41] and immune responses [19,39,42–45] may result via multiple risk factors. To consider the complex interplay between these regulatory networks we use a *systems biology* approach, which encompasses the collection of information from the biological literature to identify possible mechanistic interactions, and then translate those interactions into mathematical models that integrate experimental and clinical data. With these models, we perform in-silico experiments to investigate: (a) the synergistic effect of risk factors to uncover the underlying mechanisms that define disease onset and progression; and (b) the effects of treatments to alleviate symptoms and prevent disease progression.

Motivated by the lack of understanding of the pathogenic mechanisms and the current lack of effective treatments, in this thesis, we develop mathematical models of AD to elucidate the intricate biochemical and cellular interactions involved in the development of the disease. This mathematical description allows the exploration of mechanisms that underlie the pathogenic process of AD, and forms the basis for the ultimate goal of this thesis: the construction of a computational framework to design treatment schedules to prevent the onset and progression of AD and the long-term management of flare control.

1.2 Aims and objectives

The objective of this thesis is to use a systems biology approach to construct mathematical models, with the aim of understanding the mechanisms with which disruption of physiological processes in the epidermis lead to the development and progression of AD. Furthermore, based on the development of these mechanistic models we aim to develop computational, patient-specific therapeutic interventions to prevent the onset and progression of AD, as well as, to facilitate management of the symptoms for severe and chronic AD. The two main aims can be summarized as follows:

- to understand the underlying mechanisms involved in the pathogenesis of AD and elucidate the physiological processes that are disrupted; and
- to design patient-specific treatment strategies for prevention and management of AD flares.

To successfully achieve these aims, two things are required:

- a quantitative framework in the form of a mathematical model; and
- a computational framework with which we can identify the frequency and dosing of the treatments.

1.3 Thesis overview

The thesis overview is as follows:

- **Chapter 2:** This chapter initially presents the relevant information on AD pertaining to this thesis. Specifically, we discuss the relevant genetic and environmental risk factors involved in the pathogenic mechanisms of AD. Then, a brief overview on the systems-level investigation used in this thesis is discussed, as well as the main previous mathematical models of AD which this research is based. Finally, a toy hybrid mathematical model is presented and analysed to prepare the reader for the results presented in Chapter 3.
- **Chapter 3:** This chapter introduces the reader to the first hybrid mathematical model describing the pathogenic mechanisms of AD. Particularly, with this model we elucidate the underlying mechanisms of the progression of AD by incorporating adaptive immune responses. The model has a "double-switch" motif with the first switch representing the protease-dependent regulation of innate immune responses (equivalent to an AD flare), and the second switch represents the onset of systemic T_H2 sensitisation, which is associated with worsening of AD symptoms. We show that the hybrid model can replicate clinical and experimental data, therefore supporting the idea that it provides a plausible mechanistic interpretation for the onset and progression of AD. Furthermore, we explore how known AD genetic risk factors predispose to systemic T_H2 sensitisation and how preventive emollient treatment can reduce the risk of sensitisation.

- **Chapters 4 and 5:** These chapters present a computational framework based on optimal control theory, that enables the design of patient-specific treatment protocols. Specifically, our method designs proactive treatment schedules for the optimal use of corticosteroids for patients suffering from moderate to severe AD, with constant use of either emollients (Chapter 4) or coal tar treatment (Chapter 5). Our method illustrates the potential use of numerical simulations to inform clinicians on the best approach to apply corticosteroids to achieve long-term management and prevention of AD flares. We illustrate the design of patient-specific treatments by stratifying patients who react successfully or unsuccessfully to the treatment regimens, based on their genetic profile. Finally, we explore how non-adherence to the optimally calculated treatment protocols affect the long-term management of AD.

- **Chapter 6:** This chapter presents a mathematical model of the regulatory network controlling epidermal homeostasis through the skin barrier component filaggrin. The model is composed of regulatory interactions combining positive and negative feedback mechanisms with delay in order to explore the characteristic self-recovery property of the skin barrier that is achieved by balancing differentiation, proliferation, and desquamation processes. We assess how skin barrier perturbation or genetic factors can affect the recovery of the barrier and predispose to diseases such as AD.

- **Chapter 7:** This chapter presents the general conclusions and possible future extensions of the results presented in the previous chapters. Additionally, it highlights the contribution of this thesis towards the mathematical modelling of AD and the design of computational treatments, as well as, noting potential caveats.

1.4 Publications

- Elisa Domínguez-Hüttinger, Panayiotis Christodoulides, Kosuke Miyauchi, Alan D. Irvine, Mariko Okada-Hatakeyama, Masato Kubo, and Reiko J. Tanaka. Mathematical modeling of atopic dermatitis reveals "double-switch" mechanisms underlying 4 common disease phenotypes. *Journal of Allergy and Clinical Immunology*, 139(6):1861-1872.e7, June 2017. *Reproduced in Chapter 3.*

- Panayiotis Christodoulides, Yoshito Hirata, Elisa Domínguez-Hüttinger, Simon G. Danby, Michael J. Cork, Hywel C. Williams, Kazuyuki Aihara and Reiko

J. Tanaka. Computational design of treatment strategies for proactive therapy on atopic dermatitis using optimal control theory. *Philosophical Transactions of the Royal Society A: Mathematical, Physical & Engineering Sciences*, 375(2096):20160285, June 2017. *Reproduced in Chapter 4.*

Chapter 2

Literature review

In this chapter we first present a brief background on AD discussing its main clinical features, associated socioeconomic burden, its complex multifactorial pathogenesis, and relevant treatments (Section 2.1). The next section focuses on the systems biology approach used in this thesis (Section 2.2). We then discuss the main previous mathematical models of AD on which this research is based (Section 2.3). In the final section, we describe a simple hybrid mathematical model and analyse its behaviour for a specific set of parameters (Section 2.4).

2.1 AD background

Atopic dermatitis (AD) is a common skin disease characterised by the trifecta [46] of a defective skin barrier (manifesting as dry and scaly skin [47]), dysfunctional immune responses (manifesting as recurrent [48] or chronic [49] inflammation), and susceptibility to skin infections [50, 51]. A possible causal relationship exists between the aforementioned characteristics, summarised as follows: diminished protective capabilities of the skin barrier can result in increased infiltration of pathogens or allergens through the skin, which can activate innate or adaptive immune responses that induce inflammation [41, 52]. These in turn, can interfere with epidermal differentiation programs [53, 54], leading to further impaired barrier function. It is still debated [10, 55] whether a defective barrier is the primary cause of AD that results in aberrant immune responses (outside-inside hypothesis [56]), or an immunologic disturbance that causes epidermal

barrier dysfunction (inside-outside hypothesis [57]). However, given the complexity of AD, it might be possible that both co-exist as primary defects. Evidence for either are discussed further in Section 2.1.2.

AD is recognised as having two distinct forms, namely, extrinsic [55], which is associated with specific IgE-mediated sensitisation to external allergens, and intrinsic [58], which is not accompanied by sensitisation but still manifests with the similar symptoms. However, exposure to allergens can induce systemic sensitisation, a hallmark of allergic diseases [6, 59], which can predispose individuals to develop AD [60]. Systemic allergy sensitisation is therefore an important part of its pathogenic process, however, its mechanisms are not fully understood [61]. Furthermore, AD is frequently associated with other allergic diseases [55] and has been recognised as the first step in the so-called "Atopic March" [62], a series of allergic diseases starting from AD and progressing to asthma, allergic rhinitis, and chronic sinusitis [17, 63]. This suggests roots of common pathogenic mechanisms [60, 62]. Given the importance of systemic sensitisation, in Chapter 3 we introduce a mathematical model that describes potential mechanisms for its development.

2.1.1 Epidemiology and socioeconomic burden

AD is one of the most common skin diseases, with onset usally in early childhood [17]. Current prevalence statistics of AD range from 1% to 30% [8, 64–69] in children, depending on geographical location, and 1-3% in adults [17, 64]. In addition, there has been an increasing incidence, especially in industrialised countries [17, 70], suggesting that environmental factors are involved in AD pathogenesis [71]. Eighty-five percent of AD cases manifest within 5 years of age [55], however, 70% of patients have spontaneous remission before adolescence [17].

Although not life threatening, AD has a high social impact evident from consistently low quality of life indices reported by patients and their corresponding caregivers, compared to the unaffected population [72–74] and patients with other skin diseases [75–77]. Patients experience psychosocial effects [78] such as sleeping disorders [79], anxiety [80], and depression [23] and are often described as having difficulty in social interactions due to their symptoms [72, 81–83]. Furthermore, in one study, AD patients showed significantly greater loss of work productivity [80]. From an economic standpoint, AD presents a burden to the affected families, as well as, to the healthcare system. Individ-

ual annual costs in Australia, North Korea and Singapore range from USD 1000 to 6000 per person [84], while estimated national costs of treatment are as high as USD 3.8-5.3 billion per year in the US [4,85] and EUR 3.5 billion in Germany [86]. The wider socioeconomic impacts will continue to burden individuals and society if the current lack of understanding of the pathogenic mechanisms and development of effective treatments remain unresolved.

2.1.2 Genetic and environmental risk factors

AD can develop as a consequence of defective regulatory genetic networks controlling skin barrier function [9, 19, 39–41] and immune responses [19, 39, 42–45], which result from the complex interplay between genetic and environmental risk factors [30,87] (Fig. 2.1). These gene-environment interactions make it increasingly complicated to uncover the pathogenic mechanisms of AD and devise effective treatments. This complexity, coupled with the heterogeneity of severity [32], the varied clinical phenotypes of AD [33–35], and genetic variability in world-wide populations [36], further contribute to the lack of understanding of the aetiology and pathogenic mechanisms.

Evidence suggests that the main genes predisposing to the development of AD can be divided into two groups [64]: (i) epidermal barrier function; and (ii) immune-mediated pathways [88]. Gene loci connected to epidermal homeostasis have been identified by Genome-Wide-Association Studies (GWAS) [89], with the filaggrin (*FLG*) gene, encoding an important structural protein of the epidermal barrier, being among the most widely replicated [40,90]. Mutations in the *SPINK5* gene, which leads to loss of the protease inhibitor LEKTI and subsequent enhanced activity of kallikrein (KLK) proteases [14, 91], have been associated to AD [92]. Defects in the innate immune system, such as diminished recruitment of neutrophils, toll-like receptor defects, and reduced levels of anti-microbial peptides [93], have been shown to affect the development and severity of AD [50]. Inflammatory genes, including many encoding T_H2 cytokines [10, 88], have also been linked to its development, illustrating an adaptive immune defect [94]. Nevertheless, although genetic defects explain many subgroups of AD patients, they cannot explain the great heterogeneity of AD phenotypes [35].

Although *FLG* gene mutations are the most widely replicated AD genetic risk factor, only 30%-40% [35, 95] of AD patients present with *FLG* mutations suggesting that environmental factors or other unidentified genetic loci could play a role its pathogen-

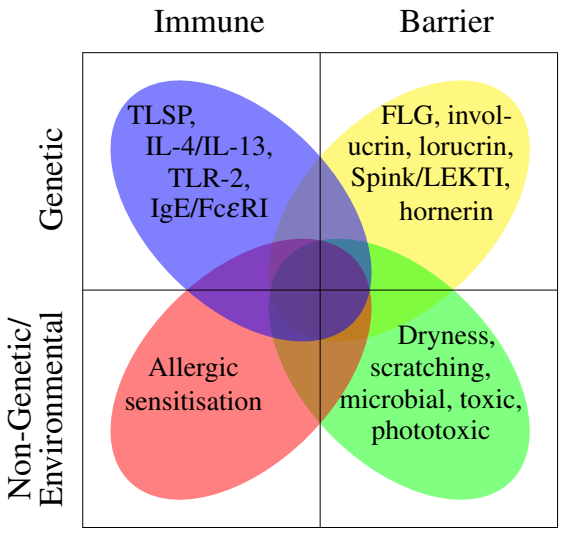


Figure 2.1: Pathogenic mechanisms of AD. Genetic and environmental factors related to the skin barrier and immune system, which can drive the development of AD. Adapted from [35].

esis. Gene expression of filaggrin can also be altered by acquired factors, for example T_H2-mediated immune responses that affect terminal differentiation programs [96–98], reinforcing the interplay between impaired epidermal function and immune responses. Furthermore, a weak epidermal barrier can result in increased infiltration of pathogens or allergens [99,100] that can activate inflammatory circuits [100,101] and lead to severer AD symptoms. Additional environmental factors that can promote an AD phenotype are noted in the literature, such as hard water [30], detergents and surfactants [30], among others [19, 41–45]. Persistent percutaneous aggravation from specific allergens or irritants can cause IgE responses, typical of extrinsic AD, and cause allergic sensitisation [100, 102]. Moreover, late stages of AD are characterised by allergic sensitisation [100, 102, 103], which is associated with an irreversible impairment of adaptive immune responses via systemic T_H2 sensitisation [35] and worsening of AD symptoms. Given that systemic T_H2 sensitisation is characteristic of the late stages of AD [102], in order to understand the onset and progression of the disease it is relevant to uncover the underlying mechanisms that induce it. It should be noted that not all patients diagnosed with AD have a specific IgE-mediated sensitisation to allergens [101], further cementing the gene-environment interaction.

2.1.3 Treatments for AD

A cure for AD does not currently exists and treatments focus on the relief of symptoms that develop through its complex pathogenic mechanisms. Cornerstone treatments for mild-to-moderate AD include topical moisturisers [25], which improve skin barrier function and reduce transepidermal water loss (TEWL) [94, 104], and corticosteroids [105], which reduce inflammation by inhibiting the release of proinflammatory cytokines [25]. Patients not responsive to corticosteroids or reluctant to use them, due to steroid phobia [8], are typically prescribed steroid-sparing treatments such as topical calcineurin inhibitors [106, 107], which address cutaneous inflammation while also lacking many of the side-effects of corticosteroids [3].

The skin of AD patients is prone to secondary bacterial infection and is frequently inhabited by *Staphylococcus* and *Streptococcus* species [1, 108], necessitating the use of antibiotics [70]. In cases of refractory AD, more potent corticosteroids are necessary [65], but long-term use of potent steroids has been associated to cutaneous adverse affects [25], such as skin atrophy [23], as well as systemic side-effects [23]. Finally, for advanced and severe cases of AD, systemic treatments are available [25, 28, 109–111], but such treatments are associated with several risks [109, 112] or are impractical and therefore rarely recommended [109].

Recently, a new form of treatment with a drug called dupilumab, a monoclonal antibody targeting IL4 and IL13 signalling, has shown great success in the treatment of difficult to treat AD [68]. Phase III clinical trials showed improved clinical signs and symptoms, as well as, psychosocial symptoms and quality of life [113], however, due to unwanted side-effects further studies have been recommended to prove its safety [114]. Nevertheless, the FDA has recently approved dupilumab injections, marketed with the name Dupixent, for the use against moderate to severe AD.

Traditional treatment regimens follow a reactive approach in the application of topical anti-inflammatory agents, however, long-term prevention of flares is difficult to maintain [115]. Since even the non-affected skin of AD patients presents with immunological defects [96, 116] a proactive approach (or weekend therapy) is now advocated for patients with frequent outbrakes of moderate-to-severe AD [117–119]. This treatment strategy entails an initial symptom stabilisation phase with topical application of corticosteroids or calcineurin inhibitors [120, 121] and a secondary maintenance phase with low-dose intermittent (usually 2-3 days weekly) application of topical anti-inflammatory treatments

in commonly affected areas [28, 117, 122, 123].

2.1.4 Skin barrier function

The outermost layer of the skin is termed the epidermis [124] and plays a critical role in epithelium tissue homeostasis as it posseses physical, chemical, microbial, and immunologic barrier functions [49, 125, 126]. However, most of these defensive functions seem to be localised in the most superficial layer of the epidermis, the stratum corneum [127] (Fig. 2.2). Specifically, the stratum corneum protects from external stressors [128], by serving as the first line of defence against invading pathogens and allergens [40, 129], and helps maintain internal fluid and electrolyte homeostasis [53] by providing an occlusive interface that restricts water loss. Furthermore, human epithelium is often colonised by non-pathogenic bacteria that provide a microbiological barrier to infection by competing with pathogens for nutrients [126]. These non-pathogenic bacteria, may also be able to produce antimicrobial substances that prevent infection [126].

The epidermal barrier is a result of the tight regulation of cell proliferation, differentiation and migration processes [130, 131], as well as, degradation of skin cells at the top layer of the epidermis (desquamation) [132–134]. Stratified epithelial cells, that cover the epidermis, are continuously renewed through proliferation of keratinocytes, which constitute the major epidermal cell type [124], with the differentiation program, from viable to non-viable keratinocytes (corneocytes), involving a complex set of biochemical events [135, 136].

At the upper levels of the skin, the formation of the stratum corneum results from corneodesmosome-mediated intercellular cohesion of corneocytes [135], which are embedded in a lipid/protein envelope (cornified envelope) [137]. Filaggrin protein [40, 90, 138] and other terminal differentiation products are expressed, which enable the cross-linking of the cornified envelope with the keratin cytoskeleton [55]. The formation of the cornified envelope, cohesion via tight junctions, and the cross-linking to the cytoskeleton confer structural stability to the skin barrier and are determinants for its proper function. Finally, the process of desquamation through KLK-induced degradation of corneodesmosomes [139], leads to the renewal of the stratum corneum.

A key property of a healthy skin barrier is the return to a homoeostatic state in response to skin barrier damage [140, 141]. This property is still not well understood mechanistically and in Chapter 6 we propose mathematical models of the regulatory structures

filaggrin into a mechanical structure called the cornified envelope. Finally, the lamellar bodies release lipids precursors and lipid enzymes that form a lipid envelope that is associated with CE.

5. As the corneocytes move apically corneodesmosomes are degraded by extracellular proteases that ultimately lead to the detachment of filaggrin from th CE-LE structure. Filaggrin is further degradated into amino acid that have special functional role in the upper SC. The collection of amino acids is termed the NMF.

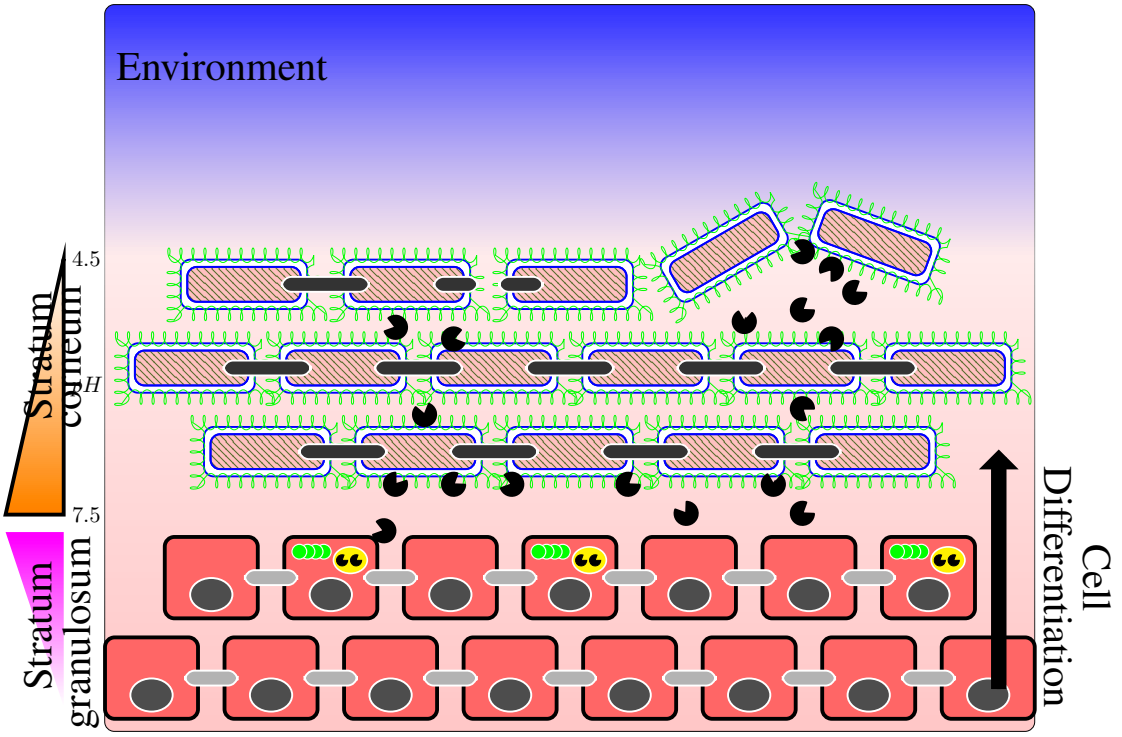


Figure 2.2: Schematic representation of the structure and functions of the epidermis. Keratinocytes from the lower level of the epidermis (stratum basale - not shown in figure) differentiate into the stratum granulosum (red blocks). Cells in the stratum granulosum release proteins (such as FLG - green circles) and lipids structures that contain enzymes (such as KLKs - noted in black), becoming anucleated cells (corneocytes), thus forming the stratum corneum. Corneodesmosomes (black elongated rods) bind the corneocytes together which are embedded in the cornified envelope (green mesh). KLK is the stratum corneum cleave the corneodesmosomes causing desquamation This forms the skin barrier that protects against the penetration of environmental stimuli but also restricts the flow of water.

involved in this process in order understand it in the context of AD.

2.2 Systems-biology approach

The realisation of the complexity and variability of human biology [142], as well as, the large volume of data generated by experimental approaches in molecular biology has led to the creation of new fields such as systems biology, bioinformatics, and synthetic biology [143–145]. In the core of these fields is the study of biological systems, for example biochemical and cellular systems. Such biological systems can be represented by complex, highly interconnected regulatory networks and subsequently translated into

precise mathematical terms as mathematical models, in order to provide insight into their dynamical properties [146, 147]. As such, mathematical modelling has emerged as a substantial tool "for formumating mechanistic hypotheses precisely and for deriving with confidence physiological implications" [146] of biological systems.

Multidisciplinary research performed by biologists, mathematicians, physicists, and engineers has provided solutions in the areas of preemptive medicine, diagnostic tools, and target oriented molecular therapies [148–152], but has also helped uncover salient features of disease pathogenic mechanisms [152–155]. Often the latter involves the identification of biochemical or cellular networks of interest and how the deregulation of their mechanistic properties leads to loss of function. In this sense, the failure of complex biological control mechanisms leads to a pathophysiological phenotype. Examples include pathogen [156] or bacterial infection [157, 158], AD [132–134], blood iron homeostasis [159], and immune regulation by regulatory T cells [160]. Therefore, with system-level approaches we can characterise important biological control mechanisms that ultimately improve our understanding of pathogenic processes. This understanding can potentially guide the design of biomarkers and guide the development of novel preventive or therapeutic treatments with clinical implications.

To investigate the mechanisms of AD pathogenesis, we propose following a systems biology approach. Specifically, we define a systems biology approach as the use of engineering and computational methodologies to develop mathematical models that represent pivotal biochemical and cellular networks of biological systems. These models, when integrated with biological and clinical information, can be used to decipher the control mechanisms of biological systems, predict disease outcome, and guide development of novel treatments.

The suggested systems biology approach followed in this thesis is motivated by the complex biological processes involved in the development of AD. Specifically, our mathematical models are represented by sets of Ordinary-Differential Equations (ODE) or Delay-Differential Equations (DDE) with components that operate at different timescales. This approach lends itself naturally to the study of complex interconnected regulatory networks, where there is a need to investigate their feedback mechanisms and the synergistic effects of multiple risk factors. Furthermore, we can explore the effects of multiple targeted treatments on the components of the regulatory networks, thus developing combinatorial treatment approaches. Treatment application is a dynamic process and identifying temporal protocols requires the use of dynamic optimisation techniques

[161]. The design of dynamically changing treatment protocols is accomplished with the use of optimal control theoretic tools [162–165], which require the systematic and quantitative framework of a precise mathematical model.

In this thesis, we build on previous research from our group [166, 167] and develop the first hybrid dynamical model of AD. The aim of this model is to uncover the underlying mechanisms of AD pathogenesis by investigating the intricate network of interactions between skin barrier function, innate and adaptive immune responses, and environmental stimuli. By developing this mathematical model we are able to achieve our ultimate aim: the design of treatments to prevent the development or deterioration of AD phenotypes and the development of protocols for the management of symptoms in severe AD patients.

2.3 Previous mathematical models of AD

2.3.1 KLK Model

The first model to capture the clinical characteristics of AD was presented by Tanaka et al. [166]. A systems-level investigation was used where the authors developed a mathematical model represented by a set of ODE, which integrates microarray data of Protein Activated Receptor (PAR) activity for both healthy and AD patients. This mathematical model represents key biochemical reactions of enzymatic activity in the epidermis that regulate barrier function and innate immune responses. As such, with this model the outbreak of inflammation in AD patients caused by an external stimulus was investigated. This external stimulus leads to the overactivation of enzymes found in the skin, namely kallikreins (KLK5), and subsequent activation of their downstream targets, such as PAR2, that can induce an immune response.

We refer to the model presented in [166] as the *KLK Model* and is described by the

following system of equations:

$$[KLK5^*\dot{L}EKTI](t) = k_{\mathrm{a}}[KLK5^*](t)[LEKTI](t) - k_{\mathrm{d}}[KLK5^* - LEKTI](t) \quad (2.1a)$$

$$- \delta_{\mathrm{LK}}[KLK5^* - LEKTI](t), \quad (2.1b)$$

$$[LE\dot{K}TI](t) = -k_{\mathrm{a}}[KLK5^*](t)[LEKTI](t) + k_{\mathrm{d}}[LEKTI - KLK5^*](t) \quad (2.1c)$$

$$- \delta_{\mathrm{L}}[LEKTI](t) + t_L(m_{\mathrm{L}} + f_{\mathrm{LS}}S + f_{\mathrm{L}}[PAR2^*](t)), \quad (2.1d)$$

$$[KL\dot{K}5^*](t) = -k_{\mathrm{a}}[KLK5^*](t)[LEKTI](t) + k_{\mathrm{d}}[LEKTI - KLK5^*](t) \quad (2.1e)$$

$$+ k\frac{[KLK5^*](t)[KLK5](t)}{[KLK5^*](t) + C_{\mathrm{K}}} - \delta_{\mathrm{K}^*}[KLK5^*](t), \quad (2.1f)$$

$$[K\dot{L}K5](t) = -k\frac{[KLK5^*](t)[KLK5](t)}{[KLK5^*](t) + C_{\mathrm{K}}} - \delta_{\mathrm{K}}[KLK5](t) + m_{\mathrm{K}} + f_{\mathrm{KS}}S \quad (2.1g)$$

$$+ f_{\mathrm{K}}[PAR2^*](t), \quad (2.1h)$$

$$[P\dot{A}R2](t) = -k\frac{[KLK5^*](t)[PAR2](t)}{[KLK5^*](t) + C_{\mathrm{P}}} - \delta_{\mathrm{P}}[PAR2](t) + m_{\mathrm{P}}, \quad (2.1i)$$

$$[P\dot{A}R2^*](t) = k\frac{[KLK5^*](t)[PAR2](t)}{[KLK5^*](t) + C_{\mathrm{P}}} - \delta_{\mathrm{P}^*}[PAR2^*](t), \quad (2.1j)$$

where the dynamic variables $[KLK5^*LEKTI](t)$, $[LEKTI](t)$, $[KLK5^*](t)$, $[KLK5](t)$, $[PAR2](t)$, $[PAR2^*](t)$ represent the concentrations of activated kallikrein and protease inhibitor complex, protease inhibitor, activated kallikrein, inactivated kallikrein, inactivated protease activated receptors, and activated protease activated receptors, respectively.

The model equations were developed based on mass-action and Michaelis-Menten kinetics. An analytically tractable initial condition can be identified by setting $\dot{\boldsymbol{x}} = \mathbf{0}$ (where the overdot notation represents the time derivative of the variable i.e $\dot{\boldsymbol{x}} = \frac{d\boldsymbol{x}}{dt}$); that initial condition corresponds to the non-inflammatory state with $[PAR2^*]_{ss} = 0$. The parameters of the model were non-dimensionalised based on the parameter k_{a} and include association/dissociation rates, activation rates, basal degradation rates, and feedback modulation strengths of the constituent molecules. The parameter S corresponds to an external stimulus (such as environmental pathogen) which increased levels can lead to the initiation of inflamatory responses in the skin. The schematic of the model is given in Fig. 2.3 and a description of the model parameters with their nominal

Table 2.1: Definition of model parameters and their nominal values for the *KLK Model* (Eq. 2.1). Parameters are normalised with respect to k_a. Adapted from [166].

Symbol	Name	Nominal value
k_a	$LEKTI - KLK5^*$ association rate	1
k_d	$LEKTI - KLK5^*$ dissociation rate	1
k	$KLK5$ activation rate	10
k_P	$PAR2$ activation rate	$\approx k$
δ_L	$LEKTI$ degradation rate	0.5
δ_K	$KLK5$ degradation rate	1
δ_{LK}	$LEKTI - KLK5^*$ degradation rate	$\approx \delta_K$
δ_{K^*}	$KLK5^*$ degradation rate	$\approx \delta_K$
δ_P	$PAR2$ degradation rate	0.5
δ_{P^*}	$PAR2^*$ degradation rate	$\approx \delta_P$
t_L	$LEKTI$ production capability	1
C_K	Half-saturation of KLK activation	50
C_P	Half-saturation of $PAR2$ activation	$\approx C_K$
m_P	Basal production rate of $PAR2$	10
m_L	Basal production rate of $LEKTI$	1
m_K	Basal production rate of $KLK5$	0
f_{KS}	Rate of $KLK5$ production by stimulus	0.5
f_{LS}	Rate of $LEKTI$ production by stimulus	0.05
f_K	Feedback strength from $PAR2^*$ to $KLK5$	0-1
f_L	Feedback strength from $PAR2^*$ to $LEKTI$	0-0.5

values are given in Table 2.1.

The model focuses on the regulation of KLK5 activity in the upper levels of the epidermis and considers the mechanisms of autoactivation of KLK5, inhibitory regulation of KLK5 through LEKTI, activation of PAR2 by KLK5 and, finally, feedback regulation from PAR2 to both LEKTI and KLK5. The protease KLK5 mediates the control of skin desquamation by enzymatically cleaving corneodesmosomes that connect the skin cells in the upper epidermis. Furthermore, KLK5 modulates innate immune responses through the activation of PAR2, which increase the expression of pro-inflammatory cytokines [103,168]; a clinical sign prevalent in patients with AD. Therefore, the regulatory structure proposed by the authors combines dual-positive feedback regulation of active KLK (KLK*) and its inhibitor LEKTI by inflammation-inducing PAR2.

In their analysis Tanaka et al. [166], explored the effects of both genetic factors, in the form of deficient expression of the protease inhibitor LEKTI, and environmental factors such as increased skin pH; both of these have been shown to represent risk factors which

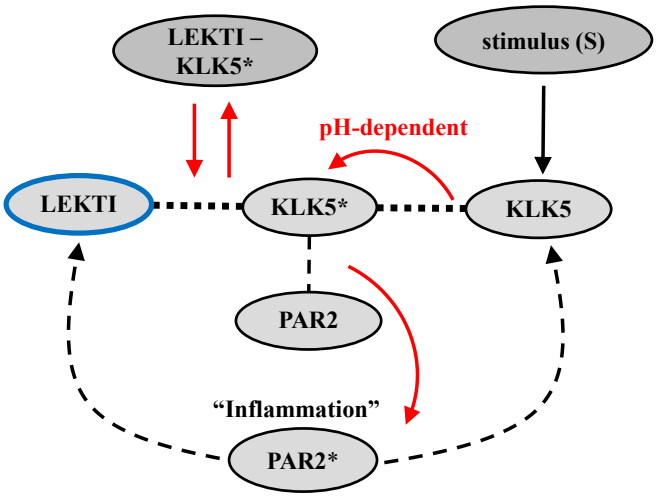


Figure 2.3: Regulatory network of the biochemical interactions controlling protease activity and PAR2-mediated inflammation (*KLK Model*). Red arrow denote reactions that are pH-dependent. Adapted from [166].

predispose to the disease.

Here we replicate the bifurcation analysis presented in [166], using the numerical continuation software MATCONT [169], which illustrates that the model can display bistable behaviour (Fig. 2.4a). The steady-state corresponding to low inflammation (i.e low $[PAR2^*]_{ss}$) loses stability via a *transcritical* (TC) bifurcation [170] as the stimulus (S) increases to the activation threshold (S^+). For the inflammation to stop, the stimulus needs to decrease to the de-activation threshold (S^-), which is lower than S^+ illustrating that the model exhibits hysteretic behaviour. The steady-state corresponding to high inflammation undergoes a *saddle-node* (SN) bifurcation at S^-.

The steady-state behaviour of activated PAR2 and KLK5 is displayed in Fig. 2.4b and Fig. 2.4c, respectively, for the risk factors corresponding to deficient LEKTI expression ("Low LEKTI", blue) and increased skin pH ("High pH", red). Both risk factors result in lower activation and inactivation thresholds (S^+ and S^-, respectively) of protease-mediated immune responses (Fig. 2.4b) and KLK5 activity (Fig. 2.4c). This leads to increased susceptibility to stimulus, due to lower S^+, and a more persistent immune response, due to lower S^-. The level of active KLK5 for both risk factors is increased for the same level of stimulus (Fig. 2.4c, red and blue), compared to the control (Fig. 2.4c, black).

We will use this model in the development of our hybrid model (Chapter 3) by approx-

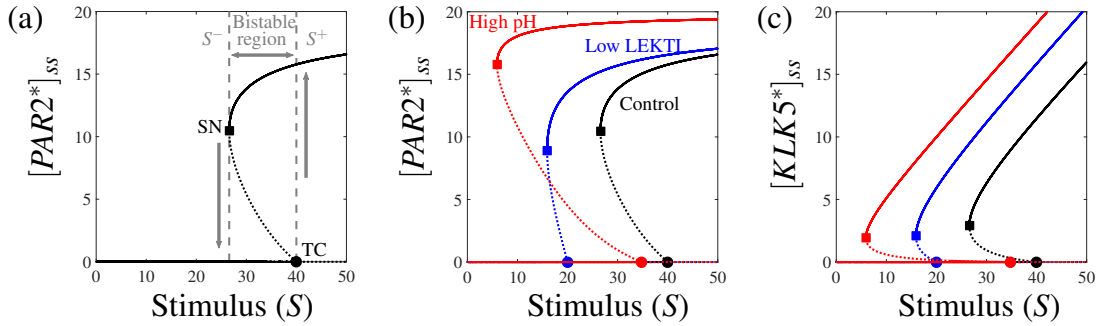


Figure 2.4: The *KLK Model* displays bistable behaviour with respect to the stimulus. (a) Steady-state behaviour of $[PAR2^*]_{ss}$ corresponding to protease-mediated immune responses as a function of the stimulus. Dashed grey lines correspond to the activation (S^+) and inactivation (S^-) thresholds. (b) Steady-state behaviour of $[PAR2^*]_{ss}$ for the risk factors of deficient LEKTI expression (blue) and increased skin pH (red). (c) Steady-state behaviour of $[KLK5^*]_{ss}$ corresponding to the level of active KLK, for the risk factors of deficient LEKTI expression (blue) and increased skin pH (red). Solid and dotted lines correspond to the stable and unstable steady-states, respectively. Squares and circles denote *saddle-node* (SN) and *transcritical* (TC) bifurcations, respectively.

imating the steady-state behaviour of the low and high states of activated PAR2 and KLK5.

2.3.2 A multi-scale model of AD

In [167] a multi-scale model of epidermal homeostasis was developed that considers the interplay between protease-activated innate immune responses, epidermal permeability function, and the intrusion of pathogens through the skin barrier. The authors consider the natural separation of time scales between fast inflammation-inducing biochemical reactions and slow morphogenic processes that establish the epidermal barrier and its homeostatic function. Specifically, by invoking the quasi-steady state assumption [171], they combine the biochemical network introduced in [166] (the *KLK Model*, Section 2.3.1) with the tissue-level property of epidermal permeability in an integral-differential-algebraic model, in order to investigate the early-phase pathogenic mechanisms of AD.

The quasi-steady state assumption can be applied due to the different time-scales that the dynamic variables operate. While the variables in the *KLK Model* operate on the slower time-scale of minutes [132], the tissue-levels properties (including cell proliferation and differentiation) operate on the time-scale of hour or days [172, 173]. As such, the variables of the *KLK Model* achieve their homeostatic behaviour faster than the

variables describing the tissue-level properties, and can therefore be substituted by a set of algebraic equations. The schematic of the network is given in Fig. 2.5 and the mathematical model is described by the following system of equations:

$$\dot{S}(\tau) = S_{\text{out}} \frac{\tilde{P}}{B(\tau) + \epsilon} - S(\tau)(f_{\text{IP}} I_{\text{P}}(\tau) + I_0), \tag{2.2a}$$

$$\dot{B}(\tau) = \frac{b_{\text{pre}}}{1 + k_L [PAR2^*]_{\text{ss}}} \Big(1 - \frac{B(\tau)}{\tilde{B}}\Big) - d_{\text{K}} [KLK5^*]_{\text{ss}} B(\tau), \tag{2.2b}$$

$$I_{\text{P}}(\tau) = \int_{x=0}^{x=\tau} [PAR2^*]_{\text{ss}} e^{-\tau + x} dx, \tag{2.2c}$$

and the algebraic equations describing the biochemical events:

$$0 = k_{\text{a}} [KLK5^*]_{ss} [LEKTI]_{ss} - k_{\text{d}} [KLK5^* - LEKTI]_{ss} \tag{2.3a}$$

$$- \delta_{\text{LK}} [KLK5^* - LEKTI]_{ss}, \tag{2.3b}$$

$$0 = -k_{\text{a}} [KLK5^*]_{ss} [LEKTI]_{ss} + k_{\text{d}} [LEKTI - KLK5^*]_{ss} \tag{2.3c}$$

$$- \delta_{\text{L}} [LEKTI]_{ss} + t_L (m_{\text{L}} + f_{\text{LS}} S + f_{\text{L}} [PAR2^*]_{ss}), \tag{2.3d}$$

$$0 = -k_{\text{a}} [KLK5^*]_{ss} [LEKTI]_{ss} + k_{\text{d}} [LEKTI - KLK5^*]_{ss} \tag{2.3e}$$

$$+ k \frac{[KLK5^*]_{ss} [KLK5]_{ss}}{[KLK5^*]_{ss} + C_{\text{K}}} - \delta_{\text{K}^*} [KLK5^*]_{ss}, \tag{2.3f}$$

$$0 = -k \frac{[KLK5^*]_{ss} [KLK5]_{ss}}{[KLK5^*]_{ss} + C_{\text{K}}} - \delta_{\text{K}} [KLK5]_{ss} + m_{\text{K}} + f_{\text{KS}} S \tag{2.3g}$$

$$+ f_{\text{K}} [PAR2^*]_{ss}, \tag{2.3h}$$

$$0 = -k \frac{[KLK5^*]_{ss} [PAR2]_{ss}}{[KLK5^*]_{ss} + C_{\text{P}}} - \delta_{\text{P}} [PAR2]_{ss} + m_{\text{P}}, \tag{2.3i}$$

$$0 = k \frac{[KLK5^*]_{ss} [PAR2]_{ss}}{[KLK5^*]_{ss} + C_{\text{P}}} - \delta_{\text{P}^*} [PAR2^*]_{ss}, \tag{2.3j}$$

where, $S(\tau)$ are the infiltrating pathogens, $B(\tau)$ corresponds to the collective property of barrier integrity, and I_{P} is the level of immune responses. The variables $[KLK5^*]_{\text{ss}}$ and $[PAR2^*]_{\text{ss}}$ represent the steady-state values of active kallikreins and protease-activated receptors, respectively, as discussed in Section 2.3.1. A description of the model parameters and their nominal values are given in Tables 2.1 and 2.2.

Note that barrier integrity ($B(\tau)$) is a term combining many biological processes involved in the self-recovery and proper function of the skin barrier (proliferation/differentiation of corneocytes, cohesion of corneocytes, lipid content etc). However, for simplicity, the authors consider a phenomenological representation of self-recovery dynamics via a

Table 2.2: Definition of parameters and their nominal values for the multi-scale model of AD (Eq. 2.2). Adapted from [167].

Symbol	Name	Nominal value
S_{out}	Concentration of external stimulus	95
$\tilde{P}$	Nominal skin permeability	0.4
f_{IP}	Strength of stimulus eradication by $PAR2^*$-mediated immune reactions	0.8
I_0	$PAR2^*$-independent immune reactions	1
b_{pre}	Concentration of skin barrier precursors	0.5
k_L	Strength of lipid release inhibition by $PAR2^*$	10
$\tilde{B}$	Nominal skin barrier integrity	1
d_K	Rate of desquamation by KLK^*	0.1
ϵ	Minimum barrier integrity	001

production term $\left(1-\frac{B(\tau)}{\tilde{B}}\right)$. In Chapter 6 we propose mathematical models, represented by delay-differential equations, describing the mechanisms with which the self-recovery property can be achieved.

The regulatory network proposed retains the feedback structure of the biochemical interactions proposed in [166] and is composed of positive and negative feedback regulation at the tissue level. Specifically, healthy barrier function reduces the infiltration of pathogens, however, PAR2-induced inflammation, due to the presence of these pathogens, can interfere with barrier recovery processes, thus, resulting in a positive feedback loop. Infiltration of pathogens activate PAR2 signalling, resulting in inflammation that eradicates the stimulus via a negative feedback. Finally, barrier integrity is controlled by the enzymatic activity of KLK, which when excessive, can diminish the protective capabilities of the barrier (Fig. 2.5).

With this model, the authors investigated common risk factors related to AD development, as explored in [166], as well as, risk factors related to skin barrier function. Specifically, they studied risk factors resulting in high skin permeability, represented as deficient *FLG* expression ("Low *FLG*"), and weak immune defences, represented as deficient eradication of infiltrating pathogens ("'Low AMP'). Coincidence of multiple risk factors increased the propensity to develop AD and lead to increased disease severity, while each risk factor was associated with a distinct dynamic signature. The proposed model architecture and the choice of parameters resulted in the model exhibiting qualitative behaviours replicating clinically relevant symptoms of AD: (a) healthy recovery of the epidermal function resulting in homeostasis; (b) oscillations with periodic loss of

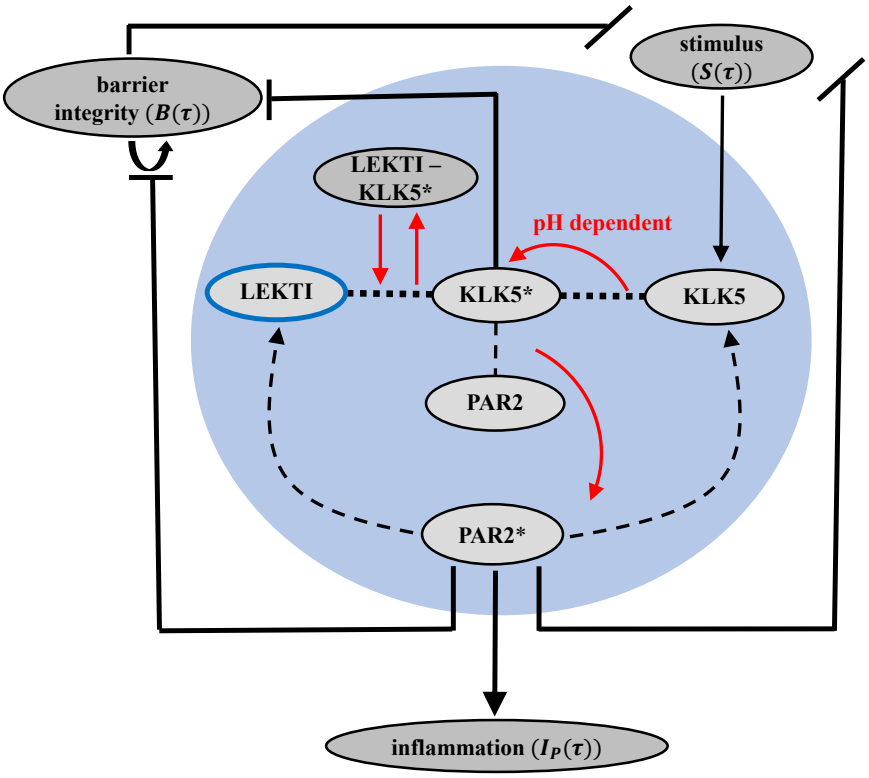


Figure 2.5: Regulatory network of the biochemical and tissue-level interactions controlling epidermal permeability function (mutli-scale model). Inner circle: biochemical network proposed in [166]. Adapted from [167].

homeostasis frequently observed in patients with mild AD and manifesting as an AD flare; and (c) persistent damage as observed in severe AD patients.

The system-level analysis, investigating the interplay between protease-dependent immune responses, barrier function, and infiltrating pathogens described the early-phases of AD pathogenesis, elucidating disease onset mechanisms via known risk factors. This mathematical model, however, does not take into account adaptive immune responses, which are known to be activated in chronic AD patients [5, 102, 103, 174]. In order to understand the pathogenic processes involved in the onset and progression of AD, we develop a hybrid model (Chapter 3) using as a basis the model proposed by Dominguez et al. [167]. Our model considers adaptive immune responses mediated via dendritic cells [45,127,175] that characterise the late-stages of AD. The development of the hybrid system was motivated by its computational simplicity, which enabled us to explore the effect of treatments. We therefore then propose a computational framework for the de-

sign of patient-specific treatment strategies (Chapters 4 and 5) for proactive treatment in the management of severe AD. The protocols for proactive treatment strategies form the first comprehensive approach to develop model-based, closed-loop treatments of AD using optimal control theory.

2.4 A toy hybrid model

The model developed in Chapter 3 is termed a *hybrid model*. Generally speaking hybrid dynamical systems are those that exhibit continuous state evolutions, as well as, discrete state jumps and/or involve continuous and discrete inputs and outputs [176,177]. In the literature they belong in the wider class of *non-smooth dynamical systems* [178]. Such systems are quite pervasive in mathematical biology, for example to simulate the firing dynamics of neurons [179], transcription factor regulation of gene-expression [180–182], and cell decision making and division [183–185], and have amassed attention in both academic and industry circles [186].

Hybrid dynamical systems have been noted to exhibit richer and more complicated behaviour compared with their smooth counterparts [187]. In order to view this idea we analyse here a simple linear one-dimensional hybrid dynamical system. Analogous one-dimensional linear dynamical systems cannot exhibit oscillatory behaviour, while as we will see in the example, the system displays regular oscillations.

The simple hybrid dynamical system is described by the following equation:

$$\dot{x} = R(x) - x(t), \tag{2.4}$$

where

$$R(x) = \begin{cases} \alpha, & x(t) > x^- \quad (2.5) \\ \beta, & x(t) < x^+, \quad (2.6) \end{cases}$$

with $\alpha, \beta, x^-, x^+ \in \mathbb{R}$.

The state evolution across time is governed by a linear ODE[1], however, at discrete points in phase space the equations governing the trajectory of the system abruptly

[1] This will result in a solution given by either a negative or positive exponential depending on the initial condition and the choice of α and β.

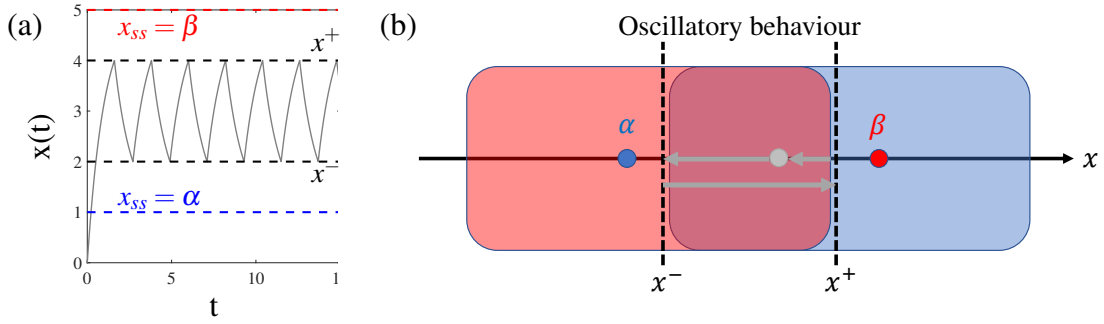


Figure 2.6: Oscillatory behaviour of the toy hybrid model defined by Eq. (2.4). (a) Numerical simulation of the time evolution of the state (grey) with initial condition $x(0) = 0$, switching boundaries $x^- = 2$ and $x^+ = 4$ (black dashed lines), and model parameters defining the equilibria of the system: $\alpha = 1$ (blue dashed line) and $\beta = 5$ (red dashed line). (b) Schematic representation of the oscillatory behaviour of the hybrid system given by the grey arrows. Red and blue region denote the *domain of definition* when $R(x) = \beta$ and $R(x) = \alpha$, respectively. Red, and blue circles denote the system equilibria with $R(x) = \beta$ and $R(x) = \alpha$, respectively, and the grey circle denotes the initial condition ($x(0)$).

change, as determined by the function $R(x)$. Therefore, the complete evolution of the hybrid system involves a collection of two *subsystems*; this type of hybrid systems are known as *switched-hybrid systems* [188,189]. The aforementioned discrete points in the phase space, where there is such a change in the mode of operation, are called *switching boundaries* or *switching manifolds* and are denoted here as x^- and x^+.

To determine the behaviour of this simple hybrid system we need to provide an initial condition ($x(0)$) for Eq. (2.4), as well as, an initial state for the switch $R(x)$ (Eq. (2.5) and (2.6)), thus defining which subsystem is currently governing the evolution. The only restriction is that the initial condition ($x(0)$) is *viable* given the choice of the initial state of the switch: if $R(x) = \alpha$ then any initial condition $x(0) < x^-$ is not viable since it is out of the *domain of definition* of the governing subsystem.

To analyse the behaviour of the hybrid system we first determine the equilibria of each subsystem. These are given by $x_{ss} = \alpha$, when $R(x) = \alpha$, and $x_{ss} = \beta$, when $R(x) = \beta$. The natural behaviour of the system will depend on the position of the switching boundaries (x^- and x^+) relative to the equilibria. For the system to exhibit oscillatory behaviour the following conditions must hold: $\alpha < x^- < x^+ < \beta$.

The resulting time evolution with $x(0) = 0$, $x^- = 2$, $x^+ = 4$, $\alpha = 1$, and $\beta = 5$ is shown in Fig. 2.6a. Since both equilibria are outside the domain of definition of each governing subsystem the switching boundaries are hit, therefore, changing the mode of operation

periodically, leading to oscillations. A schematic representation for this process is shown in Fig. 2.6b.

Chapter 3

A hybrid model of atopic dermatitis

This chapter presents the first hybrid mathematical model of AD pathogenesis (Fig. 3.1) that we recently developed to investigate the mechanisms behind onset and progression of AD.

Previously developed AD models [166, 167] focused on the early stages of AD and did not consider the effects of adaptive immune responses. In order to have a broader description for the onset and progression of the disease, our new model incorporates adaptive immune responses, which are activated in the late stages of AD. The late stages of AD are characterised by an irreversible impairment of adaptive immune responses via systemic T_H2 sensitisation [35]. Therefore, it is relevant to understand the underlying mechanisms that induce systemic T_H2 sensitisation.

We show that the developed hybrid model can replicate clinical and experimental data, hence demonstrating that it provides a plausible mechanistic explanation for onset and progression of AD; this addresses the first aim of this thesis. Furthermore, this model is an essential ingredient to address the lack of effective treatment protocols to prevent the onset of AD and to manage its symptoms, as it provides a necessary mathematical framework to investigate the effects of treatments on disease progression. We use this mechanistic model to develop a computational method that will enable the design of patient-specific effective treatment protocols in Chapter 4.

In collaboration with Dr Elisa Domínguez-Hüttinger we developed the reaction network

and its precise mathematical description. Furthermore, we developed the MATLAB code to numerically integrate the hybrid system and conducted bifurcation analysis to identify its dynamic behaviours. Our clinical and experimental collaborators, Dr Kosuke Miyauchi, Professor Alan D. Irvine, Dr Mariko Okada-Hatakeyama, and Dr Masato Kubo, have contributed in providing information on the underlying biology of AD and its clinical relevance. The mice experimental data demonstrated in the paper was provided by Dr Masato Kubo (Appendix A.1 and A.3).

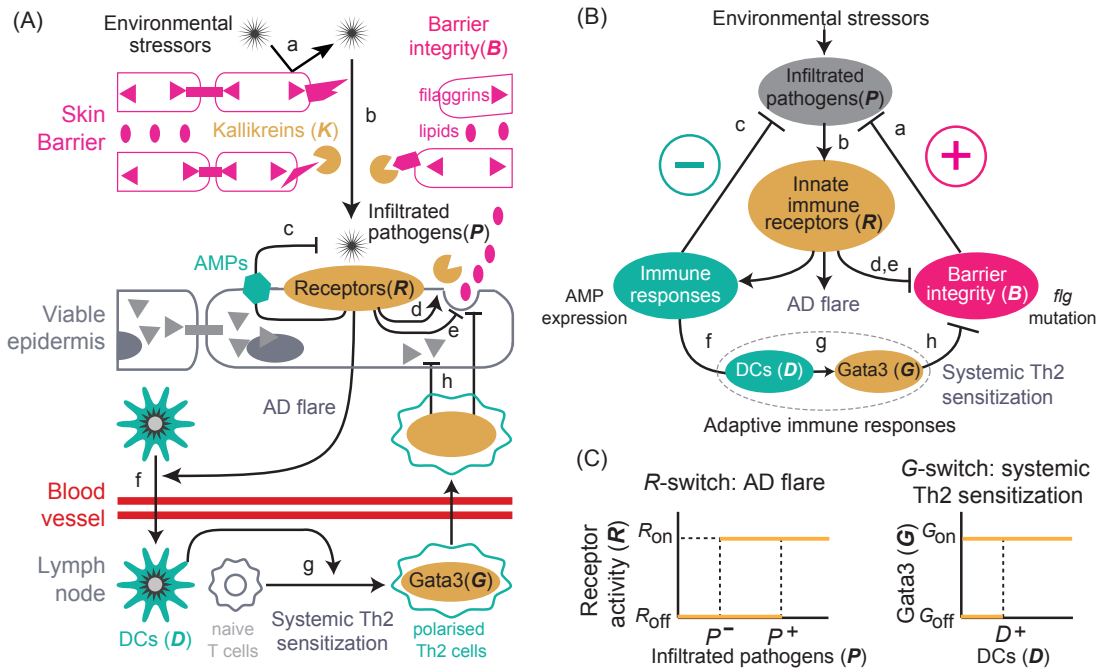


Figure 3.1: Mechanistic model of AD pathogenesis with a double-switch motif. A, Schematic diagram of the processes included in the model. Italics denote the state variables in the model equations (Eq. (3.1)). B, Control structure of the system regulating AD flares through positive and negative feedback. C, R-switch (reversible activation of innate immune receptors) and G-switch (irreversible GATA-3 transcription).

The rest of the chapter represents a variation of the contents of our paper *"Mathematical modeling of atopic dermatitis reveals "double-switch" mechanisms underlying four common disease phenotypes"* [190] as it was published in the *Journal of Allergy and Clinical Immunology*, under a Creative Commons licence in June 2017. The original article can be found under `http://www.sciencedirect.com/science/article/pii/S0091674916314336?via%3Dihub`.

3.1 Introduction

Atopic dermatitis (AD) is a common chronic skin disease, characterized by persistent skin inflammation and a defective skin barrier prone to infections [24]. While AD affects up to 25% of children worldwide [191], with a continuous increase in the number of patients and treatment costs [192], clear guidance and consensus for effective treatment strategies for prevention, and induction of remission, are yet to be fully established [193]. The scientific basis for recent clinical recommendations of "proactive therapy" is largely based on clinical trial data with limited duration and scope [123], and waits to be further strengthened by a better understanding of the pathogenic mechanisms of AD. A system-level understanding of AD pathogenesis, however, may lie beyond the ethical and practical reach permitted by clinical and experimental studies, and could be supported by a systematic, extensive investigation of the disease dynamics using mathematical models [194, 195].

Previous studies have identified genetic and environmental risk factors for AD onset including defects in skin barrier function (the filaggrin gene encoding profilaggrin [196–199] and 30 other putative loci for skin barrier function) and in the immune system, including innate and adaptive immunity [50, 89, 200]. In addition, microbiome composition has been shown to play a critical role [51, 70]. Each of these risk factors perturbs the system of strongly intertwined regulatory interactions between the keratinocytes (which along with the extracellular lipids provide the barrier function and also initiate many innate immune responses in the epidermis) and mediators of the adaptive immunity such as dendritic cells (DCs) and T cells. Perturbations triggered at one part of the system can propagate to another part through interactions, causing synergistic effects of risk factors and a gradual aggravation of the AD phenotype from a mostly asymptomatic mild phenotype at its early stage [112] to a severe treatment-resistant form [90]. Understanding of this dynamic pathogenesis thus requires elucidation of the synergistic effects of multiple risk factors on AD pathogenesis (e.g., mutations in skin barrier components accompanied by environmental insults) and the dynamic interplay between the skin barrier, immunity and environment, as suggested by several clinical [19, 200] and animal or *in vitro* experimental studies [129, 138, 201, 202].

In this chapter, we develop a mathematical *in silico* model of AD pathogenesis that describes the complex and dynamic interplay between skin barrier function, immune responses, and environmental stressors, based on clinical and experimental data and our

previous model of the early stage of AD [167]. Through systematic and mathematical investigation of the synergistic effects of the risk factors on dynamic progression of AD pathogenesis, we tested the hypothesis that genetic risk factors predispose patients to AD progression and decrease the threshold for environmental stressors to drive severe AD [91]. We uncover mechanisms underlying AD onset and progression, explore effective treatment strategies to prevent progression of AD, and answer three basic questions about onset, progression and prevention of AD: (1) Why do some patients with genetic AD risk factors appear initially asymptomatic but then easily develop clinically severe AD? (2) Why do some patients progress to severe AD, while the others stay with mild AD? (3) What are the underlying mechanisms behind effective prevention of AD development by emollients in neonates, as demonstrated in recent clinical trials? [203, 204]

3.2 Methods

Model description

The proposed model of AD pathogenesis (Fig. 3.1) is described by a hybrid system,

$$\frac{dP(t)}{dt} = P_{env}\frac{\kappa_P}{1+\gamma_B B(t)} - (\alpha_I R(t) + \delta_P)P(t) \tag{3.1a}$$

$$\frac{dB(t)}{dt} = \frac{\kappa_B(1-B(t))}{\Big(1+\gamma_R R(t)\Big)\Big(1+\gamma_G G(t)\Big)} - \delta_B K(t)B(t) \tag{3.1b}$$

$$\frac{dD(t)}{dt} = k_D R(t) - \delta_D D(t), \tag{3.1c}$$

for the dynamics of the three variables, $P(t)$, $B(t)$, and $D(t)$, denoting the infiltrated pathogen load (in milligrams per milliliter), the strength of barrier integrity (relative to the maximum strength), and the concentration of DCs in the lymph node (cells per milliliter), respectively. The dynamics of $P(t)$, $B(t)$, and $D(t)$ depend on the dynamics of the three additional variables, $R(t)$, $G(t)$, and $K(t)$, denoting the levels of activated immune receptors, *Gata3* transcription (relative to the maximum transcription level), and active kallikreins, respectively.

The infiltrated pathogen load (P), increases by the penetration of environmental stress load (P_{env}) through the barrier (B). P is eradicated by innate immune responses trig-

gered by inflammation (R) and is also naturally degraded. The barrier function, (B), is determined by the balance between its production and degradation. The barrier production is described by a phenomenological representation of its capacity to self-restore the nominal barrier function following its disruption, and is compromised by innate immune responses triggered by inflammation (R) and cytokines produced by differentiated T_H2 cells which increases according to G. The degradation of the barrier occurs as a result of desquamation mediated by active kallikreins, (K). The DCs (D) increases while inflammation (R) persists and degrades naturally. In Eq. (3.1) we use simple mathematical terms based on the law of mass action with zero order production and first order degradation terms, except for the barrier production term, $k_{\mathrm{x}}(1-x(t))$, which represents the phenomenological recovery of skin barrier in response to disruption [140]. The inhibitory rates are described in the form of $1/(1+x(t))$.

The dynamics of $R(t)$, $G(t)$, and $K(t)$ is described by a perfect switch (Fig. 3.1, C),

$$(R(t), K(t)) =$$

$$\begin{cases} (R_{off}, K_{off}) & if\ P(t) < P^- \ or\ \{P^- \leq P(t) \leq P^+ \ and\ R(t^-) = R_{off}\} \\ (R_{on}, K_{on} = m_{on}P(t) - \beta_{on}) & if\ P(t) > P^+ \ or\ \{P^- \leq P(t) \leq P^+ \ and\ R(t^-) = R_{on}\} \end{cases} \tag{3.2}$$

$$G(t) = \begin{cases} G_{off} & if\ D(t) < D^+ \ and\ G(t^-) = G_{off} \\ G_{on} & if\ D(t) \geq D^+ \ or\ G(t^-) = G_{on} \end{cases} \tag{3.3}$$

where t^- is a time slightly before the time t, as they change abruptly within hours [205, 206], in a much faster time-scale than for $P(t)$, $B(t)$, and $D(t)$ that change over weeks [140, 207].

The nominal values of model parameters (Table 3.1) [129, 140, 166, 167, 207–210] were taken from the previously published model of the early stage of AD [167] (P_{env}, γ_{B}, κ_{B}, α_{I}, δ_{P}, κ_{B}, γ_{R}, δ_{B}), obtained by approximation of the bifurcation diagrams previously derived [166, 208] (P^-, P^+, R_{off}, R_{on}, K_{off}, m_{on}, β_{on}, D^+, G_{off}, G_{on}), or derived [129, 140, 207, 209, 210] from experimental literature (γ_{G}, κ_{D}, δ_{D}).

The parameters P^-, P^+, R_{off}, R_{on}, K_{off}, m_{on}, β_{on} were estimated from bifurcation

diagrams presented in [166] (reproduced in Section 2.3.1) in the following way: With the nominal parameter set (Table 2.1) P^- and P^+ represent the pathogen concentration at which saddle-node bifurcations occur, as discussed in Section 2.3.1. Parameters R_{off} and R_{on} represent the level of inflammation via $PAR2$ activation and are approximated as horizontal lines (see Fig. 2.4b). Finally, parameters K_{off}, m_{on}, and β_{on} represent the level of $KLK5$ activation and are approximations of the Fig. 2.4c. The parameters m_{on}, and β_{on} are derived by approximating a linear line. Similar analysis was performed to estimate D^+, G_{off}, and G_{on} from [208].

The novelty of this model stems from its construction as a hybrid model and the addition of the effects of adaptive immune responses to the previously published papers [166] and [167]. The effects of the adaptive immune responses are considered through the accumulation of dendritic cells (Eq. (3.1c)), which introduce three new parameters, namely: γ_{G}, κ_{D}, δ_{D}. These parameters were identified using a qualitative approach from mouse or human data ([129,207,209,210]) in order to replicate the following qualitative features: (i) increased concentration of dendritic cells when innate receptors are active (accumulation of dendritic cells via the parameters κ_{D} and δ_{D}). These two parameters were varied so as to replicate the increase/decrease of dendritic cell concentration as depicted in [207, 209, 210], which leads to sensitisation occuring after $t_{\text{on}} = 2.02$ days of continuous innate receptor activation. The parameters where estimated by minimising the least squared error between the model predictions and the data; and (ii) the spontaneous worsening of barrier integrity after sensitisation (via the parameter γ_{G}). The parameter γ_{G} is included through the term $1/(1+\gamma_G G(t))$ (Eq. (3.1b)) that effectively represents a reduction in the expression of skin barrier precursors and increases the time required for the skin barrier to reach homeostasis. This qualitatively replicates the experimental observations in human data [129].

Model analysis

Model analysis was conducted using MATLAB version R2014a (The MathWorks, Inc., Natick, MA, USA). We used *ode15s* for numerical integration of the system from the steady states as the initial conditions, and *output* function to update the switching variables at each step of the iteration. In the subsequent sections the two most common genetic risk factors of AD will be investigated, relating to skin barrier permeability (e.g. mutations in the FLG gene) and the capacity to eradicate infiltrated pathogens (through regulators of antimicrobial peptide expression e.g. TLRs and NK-κB), that

Table 3.1: Definition of model parameters and their nominal values for Eq. 3.1.

Symbol	Name	Nominal value	Ref.
P_{env}	Environmental stress load	95 (mg/ml)	[167]
γ_{B}	Barrier-mediated inhibition of pathogen infiltration	1	[167]
κ_P	Nominal skin permeability	0.6 (1/day)	[167]
α_I	Rate of pathogen eradication by innate immune responses	0.25 (1/day)	[167]
δ_{P}	Basal pathogen death rate	1 (1/day)	[167]
κ_B	Barrier production rate	0.5 (1/day)	[140, 167]
γ_{R}	Innate immunity-mediated inhibition of barrier production	10	[167]
δ_B	Rate of kallikrein-dependent barrier degradation	0.1	[167]
γ_{G}	Adaptive immunity-mediated inhibition of barrier production	1	[129]
κ_D	Rate of DC activation by receptors	4 cells/(ml × day)	[207, 209]
δ_D	Rate of DC degradation	0.5 (1/day)	[210]
P^-	Receptor inactivation threshold	26.6 (mg/ml)	[166]
P^+	Receptor activation threshold	40 (mg/ml)	[166]
D^+	Gata3 activation threshold	85 (cells/ml)	[208, 209]
R_{off}	Receptor-off level	0	[166]
R_{on}	Receptor-on level	16.7	[166]
G_{off}	Gata3-off level	0	[208]
G_{on}	Gata3-on level	1	[208]
K_{off}	Kallikrein-off level	0	[166]
m_{on}	Slope of the linear relation between $P(t)$ and K_{on}	0.45	[166]
β_{on}	Y-intercept of the linear relation between $P(t)$ and K_{on}	6.71	[166]

are represented by the model parameters κ_P and α_I, respectively. Our model analysis investigated the ranges of $0 \leq \alpha_I \leq 0.3$ and $0 \leq \kappa_P \leq 1$. The dynamic trajectories were calculated for 1054 pairs of α_I, κ_P uniformly sampled (an interval of 0.01 for α_I and 0.03 for κ_P).

Epidermis-specific signal transducer and activator of transcription 3 knockout mice

We developed keratinocyte-specific signal transducer and activator of transcription 3 (*Stat*3) knockout ($Stat3^{f/f}$) mice with the B6X129 mixed background [211]. All mice used in this study were maintained under pathogen-free conditions. Animal care was conducted in accordance with guidelines of the RIKEN Yokohama Institute.

Development of AD phenotypes in epidermis-specific *Stat*3 knockout mice

Expression levels of 11 nuclear factor κB (NF-κB) target genes (*Bcl2, Ddx26b, Gadd45b, Icam1, Icam2, Icam4, Icam5, Il1b, Tnf, Traf1, Traf2* and *Vcam1*) selected from the Kyoto Encyclopedia of Genes and Genomes database (`http://www.genome.jp/kegg-bin/show_pathway?ko04064+K02580`) were quantified from sorted ear samples of 2-, 5-, 8-, and 10-week-old $Stat3^{f/f}$ mice. By using total RNA isolated with TRIzol, cDNAs were synthesized with NEBNext Ultra RNA Library Prep Kit for Illumina (New England Biolabs, Ipswich, Mass), according to the manufacturer's instructions. Comprehensive expression analysis was performed by mRNA sequence (single-ended 50-base pair reads) using the HiSeq 3000 system (Illumina, San Diego, Calif; GEO accession number GSE86071). Read alignment (mm9) was performed using TopHat2 v2.0.8 and expression level was determined by Cufflinks, version2.1.1 with default settings. We calculated mean expression levels of the NFκB target genes over the 2 mice per cohort (asymptomatic and AD phenotype) and normalized them by using wild-type (WT) dynamics.

Severity of the AD symptoms was assessed in 11 mice at 51 time points by examining the areas of the skin lesion: no lesions (score 0), periocular lesions (score 1/5), lesions on a half side of the face (score 2/5), on a complete side of the face (score 3/5), on the whole face (score 4/5), or on the whole face and ears (score 5/5). The time of systemic

sensitisation (t = 0) corresponds to the time when the IgE levels increase to 10% of the maximal IgE level measured for each mouse.

3.3 Results

Model overview

Our proposed mathematical model of AD pathogenesis (Fig. 3.1, A and B) is a system-level representation of the prominent interactions between environmental stressors, skin barrier integrity and immune responses, that were identified based on the empirical evidence from numerous clinical [102, 108, 129, 139, 199, 212] and experimental *in vivo* [139,168,201,213–215] or *in vitro* [216–218] studies. The model is described by a hybrid system of three ordinary differential equations (Eq. (3.1)) and includes a double-switch motif with two concatenated bistable switches (Eqs. (3.2) and (3.3)), as detailed below. The first switch is responsible for onset of AD flares and the second switch for progression to severe AD. This mathematical model includes only the major cellular and biochemical regulators required to describe a global regulatory structure and mechanisms underlying onset, progression and prevention of AD, rather than explicitly incorporating the fine details of the complex molecular and cellular processes that control epidermal function.

Our model results are validated by clinical and experimental data derived from mouse models with perturbations in either skin barrier function, immune responses or environmental stressors, the interplay of which is investigated in our model: mouse models with barrier deficiency (flaky tail [*ft*] mice [138,201] with the double mutation involving filaggrin gene (*Flg*) and *Tmem79*, which encodes lamelar granules [219], filaggrin null [$Flg^{-/-}$] mice [202], and *Tmem79*-deficient mice [220,221]), keratinocyte-specific *Stat3* knockout mice with dysregulated immune responses [211, 222, 223], and mouse models in which AD symptoms are induced solely by environmental stressors [52, 224].

A first switch for onset of AD flares

The first part of the model (processes a-e in Fig. 3.1, A and B, described below) elucidates the mechanisms of how the activity of the first switch (switch-like activation of innate immune receptors) is regulated and leads to AD flares.

Healthy barrier integrity protectsdy from environmental stressors (process a) and is maintained by a combination of regulated processing of filaggrin [201] and lipid contents, which constitute lipid envelopes of corneocytes. When barrier integrity is compromised by, for example, excessive skin desquamation through active kallikreins [139], environmental stressors, including pathogens (e.g., *Staphylococcus aureus*) [108], infiltrate the barrier and stress the viable epidermis. They are recognized by innate immune receptors, such as Toll-like receptors (TLRs), which recognize danger-associated molecular patterns and pathogen-associated molecular patterns [205, 217]. Activation of the innate immune receptors triggers innate immune responses to eradicate the infiltrated pathogens through release of antimicrobial peptides (process c) [205, 217], further activates kallikreins (process d) [205], interferes with the *de-novo* production of skin barrier lipids (process e) [213], and triggers inflammation [214], resulting in AD flares with increased levels of IL-33 [225], thymic stromal lymphopoietin [168], and other alarmin cytokines [226].

Activation of the innate immune receptors is modelled by a reversible bistable switch [166] between the off and on states ($R = R_{off}$ and R_{on}) with the activation (P^+) and inactivation (P^-) thresholds for the amount of environmental stressors, such as pathogen load, that are recognized by the innate immune receptors (Fig 3.1, C, R-switch). When the R-switch is on, clinical symptoms of AD flares appear as increased inflammation accompanied by decreased barrier integrity. Our model demonstrates that activation of the innate immune receptors and the subsequent onset and resolution of AD flares is mainly regulated by a combination of negative and positive feedbacks through innate immune responses and barrier integrity (Fig 3.1, B). The relative strengths of the feedbacks can be associated with the 2 most prominent genetic risk factors of AD: mutations in the *FLG* gene [196, 197], which results in a higher skin barrier permeability [202], and a dysregulated expression of innate immune system components [89], including regulators of antimicrobial peptide expression (e.g., TLRs [227], nucleotide-binding oligomerization domains [50], and NF-kB [228]), leading to dysfunctional immune responses and a diminished capacity to eradicate the infiltrated pathogens.

Synergistic effects of genetic risk factors and environmental triggers on dynamic phenotypes for AD flares

We investigated the effects of the two most common genetic risk factors of AD with our model by varying the model parameters that quantify skin barrier permeability

(κ_P) and the capacity to eradicate infiltrated pathogens (α_I) in Eq. (3.1). These analyses correspond to examining carriers of different variations of the genetic risk factors and observing how AD can be developed and proceeded in each cohort as a result of the synergistic effects of the environmental stressors and the two genetic risk factors. Our model analysis revealed the following four qualitatively different *dynamic phenotypes* (Fig. 3.2, A and B) in response to environmental stressors (e.g. pathogenic challenges). Fig. 3.2A represents a co-dimension 2 bifurcation diagram with respect to the parameters (κ_P, α_I) which is derived by examining the position of the equilibria of each subsystem of the hybrid model with respect to the switching manifold P^- and P^+. Specifically, the bifurcation diagram (Fig. 3.3, A) of the proposed model was numerically obtained using the methodology described in Oyarzún et al [229] to identify the 4 qualitatively different *dynamic phenotypes* with respect to the relative strengths of the feedbacks determined by skin barrier permeability (κ_P) and immune responses (α_I). The steady states for barrier integrity were calculated analytically for the *recovery*, *bistability*, and *chronic damage* dynamic phenotypes, and numerically obtained for the *oscillation* dynamic phenotype by taking the mean of the mean-over-time over the corresponding parameter region for (α_I,κ_P) or by taking the mean for varied levels of skin barrier permeability (κ_P) with an α_I value of 0.25. The basins of attraction for the *bistability* dynamic phenotype for (α_I,κ_P)=(0.04, 0.65) were numerically determined by integrating the system from the points of tangency, (P^-, B^-) and (P^+, B^+), identified by solving $\dot{P}(t) = 0$ at $P(t) = P^-$ and P^+, respectively (Fig. 3.3, F).

When these intrinsic genetic defects do not exist, a quick recovery of the system to the healthy steady state (Fig. 3.2, B *grey*), with homeostatic barrier integrity and no AD flares ($R = R_{off}$), is achieved after a transient decrease in the barrier integrity and transient AD flares (*recovery* dynamic phenotype Fig. 3.2, A *grey*); simultaneous existence of these two genetic risk factors results in convergence of the system to the unhealthy steady state (Fig. 3.2, B *red*), corresponding to a chronically decreased barrier integrity and persistent AD flares ($R = R_{on}$), which potentially leads to chronic tissue damages (*chronic damage* dynamic phenotype Fig. 3.2, A *red*); genetic defects leading to dysregulated immune responses result in bistability (Fig. 3.2, B *yellow*), where either the healthy or unhealthy steady state is achieved (*bistability* dynamic phenotype Fig. 3.2, A *yellow*); genetic defects leading to high skin barrier permeability results in persistent oscillatory dynamics (Fig. 3.2, B *teal*) due to the switching of R between R_{on} and R_{off} (*oscillation* dynamic phenotype Fig. 3.2, A *teal*). The aforementioned results correspond to co-dimension 2 bifurcation analyses of the model described by Eq. (3.1)

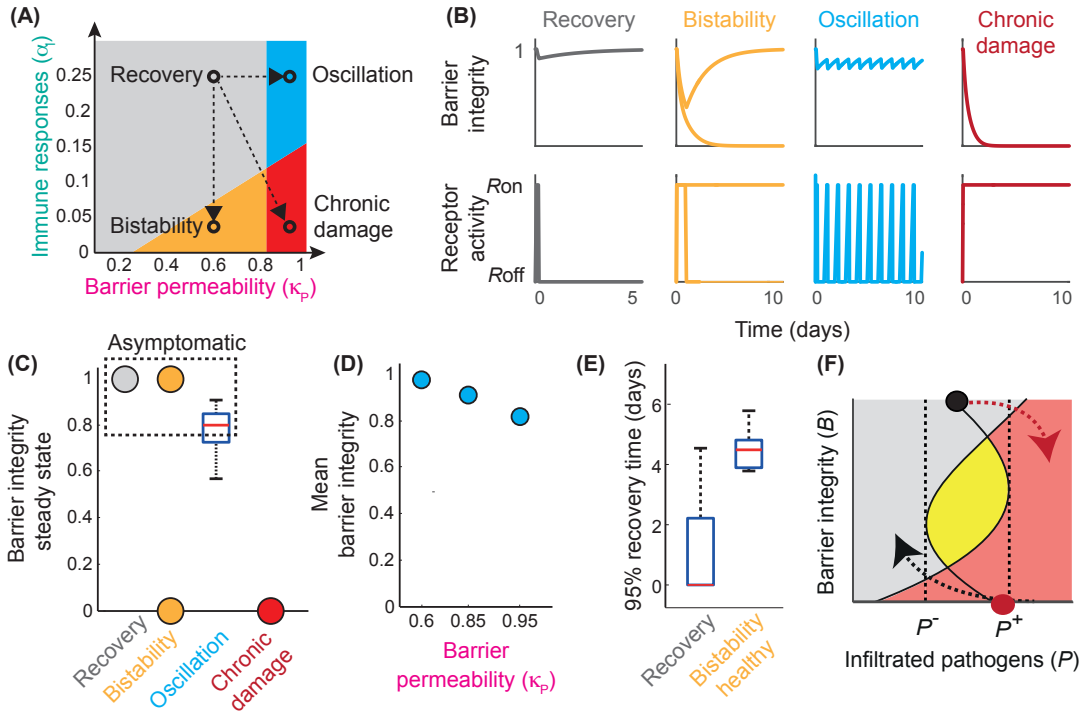


Figure 3.2: Computationally predicted effects of the 2 main genetic risk factors on the dynamic response to environmental stressors. A, Schematic of the bifurcation diagram. The circles in Fig. 3.2, A, represent the parameter values used to generate the example dynamics for each of the 4 dynamic phenotypes (B). C, Steady states of barrier integrity. D, Dose dependency of filaggrin deficiency on mean barrier integrity. E, Time required to regain 95% of the healthy steady state of barrier integrity. F, Basin of attraction in the (P, B)-space. The basins of attraction of the healthy (black circle) and unhealthy (red circle) steady states are represented by the grey and red regions. The states in the yellow region converge to the healthy steady state if the initial condition is $R = R_{off}$ and to the unhealthy steady state if the initial condition is $R = R_{on}$

with respect to the parameters κ_P and α_I.

The steady state barrier integrity for the *oscillation* dynamic phenotype (Fig. 3.2, A *teal*) is computationally predicted to be indistinguishable from that of the healthy steady state (Fig. 3.2, C), with a slightly lower mean but with an increased variability. These long-term dynamic behaviours are concordant with a slightly lower but more variable skin barrier integrity observed in $Flg^{-/-}$ [202] and ft [138, 201] mice, compared with that seen in WT mice. Our model analysis further predicts gradual decrease of the steady state barrier integrity for increased barrier permeability (κ_P), corresponding to the dose-dependent effects of filaggrin deficiency on the severity of AD symptoms [197] (Fig. 3.2, D).

The *bistability* dynamic phenotype (Fig. 3.2, A *yellow*) may also be asymptomatic (or subclinical) if it converges to the healthy steady state. However, our model analysis demonstrates that the healthy steady state of the *bistability* dynamic phenotype is distinguishable from that of the *recovery* dynamic phenotype based on the much longer time for recovery to regain the same healthy steady state from transient barrier damage (Fig. 3.2, E) because of the existence of the second stable (unhealthy) steady state. This model prediction is consistent with slower skin barrier recovery following tape stripping observed in non-lesional skin of patients with AD compared with healthy subjects [116] and in inflamed compared with non-inflamed human skin [141].

The boundaries of the basins of attraction for the *bistability* dynamic phenotype are computationally obtained by finding the points of tangency between the switching thresholds for the reversible R-switch, P^+ and P^-, and the $(P(t), B(t))$-trajectories on the phase plane (Fig. 3.2, F). The system moves from the healthy to the unhealthy steady state if external inputs (e.g., environmental aggressors) push the system into the unhealthy basin of attraction. This worsening of the state was observed in *ft* mice [138, 201, 202], as well as in *Stat3* knockout mice, which demonstrated AD symptoms only after challenged with haptens or LPS, an activating ligand of the innate immune receptor TLR4 [230] (see Fig. A.1). Likewise, the system can move back to the healthy from the unhealthy steady state if external inputs (e.g., treatments) bring the system back to the healthy basin of attraction, achieving remission. Once the remission is induced, maintenance therapy to keep the system in the healthy basin of attraction may achieve control of AD symptoms [120]. This potential switching between the healthy and unhealthy steady states, by environmental aggressors or treatments, is a distinguished feature of the *bistability* dynamic phenotype, and is not observable in the *recovery* and *chronic damage* dynamic phenotypes. Note that Fig. 3.2F corresponds to a static phase plane depiction of the basins of attraction of the two stable equilibria for a specific set of the (κ_P, α_I)-parameters. Varying these parameters within the range of *bistability* dynamic phenotype (Fig. 3.2, A *yellow*) will result in geometrically different basins of attraction as the points of tangency will change.

A second switch for progression of AD

The second part of the model (processes f-h in Fig. 3.1, A and B, as described below) includes the main biochemical and cellular players for the allergy-mediating (T_H2) adaptive immune responses triggered by AD flares and is a system-level synthesis of several

lines of empiric evidence from clinical and experimental studies. Using this model, we elucidate mechanisms behind progression of AD to establish systemic T_H2 sensitisation (including elevated IgE, a marker of a T_H2-skewed AD phenotype), and systematically investigate how the duration and frequency of AD flares affect the onset of systemic inflammation, including allergic inflammation.

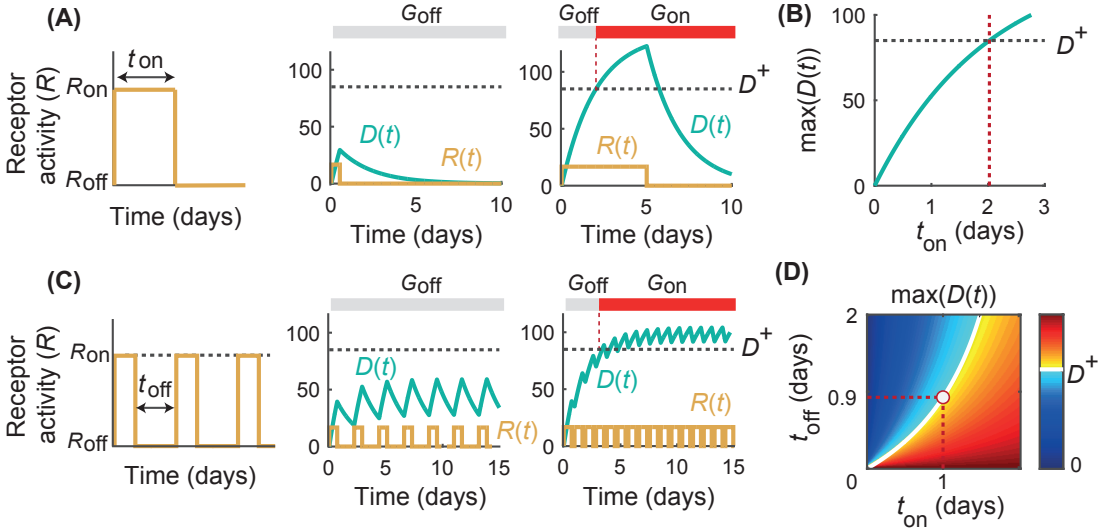


Figure 3.3: Proposed mechanisms of AD progression through a double switch. The G-switch is turned on by accumulation of DCs beyond D^+ because of transient AD flares (A) with a flare time (t_{on}) of longer than 2.02 days (B) or periodic AD flares (C) with a sufficiently small relaxation time (t_{off}) as a function of ton (D).

Activation of innate immune receptors causes AD flares with increased levels of cytokines (including thymic stromal lymphopoietin [168]), alarmins (such as IL-33 [225]), and others [226], which together contribute to activation of dendritic cells (DCs) in the epidermis [215]. These activated DCs migrate to lymph nodes (process f), where they increase the levels of IL-4 [215] and induce expression of *Gata3* [212] (process g), the master transcriptional regulator that controls the irreversible differentiation of naïve T cells into T_H2 cells [215, 218]. Differentiated T_H2 cells then migrate back to the epidermis, where they contribute to establish an allergic and pro-inflammatory micro-environment [102] and release cytokines that down-regulate the expression of several epidermal terminal differentiation markers, including filaggrin [129] (process h), thereby further compromising the barrier integrity [199]. Compromised barrier integrity results in persistent inflammation even in the absence of the additional environmental stressors.

The transcription level of *Gata3* is modelled by an irreversible switch [208] (Fig. 3.1,

C, G-switch): The transcription remains off ($G = G_{off}$) until sufficient numbers of DCs accumulate in the lymph nodes to reach the activation threshold (D^+), with which the transcription initiates ($G = G_{on}$) and persists even if the DCs disappear (D = 0). We assume that *Gata3*-mediated polarization of T cells to T_H2 cells is a hallmark of systemic T_H2 sensitisation and that the progression of AD from a mild to more severe phenotype is mediated by this irreversible G-switch.

Accordingly, our model of AD pathogenesis suggests that systemic T_H2 sensitisation is established if AD flares persist long enough so that $D(t)$ accumulates during the AD flares ($R = R_{on}$) and reaches D^+ to turn on the G-switch (Fig. 3.3, A, *right*). AD flares that do not persist long enough do not turn on the G-switch because $D(t)$ stays lower that D^+ (Fig. 3.3, A, *center*). Our model analysis predicts that a flare time (t_{on}) longer than 2.02 days turns on the G-switch (Fig. 3.3, B, Eq. (A.6)), which is consistent with the experimental observations that the peak of *Gata3* expression is reached in approximately 2 days after in vitro stimulation of T_H2 cell differentiation, inducing a stable Gata3-mediated T cell differentiation [218]. Systemic T_H2 sensitisation is spontaneously established in the *chronic damage* dynamic phenotype due to persistent AD flares and subsequent continuous accumulation of DCs to surpass D^+, turning on the G-switch.

Periodic AD flares, as in the *oscillation* dynamic phenotype, are also predicted to turn on the G-switch if the relaxation time (t_{off}) between AD flares (when $R = R_{off}$) is too short to prevent a gradual accumulation of DCs that eventually surpass the threshold D^+ (Fig. 3.3, C, *right*). The minimum relaxation time, above which the G-switch stays off, is analytically obtained as a function of the flare time (t_{on}; white line in Fig. 3.3, D, obtained by using Eq. (A.7)). For example, the R-spikes with a t_{on} of 1 day turns on the G-switch if t_{off} is shorter than 0.93 days (Fig. 3.3, D, *red circle*). Our model simulation for R-spikes with a t_{on} of 1 day and t_{off} of 0.9 days predicts turning on of the G-switch within 10 days, which is consistent with several features of AD skin, including T_H2 cell infiltration, observed in mice after repeated application of oxazolone once every other day over 10 days [224].

Four AD phenotypes classified by a double switch

Taken together, our model of AD pathogenesis is characterized by a double switch with two concatenated bistable switches (R- and G-switches), the status of which represents

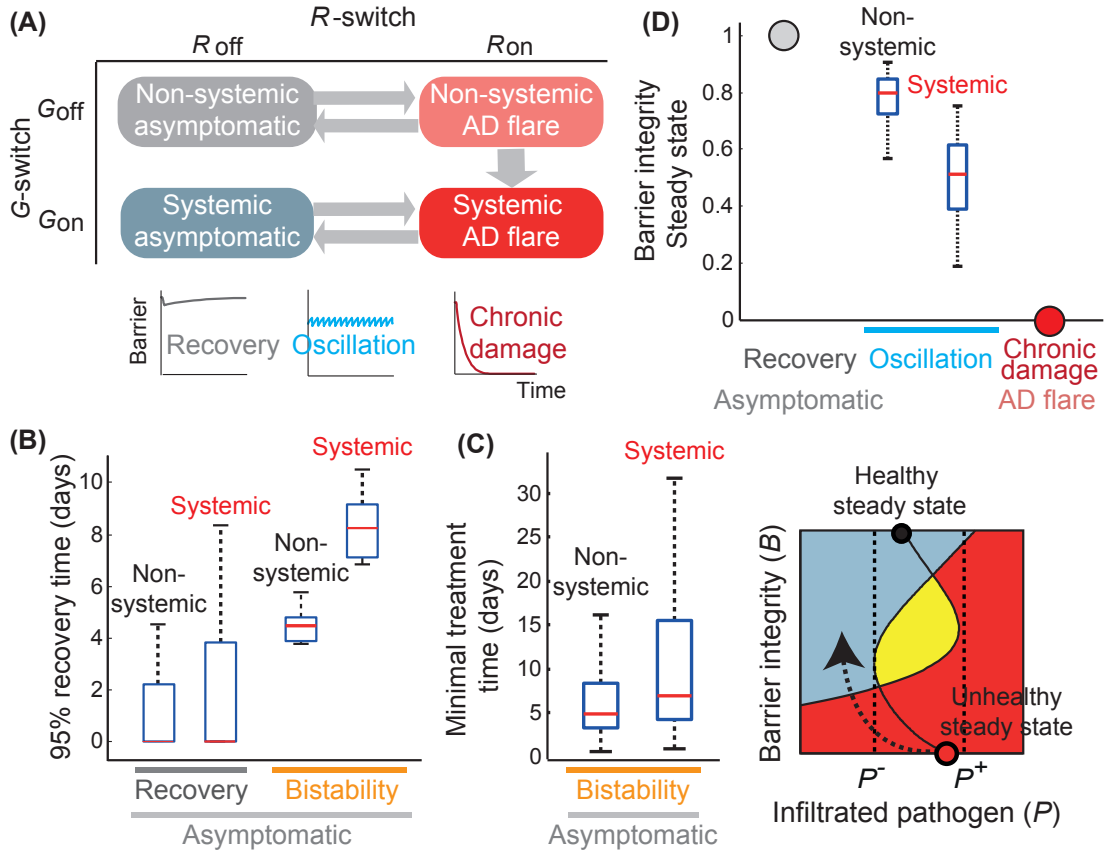


Figure 3.4: Four AD phenotypes described by the status of the double switch. A, The R-switch distinguishes between asymptomatic ($R = R_{off}$) and symptomatic ($R = R_{on}$), and the G-switch distinguishes between non-systemic ($G = G_{off}$) and systemic ($G = G_{on}$) phenotypes. B-D, Systemic phenotypes demonstrate severe AD symptoms compared with non-systemic counterparts, as computationally predicted by a longer 95% recovery time (Fig. 3.4, B), longer treatment time required for remission (Fig. 3.4, C), and lower barrier integrity (Fig. 3.4, D).

four AD phenotypes of different severity (Fig. 3.4, A). The state of the R-switch determines whether the phenotype is asymptomatic ($R = R_{off}$) or symptomatic (AD flare, $R = R_{on}$), and the state of the G-switch determines whether it is systemic ($G = G_{on}$) or non-systemic ($G = G_{off}$).

For the symptomatic case, in which the R-switch is constantly on and AD flares persist, as in the *chronic damage* or *bistability* (unhealthy) dynamic phenotype, the non-systemic symptomatic (R_{on}, G_{off}) state appears only transiently as it inevitably progresses, after a flare time of t_{on}=2.02 days (Fig. 3.3, B), to the (R_{on}, G_{on}) state corresponding to the systemic symptomatic phenotype, the most severe AD phenotype

with an impaired barrier integrity, systemic inflammation and infection.

The asymptomatic case, in which the R-switch turns off after transient AD flare as in the *recovery* or *bistability* (healthy) dynamic phenotype, corresponds to either non-systemic asymptomatic (healthy) phenotype in the (R_{off}, G_{off}) state or systemic asymptomatic phenotype in the (R_{off}, G_{on}) state with subclinical inflammation caused by T_H2-related cytokines. The systemic phenotype demonstrates more severe AD symptoms compared with its non-systemic counterpart, which are computationally characterized by a longer 95% recovery-time (Fig. 3.4, B). The 95% recovery times were numerically obtained by $t_{95\%} - t_{min}$, where $\mathrm{B}(t_{95\%}) = 0.95$ and $B(t_{min})$ is the minimum barrier integrity achieved after a transient AD flare. This was suggested by experiments in both WT and $Flg^{-/-}$ mice, which recovered from hapten challenge if unsensitised (non-systemic) but did not recover within two days if sensitised (systemic). The more severe symptoms are also computationally predicted by a longer treatment time required for remission (Figs. 3.2, F, and 3.4, C *right*) to drive the system from the unhealthy steady state to the healthy basin of attraction for the systemic than non-systemic phenotype because of the enlargement of the unhealthy basin of attraction. The minimal treatment times to achieve remission were numerically determined by evaluating the fold-decrease of P_{env} with which the state $(P(t), B(t))$ enters the healthy basin of attraction. This prediction is in agreement with the clinical observation that a much higher treatment effort is required to relieve AD symptoms during the chronic phase of AD, which is characterized by high IgE levels (systemic) [112].

The more severe symptoms for the systemic compared with the non-systemic phenotype are also computationally predicted for the case in which the R-switch is switching between R_{off} and R_{on}, as in the oscillation dynamic phenotype, by a decrease in the mean and an increase in the variance of the steady state of the barrier integrity (Fig. 3.4, D). This prediction is consistent with the increase in the mean and variance of the transepidermal water loss (an indicator of the barrier defect) measured in *ft* mice after the induction of systemic T_H2 sensitisation [138].

Genetic risk factors predispose to systemic T_H2 sensitisation

Here we use our mathematical model of AD pathogenesis to investigate the synergistic effects of environmental and genetic risk factors on AD progression. Specifically, we calculate the minimum stress load (the strength of the environmental stressors, P_{env})

that can turn on the G-switch by its continuous challenge through an AD flare of a single-pulse (Fig. 3.5, A, *left*) or of transient oscillation (Fig. 3.5, A, *right*) for different dynamic phenotypes caused by synergetic effects of the genetic risk factors (Fig. 3.2, A, and B). Turning on the G-switch (systemic T_H2 sensitisation) might appear as a dramatic increase in the severity of AD symptoms, as observed in *ft* and $Flg^{-/-}$ mice on ovalbumin (OVA) challenges [138,202]. The minimum stress load was experimentally evaluated in the dose response in WT mice, in which a systemic AD phenotype was developed through challenges with high (10%) but not lower ($\leq$ 2%) concentrations of *S. aureus* in culture supernatant [52], and by 10 repeated, but not single, oxazolone challenges [224].

Our model simulations predict that the minimum stress load is significantly lower for the *bistability* or *oscillation* dynamic phenotypes that arise in the context of genetic risk factors compared with the *recovery* dynamic phenotype, which is mainly observed when the intrinsic genetic defects do not exist (Fig. 3.5, B). This model prediction suggests that the genetic risk factors make the patients susceptible to smaller environmental stressors in developing systemic T_H2 sensitisation and is concordant with the experimental observation [201] of a low concentration (0.02%) of oxazolone-induced allergic contact dermatitis in *ft* mice but not WT mice and a higher concentration (0.5%) of oxazolone-induced allergic contact dermatitis also in WT mice.

Our predicted increase in the susceptibility to environmental stressors might explain the spontaneous appearance of AD symptoms in some, but not all, carriers of genetic risk factors for AD, as demonstrated in $FLG^{-/-}$ patient cohorts [196]. Carriers of the genetic risk factors who initially appear asymptomatic (as in the *bistability* or *oscillation* dynamic phenotypes; Fig. 3.2 C) can demonstrate a sudden and sharp worsening of the AD symptoms when they experience systemic T_H2 sensitisation, even with naturally occurring (small) fluctuations in the environment (Fig. 3.5, B). This observation also implies a possible mechanism behind the dose-dependent effects of filaggrin deficiency on AD symptoms [197] because the G-switch is turned on by a smaller environmental load for stronger filaggrin deficiency (Fig. 3.5, C).

To test the model-predicted outcome that small and naturally occurring environmental fluctuations can trigger a sudden and sharp worsening of the AD symptoms through systemic T_H2 sensitisation in carriers of the genetic risk factors, we evaluated the temporal changes of AD symptoms for *Stat3* knockout mice in the natural environment with small environmental stressors. Half of the mice developed an AD phenotype after

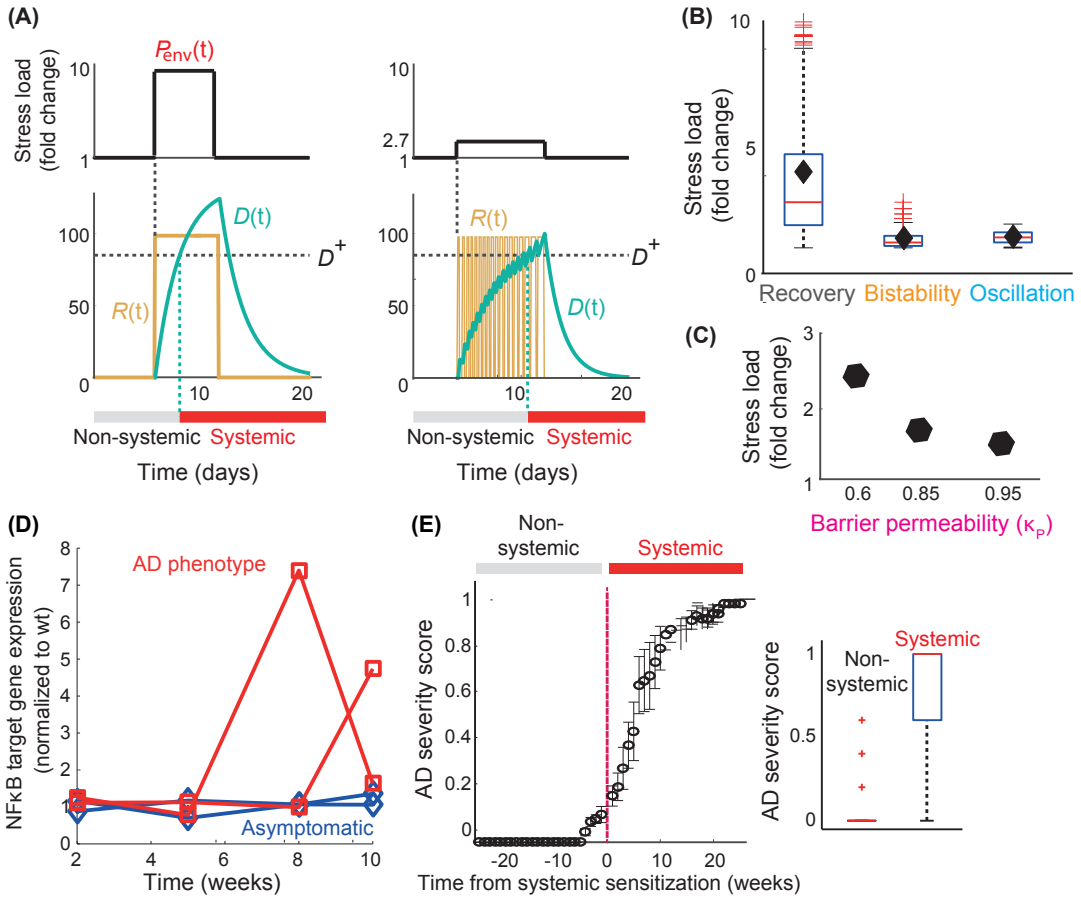


Figure 3.5: Genetic risk factors increase the susceptibility to environmental stressors in developing systemic T_H2 sensitisation. A, Transient increases in the environmental stress load can trigger systemic T_H2 sensitisation. B and C, Minimum stress load decreases with genetic risk factors (Fig. 3.5, B) in a dose-dependent manner (Fig. 3.5, C). D and E, Stat3 knockout mice with AD symptoms had higher NF-κB activity (Fig. 3.5, D), and the severity of the symptoms increased sharply after T_H2 sensitisation (Fig. 3.5, E).

30 weeks, whereas the others remained asymptomatic. Mice that demonstrated an AD phenotype exhibited a much higher expression of the NF-κB-target genes (a marker of ubiquitous environmental triggers [230];Fig. 3.5, D), suggesting that naturally occurring environmental triggers contributed to the observed development of the AD phenotype. Together with the observations in *Stat3* knockout mice that a long-lasting exposure to OVA (environmental stressor) triggered a sharp increase in the levels of IgE (see Fig. A.2) and that AD symptoms sharply increased after allergic systemic T_H2 sensitisation (increase of IgE; Fig. 3.5, E), these experimental results suggest that naturally occurring fluctuations in environmental stressors can trigger systemic T_H2 sensitisation in

mice with a genetically defective background and worsen their AD symptoms, which is consistent with the model-predicted outcome.

Prevention of AD symptoms by emollient treatments

We further derived the minimum stress load that can turn on the G-switch in the presence of continuous application of emollients computationally. In this analysis the stress load represents the external pathogen concentration (parameter P_{env}). Increasing P_{env} results in a shift of the equilibria of the system (Eq. (3.1)) that may activate the R-switch and subsequently cause T_H2 sensitisation (activation of G-switch). Applying emollients constantly counteracts the shift of the equilibria, caused by the external pathogen, and thus increases the minimum stress load that can cause T_H2 sensitisation. Emollient treatments are modelled by adding a constant production term to the barrier production rate dB/dt (Eq. (3.1b)) resulting in the equation $\frac{d\tilde{B}(t)}{dt} = \frac{dB(t)}{dt} + E$. The constant nominal value of emollient treatment was chosen to be 1.5 (dimensionless units) and was chosen arbitrarily. The main hypothesis we wanted to test is if emollients can be used to lower the risk of T_H2-mediated sensitisation.

The minimal stress load that can trigger systemic T_H2 sensitisation (Fig. 3.6, A, B, and C) was numerically determined by evaluating whether the $D(t)$ surpasses the threshold (D^+) for all the parameter combinations of (κ_P,α_I) within the *recovery* (Fig. 3.2, A *grey*), *bistable* (Fig. 3.2, A *yellow*), and *oscillation* (Fig. 3.2, A *teal*) dynamic phenotypes. Note that since Eq. (3.1c) is decoupled from the other equations (except for the instantaneous moment when the G-switch is activated) the only parameters determining DC accumulation, and by extension T_H2 sensitisation, in the model are k_D and δ_D; hence the duration the R-switch is required to be active such that the G-switch is activated is constant $t_{on} = 2.02$ days and is independent of the parameters κ_{P} and α_{I}. The ratio of minimal stress load (Fig. 3.6, D) is defined as the ratio of the nominal P_{env} ($P_{\mathrm{env}} = 95$, Table 3.1) and the increased P_{env} that may induce T_H2 sensitisation. All the boxplots (Fig. 3.6) show the minimum, first quartile, median, third quartile, and maximum values.

The model predictions confirm that emollient treatments, which strengthen barrier integrity and resistance [104], reduce the susceptibility to environmental stressors in developing systemic T_H2 sensitisation in all asymptomatic patient cohorts considered, as demonstrated by a more than 2-fold increase in the minimum stress load required to

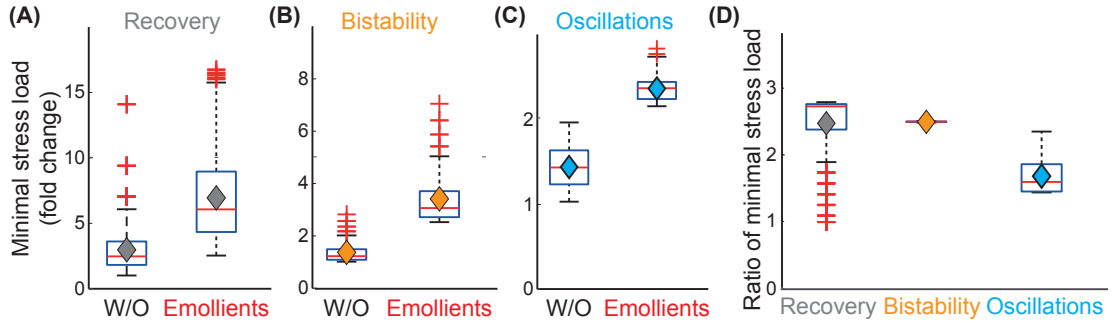


Figure 3.6: Emollient treatments prevent the progression to severe AD by increasing the computationally predicted minimum stress load required to drive systemic inflammation in *recovery* (A), *bistability* (B), and *oscillation* (C) dynamic phenotypes by approximately 2-fold (D).

turn on the G-switch (Fig. 3.6, D). These computational results suggest that topical applications of emollients can counteract the effects of the two genetic risk factors investigated in this article (weak barrier integrity and dysregulated immune responses) that asymptomatically increase the susceptibility to environmental stressors and effectively decrease the propensity to develop systemic T_H2 sensitisation in response to naturally occurring fluctuations in the environment.

Importantly, our model analysis suggests preventive effects of emollients against the progression of AD through a dynamic interplay between barrier integrity and immune reactions for diverse patient cohorts with different genetic risk factors and not only for those with weak barrier integrity. This prediction is concordant with the results of clinical trials that demonstrated the effective prevention of the development of AD in newborns both with and without filaggrin mutations [203, 204] and recently observed preventive effects of emollients in AD mouse models with weak immune responses caused by Jak1 hyperactivation, in which the incidence of AD symptoms was dramatically reduced by regular application of petrolatum on their skin [231].

3.4 Discussion

This article proposes the first mathematical model of AD pathogenesis that reproduces gradual progression from a mostly asymptomatic mild phenotype at its early stage to a severe treatment-resistant form. Our model is a mechanistic representation of the main feedback control structures that regulate the dynamics of AD flares through the relative strength of barrier function (permeability) and immune responses, corresponding to

positive and negative regulation (Fig. 3.1).

We computationally demonstrated that the strengths of the two well-known risk factors, dysregulated immune responses and high skin barrier permeability, determine the dynamic phenotypes of AD flare by the R-switch and that patients with either of the genetic risk factors may appear asymptomatic initially (Fig. 3.2). Long-lasting or frequent AD flares trigger the activation of the G-switch, which underlies the onset of systemic T_H2 sensitisation (Fig. 3.3), a hallmark event for the progression from mild to clinically severe AD (Fig. 3.4). Our model simulations suggested that the genetic risk factors predispose the carriers to develop a severe AD phenotype, even in response to naturally occurring fluctuations in environmental stressors (Fig. 3.5). These susceptible patient cohorts could benefit from preventive emollient treatments, which increase the threshold stress load that drives systemic T_H2 sensitisation (Fig. 3.6).

Our model analysis identified a double switch as a key regulatory motif that determines AD phenotypes of different severity (Fig. 3.4). The first switch (R-switch) is responsible for the onset of reversible AD flare, and frequent or long-lasting AD flares can trigger the second switch (G-switch), leading to the irreversible progression to severe AD through systemic T_H2 sensitisation (Fig. 3.7). Description of the AD phenotypes by the status of the R- and G-switches in our model allows us to uncover and quantitatively investigate the dynamic mechanisms behind worsening or improvement of AD symptoms, which are often evaluated clinically by an AD score (SCORAD) associated with increased IgE and pro-inflammatory cytokine levels [5]. The synergistic effects of environmental and genetic risk factors of AD progression determine the dynamics of the R- and G-switches, which govern a dramatic worsening of AD symptoms through the onset of systemic T_H2 sensitisation (G-switch on) and could be a target for effective treatment to prevent the progression to a severe form of AD.

Our model simulations reproduced several sets of experimental and clinical results, providing plausible mechanistic, quantitative and coherent explanations for dynamic mechanisms behind the onset, progression, and prevention of AD. This experimentally validated, quantitative, systems-level mathematical framework can be used to uncover possible early biomarkers and to investigate new and better treatment options to reverse and control AD symptoms and prevent progression from mild to clinically severe forms of AD. For example, application of predictive control [232] to our model will allow us to computationally design optimal treatment regimens, with minimal treatment times and strengths for effective proactive treatment [120, 123], while reducing the risk of the

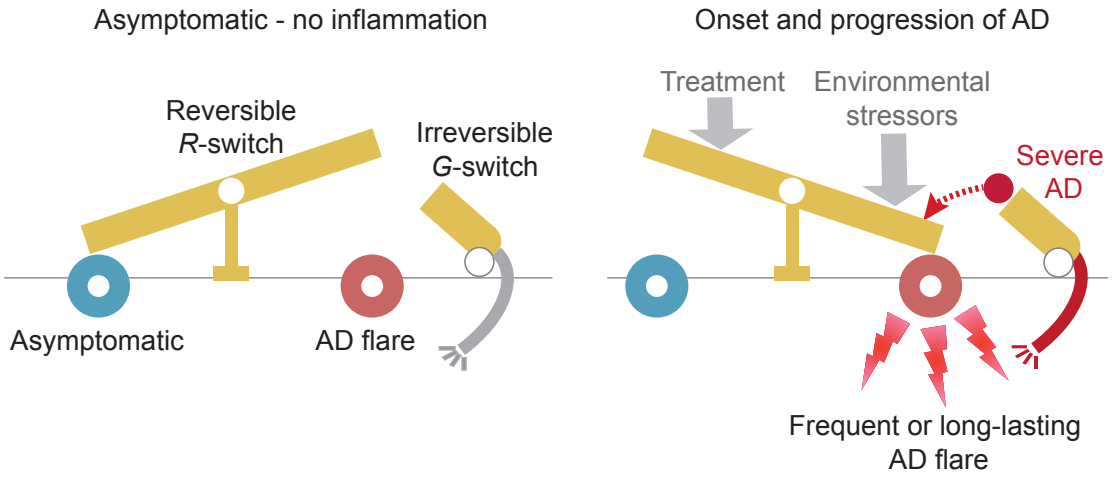


Figure 3.7: "Double-switch" mechanism for onset and progression of AD proposed in this article. Environmental stressors might cause onset of the first reversible switch leading to AD flares, which can be reversed by treatments. Frequent or long-lasting AD flares can trigger the second irreversible switch resulting in progression to severe AD.

side effects, such as skin atrophy and barrier damage [233, 234]. Our model could also be used to investigate early warning signals [235] to identify asymptomatic but high-risk patient cohorts by their characteristic dynamics in the barrier integrity, such as higher variability (Fig. 3.2, C) or a slower recovery (Fig. 3.2, E) and identify who might benefit from early treatments that prevent incipient disease development. Other promising future research includes application of machine learning methods [236] to a large set of clinical data with multiple variables to predict the likelihood of onset, progression, and prevention of AD. It would be also worth evaluating the stochastic effects of the genetic variants when such data becomes available.

Consolidating effective treatment strategies for AD will potentially reduce the social and economic burden of this disease by decreasing clinical symptoms and undesired side effects of the treatments that are associated with the advanced stage of AD. The proposed "double switch" motif provides a coherent explanation of underlying mechanisms behind dynamic onset, progression, and prevention of AD. The same motif can be found and reveal similar mechanisms underlying the onset, progression and prevention of other multi-stage and multi-factorial diseases, such as cancers, diabetes, and cardiovascular disease, which are caused by a complex interplay between genetic and environmental factors.

Chapter 4

Computational design of corticosteroid and emollient treatment

This chapter describes a computational framework to design patient-specific treatment strategies based on the model proposed in Chapter 3. We will identify the optimal frequency and dosing of corticosteroid treatment that enables long-term management of the symptoms of AD.

We incorporate the effects of cornerstone treatments for AD in the mathematical model presented in Chapter 3, by means of simple mathematical forms. Specifically, we introduce the effects of emollients, which improve skin barrier function [94, 104], and corticosteroids, which reduce inflammation [25]. The applied treatments mimic a proactive approach for the maintenance of symptoms, which is directed towards patients with frequent outbrakes of flares [117–119]. Our computational framework enables the design of dynamic treatment protocols by solving a sequence of optimal control problems and optimising an objective function using a Differential Evolution algorithm (Appendix C).

Dr Yoshito Hirata assisted in the development of the MATLAB code to identify the optimal scheduling and dosing of treatments. Dr Elisa Domínguez-Hüttinger helped to develop the mathematical description of the treatments and add the biological and clinical interpretation of the results. Our clinical and experimental collaborators, Professor Hywel C. Williams, Professor Michael J. Cork, and Dr Simon G. Danby, have

contributed in putting this computational work into a realistic clinical context.

The rest of the chapter represents a variation of contents of our paper *"Computational design of treatment strategies for proactive therapy on atopic dermatitis using optimal control theory"* [237] as it was published in the journal *Philosophical Transactions of the Royal Society A: Mathematical, Physical & Engineering Sciences*, under a Creative Commons licence in June 2017. The original article can be found under `http://rsta.royalsocietypublishing.org/content/375/2096/20160285.long`.

4.1 Introduction

Atopic dermatitis (AD) is a chronic inflammatory disease, characterised by recurrent skin inflammation and a defective permeable skin barrier, that is considered to be caused by complex interactions of genetic and environmental risk factors [24, 193]. AD affects up to 25% of children world-wide and has a high socioeconomic impact [85]. AD is associated with constant itching that may result in chronic sleep loss, and the resultant scratching can cause bleeding and skin infections. The current mainstay of AD treatment is to control the AD symptoms by topical application of corticosteroids or calcineurin inhibitors to reduce the inflammation, in addition to application of emollients to improve the barrier integrity [24, 191, 238]. However, only 24% of AD patients and carers believe that they adequately manage the symptoms by the current main treatments [23]. This is partly because clear guidance and consensus for effective treatment strategies in terms of frequency, duration and potency are yet to be fully established [2, 191, 193], while patients are often advised to minimise the use of the corticosteroids because of a fear of skin thinning [30].

As a result of the complex underlying mechanisms of AD pathogenesis, AD patients demonstrate a wide spectrum of clinical phenotypes thereby greatly benefitting from personalised treatment [239]. Recently, long-term management of AD focuses on prevention of flares by the so-called "proactive therapy" [120, 123]. Following initial induction of remission to "get control", proactive therapy aims to "keep control" by preventing AD flares (inflammation) and achieving skin barrier stabilisation. This is achieved by intermittent and scheduled use of low-dose topical corticosteroids or calcineurin inhibitors to the areas of the body that frequently have recurrent flares, even in the absence of the flares. Ideally, effective treatment schedules for proactive therapy can be tailored to each patient, based on the patient's information, such as genetic risk factors, how the

symptoms have evolved, and the responses to the treatments. This paper investigates the potential of a computational method to inform the design of such personalised effective treatment schedules for proactive therapy, in terms of frequency, duration and potency.

In Chapter 3 we proposed a mathematical model of AD pathogenesis, as an *in silico* and quantitative framework that coherently explains underlying mechanisms of common AD phenotypes [190]. The model is a system-level representation of the complex and dynamic interplays between immune responses, skin barrier function and environmental triggers that determine AD pathogenesis; specifically how AD flares start and how AD symptoms exacerbate. Our model simulations reproduced several sets of experimental and clinical results, providing plausible mechanistic and quantitative explanations for dynamic mechanisms behind onset, progression and prevention of AD.

In this chapter, we extend this experimentally validated mathematical model of AD pathogenesis and propose a new model which includes the effects of treatments on the pathogenesis of AD. We then use the mathematical model to computationally design the personalised optimal treatment schedules for proactive therapy by solving the optimal control problems recursively using a differential evolution (DE) algorithm [240, 241], which is an efficient global optimisation technique to solve our non-convex optimisation problem.

4.2 Mathematical model of treatment effects on AD pathogenesis

We consider a mathematical model of treatment effects on AD pathogenesis (Fig. 4.1(a)) obtained by incorporating the dynamic effects of treatments in the previous mathematical model of AD pathogenesis [190]. The proposed model is described by a set of three differential equations,

$$\dot{P}(t) = P_{\text{env}} \frac{\kappa_{\text{P}}}{1+\gamma_{\text{B}} B(t)} - \Big(\alpha_{\text{I}} \frac{R(t)}{1+\beta_1 C(t)} + \delta_{\text{P}}\Big) P(t), \tag{4.1a}$$

$$\dot{B}(t) = \frac{\kappa_{\text{B}}(1-B(t))}{\Big(1+\gamma_{\text{R}} \frac{R(t)}{1+\beta_2 C(t)}\Big)\Big(1+\gamma_{\text{G}} \frac{G(t)}{1+\beta_3 C(t)}\Big)} + E(t) - \delta_{\text{B}} K(t) B(t), \tag{4.1b}$$

$$\dot{D}(t) = \kappa_{\text{D}} \frac{R(t)}{1+\beta_4 C(t)} - \delta_{\text{D}} D(t), \tag{4.1c}$$

where $P(t)$ is the amount of infiltrated environmental stressors (milligrams per milliliter), such as pathogens, that trigger skin inflammation (an AD flare) through activation of innate immune receptors ($R(t)$), $B(t)$ denotes the degree of skin barrier integrity (relative to the maximum strength), and $D(t)$ denotes the level of inflammation markers (cells per milliliter), including pro-inflammatory cytokines (such as TSLP or IL33) and activated dendritic cells (DCs). We will consider moderate to severe AD patients as determined by the combination of parameters κ_P and α_I (Fig. 3.2, A *red*) which suffer from chronic AD and are susceptible from relapsing flares. As such the initial conditions of the state variables will vary depending on the choice of (κ_P, α_I).

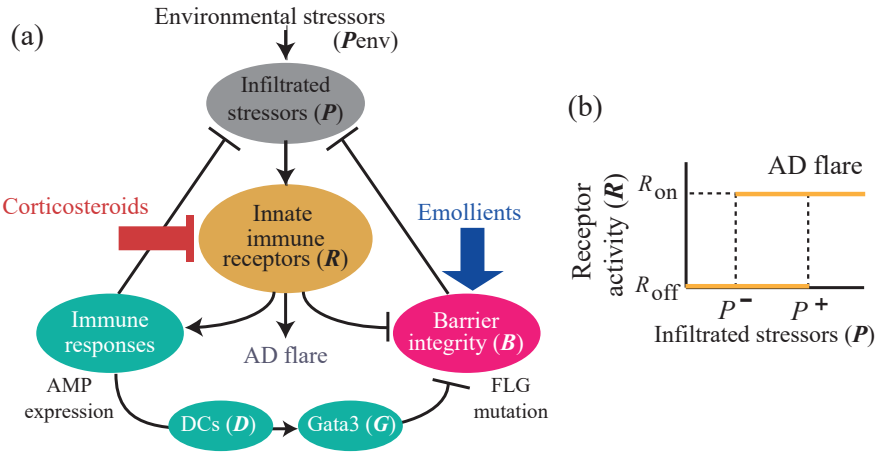


Figure 4.1: Mathematical model of treatment effects on AD pathogenesis. (a) A model schematic and (b) a perfect reversible switch for the AD flare triggered by infiltrated pathogens. The italics denote the model variables.

The triple of state variables, $(P(t), B(t), D(t))$, represents the patient's disease status described by the levels of infection, barrier defects and inflammation. The variables $E(t)$ and $C(t)$ respectively represent the potency of emollients and corticosteroids that are applied to achieve skin barrier stabilisation and to prevent infection and inflammation. The parameters, β_1, β_2, β_3 and β_4 represent the relative effects of corticosteroids on the relevant processes (Table 4.1). Other model parameters and their nominal parameter values are taken from [190] (Table 3.1) with the exception that we set $\delta_P = 1.6$ (1/day).

The proposed model describes the effects of the treatments on AD pathogenesis in a simple form, rather than explicitly incorporating the fine details of the complex molecular and cellular processes. The infiltrated stressors or pathogens, $P(t)$, increase by the

Table 4.1: Description of simulation parameters and their nominal values for Eq. 4.1.

Symbol	Name	Nominal value
β_1	Corticosteroid-mediated rate of reduction of AMP expression	0.005 (a.u[1])
β_2	Corticosteroid-mediated rate of reduction in barrier damage	10 (a.u)
β_3	Corticosteroid-mediated rate of reduction of T_H2 cytokine production	10 (a.u)
β_4	Corticosteroid-mediated rate of reduction of dendritic cell maturation	10 (a.u)
$\bar{E}$	Potency of constant emollients applied	0.04
$C_{\max}$	Maximum potency of corticosteroids during the remission phase	50
$C^i_{\max}$	Maximum potency of corticosteroids during the i-th maintenance cycle	50
$T_{\mathrm{r}}^{\max}$	Maximum duration of the induction phase	8 (weeks)
T_{m}	Duration of each maintenance cycle	1 (week)
k_1	Penalty weight for treatment duration	0.5 (d.u[2])
k_2	Penalty weight for total amount of treatment	1 (d.u)
k_3	Penalty weight for deviation of the final level of P from the target level	10 (d.u)
k_4	Penalty weight for deviation of the trajectories of P from the target level	10 (d.u)
$\hat{P}_{\mathrm{r}}$	Target level of P during induction phase	24 (mg/ml)
$\hat{P}_{\mathrm{m}}$	Target level of P during maintenance phase	26 (mg/ml)

penetration of environmental stressors, P_{env}, through the barrier, $B(t)$. P is eradicated by innate immune responses triggered by inflammation ($R(t)$) and is also naturally degraded. Topical application of corticosteroids ($C(t)$) provides an anti-inflammatory action [238], resulting in reduced antimicrobial protein (AMP) expression, and hence reduced pathogen eradication [242]. The production of $B(t)$ is described phenomenologically in its capacity to self-restore the nominal barrier integrity ($B = 1$) following its disruption, and is compromised by innate immune responses triggered by inflammation and by cytokines produced by differentiated T_H2 cells (where the differentiation is controlled by the master transcription regulator *Gata 3*, $G(t)$). Topical application of corticosteroids reduces both inflammation and release of cytokines [191, 243], resulting in improved skin barrier function [107]. Application of emollients enhances skin barrier

[2]Arbitraty units (a.u) related to the potency of corticosteroids or emollients.
[2]Dimensionless units (d.u) since the terms in the objective function are normalised.

integrity [191, 238], and hence reduces AD symptoms [244]. The degradation of the barrier occurs as a result of desquamation mediated by active kallikreins, $K(t)$. The level of inflammation markers, $D(t)$, increases while inflammation ($R(t)$) persists and degrades naturally.

The main aim of proactive therapy is to prevent AD flares that are assumed to occur as a result of activation of the innate immune receptors. We model the occurrence of an AD flare by a perfect reversible switch between the off- and on-states ($R = R_{\text{off}}$ and R_{on}) with P^+ and P^- denoting, respectively, the activation and inactivation threshold for the infiltrated stressors (pathogens) that are recognised by innate immune receptors (Fig. 4.1(b)) [190]. An AD flare occurs when the level of the stressors increases above P^+, and stops when it decreases below P^-. A similar switching behaviour is assumed for K [190].

Here, we consider moderate to severe AD patients, who could benefit from proactive therapy for flare prevention and skin barrier stabilisation. The severity of the AD symptoms is characterised in our model by two model parameters, κ_{P} and α_{I}, that correspond to the level of the genetic risk factors: mutations in the FLG gene (κ_{P}) and a dysregulated expression of innate immune system components (α_{I}) including regulators of antimicrobial peptide expression (eg. TLRs and NF-κB) [167, 190]. A lower α_{I} indicates dysfunctional immune responses and a diminished capacity to eradicate the infiltrating pathogens, and a higher κ_{P} results in a higher skin barrier permeability leading to increased infiltration of stressors that can cause the recurrence of AD flares. To simulate these moderate to severe AD patients, we pick the values of $(\alpha_{\text{I}}, \kappa_{\text{P}})$ from the parameter region for which a unique pathological steady state exists that corresponds to the high level of stressors leading to persistent AD flare and completely damaged skin barrier. We also assume $R_{\text{off}} = 1$ and $K_{\text{off}} = 1$ to model the effects of subclinical inflammation in non-lesional skin of severe AD patients [120], and $G(t) = 1$ corresponding to systemic T_H2 sensitisation due to the persistent AD flare [190].

4.3 Optimal control problem formulation

Using the proposed model, we computationally design optimal treatment strategies for proactive therapy with a combination of emollients and corticosteroids. The proactive therapy consists of two phases: an "induction of remission" phase where we aim to suppress the clinical inflammation, followed by a "maintenance of remission" phase

where we apply intermittent but scheduled treatment to prevent the recurrence of an AD flare [120, 123]. We refer the two phases as "induction phase" and "maintenance phase" hereafter. The induction phase aims to "get control", and the maintenance phase aims to "keep control" [120]. To comply with the current clinical recommendations [109, 191] we assume that emollients are applied constantly throughout both phases at a low level, $\bar{E}$, which is insufficient to achieve remission by itself for the moderate to severe AD patients [26]. We therefore design the optimal schedules for application of corticosteroids that can induce and maintain the remission. We consider the on-off treatment at discrete times, reflecting the daily application or non-application of corticosteroids with different potencies (Fig. 4.2(a)).

We formulate the problem as finding optimal treatment strategies that minimise the duration and potency of the treatments that effectively move the state variables from the initial pathological steady state $(P(0), B(0), D(0)) = (33.4, 0.012, 122)$ (nominal κ_P and α_I parameters) to a specified target state (Fig. 4.2(b)), while the dynamics of the state variables are determined by our model . The target state is defined by a target level of $P(t)$ that does not lead to recurrence of AD flare (Fig. 4.1(b)), as the proactive therapy aims to prevent AD flares. The objective function, J, is described by

$$J = k_1 J_1 + k_2 J_2 + k_3 J_3 + k_4 J_4, \tag{4.2}$$

where J_1 is the penalty for the treatment duration, corresponding to the patients' burden to apply the treatments, J_2 is the penalty for the total amount of the treatment applied (duration $\times$ potency), representing the financial cost as well as the risk of the side effects due to the excessive use of corticosteroids, J_3 is the penalty for the final state to be deviated from the target state, and J_4 is the penalty for the trajectory to be deviated from the target state. The functions J_1, J_2, J_3 and J_4 are defined for the induction and maintenance phases as shown below. We assume $k_3 = k_4$ (the coefficients for the penalty on the deviation from the target state) for simplicity.

Induction of remission phase

In the induction phase, we assume that corticosteroids are constantly applied during the calculated optimal duration, T_{r}. The optimal problem to be solved is formulated so as to find a pair of values $(T_{\mathrm{r}}, \bar{C})$, where T_{r} is the duration of the induction phase and $\bar{C}$ is the potency of corticosteroid to be constantly applied during this phase, that minimise

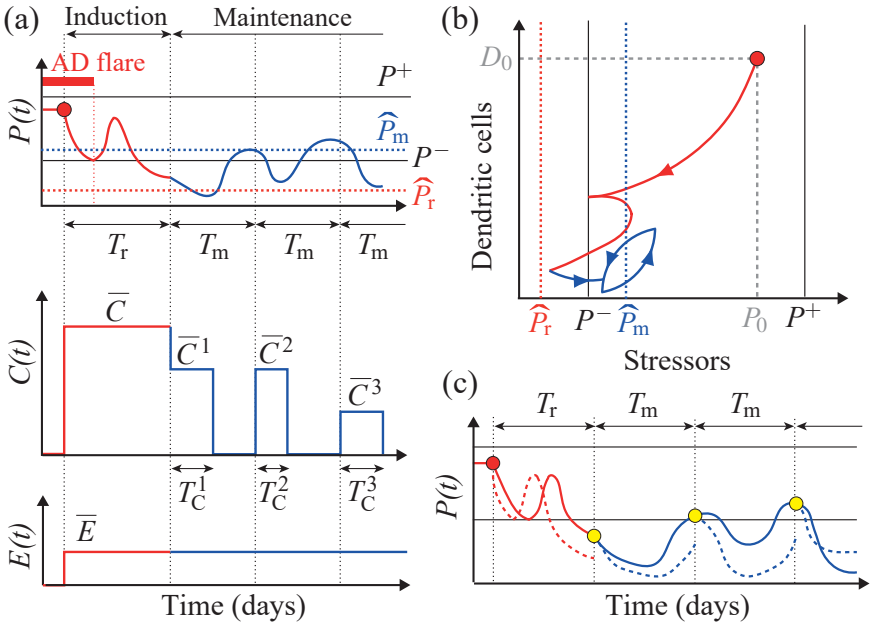


Figure 4.2: Optimal control problem formulation to design treatment strategies for proactive therapy for AD. The whole period consists of the induction phase (red) and maintenance phase (blue). (a) Example dynamics of the pathogen state variable ($P(t)$) with on-off treatment of corticosteroids ($C(t)$) of different potencies at discrete times, in addition to constant application of emollients ($E(t)$) of a fixed potency $\bar{E}$. (b) Example of the projected state trajectory of a patient's states, (P, D), when the optimal treatment strategy is applied. The states move from the initial state ((P_0, D_0), red circle) towards the target level, $\hat{P}_\mathrm{r}$, of the induction phase (red vertical line), and then to the target level, $\hat{P}_m$ (blue vertical line), of the maintenance phase. The state B is omitted in the figure. (c) The recursive optimal control problem to be solved. The optimal treatment strategy for each cycle (either for the duration of T_r or T_m) is determined by predicting the optimal evolution of the state variables (dashed lines) based on the measurement of the states at the beginning of the period (yellow circles). The actual evolution of the state (solid lines) can be different from the prediction, for example if the calculated optimal treatment strategy is not applied or due to model mismatch.

the objective function under the constraints $0 \leq T_\mathrm{r} \leq T_\mathrm{r}^{\max}$ and $0 \leq \bar{C} \leq C_{\max}$. We set the target level, $\hat{P}_\mathrm{r}$, to be smaller than P^- where the AD flare ceases. The objective function for the induction phase consists of $J_1 = (\frac{T_\mathrm{r}}{T_\mathrm{r}^{\max}})^2$, $J_2 = \frac{T_\mathrm{r}}{T_\mathrm{r}^{\max}}(\frac{\bar{C}}{C_{\max}})^2$, $J_3 = \Phi_\mathrm{r}(P(T_\mathrm{r})) + \left(1 - \frac{P(T_\mathrm{r})}{\hat{P}_\mathrm{r}}\right)^2$, and $J_4 = \frac{\int_0^{T_\mathrm{r}} (P(\tau) - \hat{P}_\mathrm{r})^2 d\tau}{\int_0^{T_\mathrm{r}} P(\tau)^2 d\tau}$. $\Phi_\mathrm{r}(P(T_\mathrm{r}))$ is a non-convex function to penalise failure to achieve remission and takes the values of $100 + 0.1(P(T_\mathrm{r}) - P^-)$ if $P(T_\mathrm{r}) > P^-$ and 0 otherwise.

Maintenance of remission phase

Once remission is induced, the proactive therapy proceeds to the maintenance phase, where corticosteroids are applied intermittently to prevent the recurrence of AD flares. We design the optimal treatment schedule for a week, based on the measurement of the state variables at the beginning of the week, and repeat the weekly cycle (Fig. 4.2(c)). This scenario corresponds to weekly hospital visits of the patients, where clinicians evaluate the disease state and plan the treatment strategy until the next visit. From an optimal control point of view this form a closed loop strategy.

For the i-th cycle of the maintenance phase, we calculate the optimal treatment strategy $(T_{\mathrm{C}}^i, \bar{C}^i)$ that minimises the objective function, under the constraints on the duration of corticosteroid application, $0 \leq T_{\mathrm{C}}^i \leq T_{\mathrm{m}} = 7$ days and its potency $0 \leq \bar{C}^i \leq C_{\max}^i$. For the whole duration of the maintenance phase, we set the target level, $\hat{P}_{\mathrm{m}}$, that is smaller than P^+ to avoid the recurrence of AD flare (Fig. 4.1(b)). In the next section, we investigate the effects of the choice of $\hat{P}_{\mathrm{m}}$ on the calculated optimal treatment strategies. The objective function for the i-th maintenance cycle consists of $J_1 = (\frac{T_{\mathrm{C}}^i}{T_{\mathrm{m}}})^2$, $J_2 = (\frac{\bar{C}^i}{C_{\max}^i})^2 \frac{T_{\mathrm{C}}^i}{T_{\mathrm{m}}}$, $J_3 = \Phi_{\mathrm{m}}(P(T_{\mathrm{r}} + iT_{\mathrm{m}})) + (1 - \frac{P(T_{\mathrm{r}}+iT_{\mathrm{m}})}{\hat{P}_{\mathrm{m}}})^2$, and $J_4 = \frac{\int_{T_{\mathrm{r}}+(i-1)T_{\mathrm{m}}}^{T_{\mathrm{r}}+iT_{\mathrm{m}}} (P(\tau)-\hat{P}_{\mathrm{m}})^2 d\tau}{\int_{T_{\mathrm{r}}+(i-1)T_{\mathrm{m}}}^{T_{\mathrm{r}}+iT_{\mathrm{m}}} P^2(\tau) d\tau}$.

4.4 Methods

All simulations were conducted using MATLAB version R2016a (The MathWorks, Inc., Natick, MA, USA). We used *ode45* for the numerical integration of the system, and the *events location* functionality of MATLAB to identify the switching boundaries of the hybrid system. We identified the optimal treatment strategy for the induction phase by applying a DE with 1000 generations. Starting from 30 randomly chosen initial vectors, $(\bar{C}, T_{\mathrm{r}})$, with $0 \leq \bar{C} \leq \bar{C}^{\max}$ and $0 \leq T_{\mathrm{r}} \leq T_{\mathrm{r}}^{\max}$, we found the optimal solution by evolving a population of 30 vectors at each generation, using the mutation strategy DE/rand-to-best/1 [245] with a differential weight of 0.6, and recombination with the crossover rate of 0.5. The same procedures were repeated for each maintenance cycle. The global sensitivity analysis was conducted by simultaneously varying the values of the model parameters or the weights for the objective functions from their nominal values by $\pm 50\%$ for 529 and 400 simulations, respectively.

4.5 Computational identification of optimal treatment schedules for moderate to severe AD patients

We used differential evolution (DE) to solve the optimal control problem formulated above, for different scenarios, to test the applicability of our approach. Details on the operation of DE can be found in Appendix C.

The nominal values used for the simulations for moderate to severe AD patient cohorts, such as the target levels and the constraints on the potency and duration of treatments, are summarised in Table 4.1. We first confirmed that the optimal treatment strategy calculated using the nominal parameter values suggests a length of the induction phase, T_{r}, that is clinically relevant (less than or equal to four weeks [117]). Indeed, the optimal induction period was calculated to be $T_{\mathrm{r}} = 19$ days,while the AD flare stopped within the first 3 days (Fig. 4.3(a)). We also confirmed by conducting global sensitivity analysis that this calculated optimal strategy is robust to changes of the model parameters and the choice of weighting coefficients for the objective function (Figs. B.2 and B.3).

Effects of the choice of the maintenance target level

We first investigated the effects of the choice of the target level during the maintenance phase, $\hat{P}_{\mathrm{m}}$, on the calculated optimal treatment strategies (Fig. 4.3).

In the nominal case with the nominal parameter values we set the maintenance target level to $\hat{P}_{\mathrm{m}} = 26$ mg/ml, which is lower than the deactivation threshold ($P^{-} = 26.6$ mg/ml) but higher than the induction target level ($\hat{P}_{\mathrm{r}} = 24$ mg/ml). The calculated optimal maintenance treatment (Fig. 4.3(a)) demonstrates that 3 days weekly intermittent application of corticosteroids could achieve the maintenance without recurrence of AD flare for the whole duration of the maintenance phase investigated (8 weeks).

When the maintenance target is chosen to be closer to the activation threshold ($P^{+} = 40$ mg/ml), for example $\hat{P}_{\mathrm{m}} = 30$ mg/ml, the calculated optimal treatment strategy suggests a 1 day per week application of corticosteroids to maintain the remission (Fig. 4.3(b)). This higher target level is much easier to be maintained with a smaller amount of corticosteroids. However, the resulting state corresponds to a lower barrier integrity with a higher level of infiltrated stressors compared with the nominal scenario (Fig. 4.3(a)), due to the smaller amount of corticosteroid applied. This worsening of the

state may make the patients more vulnerable to an increased level of environmental stressors due to random or natural fluctuations that can retrigger an AD flare.

On the contrary, when the maintenance target is chosen to be much lower than P^-, for example $\hat{P}_\mathrm{m} = 20$ mg/ml, the optimal treatment strategy requires an increased amount of corticosteroids, with application of more potent corticosteroids for 6 days per week (Fig. 4.3(c)). While the calculated optimal treatment strategy can successfully prevent recurrence of inflammation, this strategy is not desired due to the high amount of corticosteroids applied in total (2.7-fold increase from the nominal case).

These results suggest the importance of the choice of the maintenance target level, $\hat{P}_\mathrm{m}$, as a design criterion for optimal treatment strategies. We decided to use $\hat{P}_\mathrm{m} = 26$ mg/ml for further simulations, as it ensures the successful maintenance of remission without the need of excessive treatment amount during the maintenance phase and it may correspond to the clinically suggested so-called weekend therapy.

We also investigated the effects of the choice of the induction target, $\hat{P}_\mathrm{r}$ (figure not shown). Decrease of $\hat{P}_\mathrm{r}$ from our nominal value of $\hat{P}_\mathrm{r} = 24$ mg/ml resulted in an optimal strategy that requires an increased amount of corticosteroid (in both the potency and application time) during the induction phase, but did not affect the strategy during the maintenance phase.

Stratification of patient cohorts

To demonstrate that our approach is applicable to different patient cohorts, we computationally obtained the optimal treatment strategies for different values of two model parameters, $(\kappa_\mathrm{P}, \alpha_\mathrm{I})$. These parameters represent the two main genetic risk factors of AD, which include mutations in the FLG gene (κ_P) and dysregulated expression of innate immune system components (α_I), and depending on their values can be used to specify patient cohorts. The objective functions and targets level were the same as the nominal case.

Specifically, we investigated three patient cohorts: the nominal patient cohorts with $(\kappa_\mathrm{P}, \alpha_\mathrm{I}) = (0.85, 0.05)$ (Fig. 4.3(a)),those with even more dysfunctional immune responses described by $(\kappa_\mathrm{P}, \alpha_\mathrm{I}) = (0.85, 0.04)$ (Fig. 4.4(a)) and $(\kappa_\mathrm{P}, \alpha_\mathrm{I}) = (0.85, 0.03)$ (Fig. 4.4(b)), and those with even more compromised barrier integrity described by

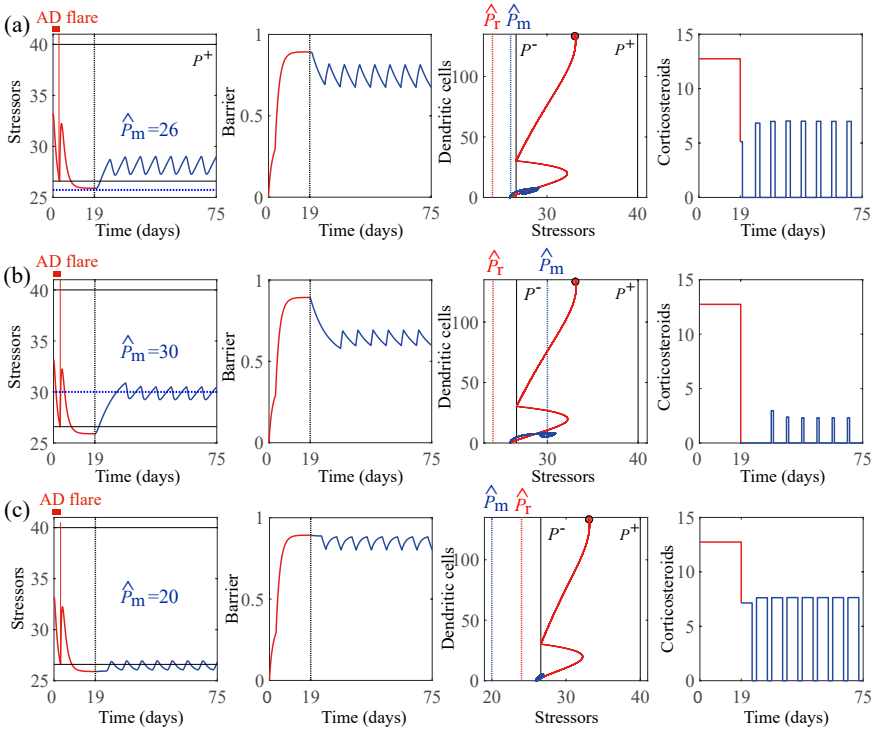


Figure 4.3: Effects of the choice of the maintenance target level (blue dotted lines) on the optimal treatment strategies calculated and the resulting dynamics of the system. The maintenance target level is set to (a) $\hat{P}_{\mathrm{m}} = 26$ mg/ml (the nominal value), (b) $\hat{P}_{\mathrm{m}} = 30$ mg/ml, and (c) $\hat{P}_{\mathrm{m}} = 20$ mg/ml, while the induction target level (red vertical lines) is set to be the same ($\hat{P}_{\mathrm{r}} = 24$ mg/ml) for all the scenarios. The dynamics during the induction phase and maintenance phase are shown in red and blue, respectively. Remission is achieved when the level of the stressors is decreased below P^-, and the AD flare reoccurs when it increases above P^+. The induction phase continues even after AD flare ceases, and tries to brings the state towards the target level.

$(\kappa_{\mathrm{P}}, \alpha_{\mathrm{I}}) = (0.9, 0.05)$ (Fig. 4.4(c)) and $(\kappa_{\mathrm{P}}, \alpha_{\mathrm{I}}) = (0.95, 0.05)$ (Fig. 4.4(d)). All the parameters, except for κ_{P} and α_{I}, were set to be the nominal values (Tables 4.1).

For the case with $(\kappa_{\mathrm{P}}, \alpha_{\mathrm{I}}) = (0.85, 0.04)$ (Fig. 4.4(a)), the calculated optimal treatment strategy was successful in achieving remission and preventing AD flares for 8 consecutive weeks, through a 20 day induction treatment followed by a 3 day weekly maintenance treatment. However, a higher total amount of corticosteroids is required with a higher potency (48% increase for the induction phase and 3.3% increase for the maintenance phase), compared to the nominal case (Fig. 4.3(a)), to combat the higher initial stressor load. When the risk factor of dysfunctional immune responses becomes even stronger, as for the case with $(\kappa_{\mathrm{P}}, \alpha_{\mathrm{I}}) = (0.85, 0.03)$ (Fig. 4.4(b)), the calculated

optimal treatment schedule failed to achieve the remission, leading to sustained or unresolved AD symptoms with a low barrier integrity. Indeed, the "maintenance" therapy we computationally calculated after 14 days of the"failed" induction of remission suggests a continuous use of corticosteroids, meaning that these virtual patients will require constant, rather than intermittent, application of corticosteroids (Fig. 4.4(b)).

For the cohorts with an increased barrier permeability ($\kappa_{\mathrm{P}} = 0.9$), an increased amount of corticosteroid (by 54.7%) is required during the maintenance phase (Fig. 4.4(c)), compared to the nominal cohort with the same $\alpha_{\mathrm{I}} = 0.05$. Further increase in the barrier permeability ($\kappa_{\mathrm{P}} = 0.95$) led to failure in inducing the remission and the optimal strategy suggests to continue the constant application of corticosteroids (Fig. 4.4(d)). Synergistic effects of the two risk factors, by increasing κ_{P} and decreasing α_{I} simultaneously ($(\kappa_{\mathrm{P}}, \alpha_{\mathrm{I}}) = (0.9, 0.04)$, figure not shown) resulted in an optimal strategy with a 5.8-fold increase in the total amount of corticosteroid (2.35-fold in the induction phase and 11.3-fold in the maintenance phase), compared to the nominal cohort. However, the optimal strategy still could not achieve the remission.

These results suggest that our approach is applicable to different virtual patient cohorts, and that it could help stratify the virtual patients into those who would benefit from the calculated optimal treatment strategies, and those who would require additional or stronger treatments, such as systemic treatment, to achieve remission. Our results also demonstrate how the treatment efforts scale with the level of the two common AD risk factors. It will be interesting to compare the computational predictions with the patients' data that relate the severity of patients' symptoms to the required treatments and the actual treatments prescribed. Evaluation of how the treatment efforts scale with the initial disease severity before the start of treatment in the clinic is an interesting future research topic.

Effects of poor adherence to suggested optimal treatment schedule

So far we have assumed that the patients follow the calculated optimal treatment schedule. However, AD patients do not necessarily always follow treatment guidelines. This problem of poor adherence to treatment could have negative effects on long-term treatment of AD [246,247]. Using our proposed approach, we investigated the effects of poor adherence to the calculated optimal treatment schedule, particularly how the future optimal treatment schedule and the evolution of the disease state are affected.

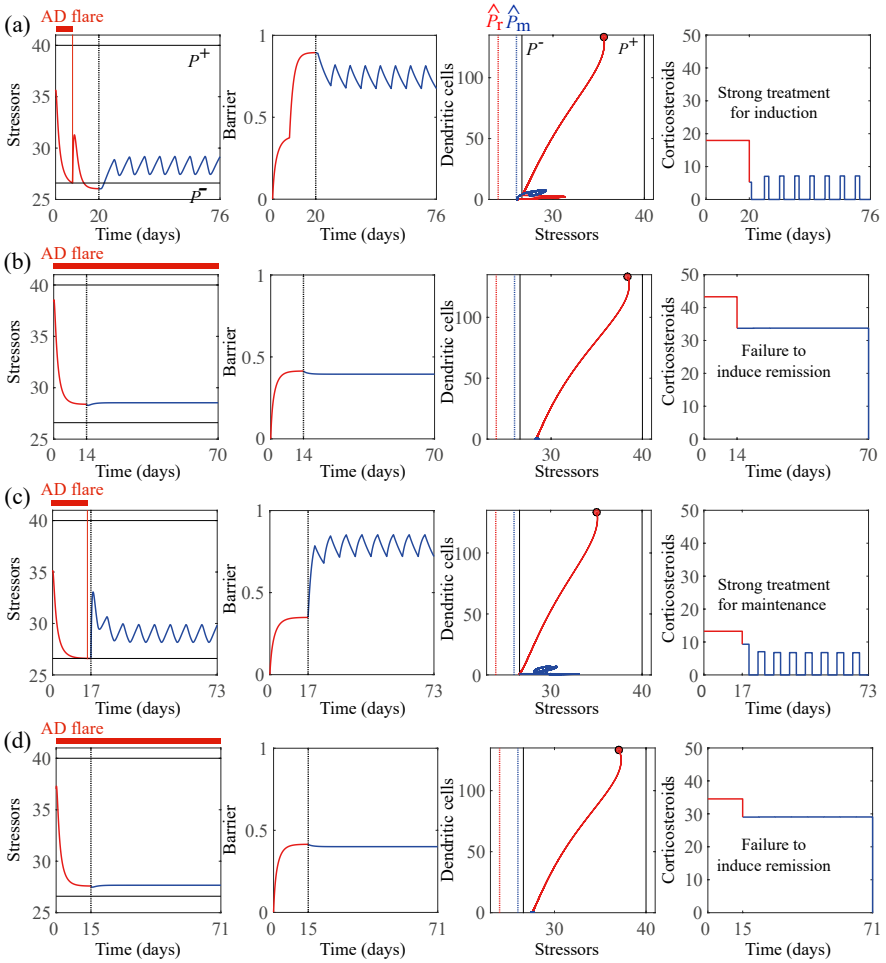


Figure 4.4: Calculated optimal treatment strategies for different patient cohorts with dysfunctional immune responses, (a) $(\kappa_{\mathrm{P}}, \alpha_{\mathrm{I}}) = (0.85, 0.04)$ and (b) $(\kappa_{\mathrm{P}}, \alpha_{\mathrm{I}}) = (0.85, 0.03)$, and compromised barrier integrity, (c) $(\kappa_{\mathrm{P}}, \alpha_{\mathrm{I}}) = (0.9, 0.05)$ and (d) $(\kappa_{\mathrm{P}}, \alpha_{\mathrm{I}}) = (0.95, 0.05)$. The dynamics during the induction phase starting from the initial state (red circles) is shown in red, and that for the maintenance phase is in blue.

Consider the case where the virtual patients do not complete the calculated optimal induction phase and stop using corticosteroids after 5 days when the AD flare disappears. This scenario can occur for example due to corticosteroid phobia. If they continue their daily emollient treatment (Fig. 4.5(a)), the optimal strategy in the subsequent weeks suggests the use of an increased amount of corticosteroid, with a 1.4-fold more potent corticosteroid for a longer period (by 1 day) during the first maintenance cycle, compared to the nominal case. The effect of non-adherence is not predicted to be dramatic, possibly because the AD flare ceased already within the first 5 days of corticosteroid use.

However, if the virtual patients also stop the daily emollient treatment (Fig. 4.5(b)), we observe the recurrence of an AD flare with a severe worsening of the symptoms (a sharp decrease in B and a dramatic increase in P and D). As a result, the calculated optimal strategy in the subsequent cycle suggests the use of a more potent corticosteroid (by 1.4-fold) than that applied during the induction phase, for 5 days. This higher potency corticosteroid is a side-effect of the constraint on the maintenance cycle duration (7 days): the treatment has less time to deal with the AD flare, compared to the induction duration constraint (8 weeks), and therefore overcompensates by increasing the potency to achieve the desired state. If instead, for this case of failed remission due to non-adherence, we change the constraints on the maintenance cycle duration from 7 days to 20 days (i.e essentially prolonging the induction phase), the calculated optimal strategy suggests the application of a 10% more potent corticosteroid, compared to that used in the induction phase, for an extra duration of 10 days (figure not show). These computational predictions suggest the benefits of continual use of emollients in reducing AD symptoms, as shown in [191].

Another scenario to consider is the non-adherence during the maintenance phase, following the successful completion of the induction phase. When the virtual patients stop their daily application of emollients for the first three maintenance cycles (Fig. 4.5(c)), it results in an immediate worsening of the symptoms (a decrease in B). The calculated optimal strategy suggests application of more potent corticosteroids (by 1.4-fold) than the nominal case for 3 days per week in the subsequent 3 weeks to maintain the remission. If in, conjunction to stopping emollient treatment, patients stop applying corticosteroids during these 3 weeks (Fig. 4.5(d)), a severe worsening of the symptoms (a sharp decrease in B and a dramatic increase in P and D) is observed. The calculated optimal strategy then suggests application of an increased amount of corticosteroid (1.5-fold more potent for 2 more days) compared to the nominal case to maintain the remission in the subsequent weeks. If they miss the treatments for 4 weeks (Fig. 4.5(e)), the AD flare reoccurs, and the optimal strategy suggests the use of a much more potent corticosteroid (by 1.35-fold) than that used during the induction phase, for the duration of 5 days.

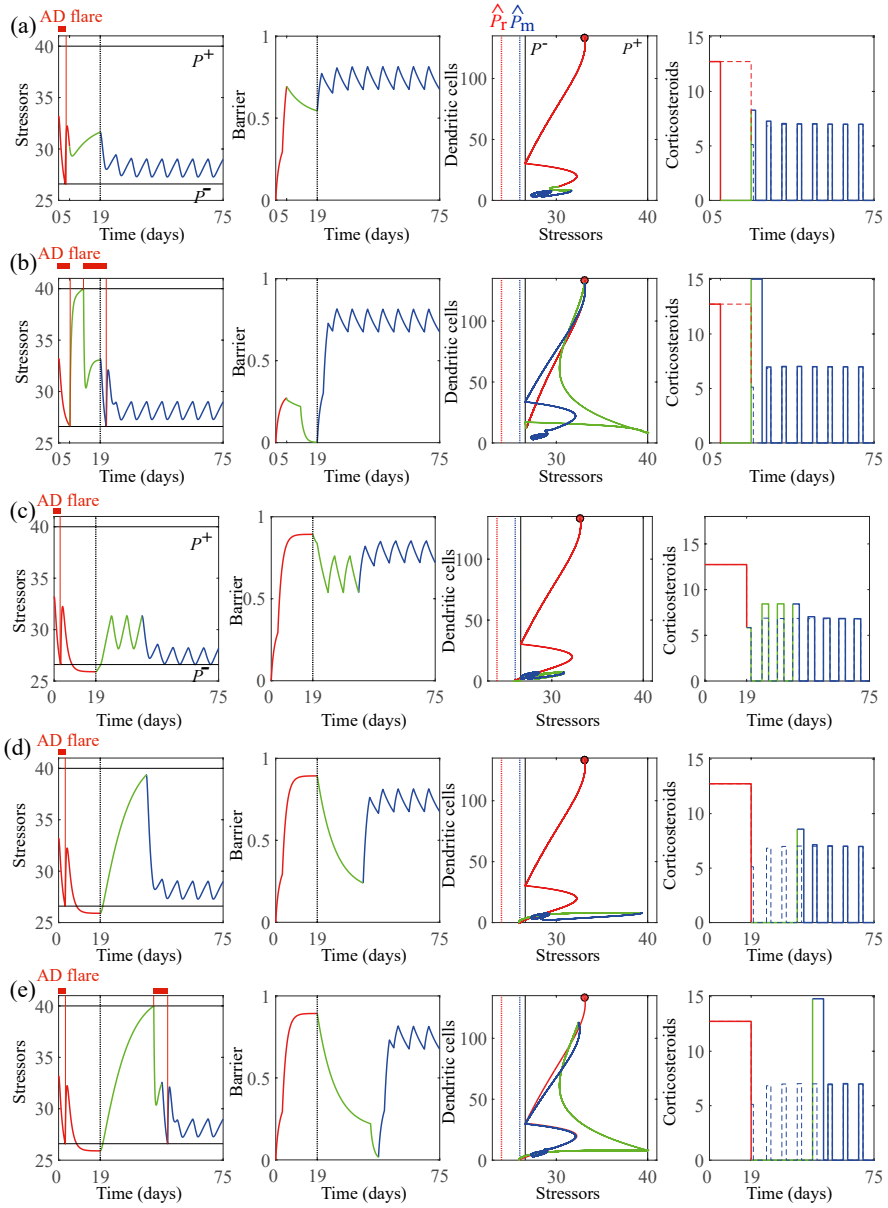


Figure 4.5: Effects of poor adherence to the calculated optimal treatment strategies during the induction phase. Non-adherence to the suggested corticosteroid treatment after 5 days in the induction phase, with continual use of emollients (a) and without use of emollients (b). Non-adherence to the suggested corticosteroid treatment during the maintenance phase, without emollient application for the first three cycles (c), and without both corticosteroid and emollient application for the first three cycles (d) and four cycles (e). Green lines represent the period during the non-adherence, and the dotted lines on the right column demonstrates the optimal strategy calculated for the nominal case where patients adhere to the suggested optimal strategy.

4.6 Discussion

In this chapter, we proposed a computational method to inform the design of patient-specific optimal treatment strategies for moderate to severe AD patients who require constant treatment for stabilisation of their AD symptoms. Our proposed framework solves optimal control problems recursively to design treatment schedules for the proactive therapy that aims to prevent AD flares and to achieve skin barrier stabilisation. The proactive therapy consists of intermittent and scheduled use of low-dose corticosteroids, in addition to a constant application of emollients, once initial induction of remission has been achieved. The objective functions to be minimised correspond to the penalties on the duration and the potency of the treatments applied, as well as the deviation from the target states we specify.

One of the main difficulties in formulating an optimal control problem is to identify appropriate objective functions. Here we systematically explored different possible target levels for the clinically relevant variables to be controlled (P), and found the most adequate maintenance target level (Fig. 4.3), which we used to derive robust treatment strategies even with poor adherence (Fig. 4.5), for our nominal patient cohorts and for patient cohorts with severer genetic risk factors (Fig. 4.4). These results suggest the importance of choosing appropriate target states to successfully maintain remission, and that our proposed mathematical framework can be used to investigate the effects of poor adherence to the optimal treatment strategies systematically. We could also identify those virtual patient cohorts that would require stronger treatments, with even higher doses or additional pharmacological substances such as antibiotics, phototherapy or systemic immunosuppressant treatment to achieve adequate disease control (Fig. 4.4). We evaluated the sensitivity of our results to the changes in the values of the weighting coefficients for the optimal control problem (k_1, k_2, k_3 and k_4) and the model parameters, for both the induction and maintenance phases, and confirmed that the optimal strategy calculated for the nominal case is robust (Figs. B.2 and B.3).

Our systematic and computational approach could be effective in: (a) informing the design of personalised optimal treatment strategies, thus addressing the issue of the current lack of clear guidance and consensus of effective treatment strategies; and (b) minimising the potential side effects of long-term use of corticosteroids. Moderate to severe AD patients require repeated treatment to stabilise their pathological state that would naturally remain unresolved if treatment is not applied. In addition, moderate

to severe AD patients usually require a combination of treatments (such as corticosteroids and emollients) to be applied to achieve successful maintenance of remission in two phases (induction and maintenance phases). Accordingly, designing the optimal treatment strategies to stabilise the AD symptoms for these patients may benefit from an advanced optimisation technique such as the one proposed in this paper.

In this chapter, we computationally obtained the optimal treatment strategy by recursively solving the optimal control problems. The proposed computational framework could be easily extended to the application of model predictive control (MPC), which uses the measured states of the system to predict and optimise the control input that minimises the objective function over a future time horizon [248]. MPC has been already successfully applied to design treatment profiles for diabetes [249, 250], prostate cancer [251] and leukemia [163, 252]. Application of MPC, i.e. inclusion of the receding horizon will allow us to obtain smoother graded therapy, as it will enable us to find the optimal treatment schedule that does not necessarily achieve the target level within each maintenance cycle, but does so gradually over a longer time period.

Our simulation results show that poor adherence to the suggested optimal treatment schedule inevitably leads to higher treatment doses in subsequent cycles and could affect long-term management of AD symptoms. To prevent poor adherence these theoretical results could be presented to patients that choose not to use the prescribed treatment, due to steroid phobia, and as such serve as an educational tool for the proper application of treatments. Our results are also consistent with the current clinical recommendations, for example the weekend therapy where corticosteroids are applied for two consecutive days per week, in addition to the daily application of emollients. Our investigation on the effects of the AD flare, that occurs during maintenance therapy, demonstrated that resuming continuous use of a more potent corticosteroid can successfully achieve remission, but results in an increase in the total amount of corticosteroids applied. As an important next step, we need to compare the computationally obtained treatment strategies with treatment options that are currently used in the clinical setting.

We also need to develop robust ways to identify model parameters from each patient's clinical data, such as initial skin thickness and pattern of eczema, in order to effectively calculate optimal treatment strategies. If the temporal data of patients become available, the information on the discrepancy between the measured values and the model prediction will be used to identify the model parameters. The approach we proposed in this paper could be a first step towards designing personalised effective treatment

strategies for prevention and adequate control of AD symptoms. Exploring personalised optimal treatment strategies in the clinical setting would be challenging if we do not apply a systematic and computational approach, because of the combinatorial explosion of treatment types, durations, potencies, and each patient's genetic and pathological profile to the disease. As the model was developed based on the pathological mechanisms of the disease, the obtained treatment strategies and the proposed framework could be applicable to different patient cohorts and different scenarios. For example, it will help to identify a way to reduce the frequency of clinic visits by placing control back in the hands of parents and children, evaluate the effects of reduced visits, and whether we can still achieve the optimal treatment strategies by monthly or bi-monthly clinical visits.

These results demonstrate a first proof of concept for the computational design of optimal treatment strategies for patients suffering with AD, using a mathematical model that describes the treatment effects in a simple form. Such frameworks could prove invaluable for personalised medicine and long-term management of the disease. We will further investigate the appropriateness of the model description of the treatment effects, using dynamic data of AD patients after application of corticosteroids and emollients.

Chapter 5

Computational design of corticosteroid and coal tar treatment

5.1 Introduction

In this chapter the mathematical model introduced in Chapter 3 is modified to accommodate the topical application of coal tar, instead of emollients, and we apply our computational framework (Chapter 4), to design treatment strategies identifying the optimal frequency and dosing of corticosteroid treatment. Our goal is to exemplify the ease with which the model can be modified to fit different treatment representations, and by extension to show the aptability of the computational method to identify optimal treatments in different settings.

Topical application of coal tar is one of the oldest treatments for AD [253], however, up until recently the molecular mechanisms, resulting in skin barrier positive effects were not readily explored nor elucidated [22, 122]. Various studies support the effectiveness of coal therapy [253, 254], and it can also be used in tandem with other treatments, such as corticosteroids and phototherapy [255].

Treatment with coal tar is suggested to have antibacterial [256], antifungal [256], and anti-inflammatory effects [122, 257], as well as antipruritic effects [22], but not all of

these are well documented [94]. A recent study [22] explored the molecular mechanisms of coal tar treatment and showed that it enhanced epidermal differentiation, increased levels of filaggrin, and inhibited the IL-4/STAT6 pathway (a pathway associated with the pathogenesis of AD [21]).

Although studies have shown no risks associated with coal tar treatment [258, 259], it should be noted that some adverse effects are documented in the literature [260–263]. The greatest concern relates to carcinogenic effects [264], therefore, safety studies are required for application to young children [265].

In Section 5.2 we introduce the mathematical model, which includes the effects of coal tar treatment in a simple mathematical form. The rest of this chapter will focus on identifying patient-specific treatment protocols for the optimal application of corticosteroid treatment accompanied with coal tar treatment following the protocols described in Chapter 4.

5.2 Mathematical model of treatment effects: corticosteroids and coal tar application

We consider the mathematical model of AD pathogenesis, presented in Chapter 2, incorporating the dynamic effects of two topical treatments: topical application of corticosteroids and coal tar preparations. The proposed model is described by a set of three differential equations,

$$\dot{P}(t) = P_{\text{env}}\frac{\kappa_{\text{P}}}{1+\gamma_{\text{B}}B(t)} - \Big(\alpha_{\text{I}}\frac{R(t)}{1+\beta_1 C(t)} + \delta_{\text{P}}\Big)P(t), \tag{5.1a}$$

$$\dot{B}(t) = \frac{(1+CT(t))\kappa_{\text{B}}(1-B(t))}{\Big(1+\gamma_{\text{R}}\frac{R(t)}{1+\beta_2 C(t)}\Big)\Big(1+\gamma_{\text{G}}\frac{G(t)}{1+\beta_3 C(t)}\Big)} - \delta_{\text{B}}K(t)B(t), \tag{5.1b}$$

$$\dot{D}(t) = \kappa_{\text{D}}\frac{R(t)}{1+\beta_4 C(t)} - \delta_{\text{D}}D(t). \tag{5.1c}$$

The variables of this model have been previously described in Section 4.2. The variables $CT(t)$ and $C(t)$ represent the potency of coal tar and corticosteroids, respectively, that are applied to achieve skin barrier stabilisation and to prevent infection and inflammation. These are the control variables that will have a direct effect on the state variables describing the dynamics of the system.

Topical application of coal tar ($CT(t)$) improves skin barrier function by increasing the expression levels of epidermal barrier component proteins (such as FLG, hornerin, and involucrin), as well as accelerating the process of epidermal morphogenesis [22]. We mathematically represent the accelerated recovery by changing the effective barrier production rate from κ_{B} to $(1+CT(t))\kappa_{\mathrm{B}}$. Topical corticosteroid treatment is applied in accordance with proactive therapy recommendations to prevent AD flares, by inhibiting the effects of innate immune responses. The parameters related to the treatments and the computational optimisation are the same as in Table 4.1, except for the nominal potency for coal tar application (calculated in Section 5.5.1). Other model parameters and their nominal values are shown in Table 3.1 with the exception that we use $\delta_P = 1.6$ as in Chapter 4. We consider, as in Chapter 4, moderate to severe AD patients as determined by the combination of parameters κ_P and α_I (Fig. 3.2, A *red*) which suffer from chronic AD and are susceptible from relapsing flares. As such the initial conditions of the state variables will vary depending on the choice of (κ_P, α_I).

5.3 Optimal control problem formulation

With the proposed model, we computationally identify the optimal duration and potency of corticosteroid treatment, given constant application of coal tar treatment. As in Chapter 4, we will use a protocol mimicking a proactive therapy, consisting of two phases: the "induction phase" and the "maintenance phase". Coal tar treatment is applied constantly at a level $\bar{CT}$ that is insufficient to induce remission by itself. Remission is achieved by the deactivation of innate immune responses, which is mediated by the R-switch.

We formulate the problem as finding treatment strategies that minimise the duration and potency of the treatments that steer the state variables from the initial pathological steady-state to a specified target state, while the dynamics of the state variables are determined by our model Eq. (5.1a) - (5.1c). The objective function, J, is a sum of four terms, as in Eq. (4.2), while the individual terms have the same interpretation as described in Section 4.3. In the next sections we describe the optimal control problems to be solved.

Induction phase

In the induction phase, we assume that corticosteroids are constantly applied during the calculated optimal duration, T_{r}. We identify the optimal pair of values $(T_{\mathrm{r}}, \bar{C})$, where T_{r} is the duration of the induction phase and $\bar{C}$ is the potency of corticosteroid, that minimise the objective function under the constraints $0 \leq T_{\mathrm{r}} \leq T_{\mathrm{r}}^{\max}$ and $0 \leq \bar{C} \leq C_{\max}$. We set the target level, $\hat{P}_{\mathrm{r}}$, to be smaller than P^{-} where the AD flare ceases. By collecting the state variables in the vector $\boldsymbol{x}(t) = (P(t), B(t), D(t))$ the Optimal Control Problem (OCP) can then be stated as,

$$\begin{aligned}
&(\bar{C}^{*}, T_{\mathrm{r}}^{*}) = \underset{(\bar{C}, T_{\mathrm{r}})}{\operatorname{argmin}}\, J(\bar{C}, T_{\mathrm{r}}, \boldsymbol{x}(t), \hat{P}_{\mathrm{r}}) \\
&\text{such that } \dot{\boldsymbol{x}} = f(t, \boldsymbol{x}(t)),\ \boldsymbol{x}(0) = \hat{\boldsymbol{x}}_{\text{measured}}, \\
&C(t) = \bar{C},\ 0 \leq \bar{C} \leq C_{\max},\ CT(t) = \bar{C}T,\ t \in [0, T_{\mathrm{r}}] \\
&0 \leq T_{\mathrm{r}} \leq T_{\mathrm{r}}^{\max},\ T_{\mathrm{r}} \in \mathbb{N},
\end{aligned} \tag{5.2}$$

where the vector $\hat{\boldsymbol{x}}_{measured}$ represents the measured state variables. The objective function for the induction phase consists of the following terms,

$$\begin{aligned}
J_1(T_{\mathrm{r}}) &= \Big(\frac{T_{\mathrm{r}}}{T_{\mathrm{r}}^{\max}}\Big)^2, \\
J_2(T_{\mathrm{r}}, \bar{C}) &= \frac{T_{\mathrm{r}}}{T_{\mathrm{r}}^{\max}}\Big(\frac{\bar{C}}{C_{\max}}\Big)^2, \\
J_3(\hat{P}_{\mathrm{r}}) &= \alpha\Phi_{\mathrm{r}}(P(T_{\mathrm{r}})) + \Big(1 - \frac{P(T_{\mathrm{r}})}{\hat{P}_{\mathrm{r}}}\Big)^2, \\
J_4(P(t), \hat{P}_{\mathrm{r}}) &= \frac{\int_0^{T_{\mathrm{r}}} (P(\tau) - \hat{P}_{\mathrm{r}})^2 d\tau}{\int_0^{T_{\mathrm{r}}} P(\tau)^2 d\tau}.
\end{aligned} \tag{5.3}$$

The term $\Phi_{\mathrm{r}}(P(T_{\mathrm{r}}))$ is a non-convex function that penalises the failure to achieve remission defined as,

$$\Phi_{\mathrm{r}}(P(T_{\mathrm{r}}), P^{-}) = \begin{cases} 1000 - (P^{-} - P(T_{\mathrm{r}})), & \text{if } P(T_{\mathrm{r}}) > P^{-},\ R(t) = R_{\text{on}} \\ 0, & \text{otherwise.} \end{cases}$$

We add a second condition for the convex function in Eq. (5.3) to have a non-zero value when $R(t) = R_{\text{on}}$. This guarantees that the optimal solution is one in which the innate immune responses are switched off independent of the choice of induction target. Without loss of generality we normalise the objective function and consider the scalar

value $\alpha = {k_3}^{-1}$.

Maintenance phase

In the maintenance phase, corticosteroids are applied intermittently to prevent the recurrence of AD flares. We design the weekly optimal treatment schedule, based on the measurement of the state variables at the beginning of the week, and then repeat the weekly optimisation cycle. For the i-th cycle of the maintenance phase, we calculate the optimal treatment strategy $(T_{\mathrm{C}}^i, \bar{C}^i)$ that minimises the objective function, under the constraints on the duration of corticosteroid application, $0 \leq T_{\mathrm{C}}^i \leq T_{\mathrm{m}} = 7$ days and its potency $0 \leq \bar{C}^i \leq C_{\max}^i$. For the whole duration of the maintenance phase, we set the target level, $\hat{P}_{\mathrm{m}}$, that is smaller than P^+ to avoid the recurrence of an AD flare. By collecting the state variables in the vector $\boldsymbol{x}(t) = (P(t), B(t), D(t))$ the Optimal Control Problem (OCP) can then be stated as,

$$
\begin{aligned}
&(\bar{C}^{\mathrm{i}*}, T_{\mathrm{C}}^{\mathrm{i}*}) = \underset{(\bar{C}^{\mathrm{i}}, T_{\mathrm{C}}^{\mathrm{i}})}{\operatorname{argmin}} J(\bar{C}^{\mathrm{i}}, T_{\mathrm{C}}^{\mathrm{i}}, \boldsymbol{x}(t), \hat{P}_{\mathrm{m}}) \\
&\text{such that } \dot{\boldsymbol{x}} = f(t, \boldsymbol{x}(t)),\ \boldsymbol{x}(T_{\mathrm{r}} + (i-1)T_{\mathrm{m}}) = \hat{\boldsymbol{x}}_{\text{measured}}, \\
&0 \leq \bar{C}^{\mathrm{i}} \leq C_{\max},\ t \in [T_{\mathrm{r}} + (i-1)T_{\mathrm{m}}, T_{\mathrm{r}} + (i-1)T_{\mathrm{m}} + T_{\mathrm{C}}^{\mathrm{i}}], \\
&CT(t) = \bar{C}T,\ t \in [T_{\mathrm{r}} + (i-1)T_{\mathrm{m}}, T_{\mathrm{r}} + iT_{\mathrm{m}}], \\
&0 \leq T_{\mathrm{C}}^{\mathrm{i}} \leq T_{\mathrm{m}},\ T_{\mathrm{C}}^{\mathrm{i}} \in \mathbb{N},
\end{aligned}
\tag{5.4}
$$

where $i = 1, 2, \ldots, N$ is the index for the i^{th} maintenance cycle. The objective function for the i-th maintenance cycle consists of the terms,

$$
\begin{aligned}
&J_1(T_{\mathrm{C}}^{\mathrm{i}}) = \Big(\frac{T_{\mathrm{C}}^i}{T_{\mathrm{m}}}\Big)^2, \\
&J_2(T_{\mathrm{C}}^{\mathrm{i}}, \bar{C}^{\mathrm{i}}) = \frac{T_{\mathrm{C}}^i}{T_{\mathrm{m}}}\Big(\frac{\bar{C}^i}{C_{\max}^i}\Big)^2, \\
&J_3(\hat{P}_{\mathrm{m}}) = \beta\Phi_{\mathrm{m}}(P(T_{\mathrm{r}} + iT_{\mathrm{m}})) + \Big(1 - \frac{P(T_{\mathrm{r}} + iT_{\mathrm{m}})}{\hat{P}_{\mathrm{m}}}\Big)^2, \\
&J_4(P(t), \hat{P}_{\mathrm{m}}) = \frac{\int_{T_{\mathrm{r}}+(i-1)T_{\mathrm{m}}}^{T_{\mathrm{r}}+iT_{\mathrm{m}}} (P(\tau) - \hat{P}_{\mathrm{m}})^2 d\tau}{\int_{T_{\mathrm{r}}+(i-1)T_{\mathrm{m}}}^{T_{\mathrm{r}}+iT_{\mathrm{m}}} P^2(\tau) d\tau}.
\end{aligned}
\tag{5.5}
$$

The non-convex function, $\Phi_{\mathrm{m}}(P(T_{\mathrm{r}}+iT_{\mathrm{m}}))$, represents the penalty on the re-occurrence of an AD flare during the maintenance phase and is defined as,

$$\Phi_{\mathrm{m}}(P(T_{\mathrm{r}}+iT_{\mathrm{m}})) = \begin{cases} 1000 + (P(T_{\mathrm{r}}+iT_{\mathrm{m}}) - P^{-}), & \text{if } P(T_{\mathrm{r}}+iT_{\mathrm{m}}) > P^{-},\ R(t) = R_{\mathrm{on}} \\ 0, & \text{otherwise.} \end{cases}$$

Without loss of generality we normalise the objective function and consider the scalar value $\beta = {k_3}^{-1}$.

5.4 Methods

All simulations were conducted using MATLAB version R2016a (The MathWorks, Inc., Natick, MA, USA). We used *ode45* for the numerical integration of the system, and the *events location* functionality of MATLAB to identify the switching boundaries of the hybrid system. We identified the optimal treatment strategy for the induction phase by applying a DE with 100 generations. Starting from 40 randomly chosen initial vectors, $(\bar{C}, T_{\mathrm{r}})$, with $0 \leq \bar{C} \leq \bar{C}^{\max}$ and $0 \leq T_{\mathrm{r}} \leq T_{\mathrm{r}}^{\max}$, we found the optimal solution by evolving a population of 40 vectors at each generation, using the mutation strategy DE/rand-to-best/1 [245] with a differential weight of 0.6, and binomial recombination with the crossover rate of 0.5. The same procedures were repeated for each maintenance cycle.

5.5 Results

The OCP's posed in Eq. (5.2) and (5.4) are solved using a DE algorithm. In the following sections, we develop optimal corticosteroid treatment protocols for patients with moderate to severe AD. We investigate the choice of pathogen target level in Section 5.5.2, in both induction ($\hat{P}_{\mathrm{r}}$) and maintenance phases ($\hat{P}_{\mathrm{m}}$). Subsequently we design patient-specific treatments with respect to known risk factors of AD (Section 5.5.3). Lastly, when treatment protocols are not adhered to by patients, innate immune responses can be reactivated inducing an AD flare. In Section 5.5.4 we explore the effects of non-adherence to the calculated treatment schedules.

5.5.1 Identification of constant potency of coal tar treatment

To stop innate immune responses, and hence induce remission, the level of pathogen ($P(t)$) in our model needs to be driven below the de-activation threshold P^-. Patients suffering from moderate to severe AD forms require antiinflammatory treatment to stabilise AD flares, since treatment with coal tar or emollient preparations are not sufficient. To emulate this in our model, we consider a constant coal tar treatment potency ($\bar{CT}$) that does not induce remission.

To identify a constant level of coal treatment that is insufficient to stop innate immune responses, we perform steady-state analysis for the pathogen level, as a function of constant corticosteroid and coal tar treatment. The analytical equations describing the steady-state value of pathogen for $R(t) = R_{\text{off}}$ and $R(t) = R_{\text{on}}$ are shown in Eq. (5.6) and (5.7), respectively, and the results are plotted in Fig. 5.1.

$$P_{\text{off}} = \frac{\alpha_2\beta_2 + \delta_B K_{off}\beta_2}{2\alpha_2 + \delta_B K_{off}} \tag{5.6}$$

where $\beta_2 = \dfrac{P_{env}\kappa_P}{(\frac{\alpha_I R_{off}}{1+\beta_1\bar{C}} + \delta_P)\gamma_B}$ and $\alpha_2 = \dfrac{\kappa_B(1+\bar{CT})}{(1+\frac{\gamma_R R_{off}}{1+\beta_2\bar{C}})(1+\frac{\gamma_G}{1+\beta_3\bar{C}})}$,

$$P_{\text{on}} = \frac{-(2\alpha_1 - \delta_B m_{on}\beta_1 - \delta_B\beta_{on}) + \sqrt{(2\alpha_1 - \delta_B m_{on}\beta_1 - \delta_B\beta_{on})^2 - 4\delta_B m_{on}\beta_1(\delta_B\beta_{on} - \alpha_1)}}{2\delta_B m_{on}}, \tag{5.7}$$

where $\beta_1 = \dfrac{P_{env}\kappa_P}{(\frac{\alpha_I R_{on}}{1+\beta_1\bar{C}} + \delta_P)\gamma_B}$ and $\alpha_1 = \dfrac{\kappa_B(1+\bar{CT})}{(1+\frac{\gamma_R R_{on}}{1+\beta_2\bar{C}})(1+\frac{\gamma_G}{1+\beta_3\bar{C}})}$.

With de-activated immune responses ($R(t) = R_{\text{off}}$), the steady-state level of pathogen is higher than the activation threshold P^+ when $\bar{C} = \bar{CT} = 0$ (Fig. 5.1a) as a consequence of reduced pathogen eradication. Note that when $\bar{C} = \bar{CT} = 0$, innate immune responses will eventually be activated since $P_{\text{off}} > P^+$. Furthermore, we observe that as the treatments are applied the steady-state value of the pathogen decreases, while with $\bar{C} = 0$ the potency of coal tar treatment, in the range $\bar{CT} \in [0, 0.1]$, cannot prevent the re-activation of immune responses, since $P_{\text{off}} > P^-$. This necessitates the use of corticosteroids during the maintenance phase for patients characterise by the nominal parameters.

When the R-switch is activated, implying the incidence of an AD flare, pathogen steady-

state levels (P_{on}) drop below P^+, even for $\bar{C} = 0$ (Fig. 5.1b). However, as a consequence of the hysteretic behaviour of the R-switch, induction of remission requires that pathogen level is driven below P^-. This again implies that for the nominal parameters singular treatment with coal tar cannot induce remission.

With the aforementioned analysis we propose using a constant coal tar potency of $\bar{CT} = 0.1$ throughout this chapter, to emulate a realistic treatment behaviour in patients with moderate to severe AD.

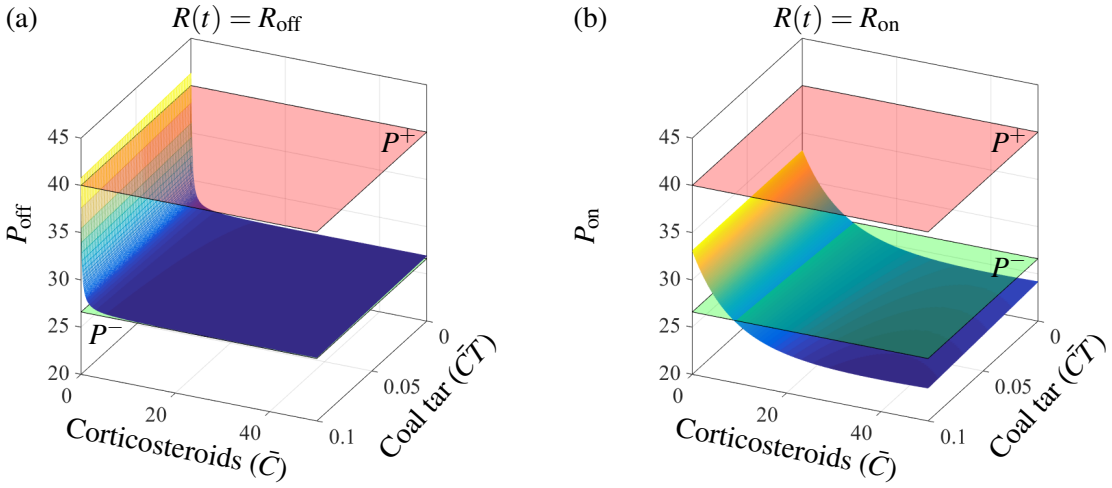


Figure 5.1: Steady-state value of pathogen with respect to constant application of corticosteroids ($\bar{C}$) and coal tar ($\bar{CT}$) with (a) de-activated ($R(t) = R_{\text{off}}$), and (b) activated ($R(t) = R_{\text{on}}$) innate immune responses. The results are plotted for $\bar{C} \in [0, 50]$ and $\bar{CT} \in [0, 0.1]$. The green and red planes indicate the de-activation (P^-) and activation (P^+) thresholds, respectively. The nominal set of parameters were used, $(\kappa_P, \alpha_I) = (0.85, 0.05)$, while the rest of the parameters are shown in Table 4.1.

5.5.2 Treatment design based on target level

By varying the pathogen target level in the optimisation we can directly affect the treatment protocols, as this level represents one measure of the disease state of the patient. Achieving a lower pathogen level requires higher potency corticosteroid treatment, which also leads to elevated barrier function. The concentration of dendritic cells increases or decreases exponentially only in the presence or absence of innate immune responses, respectively, and we therefore neglect plotting the corresponding time evolution.

In this section we investigate the outcome of the optimised corticosteroid treatment

schedule with respect to the chosen pathogen target level. We vary both the induction target level, $\hat{P}_{\mathrm{r}}$, and the maintenance target level, $\hat{P}_{\mathrm{m}}$.

Effects of the choice of induction target level

We first investigate the effects of the induction target level on the calculated optimal treatment strategies (Fig. 5.2). We sequentially increase the induction target level and observe the resulting duration and potency of corticosteroid used to induce remission.

In Fig. 5.2a we choose an induction target of $\hat{P}_{\mathrm{r}} = 22$ mg/ml, which is well below the de-activation threshold, P^{-}. The AD flare ceases after 3.3 days of treatment, indicating alleviation of AD symptoms. Upon de-activation of innate immune responsers the pathogen eradication diminishes resulting in a sudden spike of pathogen. In the induction phase, treatment with corticosteroids continues even when symptoms improve as dictated by the proactive approach. The optimal induction duration is $T_{\mathrm{r}} = 20$ days with a total applied amount of corticosteroid $T_{\mathrm{r}} \times \bar{C} = 305.3$ days×a.u[1].

For higher induction level targets of $\hat{P}_{\mathrm{r}} = 24$ mg/ml (Fig. 5.2b) and $\hat{P}_{\mathrm{r}} = 26$ mg/ml (Fig. 5.2c) the calculated induction durations are 18 and 16 days, with total amounts of corticosteroids given by 259.2 and 202.8 days×a.u, respectively. Furthermore, due to the lower potency corticosteroid applied, the AD flare stops after 3.5 and 3.9 days for induction targets set to $\hat{P}_{\mathrm{r}} = 24$ mg/ml and $\hat{P}_{\mathrm{r}} = 26$ mg/ml, respectively. Comparing the results in Fig. 5.2 it is clear that to achieve a lower pathogen level a more potent corticosteroid and longer duration of the induction phase is required, leading to higher total amounts of treatment. Note that the exact induction target cannot be achieved owing to the fact that the chosen targets are not controllable by the given treatments. This can be deduced by the analysis in Section 5.5.1, which illustrates that when $R(t) = R_{\mathrm{off}}$, pathogen levels below P^{-} cannot be achieved by the current form of treatments. However, since the objective function is a weighted sum of terms including the duration and potency of treatment, state variable trajectories and end point, the trade-off for harder to achieve target levels results in higher potency and longer duration.

These results suggest the induction target level is an important design criterion for the calculation of optimal treatment strategies. Our computational approach may provide flexibility to clinicians to implement effective treatment strategies based on the induction target level. Clinicians can use this information to make informed decisions on

[1] a.u stands for arbitraty unit.

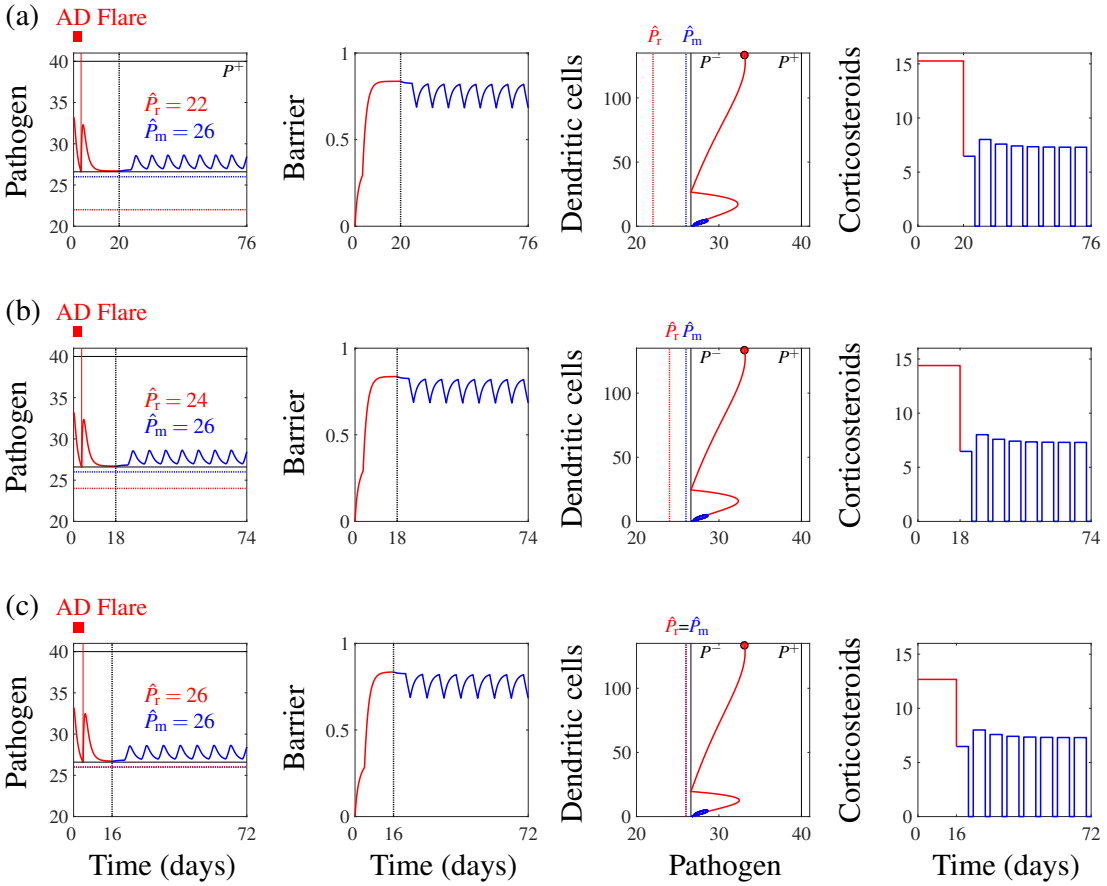


Figure 5.2: Optimally calculated treatment strategies for corticosteroids and the resulting dynamics of the model when induction target level (red dotted line) is set to (a) $\hat{P}_r = 22$ mg/ml, (b) $\hat{P}_r = 24$ mg/ml, and (c) $\hat{P}_r = 26$ mg/ml, while the maintenance target level (blue dotted line) is set to $\hat{P}_m = 26$ mg/ml. Induction phase and maintenance phase dynamics are depicted in red and blue, respectively. Vertical black dotted line indicates the end of the induction phase, while the solid black lines indicate the de-activation (P^-) and activation (P^+) thresholds. The red bar on the pathogen evolution subplot illustrates the duration of the AD flare.

the appropriate course of action and advice for the patient. Patients with severe AD symptoms may opt to use, or may be advised to use, higher potency corticosteroids for faster relief. Moreover, patients unwilling to use higher potency corticosteroids for longer durations can be given a choice for less severe treatment protocols that can still induce remission. Another interesting topic to investigate are patients that experience side-effects from treatment and how the induction target can be manipulated to induce remission without the associated side-effects.

The value of the objective function at each iteration is shown in Fig. 5.3, for the three

different induction target levels. The results indicate that convergence is achieved within the first 10 iterations.

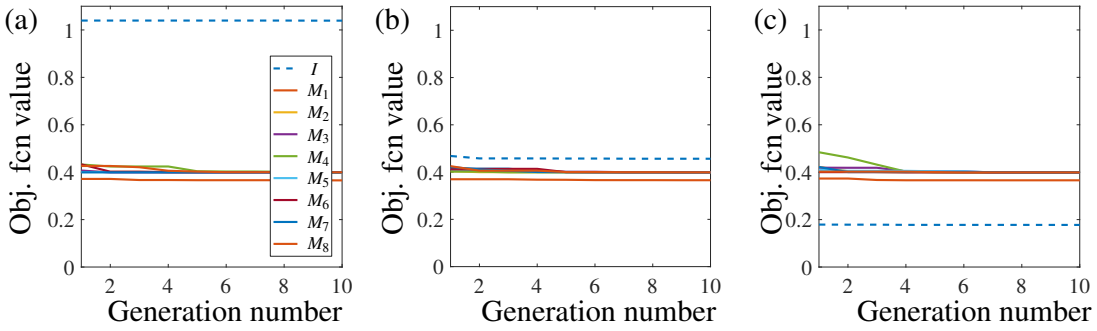


Figure 5.3: Convergence of the optimisation of the induction and maintenance phases, showing only the first 10 generations, with induction target levels set to (a) $\hat{P}_{\mathrm{r}} = 22$ mg/ml, (b) $\hat{P}_{\mathrm{r}} = 24$ mg/ml, and (c) $\hat{P}_{\mathrm{r}} = 26$ mg/ml. In the legend I stands for induction, while M_{i} stands for the i^{th} maintenance cycle.

Effects of the choice of maintenance target level

Here we study the effects of the maintenance target level on the optimally calculated treatment schedules and the resulting dynamics of the system. We first set the induction target level to a constant value ($\hat{P}_{\mathrm{r}} = 24$ mg/ml, Fig. 5.4 and $\hat{P}_{\mathrm{r}} = 22$ mg/ml, Fig. 5.5) and vary the maintenance target level.

In Fig. 5.4a the optimal treatment schedule is shown for a maintenance target level set to $\hat{P}_{\mathrm{m}} = 22$ mg/ml. The maintenance treatment strategy predicts $T_C^{\mathrm{i}} = 6$ days of corticosteroid application pair maintenance cycle, with an average potency of 9.4 a.u and total amount of $\sum_{\mathrm{i}=1}^{N} T_{\mathrm{C}}^{\mathrm{i}} \times \bar{C}^{\mathrm{i}}$ =448.9 days×a.u. This treatment protocol successfully prevents the recurrence of an AD flare for the 8 weeks investigated, while the dynamic behaviour of the model predicts low pathogen levels and high barrier integrity (on average 80.8%[2]). However, the resulting strategy proposes almost daily application of corticosteroids during the maintenance phase, which might not be well accepted by patients due to corticosteroid phobia [246], which stems from the documented unwanted side-effects [23, 233, 266].

When the maintenance target level is increased to $\hat{P}_{\mathrm{m}} = 30$ mg/ml, the calculated treatment protocol suggests periodic application of corticosteroids for 3 and 2 days, in-

[2]Mean barrier integrity is measured after the 4^{th} maintenance cycle to mitigate the transient behaviour during the initial cycles.

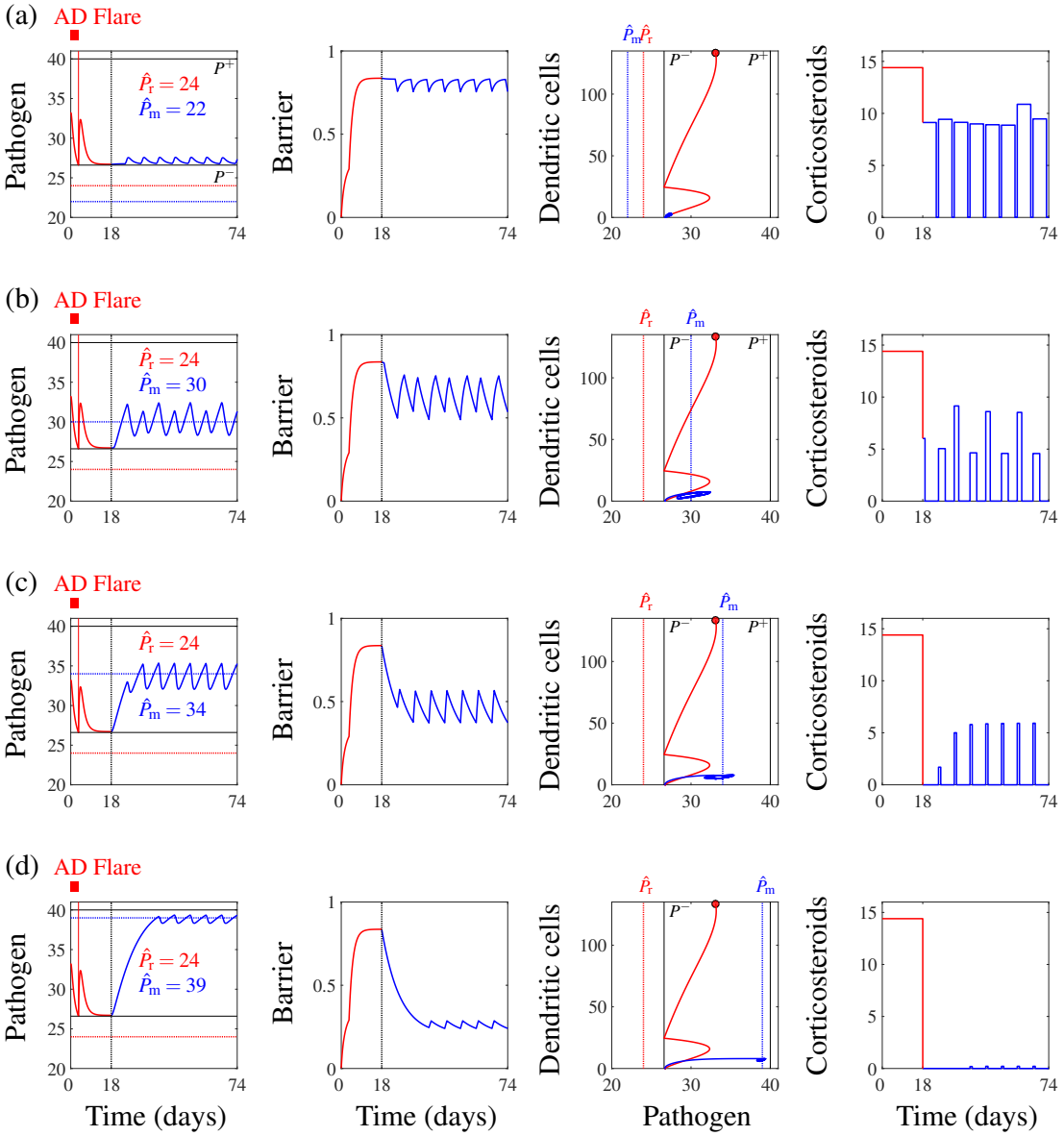


Figure 5.4: Optimally calculated treatment strategies for corticosteroids and the resulting dynamics of the model when the maintenance target level (blue dotted line) is set to (a) $\hat{P}_m = 22$ mg/ml, (b) $\hat{P}_m = 30$ mg/ml, (c) $\hat{P}_r = 34$ mg/ml, and (d) $\hat{P}_r = 39$ mg/ml, while the induction target level (red dotted line) is set to $\hat{P}_m = 24$. Induction phase and maintenance phase dynamics are depicted in red and blue, respectively. Vertical black dotted line indicates the end of the induction phase, while the solid black lines indicate the de-activation (P^-) and activation (P^+) thresholds. The red bar on the pathogen evolution subplot illustrates the duration of the AD flare.

terchangeably between successive maintenance cycles (Fig. 5.4b). Corticosteroid treatment duration during the first maintenance cycle is predicted to be 1 day. Increasing the maintenance target level relaxes the conditions on the control problem, which leads to a maintenance treatment strategy that uses 25.65% of the total corticosteroid amount used when the target was set to $\hat{P}_{\mathrm{m}} = 22$ (Fig. 5.4a). The higher target leads to a 10.5%[3] increase in the total pathogen load over the duration of the maintenance phase, compared with that shown in Fig. 5.4a, and decreased barrier function with an average of 63.1%.

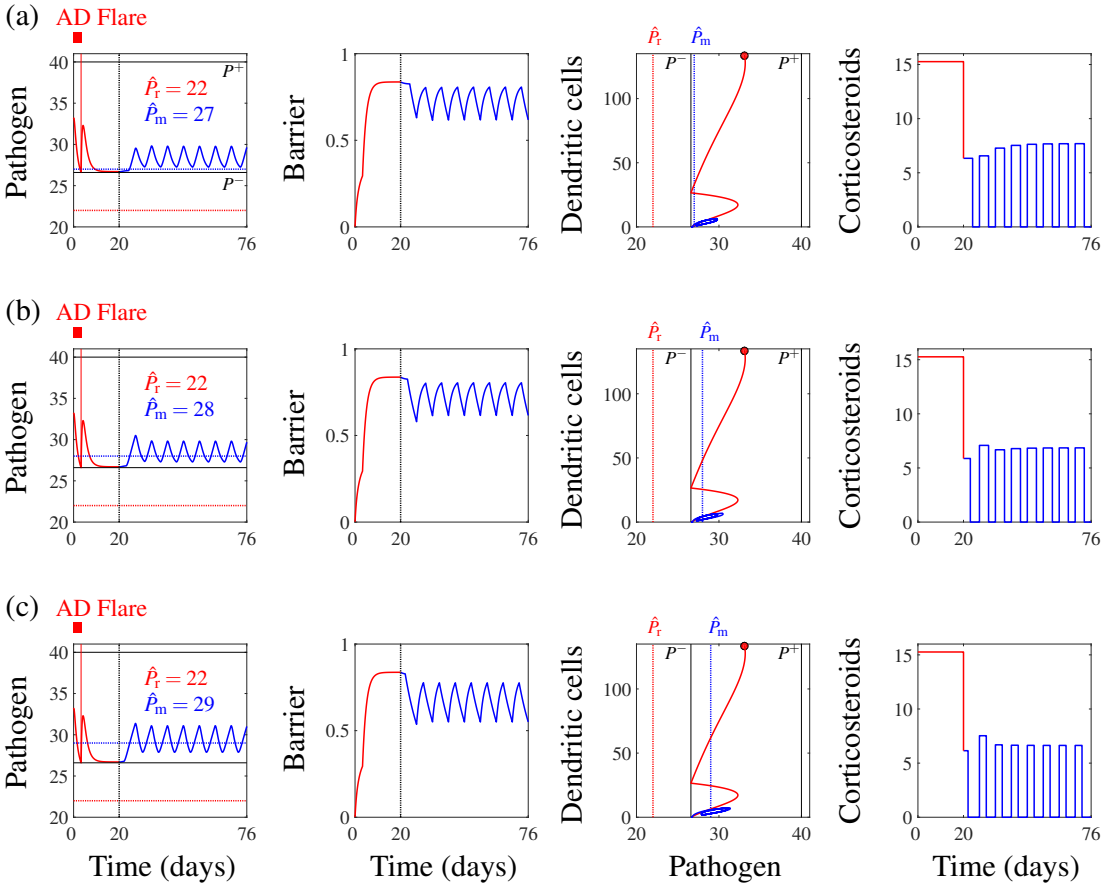


Figure 5.5: Optimally calculated treatment strategies for corticosteroids and the resulting dynamics of the model when the maintenance target level (blue dotted line) is set to (a) $\hat{P}_{\mathrm{m}} = 27$ mg/ml, (b) $\hat{P}_{\mathrm{m}} = 28$ mg/ml, and (c) $\hat{P}_{\mathrm{r}} = 29$ mg/ml, while the induction target level (red dotted line) is set to $\hat{P}_{\mathrm{m}} = 22$ mg/ml. Induction phase and maintenance phase dynamics are depicted in red and blue, respectively.

[3]Pathogen level is given by the integral $\int_{T_{\mathrm{r}}}^{T_{\mathrm{r}}+N\times T_{\mathrm{m}}} P(\tau)d\tau$, which represents the total amount of pathogen load during the maintenance phase.

Increasing the maintenance target to $\hat{P}_{\mathrm{m}} = 34$ mg/ml (Fig. 5.4c) and $\hat{P}_{\mathrm{m}} = 39$ mg/ml (Fig. 5.4d), further decreases the efforts of treatment, compared with those depicted in Fig. 5.4a, with predicted corticosteroid application of 1 day per cycle. Furthermore, as a consequence of the higher maintenance targets, the optimal maintenance protocols suggest omission of treatment during the first maintenance cycle (Fig. 5.4c) and the first three maintenance cycles (Fig. 5.4d). In addition, in Fig. 5.4c we observe that treatment potency scales until it reaches a steady-state behaviour after four maintenance cycles. Comparing the amount of corticosteroid treatment used with that depicted in Fig. 5.4a, we observe a 92% decrease when $\hat{P}_{\mathrm{m}} = 34$ mg/ml (Fig. 5.4c), and 99.8% decrease when $\hat{P}_{\mathrm{m}} = 39$ mg/ml (Fig. 5.4d). As a result of the lower treatment efforts, in Fig. 5.4c and 5.4d the state variables depicting barrier integrity is lower and total pathogen load is higher, compared with that depicted in Fig. 5.4a. Although, low treatment efforts can mitigate the negative side effects of corticosteroids, underutilization of treatment can cause re-activation of innate immune responses and AD flares due to the exposure of unexpected environmental perturbations.

All treatment protocols calculated with $\hat{P}_{\mathrm{m}} = \{22, 30, 34, 39\}$ mg/ml successfully achieve maintenance and prevent the recurrence of AD flares for the duration of 8 weeks (Fig. 5.4). However, each treatment schedule has its own shortcoming: high total amount of corticosteroid (Fig. 5.4a); irregular patterns of corticosteroid application (Fig. 5.4b), which can make adherence challenging; and low treatment efforts leading to suboptimal barrier function, increased pathogen loads, and increased susceptibility to environmental perturbations (Fig. 5.4c and Fig. 5.4d).

In Fig. 5.5a-c we computationally design treatment schedules for intermediate maintenance targets compared with those used in Fig. 5.4, while the induction target is set to $\hat{P}_{\mathrm{r}} = 22$ mg/ml. As illustrated in both Fig. 5.4 and Fig. 5.5, the induction target does not affect the long term maintenance phase treatment, except during the first few cycles. The total amount of corticosteroids used was 233.5 (Fig. 5.5a), 209.4 (Fig. 5.5b), and 154.6 days×a.u (Fig. 5.5c), which confirms the decreasing trend observed in Fig. 5.4. Setting the maintenance target to $\hat{P}_{\mathrm{m}} = 27$ mg/ml or $\hat{P}_{\mathrm{m}} = 28$ mg/ml results in a maintenance treatment strategy with corticosteroid application of 4 days per maintenance cycle (Fig. 5.5a and b), while when $\hat{P}_{\mathrm{m}} = 29$ mg/ml the resulting strategy predicts 3 days per maintenance cycle for successful maintenance of remission. Mean barrier integrity levels, and the associated standard deviations, are calculated at 72.9%±5.7% (Fig. 5.5a), 72.7%±5.7% (Fig. 5.5b), and 67.1%±6.8% (Fig. 5.5c). The mean barrier

integrity (Fig. 5.6a)[4] and standard deviation (Fig. 5.6b)[5] were statistically significant for the maintenance target level of $\hat{P}_{\mathrm{m}} = 29$ mg/ml.

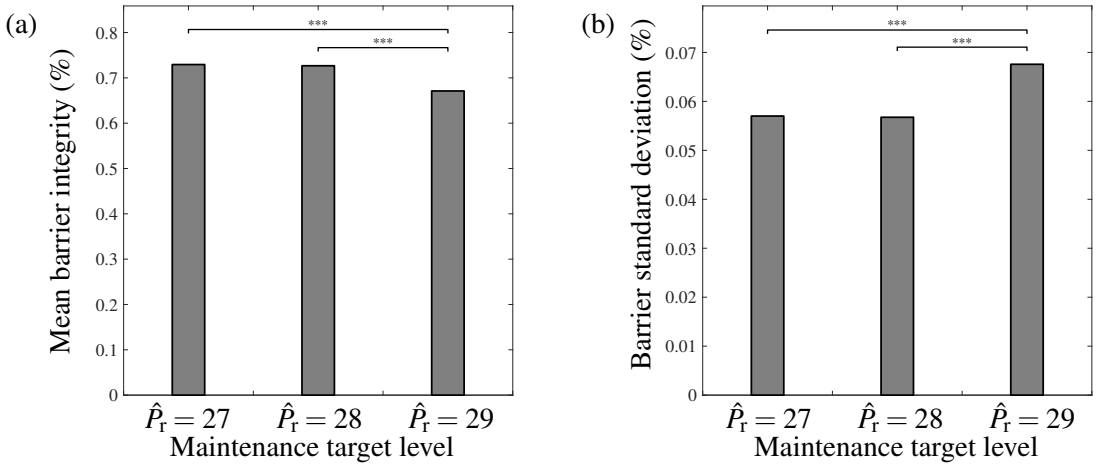


Figure 5.6: (a) Mean barrier integrity and (b) standard deviation for maintenance target level $\hat{P}_{\mathrm{m}} = 27$ mg/ml, $\hat{P}_{\mathrm{m}} = 28$ mg/ml, and $\hat{P}_{\mathrm{m}} = 29$ mg/ml, and induction target level $\hat{P}_{\mathrm{r}} = 22$ mg/ml. Significance level was set to 0.1%.

These results suggest that the maintenance target level is an important design criterion for efficient and effective optimal treatment strategies. Although, none of the simulations indicate failure of treatment, long-term maintenance protocols can be designed based on the trade-off between total treatment amount and the desired patients disease status. Our methodology does not include random fluctuations of environmental stressors, which can lead to ill-designed treatment protocols and eventual recurrence of AD flares. It would be interesting to subject the model to random fluctuations of environmental stressors and design treatments that are robust to these fluctuations. We summarise the results of the treatment amounts for the induction and maintenance phases presented in this section in Fig. 5.7.

In the subsequent analysis presented in Sections 5.5.3 and 5.5.4 we use an induction target of $\hat{P}_{\mathrm{r}} = 22$ mg/ml and a maintenance target of $\hat{P}_{\mathrm{m}} = 29$ mg/ml as the nominal targets since the treatment protocol emulates that of the proactive/weekend therapy [117].

[4]The two-sample t-test was used at a significance level of 0.1%.
[5]The two-sample F-test was used at a significance level of 0.1%.

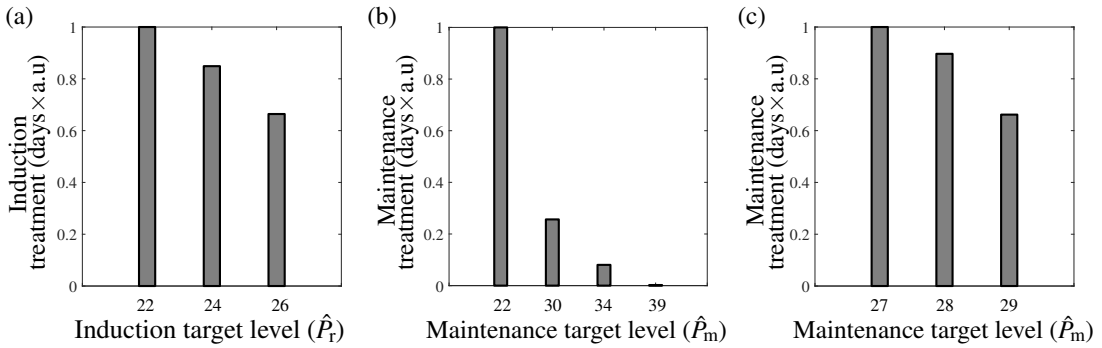


Figure 5.7: Total normalised corticosteroid treatment amount for (a) induction phase treatment ($T_r \times \bar{C}$) with induction target levels set to $\hat{P}_r = 22$ mg/ml, $\hat{P}_r = 24$ mg/ml, and $\hat{P}_r = 26$ mg/ml, when $\hat{P}_m = 26$ mg/ml; (b) maintenance treatment ($\sum_{i=1}^{N} T_C^i \times \bar{C}^i$) with maintenance target levels set to $\hat{P}_m = 22$ mg/ml, $\hat{P}_m = 30$ mg/ml, $\hat{P}_m = 34$ mg/ml, and $\hat{P}_m = 39$ mg/ml, when $\hat{P}_r = 24$ mg/ml; (c) maintenance treatment with maintenance target levels set to $\hat{P}_m = 27$ mg/ml, $\hat{P}_m = 28$ mg/ml, and $\hat{P}_m = 29$ mg/ml, when $\hat{P}_r = 22$ mg/ml.

5.5.3 Genetic risk factor-dependent treatment design

Disease severity is affected by genetic factors representing compromised skin barrier function (e.g. by mutations in the FLG gene), and dysregulated innate immune responses (e.g. mutations in TLRs and NF-κB), and are described by the parameters κ_P and α_I, respectively. We focus on designing treatment strategies for moderate to severe AD patients, which in our model are characterised by the parametric space depicted in the bifurcation diagram as red (Fig. 3.2, A). By varying these two parameters we can design treatments protocols that take into account the genotype and, thus, the corresponding severity and phenotype of AD patients. Based on the nominal target values ($\hat{P}_r = 22$ mg/ml and $\hat{P}_m = 29$ mg/ml) we will computationally design patient specific treatment protocols.

Compromised skin barrier function

To investigate the effects of compromised skin barrier function on the calculated treatment protocols we compare the nominal patient cohort $(\kappa_P, \alpha_I) = (0.85, 0.05)$ (Fig. 5.5c) with the patient cohorts described by parameters $(\kappa_P, \alpha_I) = (0.87, 0.05)$ (Fig. 5.8a), $(\kappa_P, \alpha_I) = (0.89, 0.05)$ (Fig. 5.8b), and $(\kappa_P, \alpha_I) = (0.93, 0.05)$ (Fig. 5.8c).

For the cohort described by $(\kappa_P, \alpha_I) = (0.87, 0.05)$ (Fig. 5.8a), the suggested treatment protocol successfully achieves induction of remission and AD flare prevention. The

calculated induction phase duration is 23 days, followed by maintenance treatment with 3 days corticosteroid application per cycle, except during the first cycle where 4 days of treatment is suggested. Although, the induction phase duration is increased compared to the nominal case (Fig. 5.5c), the potency of treatment decreases (decrease of 23.1%) resulting in a total treatment amount of 270 days×a.u, which represents a 11.6% decrease from the nominal case. However, during the maintenance phase, compromised barrier function leads to increased treatment efforts (increase of 39.9%). Although, this leads to increased barrier integrity (5.8% compared to the nominal case), it also indicates that long-term management of AD flares is more difficult achieve. It should also be noted that the duration of the initial AD flare is extended to 23 days (increased by 19.7 days compared to the nominal case), implying that symptoms persist for the whole duration of the induction phase.

When considering the cohort described by $(\kappa_P, \alpha_I) = (0.89, 0.05)$ (Fig. 5.8b) the calculated treatment protocol results in a 24 day induction phase and topical corticosteroid application of 4 days per cycle, during the maintenance phase. Total corticosteroid treatment during the induction and maintenance phase increases (28.8% and 45.5% increase, respectively), compared to the nominal case (Fig. 5.5c), while maintenance treatment effort scales (3.2% increase) when compared to Fig. 5.8a. Contrary to the results shown in Fig. 5.8a, the amount of treatment increases for both induction and maintenance phases, which raises speculation on the exact effect of the parameter κ_P on the induction phase dynamics. The observed non-monotonic behaviour could be attributed to the non-linearities of the model. That said, it is reasonable that compromised barrier function (leading to increased permeability to external pathogens) would require greater treatment efforts (duration or potency) to stabilise the skin barrier and protect it from increased susceptibility to external stressors. With $\kappa_P = 0.89$ (Fig. 5.8b) the AD flare ceases after 14.44 days of treatment, which is a result of the amplified induction treatment effort, whereas the AD flare persists during the induction phase when $\kappa_P = 0.87$ (Fig. 5.8a); this could be another reason contributing to the observed decrease of induction phase treatment in Fig. 5.8a, compared to the nominal case (Fig. 5.5c).

Lastly, in Fig. 5.8c the optimal treatment schedule is shown for patient cohorts decribed by parameters $(\kappa_P, \alpha_I) = (0.93, 0.05)$. In this scenario, induction of remission is unsuccessful since the de-activation threshold (P^-) cannot be achieved, and as a consequence the AD flare does not cease. Accordingly, the predicted total amount of treatment during the induction phase involves an 82.9% increase, and an 1003% increase during the

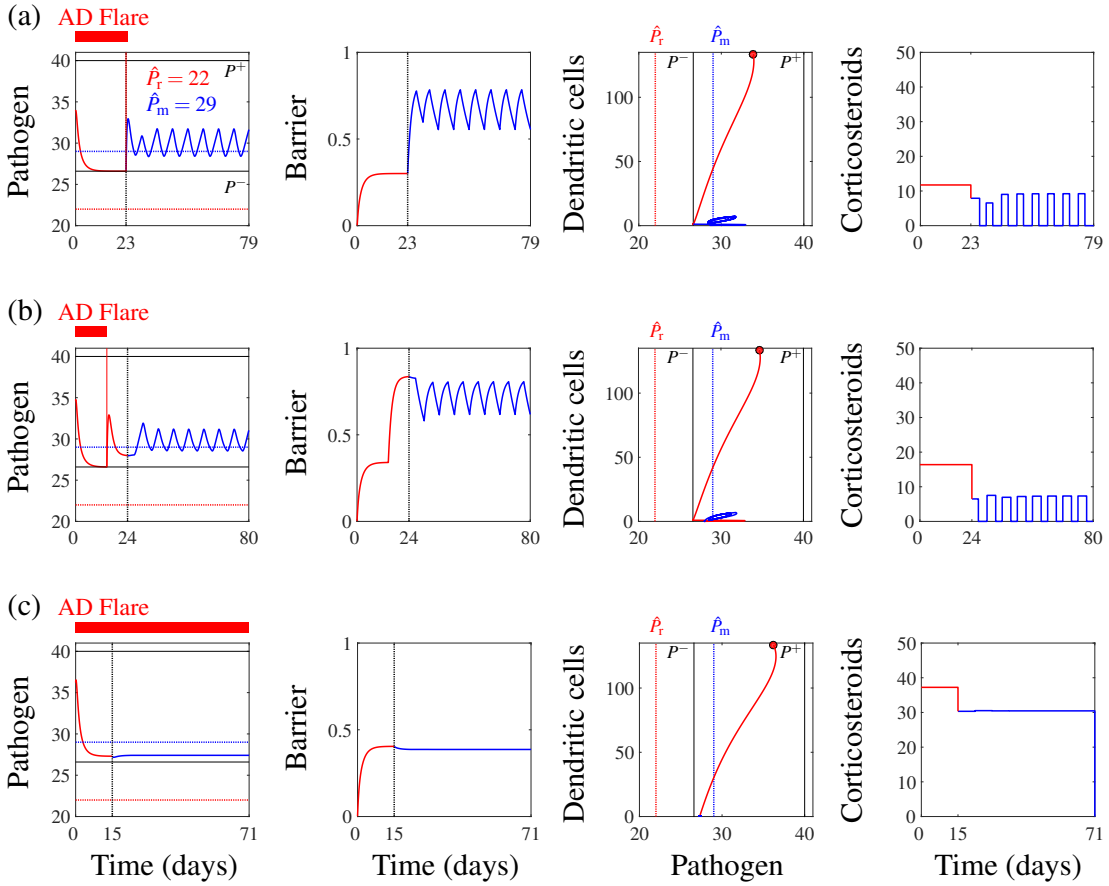


Figure 5.8: Optimally calculated treatment strategies for corticosteroids and the resulting dynamics of the model for different patient cohorts with compromised barrier integrity: (a) $(\kappa_P, \alpha_I) = (0.87, 0.05)$; (b) $(\kappa_P, \alpha_I) = (0.89, 0.05)$; and (c) $(\kappa_P, \alpha_I) = (0.93, 0.05)$. Induction phase and maintenance phase dynamics are depicted in red and blue, respectively.

maintenance phase, compared to the nominal case (Fig. 5.5c). Induction phase duration is shorter by 5 days, compared to the nominal case (Fig. 5.5c), but the potency of corticosteroid applied increases 1.44-fold. In the maintenance phase, treatments are applied continuously for the complete duration of all maintenance cycles, however, remission of the AD flare cannot be achieved. As a consequence, these patient cohorts remain symptomatic with mean barrier integrity levels diminishing greatly to 38.7%, indicating severe barrier malfunction. Nevertheless, pathogen level is kept low, which illustrates the hysteretic nature of the R-switch and the significance of deactivating it.

Dysregulated innate immune responses

We investigate the effects of dysregulated innate immune responses on the calculated treatment protocols, by comparing the nominal patient cohorts $(\kappa_P, \alpha_I) = (0.85, 0.05)$ (Fig. 5.5c) with the patient cohorts described by the parameters $(\kappa_P, \alpha_I) = (0.85, 0.045)$ (Fig. 5.9a), $(\kappa_P, \alpha_I) = (0.85, 0.04)$ (Fig. 5.9b), and $(\kappa_P, \alpha_I) = (0.85, 0.035)$ (Fig. 5.9c).

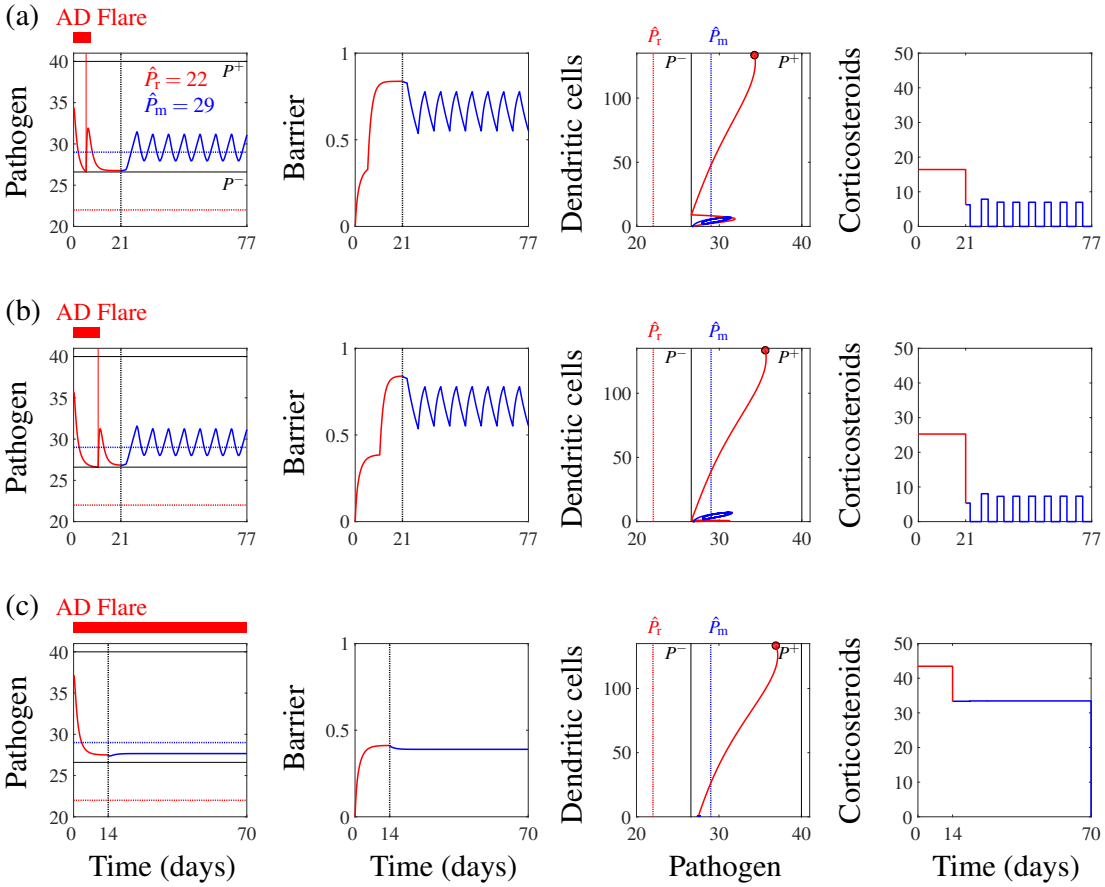


Figure 5.9: Optimally calculated treatment strategies for corticosteroids and the resulting dynamics of the model for different patient cohorts with dysregulated innate immune responses: (a) $(\kappa_P, \alpha_I) = (0.85, 0.045)$; (b) $(\kappa_P, \alpha_I) = (0.85, 0.04)$; and (c) $(\kappa_P, \alpha_I) = (0.85, 0.035)$. Induction phase and maintenance phase dynamics are depicted in red and blue, respectively.

When $\alpha_I = 0.045$ (Fig. 5.9a) our method predicts 21 days of induction phase therapy, followed by 3 days topical application of corticosteroids pair maintenance cycle. Treatment amount during the induction phase increases (12.9% increase, compared to

nominal Fig. 5.5c), and the AD flare stops after 5.6 days. Throughout the investigated maintenance phase, AD flares were prevented and a total amount of 161.7 days×a.u of maintenance therapy was used, representing a 4.6% increase from the nominal case (Fig. 5.5c).

Further scaling of treatment effort, for both induction and maintenance phase, is observed when $\alpha = 0.04$ (Fig. 5.9b) with 73.8% and 7.9% increase, respectively, compared to the nominal case (Fig. 5.5c). Increased induction treatment efforts might be caused by the propensity of patients with dysfunctional innate immune responses to have skin colonised by more pathogens, which in our model is represented by a higher steady-state pathogen level (red circle $(P(t), D(t))$-phase plots Fig. 5.9). Furthermore, comparing Fig. 5.9a and Fig. reffig:Figure6C4b with Fig. 5.5c it can be seen that genetic defects of innate immune components have a greater effect on the induction phase treatment than on the maintenance phase treatment. A possible reason for this might be the de-activation of the R-switch, which minimises the overall effect of the α_I parameter (see Eq. (5.1a)). The duration of the AD flare when $\alpha_I = 0.04$ is increased to 14 days, but it ceases before the end of the induction phase.

When immune dysregulation is more severe, for example when $\alpha_I = 0.035$ (Fig. 5.9c), induction of remission fails. The AD flare persists into the maintenance phase with considerable increases in the total amount of treatment used. As a consequence of the failed remission, barrier integrity levels remain low (39%), similar to Fig. 5.8c.

Synergistic effects of risk factors

To complete our investigation of the genetic risk factors, we simulate patient cohorts with both compromised barrier function and dysregulated innate immune responses. Specifically, we calculate the optimal treatment schedules for patient cohorts given by the combination of parameters $(\kappa_P, \alpha_I) = (0.87, 0.045)$ (Fig. 5.10a), $(\kappa_P, \alpha_I) = (0.9, 0.045)$ (Fig. 5.10b), and $(\kappa_P, \alpha_I) = (0.87, 0.04)$ (Fig. 5.10c).

For patient cohorts given by $(\kappa_P, \alpha_I) = (0.87, 0.045)$ (Fig. 5.10a) the optimal treatment schedule predicts a induction phase duration of 22 days, with application of 436.7 days×a.u amount of treatment. This corresponds to a 43% increase, compared to the induction therapy in the nominal case (Fig. 5.5c), while for patient cohorts with similarly compromised barrier function (Fig. 5.8a) or defective immune responses (Fig. 5.9a), a 61.7% and 26.6% increase is noted, respectively. For the maintenance phase,

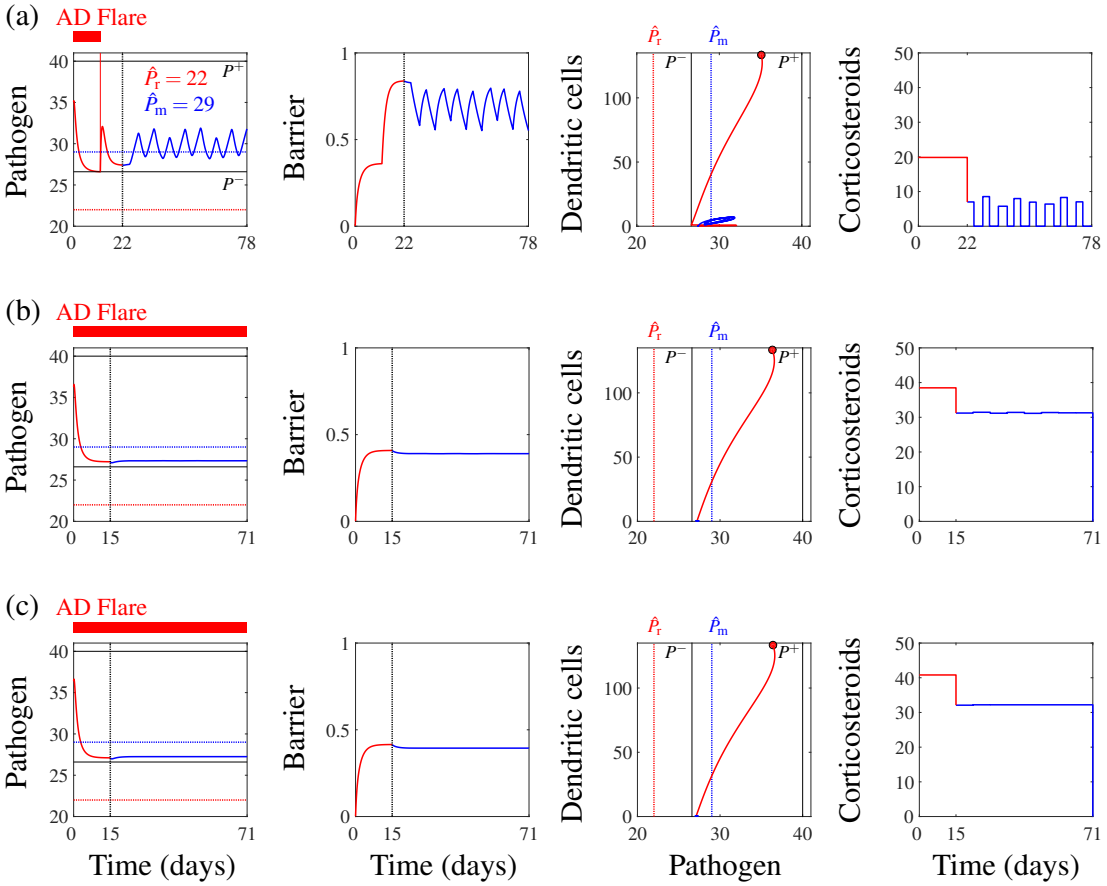


Figure 5.10: Optimally calculated treatment strategies for corticosteroids and the resulting dynamics of the model resulting from synergistic effects of the risk factors: (a) $(\kappa_P, \alpha_I) = (0.87, 0.045)$; (b) $(\kappa_P, \alpha_I) = (0.9, 0.45)$;and (c) $(\kappa_P, \alpha_I) = (0.87, 0.04)$. Induction phase and maintenance phase dynamics are depicted in red and blue, respectively.

the treatment schedule suggests 3 days of corticosteroid application per cycle for two weeks, followed by 4 days treatment per cycle for one week. The average potency used during the maintenance phase is 7.2 a.u, with an irregular potency pattern, and total maintenance therapy amounting to 186 days×a.u. By comparing the maintenance treatment amount when $(\kappa_P, \alpha_I) = (0.87, 0.045)$ with the nominal case (Fig. 5.5c), similarly compromised barrier (Fig. 5.8a), and similarly dysregulated immune responses (Fig. 5.9a), we observe a 20.4% increase, a 14% decrease and a 15% increase, respectively. Notice that although treatment effort scales for the induction phase, in the maintenance phase treatment effort decreases compared to having the single genetic risk factor (compromised barrier function Fig. 5.8a). This suggests that the synergistic effect of the risk factor on the dynamics of the system are not merely dose dependent and that a

complex interplay exists.

When we consider patients with more severe forms of AD (Fig. 5.10b and Fig. 5.10c), combining both genetic risk factors, the treatment schedule fails to induce remission. The treatments are insufficient to suppress the AD flare because the trajectories of the system cannot be driven below P^-.

We summarise the results on the treatments amounts used for the induction and maintenance phases, shown in this section, in Table 5.1.

Table 5.1: Treatment amount used during the induction and maintenance phases for risk factors conditions shown in Figs. 5.8, 5.9, and 5.10.

Figure	Induction treatment	Maintenance treatment
5.8a	270 (days×a.u)	216.3 (days×a.u)
5.8b	393.3 (days×a.u)	223.3 (days×a.u)
5.8c	558.5 (days×a.u)	1705 (days×a.u)
5.9a	344.8 (days×a.u)	161.7 (days×a.u)
5.9b	530.6 (days×a.u)	166.7 (days×a.u)
5.9c	608.5 (days×a.u)	1872 (days×a.u)
5.10a	436.7 (days×a.u)	186 (days×a.u)
5.10b	577.3 (days×a.u)	1752 (days×a.u)
5.10c	612.1 (days×a.u)	1803 (days×a.u)

5.5.4 Treatment design under non-adherence to treatments

Treatment guidelines by doctors are explained to patients after their clinical visit, where they discuss the particulars on the treatment dose and frequency. More often than not, doctors do not have the time [267] or resources [268] to properly educate patients, which can lead to misconceptions on the proper way of applying treatments. Moreover, patients [269] or their caregivers [270] might not comply with treatment specifications of corticosteroids out of fear for their adverse effects (steroid phobia) [246].

In this section we investigate the disease outcome when the treatment protocols are not followed either due to insufficient duration application or potency throughout the induction and maintenance phases.

Effects of poor adherence to optimal induction treatment schedule

In the induction phase the primary goal is to stop the AD flare and, as such, alleviate the symptoms of AD. Frequently, symptoms can subside and patients may stop using treatment. We investigate the effects of the following on the induction phase dynamics: stopping corticosteroid treatment prematurely (Fig. 5.11a); stopping both treatments prematurely (Fig. 5.11b and Fig. 5.11d); stopping corticosteroid treatment prematurely while neglecting coal tar application (Fig. 5.11c); and neglecting corticosteroid potency and duration recommendations (Fig. 5.11e).

In Fig. 5.11a we simulate a scenario in which corticosteroid treatment is stoped 16 days earlier, but still adhering to coal tar treatment. The AD flare ceases after 3.3 days and treatment discontinues almost a day later. Throughout the remaining induction phase, barrier integrity decreases without the reactivation of inflammation, however, the pathogen level increases and almost reaches the activation threshold (P^+). This situation could lead to re-initiation of the AD flare due to unpredicted external stimuli. Furthermore, there is a 9.9% increase of corticosteroid treatment during the maintenance phase, compared to the nominal case (Fig. 5.5c). Corticosteroid potency levels normalise after four maintenance cycles to the nominal case.

When both treatments are stoped 16 days earlier (Fig. 5.11b), remission is still achieved, however, the pathogen levels increase rendering the patient more susceptible to external stimuli. Maintenance treatment efforts scale compared to the nominal case (Fig. 5.5c). On the other hand, when coal tar treatment is completely neglected during the induction phase (Fig. 5.11c), the AD flare ceases after approximately 4 days. Upon discontinuationation of corticosteroid treatment, an AD flare re-initiates after 7.9 days. Induction of remission is achieved during the first maintenance cycle with 5 day treatment and a 1.79-fold increase in the potency of corticosteroid used, compared to nominal (Fig. 5.5c). The total treatment effort during the maintenance phase scales (43.3% increase), compared to the nominal case (Fig. 5.5c), however, long-term remission is still successful. Stopping both treatments 16.5 days prematurely (Fig. 5.11d), can also lead to the re-initiation of an AD flare. However, during the maintenance phase the AD flare can be stoped and prevented for the computionally calculated 8 week maintenance phase. We can conclude that cooperative treatment with both corticosteroid and other topical treatments, such as coal tar, is an important aspect of AD flare control and prevention.

Finally, we simulate the effects of not complying to the amount of induction treatment

suggested (Fig. 5.11e). In this setting, only 65% of the recommended corticosteroid potency is used and treatment is stoped 14 days earlier than the recommended 20 days (nominal case, Fig. 5.5c), while coal tar treatment is applied throughout. The AD flare ceases after 6 days, instead of 3.3 days (Fig. 5.5c), however, it is re-initiated after 9.1 days. Compared to the nominal case (Fig. 5.5c), maintenance treatment efforts scale with a 42.7% increase.

Effects of poor adherence to optimal maintenance treatment schedule

During the maintenance phase, successfully applied treatments will prevent the recurrence of AD flares or extend the duration between flares, while maintaining a healthy barrier integrity. In this section we investigate the dynamics of the model when patients do not comply to the optimally calculated maintenance treatment protocols either, by not using corticosteroids or coal tar treatment.

Consider the scenarios where the virtual patients adhere to the induction phase protocol, but discontinue both treatments during the 1^{st} to 2^{nd} (Fig. 5.12a) or 1^{st} to 3^{rd} (Fig. 5.12b) or 1^{st} to 4^{th} (Fig. 5.12c) maintenance cycles. The total maintenance treatment, when normalised for the duration, experiences a 3.9% (Fig. 5.12a), 11.7% (Fig. 5.12b), and 49.2% (Fig. 5.12c) increase, compared to the nominal case (Fig. 5.5c). Maintenance strategies with non-adherence depicted in Fig. 5.12a and Fig. 5.12b, successfully prevent the recurrence of AD flares, while in Fig. 5.12c the AD flare reoccurs 23.7 days after the induction phase ends. Nevertheless, as a consequence of the non-adherence (Fig. 5.12a and Fig. 5.12b), the pathogen level increases and barrier integrity diminishes. In addition, to induce remission in the next cycle (Fig. 5.12c), after the AD flare reoccurs, the optimal treatment strategy suggests 5 days of treatment with 1.53-fold more potent corticosteroids, compared to the nominal case (Fig. 5.5c).

In Fig. 5.12d and Fig. 5.12e we simulate the scenarios where virtual patients adhere to the maintenance therapy at the start of the maintenance phase, but stop treatment later. When patients stop both treatments during the 4^{th} to 5^{th} maintenance cycle (Fig. 5.12d), the treatment protocols can still manage to prevent the recurrence of an AD flare, however, the total maintenance therapy effort experiences a 10.7% increase, compared to nominal (Fig. 5.5c). When the 3^{rd} to 5^{th} cycles are neglected, the AD flare re-initiates (Fig. 5.12e), which implies that not ony the duration of non-adherence, but also at which cycles the non-adherence occurs, is an important factor in the long-term management of

AD (compare with Fig. 5.12b). Of course, it is clear that the maintenance target level ($\hat{P}_{\mathrm{m}}$) will also play a role in the reactivation of immune responses when non-adherence is considered. Once again, comparing to the nominal case (Fig. 5.5c), maintenance treatment efforts increase (Fig. 5.12e).

Note that the dashed lines in Figs. 5.12a-e, represent the optimal treatment protocols that would restore normal barrier function and decrease pathogen level to the maintenance target, given the non-adherence pattern. In Fig. 5.12c and Fig. 5.12e, the dashed lines indicate that the optimally calculated treatment protocols predict a progressively higher corticosteroid potency for each successive cycle.

In Fig. 5.13a and Fig. 5.13b we investigate the effects of not applying coal tar treatment. In both cases successful prevention of AD flares is predicted for the duration of the 8 weeks. However, as a consequence of not using topical coal tar treatment the total amount of corticosteroid used in the maintenance phase experiences a 2.5% (Fig. 5.13a) and 3.8% (Fig. 5.13b) increase, with respect to the nominal case (Fig. 5.5c). Although, the optimally calculated maintenance treatment protocols do not vary significantly over 8 weeks, long-term management of AD could result in overuse of topical corticosteroids.

When corticosteroid treatment is discontinued for the first four cycles, while still applying coal tar treatment (Fig. 5.13c), an AD flare reoccurs, however this occurs after 27 days instead of 23.7 days, as observed in Fig. 5.12c. Furthermore, the total normalised corticosteroid treatment increases by 51.6%, compared to Fig. 5.5c and 1.6% compared to Fig. 5.12c. Remission is achieved at the next maintenance cycle (Fig. 5.13c).

In the scenario where corticosteroid treatment is neglected for the 3^{rd} to 5^{th} cycles, while still applying coal tar treatment (Fig. 5.13d), the AD flare can be prevented. This is achieved through the barrier stabilising effects of coal tar treatment, which prevent the reactivation of inflammation, unlike the results shown in Fig. 5.12e. This illustrates the importance of applying, in conjunction antiinflammatory and barrier stabilising treatments for the successful management of the disease.

5.6 Discussion

In this chapter, we used the computational method proposed in Chapter 4 to investigate the design of patient-specific optimal treatment strategies for corticosteroids with coal tar treatment as the barrier stabilising agent. Corticosteroid treatment protocols are

designed using a proactive approach, which aims to induce remission of AD symptoms and subsequently prevent the initiation of AD flares.

We systematically investigated different target levels, both for the induction and maintenance phases (Figs. 5.2, 5.4, and 5.5). The target levels play a crucial role in the design of treatment protocols with respect to the total amount of treatment used. Depending on the clinical parameters of patients and the desired outcome, clinicians can have the option of designing mild (low duration, weak potency) or aggressive (longer duration, stronger potency) treatment protocols that can be effective.

With our computational model we were able to stratify virtual patient cohorts with respect to their responsiveness to the applied treatments. Parameter variations could represent variations in patient endotypes corresponding to different severities of compromised barrier function (Fig. 5.8), dysregulated immune responses (Fig. 5.9) or both (Fig. 5.10). As can be seen from the results in Figs. 5.8 and Fig. 5.10 the effects of treatments can be non-trivial, and to uncover effective treatments it is advantageous to use a systems biology approach that takes into account the complexity of the disease. The results in Figs. 5.8c, 5.9c, 5.10b, and 5.10c represent scenarios in which the genetic profile of the cohorts most probably matches that of recalcitrant [271] or difficult to manage AD [65] and would not benefit from a proactive treatment approach. Such patient cohorts could represent ideal candidates for systemic treatments [109] or biologic treatments [112]. This work, together with Chapter 4, represents the first step towards patient-specific treatments for AD, which take into account the disease severity as a consequence of genetic risk factors. Treatment approaches that are intelligently designed and targeted for individual patients are currently lacking [25, 28, 191] and are therefore sought after [109, 121].

We computationally investigated the effects of non-adherence to the suggested optimal treatment protocols (Figs. 5.11, 5.12, and 5.13), as a result of steroid phobia. We showed that non-adherence to the designed treatment protocols (and underutilisation of treatments) can interfere with the long-term management of AD, by diminishing the effects of treatment. In fact, a recent study concluded that concerns on the adverse effects of corticosteroids are unfounded and could be the cause of "worse outcomes for children with eczema in both the short and long term" [272]. Therefore, proper education and advice can help reduce the incidence and burden of AD. Using our approach to determine disease outcome when the specified treatment protocols are not adhered to, can provide a basis for educating patients and their caregivers of the ramifications

of undertreatment.

The duration, timing, and dose of treatments is crucial, but their exact effect on the dynamics of the disease are not easily understood in a clinical setting. With our model we can predict disease progression and design treatment strategies that can benefit the individual patient. Our systems biology approach can accommodate multiple treatments that address specific symptoms of AD emerging from its pathogenic mechanisms. The main caveat of our method is the qualitative and phenomenological form of treatments that are incorporated in our model. The acquisition of data from clinical trials exploring the effects of treatment could enable us to identify realistic treatment parameters and mathematical forms, which can enable more realistic treatment design.

In this chapter we have demonstrated the flexibility of our approach to design effective corticosteroid treatment protocols by incorporating a different type of constant barrier stabilising treatment. The application of emollients, as presented in Chapter 4, affect skin barrier integrity by an additive mathematical expression, while coal tar treatment was included in a multiplicative form. From a mathematical stand point, emollients are more effective than coal tar treatment as the they modify the steady-state value of $B(t)$ to a greater extent. However, their relative strength was chosen arbitrarily in order to reflect the fact that on their own they cannot induce remission.

Future research can possibly extend the treatment range and include antibiotics, which target pathogens colonising the skin of AD patients. Moreover, the model can possibly be extended to include the adverse effect of corticosteroid treatment such as skin atrophy. An interesting topic would be the design of treatment protocols for AD patients described by the bistable or oscillatory phenotype (Fig. 3.2, A *yellow* and *teal*, respectively). Finally, the optimisation results presented here rely on perfect measurements of the state-variables. To investigate the effects of fluctuating environmental stressors, inaccuracy of measured states, and even model mismatch we can consider a stochastic formulation of the model.

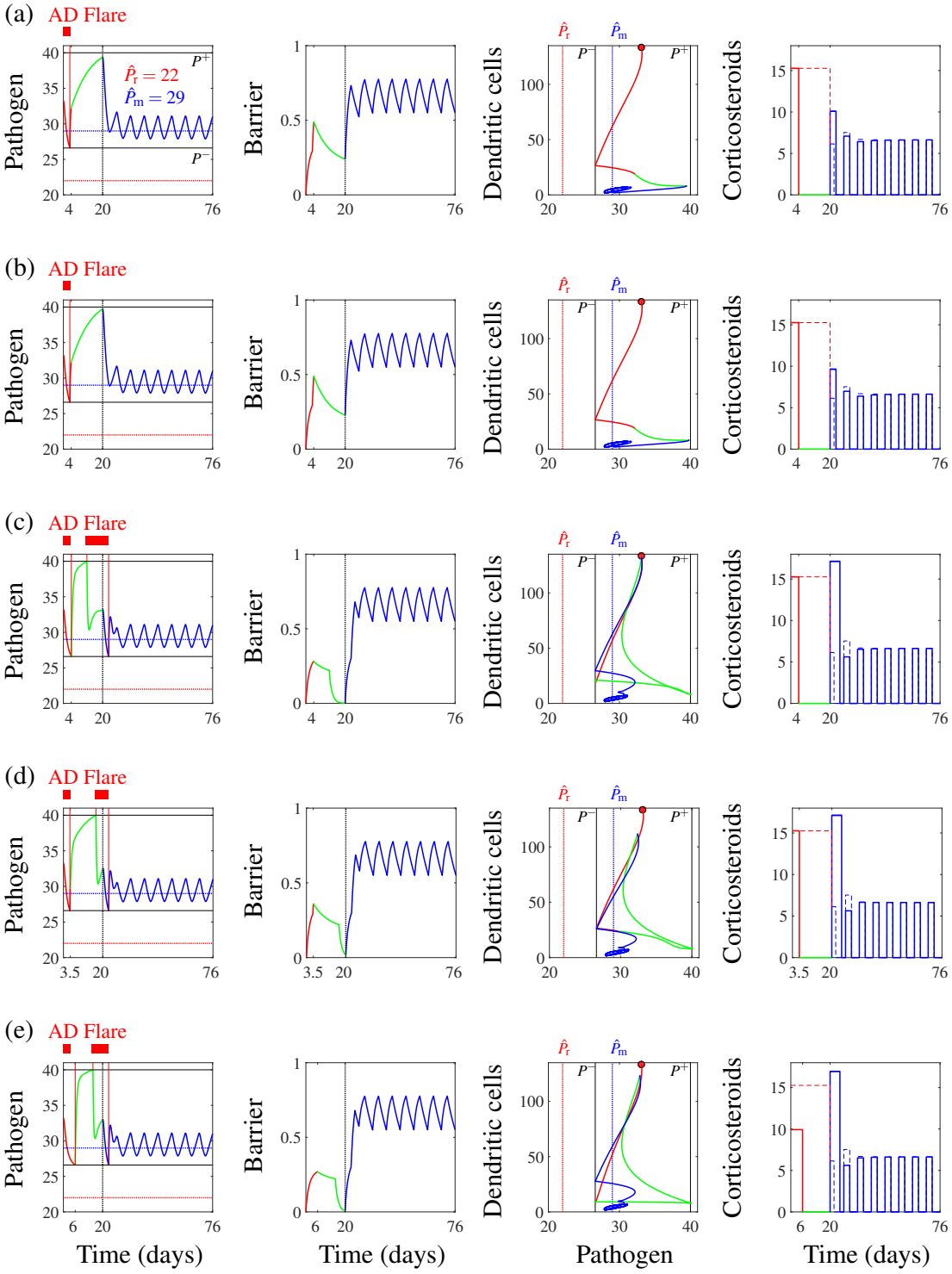


Figure 5.11: Dynamics of the model and disease progression when not adhering to the optimally calculated induction phase treatment protocol: (a) stopping corticosteroid treatment 16 days prematurely with continual use of coal tar, (b) stopping both treatments 16 days prematurely, (c) stopping corticosteroid treatment 16 days prematurely without application of coal tar, (d) stopping both treatments 16.5 days prematurely, (e) using only 65% of the recommended corticosteroid potency and stopping treatment 14 days prematurely. Induction phase and maintenance phase dynamics are depicted in red and blue, respectively. Green lines represent the period of non-adherence, and the dashed lines on the right column demonstrate the optimal strategy calculated for the nominal case (Fig. 5.5c).

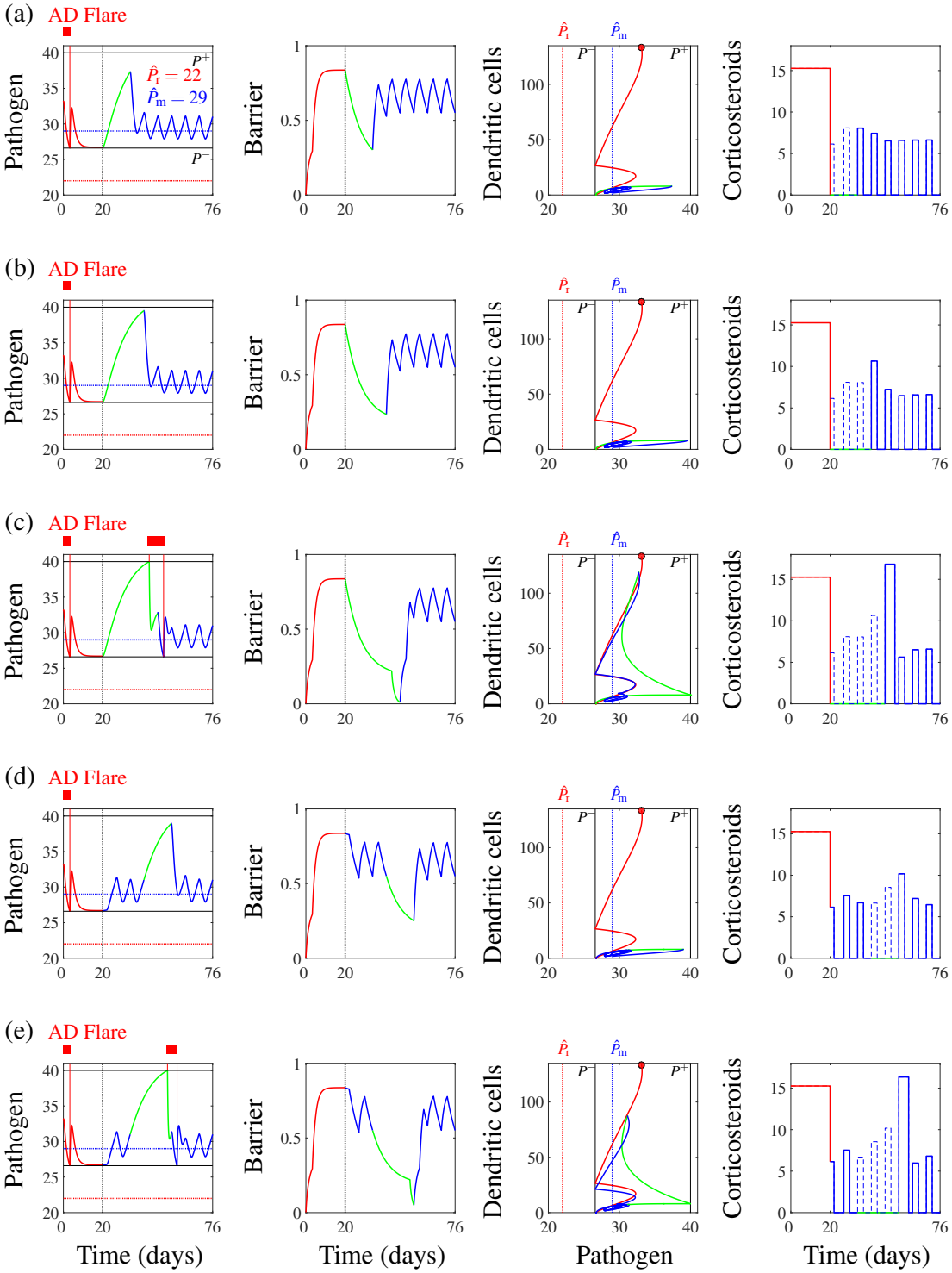


Figure 5.12: Dynamics of the model and disease progression when not adhering to the optimally calculated maintenance treatment protocol: stopping both treatments for the (a) 1^{st} and 2^{nd} cycles, (b) 1^{st} to 3^{rd} cycles, (c) 1^{st} to 4^{th} cycles, (d) 4^{th} and 5^{th} cycles , and (e) 3^{rd} to 5^{th} cycles. Induction phase and maintenance phase dynamics are depicted in red and blue, respectively. Green lines represent the period of non-adherence, and the dashed lines on the right column demonstrate the optimal strategy calculated required to normalise the dynamics of the system given the corresponding non-adherence pattern.

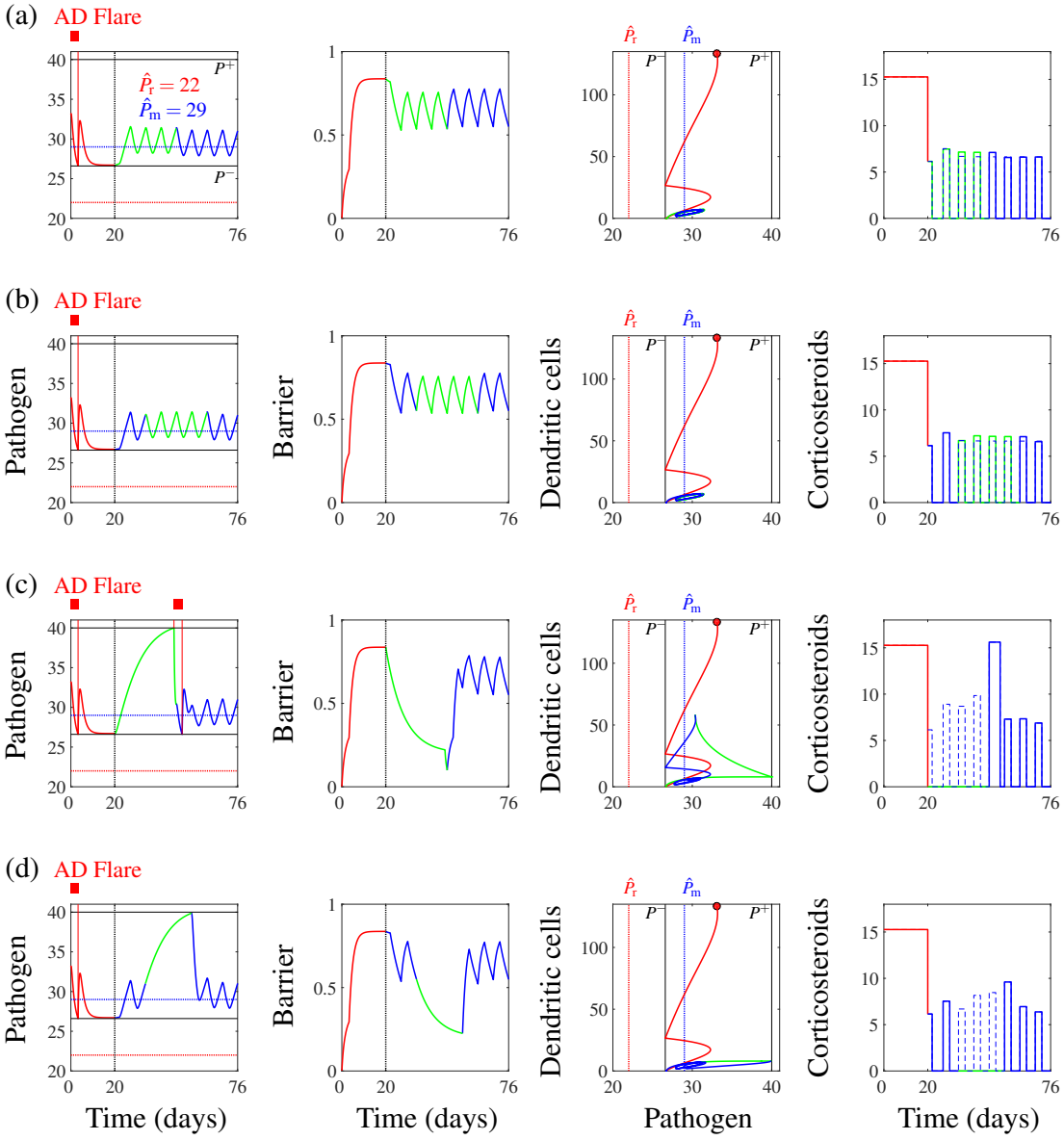


Figure 5.13: Dynamics of the model and disease progression when not adhering to the optimally calculated maintenance treatment protocol: stopping both treatments for the (a) 1^{st} and 2^{nd} cycles, (b) 1^{st} to 3^{rd} cycles, (c) 1^{st} to 4^{th} cycles, (d) 4^{th} and 5^{th} cycles , and (e) 3^{rd} to 5^{th} cycles. Induction phase and maintenance phase dynamics are depicted in red and blue, respectively. Green lines represent the period of non-adherence. The dashed lines on the right most column of Fig. 5.13a and 5.13b demonstrate the optimal strategy calculated for the nominal case (Fig. 5.5c), while in Fig. 5.13c and demonstrate the treatment required to normalise the dynamics of the system given the corresponding non-adherence pattern.

Chapter 6

Dual feedback structures with delay for epidermal homeostasis

In Chapter 3 we presented a model of AD pathogenesis. The model analysis identified the key role of a defective skin barrier in AD pathogenesis, as it increases the permeability to pathogens or allergens. This can lead to the activation of inflammatory responses that may eventually trigger adaptive immune responses and progression to severer forms of AD. Skin barrier homeostasis is achieved by the tight regulation of cell differentiation and proliferation processes [273–276] that replenish skin cells and terminal differentiation markers, and skin shedding (skin desquamation) at the upper levels of the epidermis, induced by proteases such as kallikreins [132, 139, 277]. These processes are interconnected and co-regulated through feedback mechanisms, and when properly regulated, can lead to the characteristic self-recovery of the skin barrier and return of homeostasis [278, 279]. However, impairment of these processes by risk factors such chronic inflammation [129, 280], mutations [50, 196, 197], or environmental factors [30, 41] may lead to pathological conditions such as AD [47, 56, 127].

In the model proposed in Chapter 3, the characteristic self-recovery of the skin barrier was represented phenomenologically by a production term $\kappa_{\mathrm{B}}(1 - B(\tau))$. However, this term does not allow us to explore the feedback mechanisms with which skin barrier homeostasis is maintained. In this chapter, we propose a mechanistic mathematical model representing regulatory networks of skin barrier formation. We aim to elucidate the mechanisms of self-recovery and the potential role of genetic and environmental factors that may impair this self-recovery capacity, which can lead to the progression

of AD. We specifically focus on the feedback mechanisms of skin barrier homeostasis represented as a combination of positive and negative feedbacks that operate via a delay involved in the cell differentiation processes.

The existence of dual control mechanisms, i.e positive and negative feedbacks, is ubiquitous in biological control systems [281–285]. These control mechanisms perform many functions depending on their topology and non-linearities (e.g. cooperativity to induce bistablity in MAPK cascades [286]). Negative feedback mechanisms have been associated with functions, such as homeostasis, signal adaptation and transient signal generation [287, 288], and promote robustness to parameter disturbances [289] or noise [290]. In other cases, where delays are involved in the processes, negative feedbacks can lead to unstable behaviour, such as amplitude increasing oscillations [288, 291]. Positive feedback mechanisms are associated with signal amplification and the creation of bistable switches and memory [292], and stabilise the system by locking it in one of its steady states [147, 291]. Mixed positive and negative feedback systems have been shown to exhibit homoeostatic behaviour and generate robust bistability that is involved in either reversible or irreversible reactions [146, 147, 293] or robust oscillations [283, 294]. Consequently, this information illustrates that dual control mechanisms in biological control systems can explain many physiological processes.

We present a regulatory network for skin barrier homeostasis with dual feedback mechanisms. The network is described by a set of coupled Delay Differential Equations (DDEs), where delays correspond to the de-novo synthesis of precursors of skin barrier components, such as filaggrin. We analyse the model to investigate the regulatory mechanisms that underlie self-recovery of the skin barrier and to explore how genetic risk factors or skin barrier perturbation can affect the recovery of the skin barrier or lead to pathophysiologic conditions.

6.1 Biological background

In this section we present biochemical and cellular interactions involved in the regulation of the skin barrier, in order to construct the regulatory network describing its self-recovery properties.

Skin homeostasis is maintained by a series of complex differentiation and biochemical events, that coordinately regulate the proliferation, differentiation, cornification and

desquamation of keratinocytes [295]. Balance between proliferation and differentiation of keratinocytes regulates the amount of terminally differentiated keratinocytes (corneocytes). A series of post-translational processes subsequently leads to the formation of the stratum corneum [137]. The stratum corneum provides protective functions mediated by epidermal structural components such as filaggrin [24, 296], lipids [297, 298], and corneodesmosomes [139, 299].

Inactive forms of filaggrin (profilaggrin) are expressed in the granular layer of the epidermis as part of the differentiation process of keratinocytes [39, 300] (*process a*, Fig. 6.1a). Profilaggrin is post-translationally modified (*process b*, Fig. 6.1a) into filaggrin by regulation of several enzymes, such as caspase-14 [301], furin [39], SASPase [302], and ELA2 [296]) (*process c*, Fig. 6.1a). Notably, the enzyme caspase-14 enables the processing of profilaggrin upon perturbation of the skin barrier [172]. This illustrates the existence of a negative feedback between decreased barrier function (via perturbation) and increased processing of barrier components to re-establish barrier function. More recently, the protease kallikrein-5 (KLK5) has been identified as a regulator of profilaggrin [303] (*process d*, Fig. 6.1a). Its proteolytic activity is enhanced when barrier function is compromised [30, 132, 304, 305] (*process e*, Fig. 6.1a), corresponding to regulation through negative feedback. Finally, KLK promote desquamation of the skin barrier [132, 139, 277, 306] and therefore indefectly induce degradation of filaggrin in the stratum corneum (*process f*, Fig. 6.1a). Filaggrin expression levels are affected by barrier damage, via changes in the calcium gradient in the epidermis [307–309]. Profilaggrin mRNA is reduced after mechanical [310] or chemical [308, 310] disruption, forming a positive feedback(*process g*, Fig. 6.1a), but subsequenty recovers in physiologically healthy patients [308], illustrating self-recovery properties on the gene level.

The schematic representing the epidermal homeostasis regulatory network is presented in Fig. 6.1a. Although filaggrin is an essential barrier structural protein [30, 40, 201], other components, such as lipids [128, 297, 298] and corneodesmosomes [139, 299], also play an important role in skin barrier function. Therefore, it can be assumed that skin barrier function can be tentatively expressed by the following equation:

$$Skin\ barrier\ function = f(filaggrin, lipids, cell\ cohesion\ structures, ...)$$

In our analysis of the self-recovery properties of the skin barrier, we make a further simplifying assumption, namely, that filaggrin level is analogous with barrier function

and therefore consider,

$$Skin\ barrier\ function \approx g(filaggrin).$$

Although this is a major simplification, it allows the construction of simple and qualitative mathematical models.

Table 6.1: Description of the *self-recovery model* and *skin barrier homeostasis model* parameters and their nominal values (Fitted to experimental data from [141]).

Symbol	Name	Nominal value
δ_x	Rate of filaggrin natural degradation	0.7 $(1/days)$
δ_y	Rate of profilaggrin natural degradation	0.1 $(1/days)$
δ_z	Rate of kallikrein natural degradation	0.8 $(1/days)$
f_x	Barrier-mediated inhibition of profilaggrin processing	0.2 (dm^3/mol)
f_y	Barrier-mediated precursor production	4 (dm^3/mol)
f_z	Barrier-mediated inhibition of kallikrein activity	0.5 (dm^3/mol)
f_{zx}	Kallikrein-mediated post-translation modification of profilaggrin	2 (dm^3/mol)
φ_{zx}	Kallikrein-mediated reduction of filaggrin via desquamation	4 (dm^3/mol)
k_x	Rate of profilaggrin-mediated filaggrin production	3 $(1/days)$
k_y	Rate of de-novo synthesis of profilaggrin	0.08 $(mol/dm^3 days)$
k_z	Basal activation of kallikreins	0.3 $(mol/dm^3 days)$
τ_d	Barrier-mediated time delay of precursors de-novo synthesis modulation	5 $(days)$

In the following sections, we propose a mathematical model of the regulatory network introduced in this section. The interactions of the regulatory network are translated to DDEs using mass action kinetics. A brief description of DDEs is provided in Appendix D. The resulting mathematical model is analysed using a reductionist approach [311], by decomposing it into a smaller network (Fig. 6.1b). The decomposition of the network into a smaller subnetwork will enable us to identify the feedback mechanisms that lead to the self-recovery of the skin barrier. The smaller subnetwork will be termed the "*self-recovery model*" (Section 6.3) and will include the reactions of de-novo synthesis of profilaggrin ($y(t)$) and subsequent post-translational modifications to produce filaggrin ($x(t)$) (Fig. 6.1b). Subsequently, in Section 6.4 the complete regulatory network is considered which includes the reactions of de-novo synthesis profilaggrin ($y(t)$), post-translational modification to filaggrin ($x(t)$), and KLK ($z(t)$) regulation (Fig. 6.1c).

This model will be termed the "*skin barrier homeostasis model*". The model parameters are described in Table 6.1 with their nominal values (derived from experimental data [141]).

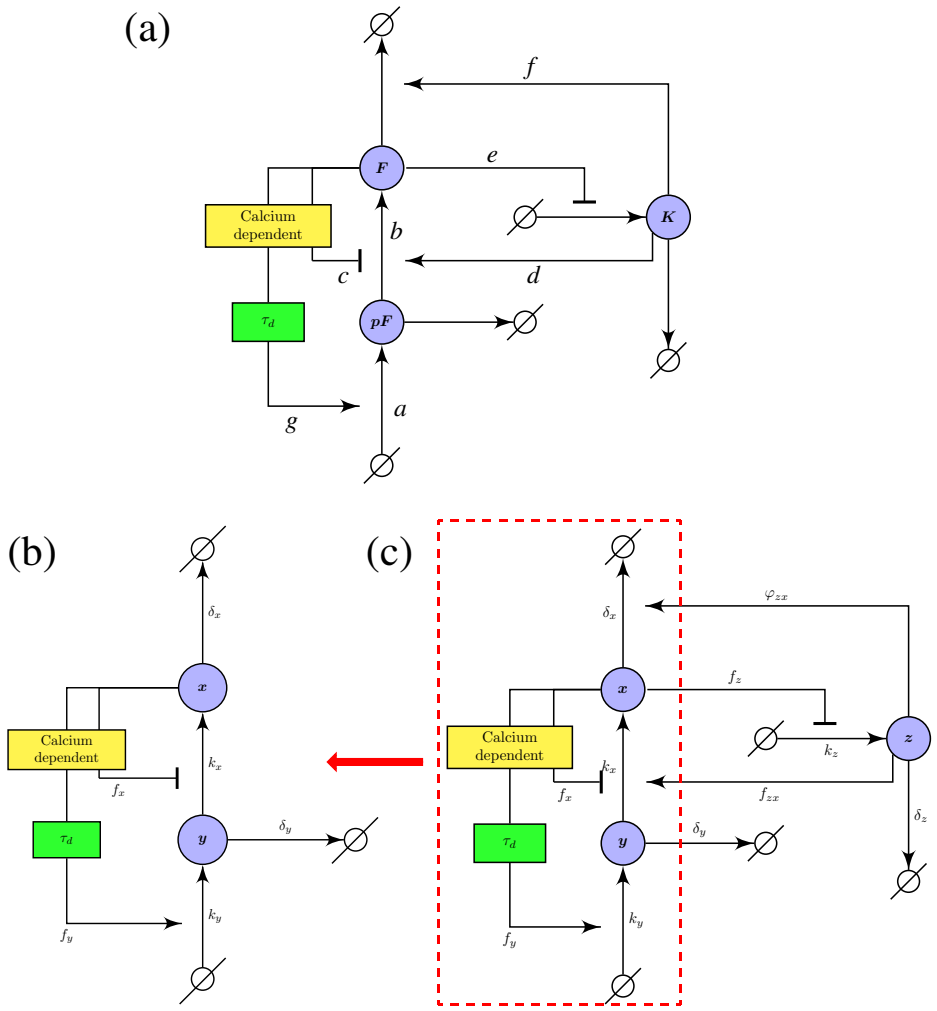


Figure 6.1: (a) Epidermal homeostasis regulatory network. Barrier precursors (pF), such as profilaggrin, are (a) produced de-novo and then (b) post-translationally modified into filaggrin, to form the epidermal barrier (F) by (c) calcium dependent pathways and (d) processing of active kallikreins (K). Compromised barrier function results in (e) enhanced proteolytic activity of kallikreins, which induces (f) skin desquamation. Precursor expression is modulated by (g) skin barrier function (level of filaggrin). Modification of the de-novo synthesis of precursors occurs via a delay. (b) Schematic of the subnetwork representing the *self-recovery model*. The nodes represent the state-variables of Eq. (6.1a) and (6.1b), filaggrin concentration (x) and profilaggrin concentration (y). (c) Schematic of the network representing the *skin barrier homeostasis model*. The nodes represent the state-variables of Eq. (6.6a) - (6.6c), filaggrin concentration (x), profilaggrin concentration (y), and active kallikrein concentration (z). Dashed red box is the *self-recovery model*. A description of the parameters is given in Table 6.1.

6.2 Methods

All simulations were conducted using MATLAB version R2016a (The MathWorks, Inc., Natick, MA, USA). We used *dde23* for the numerical integration of the system.

Parameter fitting was based on the "*skin barrier homeostasis model*" (Eq. (6.6)), since it represents the complete regulatory network and contains all of the 12 parameters (δ_x, δ_y, δ_z, f_x, f_y, f_z, f_{zx}, φ_{zx}, k_x, k_y, k_z, τ_d). We fitted the inverse TEWL measurements ($1/TEWL$) (data from [141]) to the barrier integrity levels (Eq. (6.6a)) such that the least squared error between the data and the simulation results was minimised. Minimisation was performed using the *fmincon* function in MATLAB for 12 parameters using an interior-point algorithm. We constrained the parameters to be: (i) positive; (ii) to be within the range $[10^{-3}, 100]$, in order to mitigate stiffness complications in the simulations; and (iii) based on inequality constraints identified by applying Sturm's theorem [312, 313]. All of the optimised parameters are shown in Table 6.1 and the fitted dynamics are shown in Fig. 6.4b.

6.3 Self-recovery model

6.3.1 System description

The regulatory network of the *self-recovery model* is shown in Fig. 6.1b, and the governing equations are described by a set of two DDEs of the *discrete delay type* [314]:

$$\dot{x}(t) = k_x \frac{y(t)}{1 + f_x x(t)} - \delta_x x(t), \tag{6.1a}$$

$$\dot{y}(t) = k_y(1 + f_y x(t - \tau_d)) - k_x \frac{y(t)}{1 + f_x x(t)} - \delta_y y(t), \tag{6.1b}$$

where $x(t)$ is the filaggrin content of the skin barrier, and $y(t)$ denotes the level of profilaggrin, and τ_d is a constant delay. The model parameters are stated in Table 6.1 with their values.

The proposed model describes the regulation of the barrier component filaggrin using simple mathematical terms. Filaggrin ($x(t)$) is formed via post-translational modifications [k_x] of profilaggrin ($y(t)$) (mass action). Filaggrin concentration is self-regulated

through a negative feedback $[f_x]$ and naturally degraded $[\delta_x]$. Negative feedback is modelled as a strictly decreasing shifted hyperbolic function. Profilaggrin is synthesised de-nono ($[k_y]$ basal expression) and is regulated by filaggrin via an additive delayed $[\tau_d]$ positive feedback $[f_y]$. Finally, profilaggrin is naturally degraded $[\delta_y]$.

To define a complete initial value problem we need to define the initial history function, ϕ (see Appendix D). We assume that prior to pertubation the system is in steady-state, i.e the state variables are initialised at their steady-state value, in the interval $[-\tau_d, 0)$. Therefore, we define an initial history function as a piecewise continuous function given by,

$$\phi(t) = \begin{cases} \boldsymbol{x^*}, & t \in [-\tau_d, 0) \\ \begin{bmatrix} \gamma x^* & y^* \end{bmatrix}^T, & t = 0 \end{cases} \tag{6.2}$$

where $\gamma \in [0, 1]$. We choose this functional form because it emulates instantaneous disturbance of the skin barrier. The concentration of filaggrin ($x(t)$) is instantaneously perturbed from the equilibrium point to some lower multiple of the steady-state. Such a behaviour can be achieved by tape stripping experiments on skin barrier where skin cells are directly removed from the epidermis. Combined together, Eqs. (6.1a), (6.1b), and (6.2) form an initial value problem.

6.3.2 A unique stable steady-state

The steady states of the *self-recovery model* are found by solving $\dot{\boldsymbol{x}}(t) = \mathbf{0}$ as:

$$\boldsymbol{x}^* = \begin{bmatrix} x^* \\ y^* \end{bmatrix} = \begin{bmatrix} \frac{(k_y f_y - \frac{\delta_y \delta_x}{k_x} - \delta_x) \pm \sqrt{(k_y f_y - \frac{\delta_y \delta_x}{k_x} - \delta_x)^2 + 4 \frac{\delta_y \delta_x f_x}{k_x} k_y}}{2 \frac{\delta_y \delta_x f_x}{k_x}} \\ \frac{\delta_x x^* (1 + f_x x^*)}{k_x} \end{bmatrix} \text{ or } \begin{bmatrix} -\frac{1}{f_x} \\ 0 \end{bmatrix}, \tag{6.3}$$

where $\boldsymbol{x}^*$ represents the vector form of the equilibrium points, and x^*, y^* are the individual equilibrium components. The only biophysically plausible steady-state solution is obtained with $\boldsymbol{x^*} > \mathbf{0}$[1] and is given by:

$$\boldsymbol{x}^* = \begin{bmatrix} x^* \\ y^* \end{bmatrix} = \begin{bmatrix} \frac{(k_y f_y - \frac{\delta_y \delta_x}{k_x} - \delta_x) + \sqrt{(k_y f_y - \frac{\delta_y \delta_x}{k_x} - \delta_x)^2 + 4 \frac{\delta_y \delta_x f_x}{k_x} k_y}}{2 \frac{\delta_y \delta_x f_x}{k_x}} \\ \frac{\delta_x x^* (1 + f_x x^*)}{k_x} \end{bmatrix}. \tag{6.4}$$

[1] Since these variables represent concentrations.

The steady-state solution is a function of the parameters and determing the stability of the equilibrium point. Notice that this equilibrium exists for all positive (non-zero) values of the parameters and it is always positive. Therefore, the system trajectories can exhibit two possible behaviours: (1) convergence towards the equilibrium point (if it is locally asymptotically stable) or (2) diverge to infinity.

Linear stability analysis for systems of DDEs is usually non-trivial due to the infinite dimensional spectrum (see Appendix D). In Appendix E we prove that the unique steady-state of the *self-recovery model* is locally asymptotically stable for any variation of the parameters. To further support our findings, the stability of the equilibrium is assessed using a MATLAB-compatible DDEs continuation software (DDE-BIFTOOL) [315, 316]. The results show that a bifurcation does not occur by varying the model parameters and that the equilbirum point is stable (see Appendix F).

For any variation of the parameters or initial conditions the trajectories of the system will converge to its unique steady-state since it is locally asymptotically stable. This unique steady-state represents an intact epidermis and we defined it as the *healthy state*, with high filaggrin and profilaggrin content. Therefore, due to this unique *healthy state*, the *self-recovery model* displays self-recovery dynamic behaviour. However, another determining factor for a healthy skin barrier is the speed with which recovery is achieved. In the next section we explore the dynamics of the *self-recovery model* upon perturbation of the skin barrier.

6.3.3 System dynamics

In this section the recovery dynamics of the *self-recovery model* are explored. To quantitatively assess filaggrin recovery we compute the recovery time Δt_r (Fig. 6.2) in our model, which is the time required for filaggrin content ($x(t)$) in the skin to reach its homeostatic level (x^*). The recovery time is defined as:

$$\Delta t_r \coloneqq sup\{t \in \mathbb{R} :\| x^* - x(t) \|_\infty \leq 1\%\}, \tag{6.5}$$

where $x(t)$ is filaggrin skin barrier content, x^* is the steady-state value of filaggrin, *sup* denotes the supremum of a set, and $\| \cdot \|_\infty$ denotes the infinity norm ($\| f \|_\infty = sup\{|f(x)| : x \in \mathbb{R}\}$). By adopting the preceding definition for the recovery time, it is assumed that filaggrin level has reached a homeostatic value when its concentration remains within 1% of its steady-state value. This percentage was arbitrarily chosen to

by-pass the extremely long recovery times required to reach the actual steady-state, as a consequence of the asymptotic behaviour[2].

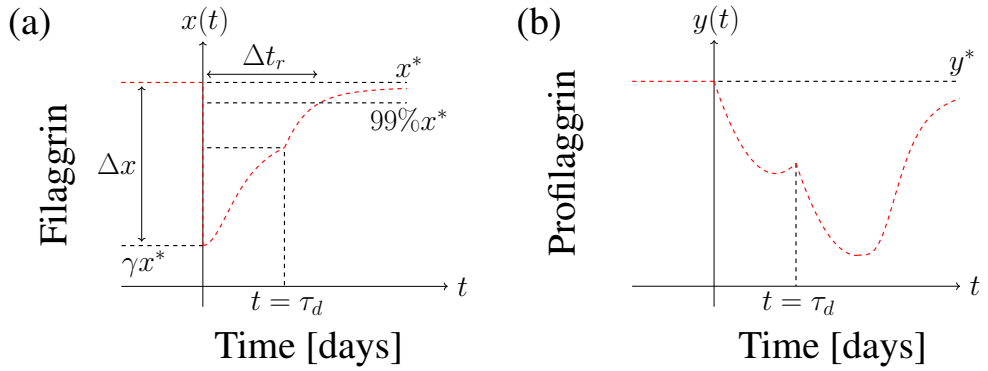


Figure 6.2: Schematic representation of the dynamics of the *self-recovery model*. (a) Filaggrin ($x(t)$) concentration is initially at a homeostatic level. At $t = 0$ the skin is perturbed, which results in a reduction of filaggrin concentration (γx^* with $\gamma \in [0, 1]$). Recovery is accomplished when filaggrin is at 99% of its steady-state value. Δt_r denotes the recovery time. (b) Profilaggrin ($y(t)$) concentration is reduced upon perturbation of the skin, but then recovers to its homeostatic value.

Barrier damage-induced effects on recovery

We simulate the effect of instantaneous skin barrier damage in order to understand the relationship between barrier-induced perturbation and the recovery time (Δt_r) (Fig. 6.3). Instantaneous damage results in an abrupt change of filaggrin content in the skin, represented as a displacement of filaggrin concentration at $t = 0$.

For all levels of the initial pertubation investigated the model demonstrates recovery to its homeostatic level (Fig. 6.3, *left* and *centre*). Initially, as a consequence of the reduction in filaggrin level profilaggrin level decreases. However, due to the delay, this extreme pertubation does not have an immediate effect on the de-novo synthesis of profilaggrin. For $t \in (0, \tau_d)$, the positive feedback modulating profilaggrin synthesis remains low since the filaggrin level is still "sensed" as high. After the duration of the delay (τ_d), de-novo synthesis is reduced significantly as a result of increased positive feedback modulation via the reduced level of filaggrin.

Recovery time (Δt_r) demonstrates a damage-dependent behaviour (Fig. 6.3, *right*). As the barrier damage pertubation increases, the recovery time also increases, with recovery

[2] $\dot{\boldsymbol{x}} \approx 0$ near the equilibrium point.

being achieved within 27 days for all levels of perturbation, given the nominal parameters in Table 6.1. Recovery time increases by 37.2% for 100% filaggrin perturbation (Fig. 6.3, *blue cross*), when compared to 40% perturbation (Fig. 6.3, *purple cross*).

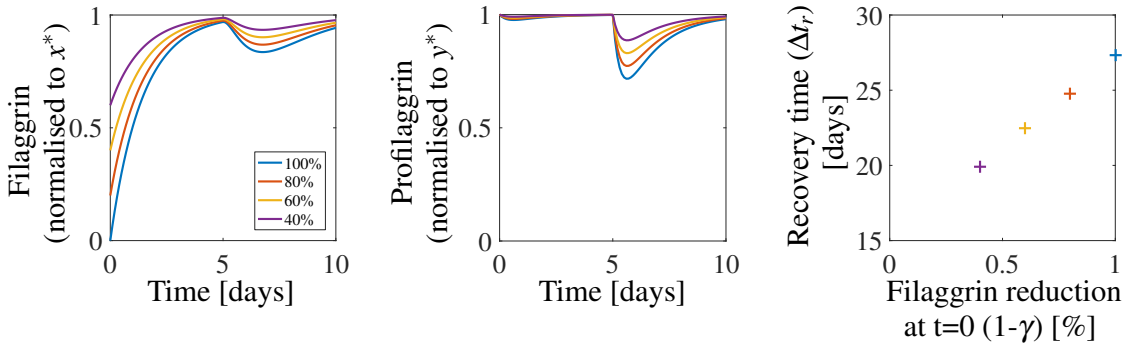


Figure 6.3: *self-recovery model* recovery dynamics with respect to instantaneous barrier damage. *Left* and *Centre*: Normalised recovery dynamics of filaggrin ($x(t)$) and profilaggrin ($y(t)$), respectively, for different levels of barrier pertubation = $\{100\%, 80\%, 60\%, 40\%\}$. *Right*: Calculated recovery time (Δt_r), after skin barrier damage, which results in a reduction of filaggrin content.

Self-recovery model summary

Utilising the information collected in Section 6.1, a regulatory network of epidermal homeostasis is constructed (Fig. 6.1a). Following a reductionist approach we decompose this network into a smaller subnetwork in order to identify the control mechanisms responsible for the recovery dynamics of the skin barrier. The constructed toy model represents the regulatory network of filaggrin processing in the skin barrier (Section 6.3.1). The model admits a unique biophysically acceptable steady-state, which is always locally asymptotically stable (Section 6.3.2). Furthermore, the model exhibits a recovery dynamic behaviour upon pertubation, with recovery times dependent on the magnitude of pertubation (Fig. 6.3).

The preliminary analysis of the dual feedback architecture of the *self-recovery model* can explain the self-recovery behaviour of the skin barrier upon perturbation. However, due to the existence of the unique stable state, this model cannot explain how the deregulation of the feedback mechanisms, genetic susceptibility, or environmental factors can lead to a disease phenotype. Nevertheless, the delay in recovery could lead to allergic sensitisation, as predicted in Chapter 3. Therefore, this regulatory network may

represent AD patients described by the (κ_P, α_I)-parametric region in grey in Fig. 3.2A. Such patients can either be non-systemic asymptomatic or systemic asymptomatic due the unique equilibrium point of Eq. (3.1a)-(3.1c) for the designated parametric region.

6.4 Skin barrier homeostasis model

6.4.1 System description

The regulatory network of the *skin barrier homeostasis model* is shown in Fig. 6.1c, and the governing equations are described by a set of three DDEs:

$$\dot{x}(t) = k_x f_{zx} \frac{y(t)z(t)}{1 + f_x x(t)} - \delta_x \varphi_{zx} x(t) z(t) - \delta_x x(t) u(t), \tag{6.6a}$$

$$\dot{y}(t) = k_y (1 + f_y x(t - \tau_d)) - k_x f_{zx} \frac{y(t)z(t)}{1 + f_x x(t)} - \delta_y y(t), \tag{6.6b}$$

$$\dot{z}(t) = \frac{k_z}{1 + f_z x(t)} - \delta_z z(t), \tag{6.6c}$$

where $x(t)$ is the filaggrin content of the skin barrier, $y(t)$ denotes the level of profilaggrin, and $z(t)$ is the concentration of active KLK. Instead of considering perturbations as a reduction in filaggrin content, a dynamic variable $u(t)$ is included, which represents a mechanical or chemical stimulus, that affects the degradation of filaggrin and is independent of natural filaggrin degradation. The stimulus variable will have the form of a pulse and will be described by the pair of parameters $(t_{\bar{u}}, \bar{u})$ representing the stimulus duration and stimulus strength, respectively (Fig. 6.4a). The model parameters are described in Table 6.1.

The proposed model describes the regulation of the barrier component filaggrin with the control of kallikrein proteases. Filaggrin $(x(t))$ is formed via post-translational modifications $[k_x]$ of profilaggrin $(y(t))$ and regulated $[f_{zx}]$ by kallikrein activity $(z(t))$ (mass action). Filaggrin concentration is self-regulated through negative feedback $[f_x]$ and naturally degraded $[\delta_x]$; degradation is modulated by the concentration of active kallikreins $[\varphi_{zx}]$. Mechanical or chemical stimuli $(u(t))$ induce barrier damage which results in a reduction of filaggrin content. Profilaggrin is synthesised de-novo ($[k_y]$ basal expression), which is regulated by filaggrin via a delayed $[\tau_d]$ positive feedback $[f_y]$, and is also naturally degraded $[\delta_y]$. Kallikreins are constitutively activated $[k_z]$ and are

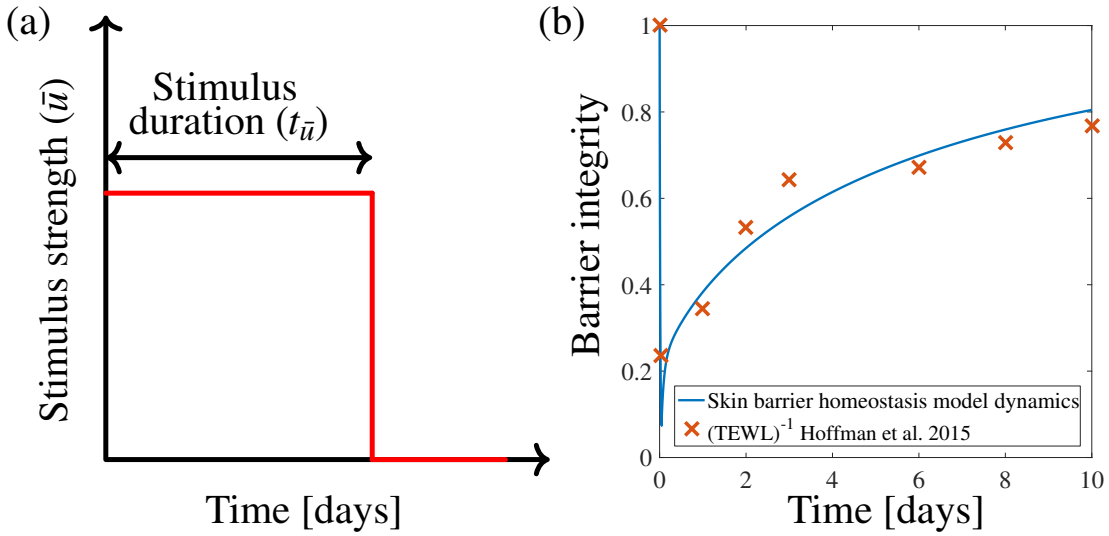


Figure 6.4: (a) Schematic representation of mechanical or chemical stimulus that induces barrier damage (Eq. 6.6a). The stimulus has the form of a pulse with strength $\bar{u}$ and duration $t_{\bar{u}}$. (b) Dynamical behaviour of the *skin barrier homeostasis model* upon pertubation (Fitted to experimental data from [141]).

regulated by filaggrin concentration through a negative feedback [f_z]. Finally, kallikreins are naturally degraded [k_z].

The initial history function for the DDEs (Eq. (6.6a)-(6.6c)) is given by,

$$\phi(t) = \boldsymbol{x}^*, \ t \in [-\tau_d, 0), \tag{6.7}$$

where $\boldsymbol{x}^* = [x^*, y^*, z^*]^T$ and corresponds to a steady-state of the *skin barrier homeostasis model*. We therefore assume that the system is in steady-state prior to pertubation.

Skin pertubation by mechanical abrasion [141] or sodium lauryl sulphate (SLS) [140] cause decreased barrier function, as observed by increased values of transepidermal tater loss (TEWL), however, skin barrier function is subsequently normalised. We fitted the model to the data presented in [141], where the skin of volunteers was mechanically abraded, and barrier integrity was measured through TEWL and measurements of Natural Moisturising Factors (NMF). The fitted dynamics of the *skin barrier homeostasis model* are shown in Fig. 6.4b. Based on the parameters calculated using the data in [141], we next explore if our system could exhibit other dynamical behaviours.

6.4.2 Bistable behaviour

To identify the number of steady-states of the *skin barrier homeostasis model*, Descartes' Rules of Signs is applied. With this tool we identify analytically parametric conditions where one unique steady-state or three steady-states exist without assessing their stability. In general, analytical stability results for systems of DDEs of order higher than two are difficult to obtain and, therefore, such an analysis is omitted here. Instead, stability is assessed using the numerical continuation software DDEBIF-TOOL (Appendix F). Note that the analysis is carried on the autonomous system i.e. with $(t_{\bar{u}}, \bar{u}) = (0, 0)$.

Conditions for the existence of three steady-states

By setting Eq. (6.6a)-(6.6c) equal to zero and substituting the expressions for y^* and z^* we reach the following polynomial expression for the x^*:

$$f(x) = (1 + f_x x^*)\big[\overbrace{\delta_y\delta_z\delta_x\varphi_{zx}f_z f_x}^{a_1} x^{*3} + \overbrace{(\delta_y\delta_z\delta_x\varphi_{zx}(f_x + f_z) - \delta_z k_y k_x f_{zx} f_y f_z)}^{a_2} x^{*2} + \overbrace{(k_z\delta_x\varphi_{zx}k_x f_{zx} - \delta_z k_y f_y k_x f_{zx} - \delta_z k_y f_z k_x f_{zx} + \delta_y\delta_z\delta_x\varphi_{zx})}^{a_3} x^* + \overbrace{(-\delta_z k_y k_x f_{zx})}^{a_4}\big] = 0. \tag{6.8}$$

Biophysically acceptable steady-states are given for non-negative steady-states, i.e ($\boldsymbol{x^* \geq 0}$, we therefore exclude the root $x^* = -1/f_x$. To identify the number of positive steady-states, without actually calculating them, we use Descartes' Rules of Signs. Since the parameters of the model are positive we have that $a_1 > 0$ and $a_4 < 0$ but a_2 and a_3 could be either positive or negative. Thus, it remains to change the signs of a_2 and a_3 in a combinatorial manner and check the possible outcomes:

Case 1: If $a_2 > 0$ and $a_3 > 0$ there is only one sign change and therefore only one positive root. Since the polynomial is of 3^{rd} degree, the remaining roots can either be negative or a complex conjugate pair.

Case 2: If $a_2 > 0$ and $a_3 < 0$ there is only one sign change which indicates one positive root leaving the remaining roots to either have a negative sign or be complex conjugate pair.

Case 3: If $a_2 < 0$ and $a_3 < 0$ then this is similar to cases 1 and 2.

Case 4: If $a_2 < 0$ and $a_3 > 0$ we have three sign changes, giving rise to three possibilities: (1) three positive roots, (2) one positive root and two negative roots, (3) one positive root and a complex conjugate pair. Negative roots are eliminated by checking the number of sign changes for $g(x) = f(-x)$, therefore leaving (1) or (3) as possibilities

Considering the aforementioned analysis, it can be concluded that our model can either have one unique steady-state or three steady-states. We are interested in exploring the possibility of bistable behaviour, since this can lead to the emergence of two stable steady-states: one representing a *healthy state* (with high levels of filaggrin and profilaggrin, while kallikrein activity is low), and the other an *unhealthy state* (with low levels of filaggrin and profilaggrin, while kallikrein activity is high). The healthy state corresponds to a competent and normal functioning skin barrier, while the unhealthy state corresponds to a dysfunctional skin barrier.

To determine exact analytical bounds on the region where three positive roots exist a more general tool from real algebraic geometry can be used, namely, Sturm's theorem [312, 313]. However, the resulting set of inequalities is usually difficult to solve analytically or even computationally. Our next step is to characterise the behaviours of the *skin barrier homeostasis model* by performing bifurcation and stability analyses using DDE-BIFTOOL.

Computational characterisation of bistability region

For the nominal parameter (Table 6.1) the system admits three equilibria. The stability of those equilibria are assessed by plotting the eigenvalues on the complex plane (Fig. 6.5). Two of the equilibria are stable (Fig. 6.5a and c), while one is unstable (Fig. 6.5b) confirming that the system exhibits bistability for the nominal parameters. We also assessed the stability of the equilibria for variations of the f_x parameter (Appendix E).

To characterise the behaviours of the *skin barrier homeostasis model* one-parameter (Fig. 6.6a) and two-parameter (Fig. 6.6b) bifurcation diagrams are plotted. We select the filaggrin degradation rate (δ_x), which represents skin desquamation, and profilaggrin post-translation modification rate (k_x) to conduct this analysis. Filaggrin degradation rate can be affected by environmental factors, such as increased pH (a known risk factor

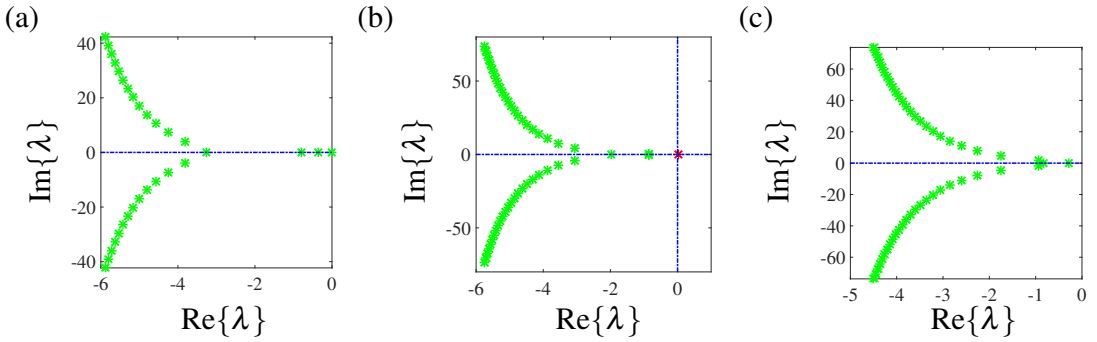


Figure 6.5: Eigenvalues associated to the equilibria of the *skin barrier homeostasis model* for the nominal parameters (Table 6.1), plotted in the complex plane. Green and red asterisks correspond to eigenvalues with $\mathrm{Re}\{\lambda\} < 0$ and $\mathrm{Re}\{\lambda\} > 0$, respectively. Blue dashed lines represent the real and imaginary axis.

of AD [317]), that increase the proteolytic activity of KLK [132] and induce excess skin desquamation. Changes in the post-translation modification of profilaggrin can interfere with the precise coordination of epidermal differentiation programs [303,318], which can lead to diseased phenotypes.

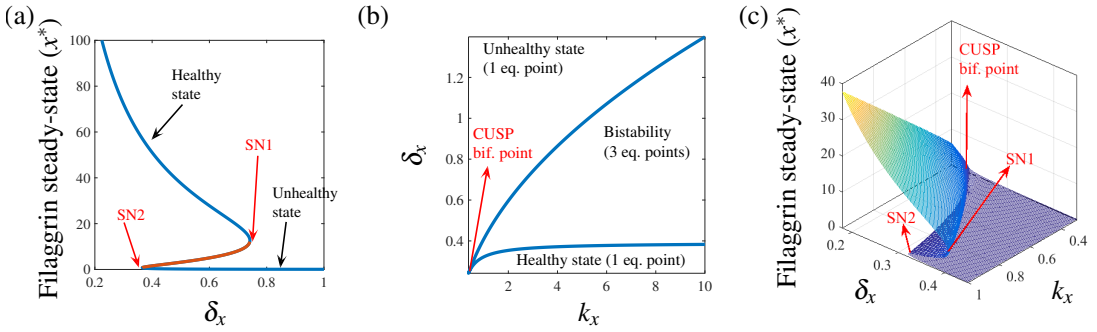


Figure 6.6: Characterisation of the bistable behaviour of the *skin barrier homeostasis model*. (a) One-parameter bifurcation with respect to filaggrin degradation rate (δ_x). Blue and red lines correspond to the stable and unstable steady-states, respectively. The healthy state corresponds to high values of filaggrin, which represents a competent barrier, while the unhealthy state corresponds to low values of filaggrin. The annotation SN denotes a saddle-node bifurcation. (b) Two-parameter bifurcation diagram with respect to the parameters (k_x, δ_x). The blue lines indicate saddle-node bifurcation and the space in-between the blue lines corresponds to the bistability region, where three steady-states exist. The annotation CUSP denotes a cusp bifurcation. (c) Filaggrin steady-state level with respect to the parameters (k_x, δ_x) denoting the saddle-node and cusp bifurcations.

By varying the filaggrin degradation rate, δ_x (Fig. 6.6a), the model is shown to exhibit bistable behaviour. The stable (blue line) steady-state of filaggrin (x^*), corresponding

to the healthy state, exists for values $\delta_x < 0.74$. At this critical value of $\delta_x^* = 0.74$, a saddle-node (SN) bifurcation [170] occurs and the steady-state disappears. The locally asymptotically stable steady-state, corresponding to the unhealthy state exists for $\delta_x > 0.36$, but disappears for lower values through a SN bifurcation. The range $\delta_x \in [0.36, 0.74]$ corresponds to the bistable region where three steady-states exist; two stable (blue lines) and one unstable (red line). This analysis predicts that high desquamation rates result in low levels of filaggrin as seen in AD patients [319].

In Fig. 6.6b we characterise the bistable region with respect to the parameters (k_x, δ_x). Varying these parameters simultaneously the region of bistability is enclosed between two branches of SN bifurcations (blue lines Fig. 6.6b). The two branches collide tangentially at the cusp bifurcation point as depicted in Fig. 6.6b. Fig. 6.6c is a three-dimensional representation of the cusp bifurcation illustrating the steady-state level of filaggrin. For combinations of high desquamation rate and low profilaggrin processing the system exhibits a unique steady-state with low filaggrin (Fig. 6.6c) and profilaggrin levels, and high KLK activity thus resulting in an unhealthy state. On the other hand, low desquamation rates and high post-translational modification rates of profilaggrin lead to a unique healthy steady-state.

6.4.3 System dynamics

In this section the dynamics of the *skin barrier homeostasis model* are simulated with respect to barrier-induced damage. We then characterise the convergence to the *healthy state* or *unhealthy state* and the recovery time (Δt_r) in the $(t_{\bar{u}}, \bar{u})$-space for the nominal parameters. Finally, the convergence behaviour, as well as, the recovery time are explored with respect to parameter changes.

Emergence of a pathological state depends on the stimulus strength and duration

To understand the stimulus effects on the dynamic behaviour of the *skin barrier homeostasis model*, we simulate different combinations of stimulus strength and duration, $(t_{\bar{u}}, \bar{u})$ (Fig. 6.7). With this analysis we can predict the minimum strength and duration combinations that drive the system from the healthy state to the unhealthy state.

For stimulus strength and duration conditions $(t_{\bar{u}}, \bar{u}) = (5, 0.5)$ (Fig. 6.7, *blue*), filaggrin and profilaggrin levels return to their homeostatic behaviour, and kallikrein activity is kept low, signifying that the system converges to the *healthy state*. By increasing stimulus strength by an order of magnitude, $\bar{u} = 50$ (Fig. 6.7, *red*), while keeping the stimulus duration the same, the dynamics illustrate convergence to the *unhealthy state*. Similarly, convergence to the *unhealthy state* is predicted with a 3-fold increase in only the stimulus duration (Fig. 6.7, *yellow*). In both cases, simulation results display low filaggrin and profilaggrin levels, while kallikrein activity is increased almost 5-fold, representing compromised barrier function.

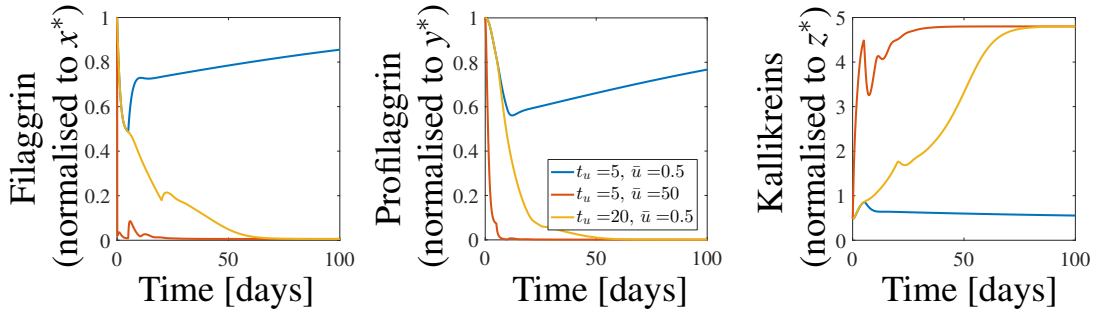


Figure 6.7: Effect of different stimuli strengths and durations on the dynamics of the *skin barrier homeostasis model*. *Left*: Normalised dynamics of filaggrin ($x(t)$), *Centre*: profilaggrin ($y(t)$), and *Right*: kallikreins ($z(t)$), with $(t_{\bar{u}}, \bar{u}) = (5, 0.5)$ (blue), $(t_{\bar{u}}, \bar{u}) = (5, 50)$ (red), and $(t_{\bar{u}}, \bar{u}) = (20, 0.5)$ (yellow).

The recovery or non-recovery behaviour and the associated recovery time, with respect to different stimuli parameters, is systematically investigated (Fig. 6.8) for the nominal model parameters. By varying the stimulus strength and duration the boundary determining convergence to the *healthy* or *unhealthy state* (Fig. 6.8, *left*) is identified. This boundary segregates the $(t_{\bar{u}}, \bar{u})$-space and describes the combinations of minimum stimulus strength and duration required to push the trajectories of the system into the basins of attraction of the *healthy* and *unhealthy states*. We will term this boundary the *$(t_{\bar{u}}, \bar{u})$-manifold* of the *skin barrier homeostasis model*. The calculated recovery time (Fig. 6.8, *right*) increases with respect to the strength or duration of stimulus, thus establishing a dose-dependent relationship between the recovery time (Δt_r), and stimulus strength and duration.

The results presented here suggest that strong enough stimuli or prolonged stimuli obstruct the recovery processes of the skin barrier and can even lead to the emergence of a pathological state. During the process of recovery, barrier function is compromised

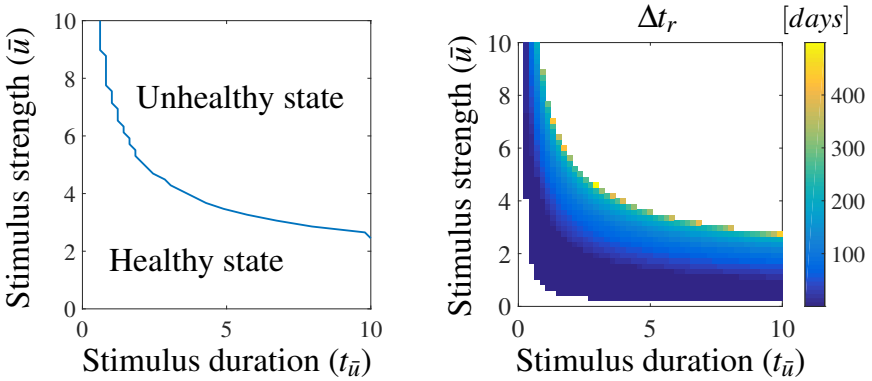


Figure 6.8: Effect of different stimuli strengths and durations on the convergence and recovery time (Δt_r) of the *skin barrier homeostasis model*. *Left:* Nominal ($t_{\bar{u},\bar{u}}$)-manifold illustrating convergence to the healthy or unhealthy state with respect to stimulus strength and duration. *Right:* Recovery time to the healthy steady-state. White space on the upper right corner corresponds to the unhealthy steady-state, while white space on the bottom left corner are cases where barrier damage is minimal and recovery time is not measured.

and increased permeability to allergens may result in the activation of inflammatory pathways [30, 47, 320]. Moreover, suboptimal barrier function conditions can increase unwanted pathogen colonisation in the skin [47, 127], further compromising the skin barrier, and exacerbating chronic inflammation [321]. It is therefore crucial to decrease recovery time with the goal of preventing disease progression.

Note that recovery times at or close to the ($t_{\bar{u},\bar{u}}$)-manifold are high (Fig. 6.8, *right*). This sluggish behaviour is characteristic of bistable systems with saddle-node bifurcations due to a bottleneck region near the bifurcation [170]. At the bifurcation point two steady-states coalesce, however, due to the influence of a saddle remnant the flows of the dynamic system are slow, which result in time delays to pass through the bottleneck [322]. This behaviour has been studied in the literature as a potential early-warning singal to identify if a disease is close to a critical transition or "tipping point" [235, 323, 324].

Robustness and recovery time with respect to parameters

In this section the "robustness" of the *skin barrier homeostasis model* is explored in response to an external stimulus, while varying certain model parameters. Parameter variations can shift the ($t_{\bar{u},\bar{u}}$)-manifold, therefore inceasing or decreasing the region of convergence of the *healthy state*. We therefore say that the system is more robust

when the region of convergence of the *healthy state* increases, and less robust for the opposite (Fig. 6.9). Furthermore, parameter variations can either increase or decrease the recovery time, therefore resulting in increased or decreased susceptibility to external stimuli, respectively (Fig. 6.10 and 6.11).

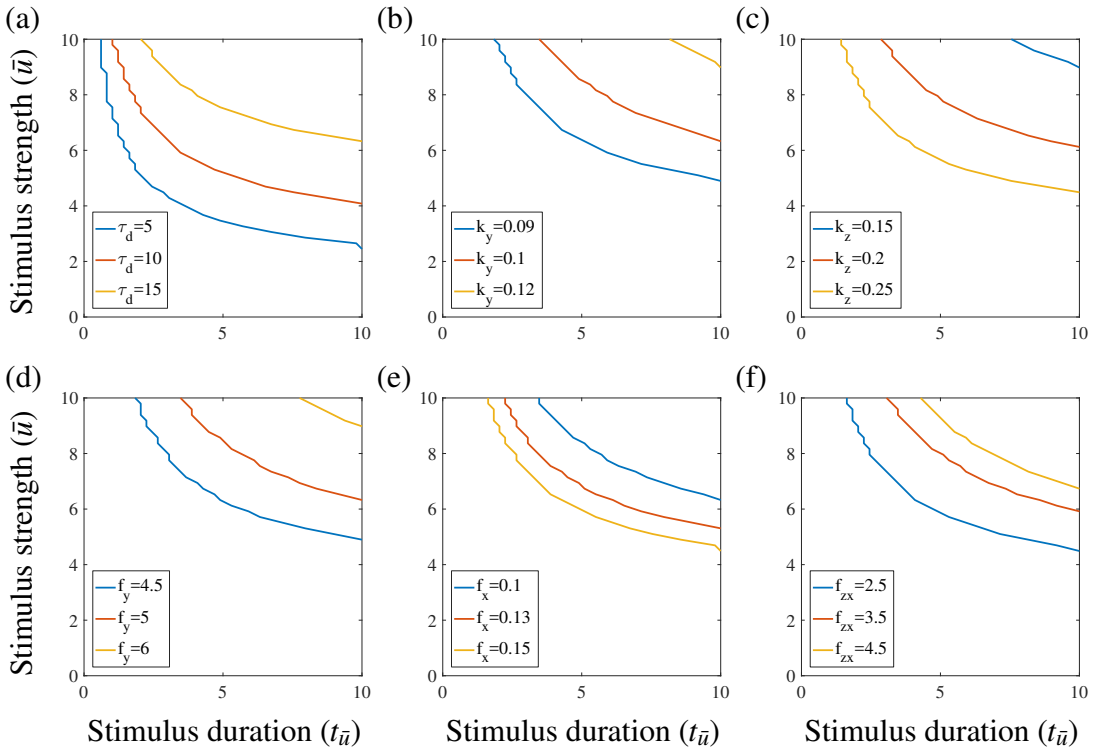


Figure 6.9: Stimulus induced $(t_{\bar{u},\bar{u}})$-manifolds of the *skin barrier homeostasis model* with respect to changes in the model parameters: (a) $\tau_d = \{5, 10, 15\}$; (b) $k_y = \{0.09, 0.1, 0.12\}$; (c) $k_z = \{0.15, 0.2, 0.25\}$; (d) $f_y = \{4.5, 5, 6\}$; (e) $f_x = \{0.1, 0.13, 0.15\}$; (f) $f_{zx} = \{2.5, 3.5, 4.5\}$. Points below and above the $(t_{\bar{u},\bar{u}})$-manifold correspond to $(t_{\bar{u}}, \bar{u})$ combinations leading to the *healthy state* and *unhealthy state*, respectively.

Increasing the delay in the feedback that modulates expression of filaggrin precursors (τ_d) increases robustness to external stimuli (Fig. 6.9a). The $(t_{\bar{u}}, \bar{u})$-region in which the system converges to the *healthy state* increases. The increased robustness is also associated with decreased recovery times (Fig. 6.10a), although, near the $(t_{\bar{u},\bar{u}})$-manifold high recovery times are predicted when $\tau_d = 15$ (days) (Fig. 6.10, *right*), possibly due to the bottleneck effect.

We next consider variations in the de-novo synthesis rate of filaggrin precursors (k_y) and basal kallikrein activity (k_z). Increasing k_y confers robustness by shifting the $(t_{\bar{u},\bar{u}})$-

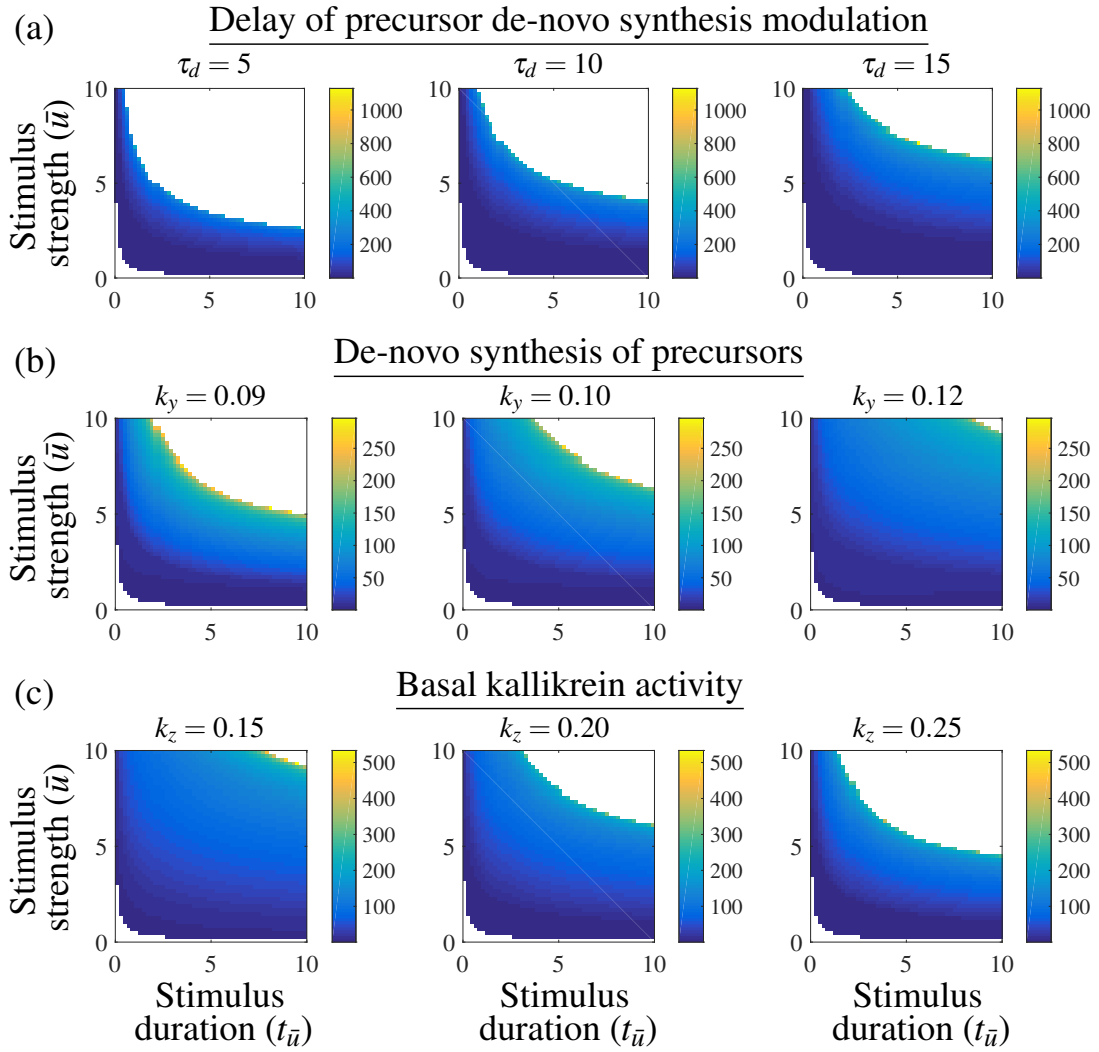


Figure 6.10: Calculated recovery time (Δt_r) for convergence to the *healthy state* for different parameter values: (a) $\tau_d = \{5, 10, 15\}$; (b) $k_y = \{0.09, 0.1, 0.12\}$; (c) $k_z = \{0.15, 0.2, 0.25\}$. White space above the $(t_{\bar{u},\bar{u}})$-manifold corresponds to the *unhealthy state*, while the white space in the lower left corner corresponds to $(t_{\bar{u}}, \bar{u})$ combinations that do not cause sufficient barrier damage.

manifold diagonally upwards (Fig. 6.9b), while the opposite is observed when k_z is increased (Fig. 6.9c). Low values of de-novo synthesis rate (k_y), mimic mutations in the filaggrin gene [95] or the effects of chronic inflammation that reduces filaggrin expression as observed in AD patients [98]. Kallikrein activity in the skin is pH-dependent [325], therefore, increased k_z values imitate aberrant KLK activity due to the increased pH level, as for example, in AD patients [317]. Recovery time is linked to the shift in the

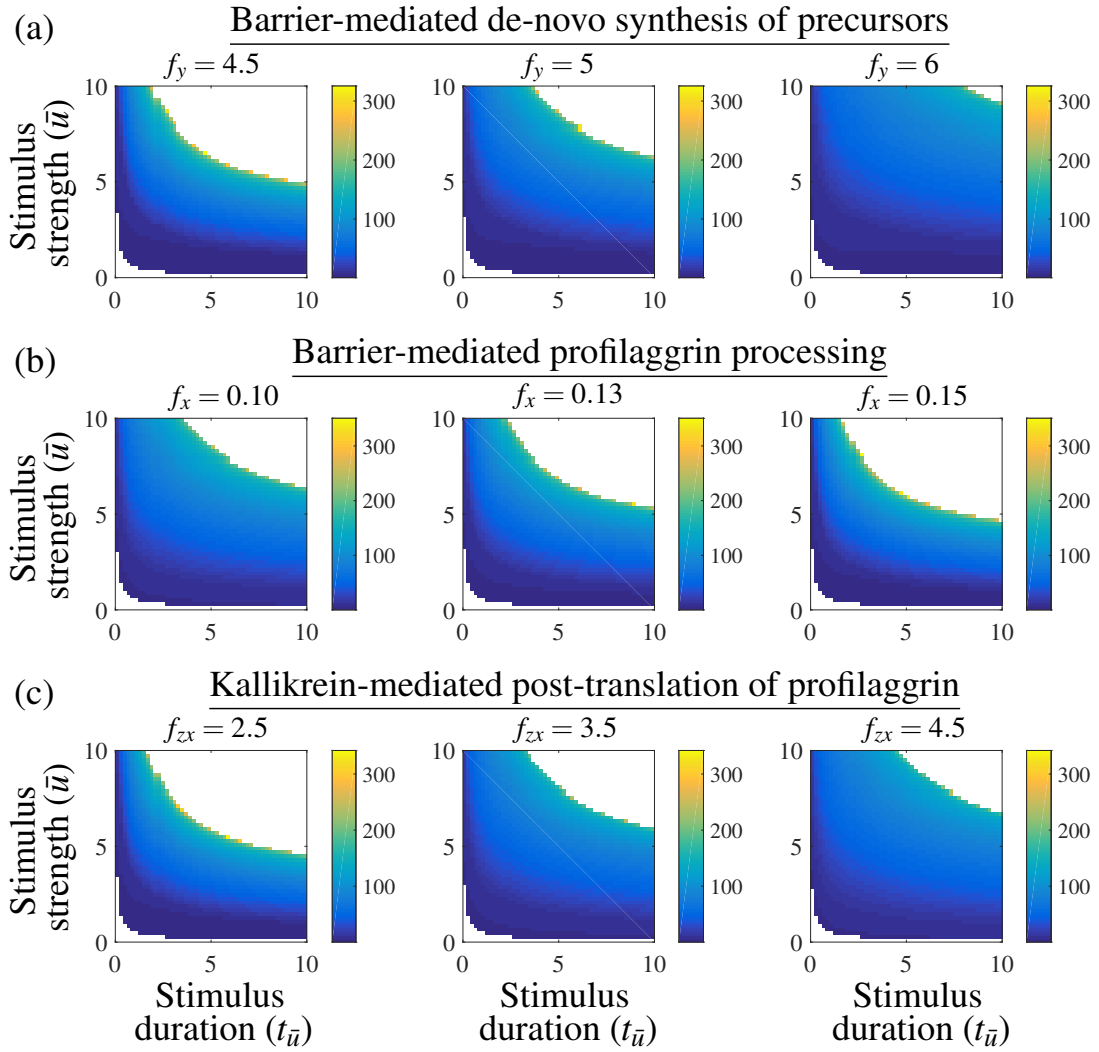


Figure 6.11: Calculated recovery time (Δt_r) for convergence to the *healthy state* for different parameter values: (a) $f_y = \{4.5, 5, 6\}$; (b) $f_x = \{0.1, 0.13, 0.15\}$; (c) $f_{zx} = \{2.5, 3.5, 4.5\}$. White space above the $(t_{\bar{u},\bar{u}})$-manifold corresponds to the *unhealthy state*, while the white space in the lower left corner corresponds to $(t_{\bar{u}}, \bar{u})$ combinations that do not cause sufficient barrier damage.

$(t_{\bar{u},\bar{u}})$-manifold and accordingly decreases as k_y increases (Fig. 6.10b), but increases as k_z increases (Fig. 6.10c).

We then explore variations in the feedback rate modulating profilaggrin de-novo synthesis, f_y (Fig. 6.9d), as well as, two feedback rates modulating profilaggrin post-translational modification, namely f_x (Fig. 6.9e) and f_{zx} (Fig. 6.9f).

High barrier-mediated precursor production rates (f_y) result in a more robust system

as the *healthy state* region of convergence increases (Fig. 6.9d). Mechanistically, higher values of f_y compensate for the decreased filaggrin level, after pertubation, by increasing the magnitude of the positive feedback $(1 + f_y x(t - \tau_d))$, hence leading to increased de-novo synthesis rates. A reduction of the barrier-mediated precursor rate can represent decreased expression of calcium sensors [326] or their downstream targets in basal keratinocytes [326, 327], which can interfere with the terminal differentiation of keratinocytes [328]. This can also lead to reduced levels of calcium in the outer epidermis observed in AD patients [307]. The corresponding recovery times are reduced (Fig. 6.11a), hence, illustrating less susceptibility to external stimuli.

Barrier-mediated profilaggrin processing operates via a negative feedback with a strength f_x. Increasing the strength of this negative feedback mimics a suppression of protease activity involved in the processing of profilaggrin, such as caspase [329], and may affect the terminal differentiation process of keratinocytes [301]. Accordingly, the $(t_{\bar{u},\bar{u}})$-manifold shifts diagonally downwards (Fig. 6.9e), which implies a decrease in robustness, while recovery times increase (Fig. 6.11b).

Kallikrein-mediated post-translation modification of profilaggrin (f_{zx}) appears to increase robustness (Fig. 6.9f), which illustrates the importance of kallikrein activity in the processing of profilaggrin and the recovery of the barrier as suggested in [303]. The activity of kallikrein-5 is reduced in the presense of alcohols due to enzyme denaturation [330], which may result in reduced processing of barrier precursors, represented in our model by low f_{zx} values. The corresponding recovery time decreases for increasing values of f_{zx} (Fig. 6.11c).

Skin barrier homeostasis model summary

In Section 6.4.1 an expanded mathematical model of filaggrin regulation is described, which includes the regulatory mechanisms of kallikreins, and is fitted to experimental data (Fig. 6.4b). The suggested regulatory structure, composed of one positive feedback and two negative feedbacks, displays recovery dynamics (Fig. 6.4b).

In Section 6.4.2 it was established that the model can exhibit bistable behaviour (Fig. 6.6) and the two stable steady-states are classified as the *healthy* and *unhealthy states*. Parameter sweeps for the parameters representing filaggrin degradation as a result of skin desquamation (δ_x) and post-translational modification of profilaggrin (k_x) revealed

the parameter regions of the existence of one unique steady-state and three steady-states, of which two are stable (Fig. 6.5). High desquamation rates (δ_x) and low profilaggrin processing (k_x) resulted in low filaggrin levels, corresponding to the unhealthy state, while the healthy state is given for low δ_x and high k_x values (Fig. 6.6c). In the region of bistability the healthy and unhealthy states co-exist and the convergence to either state depends on external stimuli, representing mechanically or chemically-induced barrier pertubation.

The dynamic behaviour of the model with respect to an external stimulus is then explored (Section 6.4.3). Prolonged exposure or strong enough stimuli were associated with increased recovery times and could eventually lead to a pathophysiologic state (Fig. 6.7). For the nominal parameter set (Table 6.1), the $(t_{\bar{u},\bar{u}})$-manifold of the system is characterised, which defines the minimum stimulus strength and duration combinations that push the trajectories of the system into the basin of attraction of the unhealthy state (Fig. 6.8a). The recovery time (Δt_r) is also characterised with respect to the stimulus parameters $(t_{\bar{u}}, \bar{u})$, and it was shown to exhibit a dose-dependent relationship with respect to stimulus strength and duration (Fig. 6.8b).

Finally, the robustness of the system and the recovery time are explored for different model parameter variations (Section 6.4.3). The delay in de-novo synthesis modulation of profilaggrin (τ_d) by barrier pertubation increased robustness (Fig. 6.9a) and lowered recovery times (Δt_r) (Fig. 6.10a). Genetic risk factors such as reduced filaggrin expression (k_y) [95, 98] and increased activity of KLK (k_z) [325], commonly presented in AD patients, resulted in longer recovery times (Fig. 6.10b and c, respectively) and lowered robustness to external perturbations (Fig. 6.9b and c, respectively). Altered calcium concentration in the epidermis modulates terminal differentiation [30], and in our model the calcium dependent feedback strengths f_y and f_x mediate its effects. Increasing f_y reduced the susceptibility (Fig. 6.9d) to external perturbations and decreased recovery time (Fig. 6.11a). Reduced caspase-14 profilaggrin processing (represented as an increase in f_x) resulted in increased susceptibility (Fig. 6.9e) and higher recovery times (Fig. 6.11b). Exploration of the feedback KLK-induced profilaggrin processing illustrated less susceptibility (Fig. 6.9f) and lower recovery times (Fig. 6.11c), for higher values of f_{zx}.

6.5 Discussion

In this chapter we propose a mathematical model that describes the feedback mechanisms that regulate epidermal homeostasis based on the key epidermal structural component filaggrin and the regulation of proteases, namely kallikreins (KLK). The regulatory network represented by the mathematical model, was constructed by assimilating information from the biological literature (Fig. 6.1a). The model describes a set of DDEs composed of dual feedback mechanisms and includes the delayed effect of altered de-novo synthesis of barrier precursors with respect to barrier damage.

To analyse this network a reductionist approach is followed by first considering a subnetwork with one negative and one positive delayed feedback (*self-recovery model*, Section 6.3). We showed that this model admits a unique stable steady-state (Section 6.3.2), given the proposed feedback architecture. Therefore, transient skin pertubation or parameter variations do not disrupt the self-recovery property, as a consequence of this unique steady-state.

Subsequently, the complete network is considered, which includes the regulation of kallikreins in addition to the previous regulatory structure, and is composed of two negative feedbacks and one positive delayed feedback (*skin barrier homeostasis model*, Section 6.4). This model exhibits recovery dynamic behaviour, which results from the topology of the feedbacks and the fitted parameters (Fig. 6.4b). The addition of KLK-mediated feedbacks, presented in the *skin barrier homeostasis model*, resulted in bistable behaviour (Fig. 6.6), and was thus able to reproduce a pathological state (unhealthy state). Therefore, this model can represent both the characteristic self-recovery of the skin barrier and the loss of homeostasis typical of severe disease.

Both the *self-recovery model* and *skin barrier homeostasis model* exhibit a dose-dependent relationship between barrier-induced damage and recovery time (Δt_r), Fig. 6.3 (*right*) and Fig. 6.8 (*right*), respectively. Moreover, combinations of sufficiently high stimulus strength and duration in the *skin barrier homeostasis model* resulted to the system converging to the unhealthy state (Fig. 6.7 and Fig. 6.8, *left*), suggesting that skin barrier perturbations can lead to a diseased phenotype [331].

We investigated parameter variation effects representing genetic and environmental risk factors of AD on the dynamics of the *skin homeostasis model*. The risk factors characterise fragility points of the regulatory network that can increase or decrease the

susceptibility to environmental perturbations (Fig. 6.9) and alter the characteristic self-recovery of the skin barrier (Fig. 6.10 and Fig. 6.11). It would not only be interesting to explore synergistic effects of multiple risk factors to determine their effect on the development of diseased phenotypes, as in Fig. 6.6b and Fig. 6.6c, but also to investigate their effects on the recovery time.

Recovery time could be a useful metric to measure disease severity and eventual progression. Slow recovery can lead to the activation of adaptive immune responses (as predicted in Chapter 3), since during the recovery time skin barrier function is at a suboptimal state and there is increased permeability to invading pathogens. The slow characteristic recovery behaviour, as a consequence of the delay in de-novo synthesis of barrier precursors or other model parameters, can be used as a potential early-warning signal [235] to identify virtual patient cohorts with susceptible genotypes. Moreover, this qualitative systems-level investigation could enable the discovery of biomarkers or the development of therapeutic interventions that target the specific fragility points of the network.

Our simple mathematical model represents the skin barrier through the production of its structural component filaggrin. However, other structural components in the epidermis, such as lipids [298], play an important role in its homeostasis. The regulation of lipids in the epidermis displays similar feedback mechanisms, as proposed in [332], with the model we constructed in this chapter. A unified regulatory network, combining lipids and structural proteins, can elucidate the mechanisms with which both of these components are co-regulated and result in the protective functions of the skin barrier. Furthermore, our model did not incorporate the modulation of filaggrin gene expression that occurs due to chronic inflammation [53], although this effect was implicitly explored through the analysis of parametric variations of k_y (Fig. 6.9 and Fig. 6.10b). Therefore, to investigate the effects of acquired filaggrin deficiencies due to chronic inflammation, the model can be extended to include feedback-downregulation profilaggrin de-novo expression. Our model was able to replicate experimental data. Integrating our mathematical model with other experimental data that measure the activity of KLK or the concentration of filaggrin and profilaggrin proteins would identify suitable parameters and provide a validated quantitative framework with predictive power.

In summary, the mechanistic model of skin barrier homeostasis proposed in this chapter provides a plausible representation of the biochemical mechanisms that are responsible for the robust self-recovery of the healthy skin. This model also suggests that strong

perturbations of the skin barrier (eg, by persistent chemical damage) can lead to a long-lasting loss of skin barrier function (convergence to a unhealthy equilibrium point) and with that, contribute to epidermal pathogenesis.

Chapter 7

Conclusion and Future work

7.1 Summary

In this thesis we constructed a mathematical model representing key regulatory interactions involved in the skin disease atopic dermatitis (AD) by assimilating information for those interactions from biological literature. The complex interplay of the regulatory interactions and the multifactorial nature of AD motivated us to use a systems biology approach in order to investigate AD pathogenesis and elucidate its underlying pathogenic mechanisms. Furthermore, the models formulated in this Thesis have established the necessary quantitative framework required to develop a computational framework for the design of treatment protocols.

The mathematical model introduced in Chapter 3, illustrates the mechanisms of regulation between epidermal barrier function, innate and adaptive immune responses, and pathogen infiltration through the epidermal barrier. Deregulation of these mechanisms, due to either genetic risk factors or environmental stressors, reproduced the multistage pathogenesis of AD from onset and then progression into severer forms. The key motif identified, that underlies the onset and progression, consisted of two concatenated bistable switches ("double switch"). The initiation of inflammation, that induces an AD flare, is regulated by innate immune receptors (R-switch), while T_H2 sensitisation is established (G-switch) by persistent or oscillatory AD flares with sufficiently short period. Varying two parameters in our model that represent the most common genetic risk factors of AD, revealed virtual cohorts with four distinct phenotypes: (a) recovery,

(b) bistability, (c) oscillations, and (d) chronic damage. With this model we also explored the effects of preventive emollient treatment and showed that emollients decrease the susceptibility to develop T_H2 sensitisation by increasing the threshold of stimulus required to induce it.

Furthermore, using our mathematical model we developed a computational framework to design temporal treatment protocols, based on optimal control theory, for the symptom management of patients suffering from moderate to severe AD (Chapter 4 and 5). With our framework we can designate specific target levels ($\hat{P}_{\mathrm{r}}$ and $\hat{P}_{\mathrm{m}}$) for the pathogen load, which result in different treatment patterns and total treatment amount. These target levels can serve as design criteria to modify the course of treatment depending on the patient's disease state or preference, in terms of corticosteroid potency, and inform clinicians on the most appropriate course of action for the relief of symptoms. Moreover, effective treatment protocols could be designed depending on the genotype of patients with respect to the most common risk factors of AD. This methodology stratified patients into groups in which treatment protocols were successful or unsuccessful; this categorisation could potentially guide clinical recommendation of treatments by suggesting alternative or additional pharmacological treatments. In addition, those unresponsive to the treatment protocols could represent AD patients with different sub-phenotypes or endotypes, and identifying such classes of patients has been suggested as being "crucial for the success of precision medicine as a new approach to patient management" [333]. Arguably, computationally assisted recommendations coupled with expert advice from clinical practitioners may help reduce the socioeconomic burden of the disease. Poor adherence to topical corticosteroid treatment by patients has been suggested as a cause for the unresponsiveness of such treatments [334] and is considered a major factor limiting treatment outcomes [335]. We therefore simulated different scenarios of non-adherence to investigate its long-term effects on the management of AD. Specifically, non-adherence to the treatment protocols during the induction or maintenance phases suggest a relapse of AD flares, and eventually symptoms, that require higher treatment doses for longer duration. Our computational results could be potentially used as a visual aid to educate patients on the side-effects of non-adherence, which could result in reducing the social and economic burden of patients living with chronic AD.

Our computational framework forms the first systematic design of treatments for AD and serves as a proof-of-concept that optimising corticosteroid dosage and frequency in a patient-specific manner can benefit certain patient cohorts. To tackle the high degree of heterogeneity in clinical phenotypes, we would like to in the future use our approach

to optimise the temporal application of multiple treatments concurrently, so as to move away from the "one size fits all" paradigm currently used [34].

To numerically integrate our hybrid mathematical model we developed a MATLAB-based computational platform using the in-build *event location* functionality. Our code uses a recursive strategy to switch between the governing subsystems of the hybrid model depending on when the switching manifolds have been reached. Each subsystem is numerically integrated and the final solution, in the predefined time span, is concatenated to give the complete solution of the hybrid model. The user only needs to define the mathematical equations of the ODE and the switching manifolds. This approach deals with hybrid systems that are continuous in the state-variables, but have a discontinuous derivative.

Finally, in Chapter 6, we constructed a mathematical model representing a regulatory network of epidermal homeostasis based on the biochemical interactions of the structural component filaggrin and kallikrein proteases. Our modelling approach utilised DDEs in order to understand the effects of the delay of de-novo filaggrin precursor expression after perturbation of the skin barrier. This model revealed plausible biological control mechanisms that lead to the recovery dynamics of the epidermal barrier. Specifically, our qualitative approach revealed that the regulatory structure, composed of one positive delayed feedback and two negative feedback mechanisms, can explain the recovery dynamics of the epidermal barrier upon perturbation. Strong stimuli with sufficiently long duration can promote the loss of skin barrier function and homeostasis, and can lead to the development of pathophysiologic conditions such as AD. We assessed the recovery dynamics by introducing the metric of recovery time, which is related to systemic sensitisation in the following way: longer recovery times result in prolonged periods where the skin barrier is at a sub-optimal state. Under this condition, individuals are susceptible to the invasion of allergens or pathogens, due to increased permeability, and can therefore lead to systemic sensitisation. Although in our model we did not specifically include the process of systemic sensitisation, we explored how this process can occur by sustained or periodic activation of innate immune receptors in Chapter 3. Furthermore, we explored the effects of genetic risk factors on the recovery dynamics of the model. Genetic risk factors decrease the robustness of the system and increase the susceptibility of the skin barrier by increasing the recovery time. The delayed recovery could be potentially used as an "early warning" signal for the detection of predisposed individuals.

With the work presented in this thesis we provide a systems-level theoretical framework for the *in silico* study of the pathogenic mechanisms of AD, the control mechanisms leading to epidermal barrier recovery, and the design of optimised patient-specific treatment protocols.

7.2 Future work

In the hybrid model, we incorporated treatments using simple mathematical terms that phenomenologically describe their effect. Specifically, emollient and coal tar treatment directly affect barrier integrity in an additive and multiplicative way, respectively, while corticosteroids inhibit inflammatory responses induced by innate immune receptors via a term $1/(1 + \beta C(t))$. Although their simplicity enabled the design of dynamic treatment protocols, exact pharmacokinetic processes, such as drug absorption, distribution, metabolism, and elimination [336], are not taken into account. Our results would greatly benefit by the acquisition and integration of dynamic data of AD patients after application of treatments, as well as, pharmacokinetic studies, in order to identify more appropriate and realistic treatment mathematical forms.

Corticosteroid treatment is associated with several documented side effects [337]. In our model we included the corticosteroid side effect associated with increased propensity to skin infections [338], which result from the reduction of inflammation-induced pathogen eradication. However, the most common side effect associated with corticosteroid use is skin atrophy. Our model could be extended to study corticosteroid-induced skin atrophy and how it may limit the potential application of corticosteroids for the treatment of AD.

Further, using our mathematical model we can incorporate other forms of treatment to identify their optimal scheduling, as well as, to explore the effects of multiple concurrent treatments. For example, the use of antibiotics in combination with corticosteroids has been suggested to produce better outcomes in AD patients prone to infection [48]. Monoclonal antibody therapy provides an exciting new pathway for the treatment of moderate to severe AD. Extending our model to specifically include the dynamics of the cytokine IL4 and the effects of dupilumab, integrated with data obtained in Phase III clinical trials [113], will allow us to investigate the use of this biologic in the treatment of AD.

To study the effects of preventive treatments, we are currently conducting a more systematic investigation by considering not only emollient, but also corticosteroid and antibiotic treatments. Our approach is based on bifurcation analysis of the hybrid model by considering the treatments as constant parameters, and we investigate how these treatments modify the regions of distinct phenotypes in the (κ_P, α_I)-parameter space (Paper submitted in the *Journal of Theoretical Biology*).

Another possible extension is the design of more advanced optimal control strategies, for example Model Predictive Control (MPC) [248]. MPC establishes a closed-feedback control strategy by measuring the evolution of the state-variables at specific intervals and identifying actuation signals across said intervals, while the optimisation of the objective function is performed over the complete future horizon. After calculating the complete sequence of actuator signals within the horizon, only the first step in the sequence is applied, establishing the receding horizon. Since there are regular measurements of the real system's states, this approach could potentially deal with problems such as model mismatch and unexpected disturbances (e.g. non-adherence to treatments or increased pathogen loads due to changes in the environment). Moreover, in all natural systems the effects of actuators is limited due to physical constraints and MPC is suitable in dealing with such hard constraints by embedding them in the optimal control problem formulation [339]. We recently submitted a conference paper exploring the design of optimal treatments using a MPC algorithm in the *IEEE-2018 5th International Conference on Control, Decision and Information Technologies*.

Further validation of model predictions is required with experimental and clinical data, especially in response to transient behaviour in the context of treatment strategies. Calibration of our model with *in vitro* and animal model data can provide clinically relevant predictions and effective design of treatment protocols. Non-invasive optimal methods such as Raman spectroscopy and multiphoton microscopy [340] can measure skin barrier hydration [104] and composition [341], which are representative of barrier integrity ($B(t)$). Cytokine levels and immune cell population measurements can be used to assess inflammation [342].

To uncover the mechanisms of acquired deficiencies in filaggrin expression patterns due to excessive inflammation, we can extend the *skin barrier homoeostasis model*, as suggested in Chapter 6, by including a second negative feedback in the regulatory structure. Furthermore, epidermal barrier lipids are another important structural component and together with filaggrin are responsible for many of the skin barrier's protective functions

[343]. The skin of AD patients manifests with deficient lipid composition and processing [344], suggesting a role in its pathogenesis, however, the underlying mechanisms with which this occurs are not readily understood. By proposing mechanistic models of lipid regulation in the epidermis we can investigate their role in the pathogenesis of AD. In the future we can consider substituting the phenomenological representation of barrier recovery in the model introduced in Chapter 3, with the mechanistic model introduced in Chapter 6. This will permit a mechanistic interpretation of the characteristic self-recovery property of the barrier in the model of AD pathogenesis and its effect on the development of systemic sensitisation.

Bibliography

[1] Rebecca Berke, Arshdeep Singh, and Mark Guralnick. Atopic dermatitis: an overview. *Am. Fam. Physician*, 86(1):35–42, jul 2012.

[2] Hywel C. Williams. Atopic Dermatitis. *N. Engl. J. Med.*, 352(22):2314–2324, jun 2005.

[3] A. Wollenberg, A. Oranje, M. Deleuran, D. Simon, Z. Szalai, B. Kunz, A. Svensson, S. Barbarot, L von Kobyletzki, A. Taieb, M de Bruin-Weller, T. Werfel, M. Trzeciak, C. Vestergard, J. Ring, and U. Darsow. ETFAD/EADV Eczema task force 2015 position paper on diagnosis and treatment of atopic dermatitis in adult and paediatric patients. *J. Eur. Acad. Dermatology Venereol.*, 30(5):729–747, may 2016.

[4] Aaron M. Drucker, Annie R. Wang, Wen-Qing Li, Erika Sevetson, Julie K. Block, and Abrar A. Qureshi. The Burden of Atopic Dermatitis: Summary of a Report for the National Eczema Association. *J. Invest. Dermatol.*, 137(1):26–30, jan 2017.

[5] E. Vakirlis, E. Lazaridou, TG Tzellos, S. Gerou, D. Chatzidimitriou, and D. Ioannides. Investigation of cytokine levels and their association with SCORAD index in adults with acute atopic dermatitis. *J. Eur. Acad. Dermatology Venereol.*, 25(4):409–416, apr 2011.

[6] W. Peng and N. Novak. Pathogenesis of atopic dermatitis. *Clin. Exp. Allergy*, 45(3):566–574, mar 2015.

[7] E. Gomez-de la Fuente. Can Atopic Dermatitis Be Prevented? *Actas Dermo-Sifiliograficas (English Ed.*, 106(4):278–284, may 2015.

[8] L. F. Eichenfield, M. Boguniewicz, E. L. Simpson, J. J. Russell, J. K. Block, S. R. Feldman, A. R. Clark, S. Tofte, J. D. Dunn, and A. S. Paller. Translating Atopic Dermatitis Management Guidelines Into Practice for Primary Care Providers. *Pediatrics*, 136(3):554–565, sep 2015.

[9] Ehrhardt Proksch, Regina Fölster-Holst, and Jens-Michael Jensen. Skin barrier function, epidermal proliferation and differentiation in eczema. *J. Dermatol. Sci.*, 43(3):159–169, sep 2006.

[10] Nanette B Silverberg and Jonathan I. Silverberg. Inside out or outside in: does atopic dermatitis disrupt barrier function or does disruption of barrier function trigger atopic dermatitis? *Cutis*, 96(6):359–61, dec 2015.

[11] Stephan Weidinger, Thomas Illig, Hansjörg Baurecht, Alan D. Irvine, Elke Rodriguez, Amalia Diaz-Lacava, Norman Klopp, Stefan Wagenpfeil, Yiwei Zhao, Haihui Liao, Simon P. Lee, Colin N. A. Palmer, Claudia Jenneck, Laura Maintz, Tobias Hagemann, Heidrun Behrendt, Johannes Ring, Markus M. Nothen, W. H Irwin McLean, and Natalija Novak. Loss-of-function variations within the filaggrin gene predispose for atopic dermatitis with allergic sensitizations. *J. Allergy Clin. Immunol.*, 118:214–219, 2006.

[12] Thomas Werfel, Jean Pierre Allam, Tilo Biedermann, Kilian Eyerich, Stefanie Gilles, Emma Guttman-Yassky, Wolfram Hoetzenecker, Edward Knol, Hans Uwe Simon, Andreas Wollenberg, Thomas Bieber, Roger Lauener, Peter Schmid-Grendelmeier, Claudia Traidl-Hoffmann, and Cezmi A. Akdis. Cellular and molecular immunologic mechanisms in patients with atopic dermatitis. *J. Allergy Clin. Immunol.*, 138(2):336–349, 2016.

[13] Bogusław Nedoszytko, Małgorzata Sokołowska-Wojdyło, Katarzyna Ruckemann-Dziurdzińska, Jadwiga Roszkiewicz, and Roman J. Nowicki. Chemokines and cytokines network in the pathogenesis of the inflammatory skin diseases: atopic dermatitis, psoriasis and skin mastocytosis. *Adv. Dermatology Allergol.*, 2(2):84–91, 2014.

[14] Jonathan J. Lyons, Joshua D. Milner, and Kelly D. Stone. Atopic Dermatitis in Children. *Immunol. Allergy Clin. North Am.*, 35(1):161–183, feb 2015.

[15] Yin-Hsiu Chien, Wuh-Liang Hwu, and Bor-Luen Chiang. The Genetics of Atopic Dermatitis. *Clin. Rev. Allergy Immunol.*, 33(3):178–190, dec 2007.

[16] Simon F Thomsen, Charlotte S Ulrik, Kirsten O Kyvik, Jacob V B Hjelmborg, Lars R Skadhauge, Ida Steffensen, and Vibeke Backer. Importance of genetic factors in the etiology of atopic dermatitis: a twin study. *Allergy Asthma Proc.*, 28(5):535–9, 2007.

[17] Sophie Nutten. Atopic dermatitis: Global epidemiology and risk factors. *Ann. Nutr. Metab.*, 66:8–16, 2015.

[18] Raffaela Campana, Sheron Dzoro, Irene Mittermann, Elena Fedenko, Olga Elisyutina, Musa Khaitov, Alexander Karaulov, and Rudolf Valenta. Molecular aspects of allergens in atopic dermatitis. *Curr. Opin. Allergy Clin. Immunol.*, 17(4):269–277, aug 2017.

[19] Michael J. Cork, Darren A. Robinson, Yiannis Vasilopoulos, Adam Ferguson, Manar Moustafa, Alice MacGowan, Gordon W. Duff, Simon J. Ward, and Rachid Tazi-Ahnini. New perspectives on epidermal barrier dysfunction in atopic dermatitis: Geneenvironment interactions. *J. Allergy Clin. Immunol.*, 118(1):3–21, jul 2006.

[20] Hans Bisgaard, Angela Simpson, Colin N.A Palmer, Klaus Bønnelykke, Irwin Mclean, Somnath Mukhopadhyay, Christian B. Pipper, Liselotte B. Halkjaer, Brian Lipworth, Jenny Hankinson, Ashley Woodcock, and Adnan Custovic. Gene-Environment Interaction in the Onset of Eczema in Infancy: Filaggrin Loss-of-Function Mutations Enhanced by Neonatal Cat Exposure. *PLoS Med.*, 5(6):e131, jun 2008.

[21] Lei Bao, Huayi Zhang, and Lawrence S Chan. The involvement of the JAK-STAT signaling pathway in chronic inflammatory skin disease atopic dermatitis. *JAK-STAT*, 2(3):e24137, jul 2013.

[22] Ellen H. van den Bogaard, Judith G.M. Bergboer, Mieke Vonk-Bergers, Ivonne M.J.J. van Vlijmen-Willems, Stanleyson V. Hato, Pieter G.M. van der Valk, Jens Michael Schröder, Irma Joosten, Patrick L.J.M. Zeeuwen, and Joost Schalkwijk. Coal tar induces AHR-dependent skin barrier repair in atopic dermatitis. *J. Clin. Invest.*, 123(2):917–927, jan 2013.

[23] Torsten Zuberbier, Seth J Orlow, Amy S Paller, Alain Taïeb, Roger Allen, José M Hernanz-Hermosa, Jorge Ocampo-Candiani, Margaret Cox, Joanne Langeraar, and Jan C Simon. Patient perspectives on the management of atopic dermatitis. *J. Allergy Clin. Immunol.*, 118(1):226–232, 2006.

[24] Stephan Weidinger and Natalija Novak. Atopic dermatitis. *Lancet*, 387(10023):1109–1122, mar 2016.

[25] Lawrence F. Eichenfield, Wynnis L. Tom, Timothy G. Berger, Alfons Krol, Amy S. Paller, Kathryn Schwarzenberger, James N. Bergman, Sarah L. Chamlin, David E. Cohen, Kevin D. Cooper, Kelly M. Cordoro, Dawn M. Davis, Steven R. Feldman, Jon M. Hanifin, David J. Margolis, Robert A. Silverman, Eric L. Simpson, Hywel C. Williams, Craig A. Elmets, Julie Block, Christopher G. Harrod, Wendy Smith Begolka, and Robert Sidbury. Guidelines of care for the management of atopic dermatitis. *J. Am. Acad. Dermatol.*, 71(1):1–17, 2014.

[26] Su Yuen Ng, Sabeera Begum, and Sze Yee Chong. Does Order of Application of Emollient and Topical Corticosteroids Make a Difference in the Severity of Atopic Eczema in Children? *Pediatr. Dermatol.*, 33(2):160–164, mar 2016.

[27] Edward Upton, Natalie Schellack, and Mojakgomo H. Motswaledi. A review of the management of childhood atopic eczema at the primary healthcare level. *Curr. Allergy Clin. Immunol.*, 29(1):30–34, 2016.

[28] Lawrence F. Eichenfield, Jusleen Ahluwalia, Andrea Waldman, Jenna Borok, Jeremy Udkoff, and Mark Boguniewicz. Current guidelines for the evaluation and management of atopic dermatitis: Acomparison of the Joint Task Force Practice Parameter and American Academy of Dermatology guidelines. *J. Allergy Clin. Immunol.*, 139(4):S49–S57, 2017.

[29] K. L. E. Hon, G. K. Ching, T. F. Leung, C. Y. Choi, K. K. C. Lee, and P. C. Ng. Estimating emollient usage in patients with eczema. *Clin. Exp. Dermatol.*, 35(1):22–26, jan 2010.

[30] Michael J Cork, Simon G Danby, Yiannis Vasilopoulos, Jonathan Hadgraft, Majella E Lane, Manar Moustafa, Richard H Guy, Alice L Macgowan, Rachid Tazi-Ahnini, and Simon J Ward. Epidermal barrier dysfunction in atopic dermatitis. *J. Invest. Dermatol.*, 129(8):1892–1908, aug 2009.

[31] Mark Boguniewicz, Joshua A. Zeichner, Lawrence F. Eichenfield, Adelaide A. Hebert, Michael Jarratt, Anne W. Lucky, and Amy S. Paller. MAS063DP is Effective Monotherapy for Mild to Moderate Atopic Dermatitis in Infants and Children: A Multicenter, Randomized, Vehicle-Controlled Study. *J. Pediatr.*, 152(6):854–859, jun 2008.

[32] A. Wollenberg, A. Seba, and A.S. Antal. Immunological and molecular targets of atopic dermatitis treatment. *Br. J. Dermatol.*, 170(SUPPL. 1):7–11, jul 2014.

[33] Shinji Noda, Mayte Suárez-Fariñas, Benjamin Ungar, Soo Jung Kim, Cristina de Guzman Strong, Hui Xu, Xiangyu Peng, Yeriel D. Estrada, Saeko Nakajima, Tetsuya Honda, Jung U. Shin, Hemin Lee, James G. Krueger, Kwang-Hoon Lee, Kenji Kabashima, and Emma Guttman-Yassky. The Asian atopic dermatitis phenotype combines features of atopic dermatitis and psoriasis with increased TH17 polarization. *J. Allergy Clin. Immunol.*, 136(5):1254–1264, nov 2015.

[34] Thomas Bieber, Angelo M. D'Erme, Cezmi A. Akdis, Claudia Traidl-Hoffmann, Roger Lauener, Georg Schäppi, and Peter Schmid-Grendelmeier. Clinical phenotypes and endophenotypes of atopic dermatitis: Where are we, and where should we go? *J. Allergy Clin. Immunol.*, 139(4):S58–S64, apr 2017.

[35] K. Eyerich and N. Novak. Immunology of atopic eczema: overcoming the Th1/Th2 paradigm. *Allergy*, 68(8):974–982, aug 2013.

[36] Joonhong Park, Dong Wook Jekarl, Yonggoo Kim, Jiyeon Kim, Myungshin Kim, and Young Min Park. Novel FLG null mutations in Korean patients with atopic dermatitis and comparison of the mutational spectra in Asian populations. *J. Dermatol.*, 42(9):867–873, sep 2015.

[37] Jochen Schmitt, Phyllis I. Spuls, Kim S. Thomas, Eric Simpson, Masutaka Furue, Stefanie Deckert, Magdalene Dohil, Christian Apfelbacher, Jasvinder A. Singh, Joanne Chalmers, and Hywel C. Williams. The Harmonising Outcome Measures for Eczema (HOME) statement to assess clinical signs of atopic eczema in trials. *J. Allergy Clin. Immunol.*, 134(4):800–807, oct 2014.

[38] P. I. Spuls, L. A A Gerbens, E. Simpson, C. J. Apfelbacher, J. R. Chalmers, K. S. Thomas, C. A C Prinsen, L. B. von Kobyletzki, J. A. Singh, H. C. Williams, and J. Schmitt. Patient-Oriented Eczema Measure (POEM), a core instrument to measure symptoms in clinical trials: A Harmonising Outcome Measures for Eczema (HOME) statement. *Br. J. Dermatol.*, pages 979–984, 2017.

[39] Peter M. Elias. Stratum Corneum Defensive Functions: An Integrated View. *J. Invest. Dermatol.*, 125(2):183–200, aug 2005.

[40] Grainne M. O'Regan, Aileen Sandilands, W.H. Irwin McLean, and Alan D. Irvine. Filaggrin in atopic dermatitis. *J. Allergy Clin. Immunol.*, 122(4):689–693, oct 2008.

[41] Peter M. Elias. Therapeutic Implications of a Barrier-based Pathogenesis of Atopic Dermatitis. *Ann. Dermatol.*, 22(3):245, 2010.

[42] William Cookson. The immunogenetics of asthma and eczema: a new focus on the epithelium. *Nat. Rev. Immunol.*, 4(12):978–988, dec 2004.

[43] Barbara S. Baker. The role of microorganisms in atopic dermatitis. *Clin. Exp. Immunol.*, 144(1):1–9, apr 2006.

[44] Andrew H. Liu. Revisiting the hygiene hypothesis for allergy and asthma. *J. Allergy Clin. Immunol.*, 136(4):860–865, oct 2015.

[45] Daniel H. Kaplan, Botond Z. Igyártó, and Anthony a. Gaspari. Early immune events in the induction of allergic contact dermatitis. *Nat. Rev. Immunol.*, 12(2):114–24, jan 2012.

[46] L Fry. *An Atlas of Atopic Eczema*. The encyclopedia of visual medicine series. Taylor & Francis, 2003.

[47] Peter M. Elias and Matthias Schmuth. Abnormal skin barrier in the etiopathogenesis of atopic dermatitis. *Curr. Allergy Asthma Rep.*, 9(4):265–272, jul 2009.

[48] Donald Y.M. Leung, Mark Boguniewicz, Michael D. Howell, Ichiro Nomura, and Qutayba A. Hamid. New insights into atopic dermatitis. *J. Clin. Invest.*, 113(5):651–657, mar 2004.

[49] I-Hsin Kuo, Takeshi Yoshida, Anna De Benedetto, and Lisa A. Beck. The cutaneous innate immune response in patients with atopic dermatitis. *J. Allergy Clin. Immunol.*, 131(2):266–278, feb 2013.

[50] Laura Y. McGirt and Lisa A. Beck. Innate immune defects in atopic dermatitis. *J. Allergy Clin. Immunol.*, 118(1):202–208, jul 2006.

[51] Heidi H Kong, J. Oh, C. Deming, S. Conlan, E. A. Grice, M. A. Beatson, E. Nomicos, E. C. Polley, H. D. Komarow, P. R. Murray, M. L. Turner, and J. A. Segre. Temporal shifts in the skin microbiome associated with disease flares and treatment in children with atopic dermatitis. *Genome Res.*, 22(5):850–859, may 2012.

[52] Yuumi Nakamura, Jon Oscherwitz, Kemp B Cease, Susana M Chan, Raul Muñoz-Planillo, Mizuho Hasegawa, Amer E Villaruz, Gordon Y C Cheung, Martin J McGavin, Jeffrey B Travers, Michael Otto, Naohiro Inohara, and Gabriel Núñez. Staphylococcus δ-toxin induces allergic skin disease by activating mast cells. *Nature*, 503(7476):397–401, oct 2013.

[53] Jacob P. Thyssen and Sanja Kezic. Causes of epidermal filaggrin reduction and their role in the pathogenesis of atopic dermatitis. *J. Allergy Clin. Immunol.*, 134(4):792–799, oct 2014.

[54] Emma Guttman-Yassky, Mayte Suárez-Fariñas, Andrea Chiricozzi, Kristine E. Nograles, Avner Shemer, Judilyn Fuentes-Duculan, Irma Cardinale, Peng Lin, Reuven Bergman, Anne M. Bowcock, and James G. Krueger. Broad defects in epidermal cornification in atopic dermatitis identified through genomic analysis. *J. Allergy Clin. Immunol.*, 124(6):1235–1244.e58, dec 2009.

[55] Thomas Bieber. Atopic Dermatitis. *N. Engl. J. Med.*, 358(14):1483–1494, apr 2008.

[56] Peter M Elias and Martin Steinhoff. Outside-to-Inside (and Now Back to Outside) Pathogenic Mechanisms in Atopic Dermatitis. *J. Invest. Dermatol.*, 128(5):1067–1070, may 2008.

[57] Donald Y.M. Leung. Atopic dermatitis: New insights and opportunities for therapeutic intervention. *J. Allergy Clin. Immunol.*, 105(5):860–876, may 2000.

[58] Anne-Marie Roguedas-Contios and Laurent Misery. What is Intrinsic Atopic Dermatitis? *Clin. Rev. Allergy Immunol.*, 41(3):233–236, dec 2011.

[59] A Repa, C Wild, K Hufnagl, B Winkler, B Bohle, A Pollak, and U Wiedermann. Influence of the route of sensitization on local and systemic immune responses in a murine model of type I allergy. *Clin. Exp. Immunol.*, 137(1):12–18, jul 2004.

[60] Jonathan M. Spergel. From atopic dermatitis to asthma: The atopic march. *Ann. Allergy, Asthma Immunol.*, 105(2):99–106, 2010.

[61] Hongwei Han, Florence Roan, and Steven F. Ziegler. The atopic march: current insights into skin barrier dysfunction and epithelial cell-derived cytokines. *Immunol. Rev.*, 278(1):116–130, jul 2017.

[62] S. C. Dharmage, A. J. Lowe, M. C. Matheson, J. A. Burgess, K. J. Allen, and M. J. Abramson. Atopic dermatitis and the atopic march revisited. *Allergy*, 69(1):17–27, jan 2014.

[63] Bruce R. Gordon. The Allergic March: Can We Prevent Allergies and Asthma? *Otolaryngol. Clin. North Am.*, 44(3):765–777, jun 2011.

[64] Sabine Hoffjan and Susanne Stemmler. Unravelling the complex genetic background of atopic dermatitis: from genetic association results towards novel therapeutic strategies. *Arch. Dermatol. Res.*, 307(8):659–670, 2015.

[65] Peter D. Arkwright, Cassim Motala, Hamsa Subramanian, Jonathan Spergel, Lynda C. Schneider, and Andreas Wollenberg. Management of Difficult-to-Treat Atopic Dermatitis. *J. Allergy Clin. Immunol. Pract.*, 1(2):142–151, mar 2013.

[66] C.Y. Zhao, E.Y. Hao, D.D. Oh, B.S. Daniel, L.K. Martin, J.C. Su, M. Rodrigues, and D.F. Murrell. A comparison study of clinician-rated atopic dermatitis outcome measures for intermediate- to dark-skinned patients. *Br. J. Dermatol.*, 176(4):985–992, apr 2017.

[67] C. G. Mortz, K. E. Andersen, C. Dellgren, T. Barington, and C. Bindslev-Jensen. Atopic dermatitis from adolescence to adulthood in the TOACS cohort: prevalence, persistence and comorbidities. *Allergy*, 70(7):836–845, jul 2015.

[68] Diamant Thaçi, Eric L. Simpson, Lisa A. Beck, Thomas Bieber, Andrew Blauvelt, Kim Papp, Weily Soong, Margitta Worm, Jacek C. Szepietowski, Howard Sofen, Makoto Kawashima, Richard Wu, Steven P. Weinstein, Neil M H Graham, Gianluca Pirozzi, Ariel Teper, E. Rand Sutherland, Vera Mastey, Neil Stahl, George D. Yancopoulos, and Marius Ardeleanu. Efficacy and safety of dupilumab in adults with moderate-to-severe atopic dermatitis inadequately controlled by topical treatments: a randomised, placebo-controlled, dose-ranging phase 2b trial. *Lancet*, 387(10013):40–52, jan 2016.

[69] Ulf Åkerström, Sakari Reitamo, Tor Langeland, Mats Berg, Lisbeth Rustad, Laura Korhonen, Marie Lodén, Karin Wirén, Mats Grände, Petra Skare, and Åke Svensson. Comparison of Moisturizing Creams for the Prevention of Atopic Dermatitis Relapse: A Randomized Double-blind Controlled Multicentre Clinical Trial. *Acta Derm. Venereol.*, 95(5):587–592, may 2015.

[70] Michael R. Williams and Richard L. Gallo. The Role of the Skin Microbiome in Atopic Dermatitis. *Curr. Allergy Asthma Rep.*, 15(11):65, nov 2015.

[71] S. G. O. Johansson, J.O'B Hourihane, J Bousquet, C Bruijnzeel-Koomen, S Dreborg, T Haahtela, M L Kowalski, N Mygind, J Ring, P van Cauwenberge, M van Hage-Hamsten, and B. Wuthrich. A revised nomenclature for allergy: An EAACI position statement from the EAACI nomenclature task force. *Allergy*, 56(9):813–824, sep 2001.

[72] E.A. Holm, H.C. Wulf, H. Stegmann, and G.B.E. Jemec. Life quality assessment among patients with atopic eczema. *Br. J. Dermatol.*, 154(4):719–725, apr 2006.

[73] F. C. Beikert, A. K. Langenbruch, M. A. Radtke, T. Kornek, S. Purwins, and M. Augustin. Willingness to pay and quality of life in patients with atopic dermatitis. *Arch. Dermatol. Res.*, 306(3):279–286, apr 2014.

[74] Carlos Lifschitz. The Impact of Atopic Dermatitis on Quality of Life. *Ann. Nutr. Metab.*, 66(1):34–40, apr 2015.

[75] Gwendoline Kiebert, Sonja V. Sorensen, Dennis Revicki, Susan C. Fagan, Joseph J. Doyle, Joel Cohen, and David Fivenson. Atopic dermatitis is associated with a decrement in health-related quality of life. *Int. J. Dermatol.*, 41(3):151–158, mar 2002.

[76] P.E. Beattie and M.S. Lewis-Jones. A comparative study of impairment of quality of life in children with skin disease and children with other chronic childhood diseases. *Br. J. Dermatol.*, 155(1):145–151, jul 2006.

[77] J.R. Olsen, J. Gallacher, A.Y. Finlay, V. Piguet, and N.A. Francis. Quality of life impact of childhood skin conditions measured using the Children's Dermatology Life Quality Index (CDLQI): a meta-analysis. *Br. J. Dermatol.*, 174(4):853–861, apr 2016.

[78] Iona H. Ginsburg. The psychosocial impact of skin disease. An overview. *Dermatol. Clin.*, 14(3):473–484, jul 1996.

[79] D. Chrostowska-Plak, A. Reich, and J.C. Szepietowski. Relationship between itch and psychological status of patients with atopic dermatitis. *J. Eur. Acad. Dermatology Venereol.*, 27(2):e239–e242, feb 2013.

[80] Jennifer Whiteley, Birol Emir, Robin Seitzman, and Geoffrey Makinson. The burden of atopic dermatitis in US adults: results from the 2013 National Health and Wellness Survey. *Curr. Med. Res. Opin.*, 32(10):1645–1651, oct 2016.

[81] Pouya Yaghmaie, Caroline W. Koudelka, and Eric L. Simpson. Mental health comorbidity in patients with atopic dermatitis. *J. Allergy Clin. Immunol.*, 131(2):428–433, 2013.

[82] Yoichi Chida, Mark Hamer, and Andrew Steptoe. A Bidirectional Relationship Between Psychosocial Factors and Atopic Disorders: A Systematic Review and Meta-Analysis. *Psychosom. Med.*, 70(1):102–116, jan 2008.

[83] Sue Lewis-Jones. Quality of life and childhood atopic dermatitis: The misery of living with childhood eczema. *Int. J. Clin. Pract.*, 60(8):984–992, 2006.

[84] Bee Wah Lee and Patrick R. Detzel. Treatment of Childhood Atopic Dermatitis and Economic Burden of Illness in Asia Pacific Countries. *Ann. Nutr. Metab.*, 66(1):18–24, apr 2015.

[85] Anthony J. Mancini, Kellee Kaulback, and Sarah L. Chamlin. The socioeconomic impact of atopic dermatitis in the United States: A systematic review. *Pediatr. Dermatol.*, 25(1):1–6, 2008.

[86] B Ehlken, M Möhrenschlager, B Kugland, K Berger, K Quednau, and J Ring. Krankheitskostenstudie bei Patienten mit atopischem Ekzem in Deutschland. *Der Hautarzt*, 56(12):1144–1151, dec 2005.

[87] Thomas Bieber. Atopic Dermatitis. *N. Engl. J. Med.*, 358(14):1483–1494, apr 2008.

[88] Bieber Thomas. Atopic Dermatitis. *Ann. Dermatol.*, 22(2):125, may 2010.

[89] Lavinia Paternoster, Marie Standl, Johannes Waage, Hansjörg Baurecht, Melanie Hotze, David P Strachan, John A Curtin, Klaus Bønnelykke, Chao Tian, Atsushi Takahashi, Jorge Esparza-Gordillo, Alexessander Couto Alves, Jacob P Thyssen, Herman T den Dekker, Manuel A Ferreira, Elisabeth Altmaier, Patrick M A Sleiman, Feng Li Xiao, Juan R Gonzalez, Ingo Marenholz, Birgit Kalb, Maria Pino-Yanes, Cheng-Jian Xu, Lisbeth Carstensen, Maria M Groen-Blokhuis, Cristina Venturini, Craig E Pennell, Sheila J Barton, Albert M Levin, Ivan Curjuric, Mariona Bustamante, Eskil Kreiner-Møller, Gabrielle A Lockett, Jonas Bacelis, Supinda Bunyavanich, Rachel A Myers, Anja Matanovic, Ashish Kumar, Joyce Y Tung, Tomomitsu Hirota, Michiaki Kubo, Wendy L McArdle, A John Henderson, John P Kemp, Jie Zheng, George Davey Smith, Franz Rüschendorf, Anja Bauerfeind, Min Ae Lee-Kirsch, Andreas Arnold, Georg Homuth, Carsten O Schmidt, Elisabeth Mangold, Sven Cichon, Thomas Keil, Elke Rodríguez, Annette Peters, Andre Franke, Wolfgang Lieb, Natalija Novak, Regina Fölster-Holst, Momoko Horikoshi, Juha Pekkanen, Sylvain Sebert, Lise L Husemoen, Niels Grarup, Johan C de Jongste, Fernando Rivadeneira, Albert Hofman, Vincent W V Jaddoe, Suzanne G M A Pasmans, Niels J Elbert, André G Uitterlinden, Guy B Marks, Philip J Thompson, Melanie C Matheson, Colin F Robertson, Janina S Ried, Jin Li, Xian Bo Zuo, Xiao Dong Zheng, Xian Yong Yin, Liang Dan Sun, Maeve A McAleer, Grainne M O'Regan, Caoimhe M R Fahy, Linda E Campbell, Milan Macek, Michael Kurek, Donglei Hu, Celeste Eng, Dirkje S Postma, Bjarke Feenstra, Frank Geller, Jouke Jan Hottenga, Christel M Middeldorp, Pirro Hysi, Veronique Bataille, Tim Spector, Carla M T Tiesler, Elisabeth Thiering, Badri Pahukasahasram, James J Yang, Medea Imboden, Scott Huntsman, Natàlia Vilor-Tejedor, Caroline L Relton, Ronny Myhre, Wenche Nystad, Adnan Custovic, Scott T Weiss, Deborah A Meyers, Cilla Söderhäll, Erik Melén, Carole Ober, Benjamin A Raby, Angela Simpson, Bo Jacobsson, John W Holloway, Hans Bisgaard, Jordi Sunyer, Nicole M Probst-Hensch, L Keoki Williams, Keith M Godfrey, Carol A Wang, Dorret I Boomsma, Mads Melbye, Gerard H Koppelman, Deborah Jarvis, W H Irwin McLean, Alan D Irvine, Xue Jun Zhang, Hakon Hakonarson, Christian Gieger, Esteban G Burchard, Nicholas G Martin, Liesbeth Duijts, Allan Linneberg, Marjo-Riitta Jarvelin, Markus M Nöthen, Susanne Lau, Norbert Hübner, Young-Ae Lee, Mayumi Tamari, David A Hinds, Daniel Glass, Sara J Brown, Joachim Heinrich, David M Evans, and Stephan Weidinger. Multi-ancestry genome-wide association study of 21,000 cases and 95,000 controls identifies new risk loci for atopic dermatitis. *Nat. Genet.*, 47(12):1449–1456, oct 2015.

[90] Maeve A. McAleer and Alan D. Irvine. The multifunctional role of filaggrin in allergic skin disease. *J. Allergy Clin. Immunol.*, 131(2):280–291, feb 2013.

[91] Peter M. Elias and Joan S. Wakefield. Mechanisms of abnormal lamellar body secretion and the dysfunctional skin barrier in patients with atopic dermatitis. *J. Allergy Clin. Immunol.*, 134(4):781–791.e1, oct 2014.

[92] Francesca Cipriani, Arianna Dondi, and Giampaolo Ricci. Recent advances in epidemiology and prevention of atopic eczema. *Pediatr. Allergy Immunol.*, 25(7):630–638, nov 2014.

[93] Margarete Niebuhr and Thomas Werfel. Innate immunity, allergy and atopic dermatitis. *Curr. Opin. Allergy Clin. Immunol.*, 10(5):463–468, oct 2010.

[94] Lynda Schneider, Stephen Tilles, Peter Lio, Mark Boguniewicz, Lisa Beck, Jennifer LeBovidge, Natalija Novak, David Bernstein, Joann Blessing-Moore, David Khan, David Lang, Richard Nicklas, John Oppenheimer, Jay Portnoy, Christopher Randolph, Diane Schuller, Sheldon Spector, Stephen Tilles, and Dana Wallace. Atopic dermatitis: A practice parameter update 2012. *J. Allergy Clin. Immunol.*, 131(2):295–299.e27, feb 2013.

[95] John Henderson, Kate Northstone, Simon P. Lee, Haihui Liao, Yiwei Zhao, Marcus Pembrey, Somnath Mukhopadhyay, George Davey Smith, Colin N. A. Palmer, W. H Irwin McLean, and Alan D. Irvine. The burden of disease associated with filaggrin mutations: A population-based, longitudinal birth cohort study. *J. Allergy Clin. Immunol.*, 121(4):872–7.e9, apr 2008.

[96] Mayte Suárez-Fariñas, Suzanne J Tintle, Avner Shemer, Andrea Chiricozzi, Kristine Nograles, Irma Cardinale, Shenghui Duan, Anne M Bowcock, James G Krueger, and Emma Guttman-Yassky. Nonlesional atopic dermatitis skin is characterized by broad terminal differentiation defects and variable immune abnormalities. *J. Allergy Clin. Immunol.*, 127(4):954–64.e1–4, apr 2011.

[97] Michael D Howell, Heather R Fairchild, Byung Eui Kim, Lianghua Bin, Mark Boguniewicz, Jasmina S Redzic, Kirk C Hansen, and Donald Y.M. Leung. Th2 Cytokines Act on S100/A11 to Downregulate Keratinocyte Differentiation. *J. Invest. Dermatol.*, 128(9):2248–2258, sep 2008.

[98] G. Mócsai, K. Gáspár, G. Nagy, B. Irinyi, A. Kapitány, T. Bíró, E. Gyimesi, B. Tóth, L. Maródi, and A. Szegedi. Severe skin inflammation and filaggrin mutation similarly alter the skin barrier in patients with atopic dermatitis. *Br. J. Dermatol.*, 170(3):617–624, mar 2014.

[99] Anna De Benedetto, Akiharu Kubo, and Lisa A Beck. Skin Barrier Disruption: A Requirement for Allergen Sensitization? *J. Invest. Dermatol.*, 132(3):949–963, mar 2012.

[100] Akiharu Kubo, Keisuke Nagao, and Masayuki Amagai. Epidermal barrier dysfunction and cutaneous sensitization in atopic diseases. *J. Clin. Invest.*, 122(2):440–7, 2012.

[101] Mark Boguniewicz and Donald Y. M. Leung. Atopic dermatitis: a disease of altered skin barrier and immune dysregulation. *Immunol. Rev.*, 242(1):233–246, jul 2011.

[102] Julia K. Gittler, Avner Shemer, Mayte Suárez-Fariñas, Judilyn Fuentes-Duculan, Kara J. Gulewicz, Claire Q.F. Wang, Hiroshi Mitsui, Irma Cardinale, Cristina de Guzman Strong, James G. Krueger, and Emma Guttman-Yassky. Progressive activation of TH2/TH22 cytokines and selective epidermal proteins characterizes acute and chronic atopic dermatitis. *J. Allergy Clin. Immunol.*, 130(6):1344–1354, dec 2012.

[103] Louise Newell, Marta E Polak, Jay Perera, Charlotte Owen, Peter Boyd, Christopher Pickard, Peter H Howarth, Eugene Healy, John W Holloway, Peter S Friedmann, and Michael R Ardern-Jones. Sensitization via Healthy Skin Programs Th2 Responses in Individuals with Atopic Dermatitis. *J. Invest. Dermatol.*, 133(10):2372–2380, oct 2013.

[104] Mark D. A. van Logtestijn, Elisa Domínguez-Hüttinger, Georgios N. Stamatas, and Reiko J. Tanaka. Resistance to Water Diffusion in the Stratum Corneum Is Depth-Dependent. *PLoS One*, 10(2):e0117292, feb 2015.

[105] J. Ring, A. Alomar, T. Bieber, M. Deleuran, A. Fink-Wagner, C. Gelmetti, U. Gieler, J. Lipozencic, T. Luger, A.P. Oranje, T. Schäfer, T. Schwennesen, S. Seidenari, D. Simon, S. Ständer, G. Stingl, S. Szalai, J.C. Szepietowski, A. Taïeb, T. Werfel, A. Wollenberg, and U. Darsow. Guidelines for treatment of atopic eczema (atopic dermatitis) Part I. *J. Eur. Acad. Dermatology Venereol.*, 26(8):1045–1060, aug 2012.

[106] Hillary C. Frankel and Abrar A. Qureshi. Comparative Effectiveness of Topical Calcineurin Inhibitors in Adult Patients with Atopic Dermatitis. *Am. J. Clin. Dermatol.*, 13(2):113–123, apr 2012.

[107] Jens Michael Jensen, Stephan Pfeiffer, Magdalena Witt, Matthias Bräutigam, Claudia Neumann, Michael Weichenthal, Thomas Schwarz, Regina Fölster-Holst, and Ehrhardt Proksch. Different effects of pimecrolimus and betamethasone on the skin barrier in patients with atopic dermatitis. *J. Allergy Clin. Immunol.*, 123(5):1124–1133, 2009.

[108] Camilla Ling Jinnestål, Emma Belfrage, Ove Bäck, Artur Schmidtchen, and Andreas Sonesson. Skin barrier impairment correlates with cutaneous Staphylococcus aureus colonization and sensitization to skin-associated microbial antigens in adult patients with atopic dermatitis. *Int. J. Dermatol.*, 53(1):27–33, jan 2014.

[109] J. Ring, A. Alomar, T. Bieber, M. Deleuran, A. Fink-Wagner, C. Gelmetti, U. Gieler, J. Lipozencic, T. Luger, A.P. Oranje, T. Schäfer, T. Schwennesen, S. Seidenari, D. Simon, S. Ständer, G. Stingl, S. Szalai, J.C. Szepietowski, A. Taïeb, T. Werfel, A. Wollenberg, and U. Darsow. Guidelines for treatment of atopic eczema (atopic dermatitis) Part II. *J. Eur. Acad. Dermatology Venereol.*, 26(9):1176–1193, sep 2012.

[110] T. Bieber and B. Straeter. Off-label prescriptions for atopic dermatitis in Europe. *Allergy*, 70(1):6–11, jan 2015.

[111] Thomas Werfel and Tilo Biedermann. Current novel approaches in systemic therapy of atopic dermatitis. *Curr. Opin. Allergy Clin. Immunol.*, 15(5):446–452, oct 2015.

[112] Alain Taïeb, Julien Seneschal, and M Djavad Mossalayi. Biologics in atopic dermatitis. *JDDG J. der Dtsch. Dermatologischen Gesellschaft*, 10(3):174–178, mar 2012.

[113] Eric L. Simpson, Thomas Bieber, Emma Guttman-Yassky, Lisa A. Beck, Andrew Blauvelt, Michael J. Cork, Jonathan I. Silverberg, Mette Deleuran, Yoko Kataoka, Jean-Philippe Lacour, Külli Kingo, Margitta Worm, Yves Poulin, Andreas Wollenberg, Yuhwen Soo, Neil M.H. Graham, Gianluca Pirozzi, Bolanle Akinlade, Heribert Staudinger, Vera Mastey, Laurent Eckert, Abhijit Gadkari, Neil Stahl, George D. Yancopoulos, and Marius Ardeleanu. Two Phase 3 Trials of Dupilumab versus Placebo in Atopic Dermatitis. *N. Engl. J. Med.*, 375(24):2335–2348, dec 2016.

[114] Maurizio Mennini, Lamia Dahdah, Alessandro Fiocchi, and Eric L Simpson. Two Phase 3 Trials of Dupilumab versus Placebo in Atopic Dermatitis. *N. Engl. J. Med.*, 376(11):1090–1091, mar 2017.

[115] A. Wollenberg and K. Feichtner. Atopic dermatitis and skin allergies - update and outlook. *Allergy*, 68(12):1509–1519, dec 2013.

[116] Ayumi Sugiura, Tsuyoshi Nomura, Atsuko Mizuno, and Genji Imokawa. Reevaluation of the non-lesional dry skin in atopic dermatitis by acute barrier disruption: an abnormal permeability barrier homeostasis with defective processing to generate ceramide. *Arch. Dermatol. Res.*, 306(5):427–440, jul 2014.

[117] J Schmitt, L von Kobyletzki, Å. Svensson, and C Apfelbacher. Efficacy and tolerability of proactive treatment with topical corticosteroids and calcineurin inhibitors for atopic eczema: systematic review and meta-analysis of randomized controlled trials. *Br. J. Dermatol.*, 164(2):415–428, feb 2011.

[118] J. Hanifin, A.K. Gupta, and R. Rajagopalan. Intermittent dosing of fluticasone propionate cream for reducing the risk of relapse in atopic dermatitis patients. *Br. J. Dermatol.*, 147(3):528–537, sep 2002.

[119] Eltjo J Glazenburg, Albert Wolkerstorfer, Anton L Gerretsen, Paul G H Mulder, and Arnold P Oranje. Efficacy and safety of fluticasone propionate 0.005% ointment in the long-term maintenance treatment of children with atopic dermatitis: Differences between boys and girls? *Pediatr. Allergy Immunol.*, 20(1):59–66, feb 2009.

[120] Ting Seng Tang, Thomas Bieber, and Hywel C. Williams. Are the concepts of induction of remission and treatment of subclinical inflammation in atopic dermatitis clinically useful? *J. Allergy Clin. Immunol.*, 133(6):1615–1625.e1, jun 2014.

[121] Robert Sidbury, Wynnis L. Tom, James N. Bergman, Kevin D. Cooper, Robert A. Silverman, Timothy G. Berger, Sarah L. Chamlin, David E. Cohen, Kelly M. Cordoro, Dawn M. Davis, Steven R. Feldman, Jon M. Hanifin, Alfons Krol, David J. Margolis, Amy S. Paller, Kathryn Schwarzenberger, Eric L. Simpson, Hywel C. Williams, Craig A. Elmets, Julie Block, Christopher G. Harrod, Wendy Smith Begolka, and Lawrence F. Eichenfield. Guidelines of care for the management of atopic dermatitis. *J. Am. Acad. Dermatol.*, 71(6):1218–1233, dec 2014.

[122] Judith Hong, Joerg Buddenkotte, Timothy G. Berger, and Martin Steinhoff. Management of Itch in Atopic Dermatitis. *Semin. Cutan. Med. Surg.*, 30(2):71–86, jun 2011.

[123] Andreas Wollenberg and Laura Maximiliane Ehmann. Long Term Treatment Concepts and Proactive Therapy for Atopic Eczema. *Ann. Dermatol.*, 24(3):253, 2012.

[124] Glynis A. Scott Anne Haake and Karen A. Holbrook. Structure and function of the skin: overview of the epidermis and dermis. In Ruth K. Freinkel Woodley and David T., editors, *Biol. Ski.*, chapter Chapter 2, pages 19–47. The Parhenon Publishing Group, 1 edition, 2001.

[125] Paola Fortugno, Laetitia Furio, Massimo Teson, Matteo Berretti, May El Hachem, Giovanna Zambruno, Alain Hovnanian, and Marina D'Alessio. The 420K LEKTI variant alters LEKTI proteolytic activation and results in protease deregulation: implications for atopic dermatitis. *Hum. Mol. Genet.*, 21(19):1–34, oct 2012.

[126] Paul Travers Murphy Kenneth and Mark Walport. Innate Immunity : The First Lines of Defense. In *Janeway's Immunobiol.*, chapter 2, pages 37–73. Garland Science, 8th edition, 2011.

[127] Peter M. Elias. The skin barrier as an innate immune element. *Semin. Immunopathol.*, 29(1):3–14, mar 2007.

[128] Kathi C. Madison. Barrier Function of the Skin: La Raison d'Être of the Epidermis. *J. Invest. Dermatol.*, 121(2):231–241, aug 2003.

[129] Michael D. Howell, Byung Eui Kim, Peisong Gao, Audrey V. Grant, Mark Boguniewicz, Anna DeBenedetto, Lynda Schneider, Lisa a. Beck, Kathleen C. Barnes, and Donald Y.M. Leung. Cytokine modulation of atopic dermatitis filaggrin skin expression. *J. Allergy Clin. Immunol.*, 120(1):150–155, jul 2007.

[130] Cédric Blanpain and Elaine Fuchs. Epidermal homeostasis: a balancing act of stem cells in the skin. *Nat. Rev. Mol. Cell Biol.*, 10(3):207–217, mar 2009.

[131] J. Nie, X. Fu, and Weidong Han. Microenvironment-dependent homeostasis and differentiation of epidermal basal undifferentiated keratinocytes and their clinical applications in skin repair. *J. Eur. Acad. Dermatology Venereol.*, 27(5):531–535, may 2013.

[132] Maria Brattsand, Kristina Stefansson, Christine Lundh, Ylva Haasum, and Torbjörn Egelrud. A Proteolytic Cascade of Kallikreins in the Stratum Corneum. *J. Invest. Dermatol.*, 124(1):198–203, jan 2005.

[133] Janet A. Fairley and Daniel Zivony. Epidermal kinetics and regulation of the cell proliferation. In Ruth K . Freinkel Woodley and David T., editors, *Biol. Ski.*, chapter Chapter 12, pages 201–209. The Parhenon Publishing Group, 1 edition, 2001.

[134] Azza Eissa and Eleftherios P. Diamandis. Human tissue kallikreins as promiscuous modulators of homeostatic skin barrier functions. *Biol. Chem.*, 389(6):669–680, jun 2008.

[135] Nathalie Jonca, Marina Guerrin, Krassimira Hadjiolova, Cécile Caubet, Hélène Gallinaro, Michel Simon, and Guy Serre. Corneodesmosin, a component of epidermal corneocyte desmosomes, displays homophilic adhesive properties. *J. Biol. Chem.*, 277(7):5024–5029, feb 2002.

[136] Fabienne Berthaud and Mila Boncheva. Correlation between the properties of the lipid matrix and the degrees of integrity and cohesion in healthy human Stratum corneum. *Exp. Dermatol.*, 20(3):255–262, mar 2011.

[137] Takeshi Matsui and Masayuki Amagai. Dissecting the formation, structure and barrier function of the stratum corneum. *Int. Immunol.*, 27(6):269–280, jun 2015.

[138] Padraic G Fallon, Takashi Sasaki, Aileen Sandilands, Linda E Campbell, Sean P Saunders, Niamh E Mangan, John J Callanan, Hiroshi Kawasaki, Aiko Shiohama, Akiharu Kubo, John P Sundberg, Richard B Presland, Philip Fleckman, Nobuyoshi Shimizu, Jun Kudoh, Alan D Irvine, Masayuki Amagai, and W H Irwin McLean. A homozygous frameshift mutation in the mouse Flg gene facilitates enhanced percutaneous allergen priming. *Nat. Genet.*, 41(5):602–608, may 2009.

[139] Jean-Pierre Hachem, Debra Crumrine, Joachim Fluhr, Barbara E. Brown, Kenneth R. Feingold, and Peter M. Elias. pH Directly Regulates Epidermal Permeability Barrier Homeostasis, and Stratum Corneum Integrity/Cohesion. *J. Invest. Dermatol.*, 121(2):345–353, aug 2003.

[140] D. R. Hoffman, L. M. Kroll, A. Basehoar, B. Reece, C. T. Cunningham, and D. W. Koenig. Immediate and extended effects of sodium lauryl sulphate exposure on stratum corneum natural moisturizing factor. *Int. J. Cosmet. Sci.*, 36(1):93–101, feb 2014.

[141] D. R. Hoffman, L. M. Kroll, A. Basehoar, B. Reece, C. T. Cunningham, and D. W. Koenig. Immediate and extended effects of abrasion on stratum corneum natural moisturizing factor. *Ski. Res. Technol.*, 21(3):366–372, aug 2015.

[142] Stephen Naylor and Jake Y Chen. Unraveling human complexity and disease with systems biology and personalized medicine. *Per. Med.*, 7(3):275–289, may 2010.

[143] Hans V Westerhoff and Bernhard O Palsson. The evolution of molecular biology into systems biology. *Nat. Biotechnol.*, 22(10):1249–1252, oct 2004.

[144] Vladimir A. Likić, Malcolm J. McConville, Trevor Lithgow, and Antony Bacic. Systems Biology: The Next Frontier for Bioinformatics. *Adv. Bioinformatics*, 2010:1–10, 2010.

[145] Jenny Rooke. Synthetic biology as a source of global health innovation. *Syst. Synth. Biol.*, 7(3):67–72, sep 2013.

[146] John J. Tyson, Katherine C. Chen, and Bela Novak. Sniffers, buzzers, toggles and blinkers: Dynamics of regulatory and signaling pathways in the cell. *Curr. Opin. Cell Biol.*, 15(2):221–231, apr 2003.

[147] Uri Alon. Network motifs: theory and experimental approaches. *Nat. Rev. Genet.*, 8(6):450–461, jun 2007.

[148] Duccio Medini, Davide Serruto, Julian Parkhill, David A. Relman, Claudio Donati, Richard Moxon, Stanley Falkow, and Rino Rappuoli. Microbiology in the post-genomic era. *Nat. Rev. Microbiol.*, 6(6):419–430, may 2008.

[149] Shao-Hua Xie, Ai-Lin Liu, Yan-Yan Chen, Li Zhang, Hui-Juan Zhang, Bang-Xiong Jin, Wen-Hong Lu, Xiao-Yan Li, and Wen-Qing Lu. DNA damage and oxidative stress in human liver cell L-02 caused by surface water extracts during drinking water treatment in a waterworks in China. *Environ. Mol. Mutagen.*, 51(August):229–235, 2010.

[150] Andrew G Hall, Sally A. Coulthard, and Julie AE. Irving. Molecular diagnostics: a healthcare perspective. *Expert Rev. Mol. Diagn.*, 3(1):13–16, jan 2003.

[151] A. Aderem, J. N. Adkins, C. Ansong, J. Galagan, S. Kaiser, M. J. Korth, G. L. Law, J. G. McDermott, Sean C Proll, Carrie Rosenberger, Gary Schoolnik, and Michael G Katze. A Systems Biology Approach to Infectious Disease Research: Innovating the Pathogen-Host Research Paradigm. *MBio*, 2(1):e00325–10–e00325–10, mar 2011.

[152] Duncan Ayers and Philip J. Day. Systems Medicine: The Application of Systems Biology Approaches for Modern Medical Research and Drug Development. *Mol. Biol. Int.*, 2015:1–8, 2015.

[153] R Fonteneau, G-B Stan, C Michelet, F Zeggwagh, F Belmudes, D Ernst, and M-A Lefebvre. Modelling the influence of activation-induced apoptosis of CD4+ and CD8+ T-cells on the immune system response of a HIV-infected patient. *IET Syst. Biol.*, 2(2):94–102, mar 2008.

[154] Mark T. Mc Auley, Alvaro Martinez Guimera, David Hodgson, Neil Mcdonald, Kathleen M. Mooney, Amy E. Morgan, and Carole J. Proctor. Modelling the molecular mechanisms of aging. *Biosci. Rep.*, 37(1):BSR20160177, feb 2017.

[155] Jana Schleicher, Theresia Conrad, Mika Gustafsson, Gunnar Cedersund, Reinhard Guthke, and Jörg Linde. Facing the challenges of multiscale modelling of bacterial and fungal pathogenhost interactions. *Brief. Funct. Genomics*, 16(February 2016):elv064, feb 2016.

[156] Reiko J. Tanaka, Neville J. Boon, Katarina Vrcelj, Anita Nguyen, Carmelina Vinci, Darius Armstrong-James, and Elaine Bignell. In silico modeling of spore inhalation reveals fungal persistence following low dose exposure. *Sci. Rep.*, 5(1):13958, nov 2015.

[157] Elisa Domínguez-Hüttinger, Neville J. Boon, Thomas B. Clarke, and Reiko J. Tanaka. Mathematical Modeling of Streptococcus pneumoniae Colonization, Invasive Infection and Treatment. *Front. Physiol.*, 8(MAR):1–14, mar 2017.

[158] Martina Cantone, Guido Santos, Pia Wentker, Xin Lai, and Julio Vera. Multiplicity of Mathematical Modeling Strategies to Search for Molecular and Cellular Insights into Bacteria Lung Infection. *Front. Physiol.*, 8(August), aug 2017.

[159] Guillem Casanovas, Anashua Banerji, Flavia D'Alessio, Martina U. Muckenthaler, and Stefan Legewie. A Multi-Scale Model of Hepcidin Promoter Regulation Reveals Factors Controlling Systemic Iron Homeostasis. *PLoS Comput. Biol.*, 10(1):e1003421, jan 2014.

[160] Masahiro Ono and Reiko J Tanaka. Controversies concerning thymus-derived regulatory T cells: fundamental issues and a new perspective. *Immunol. Cell Biol.*, 94(1):3–10, jan 2016.

[161] Colin W. Clark, Morton I. Kamien, and Nancy L. Schwartz. Dynamic Optimization: The Calculus of Variations and Optimal Control in Economics and Management. *Am. J. Agric. Econ.*, 64(1):167, feb 1982.

[162] S. N. Avvakumov and Yu. N. Kiselev. Construction of Optimal Control Laws for a Model of Information Diffusion in a Social Group. *Comput. Math. Model.*, 26(1):61–86, jan 2015.

[163] Devaraj Jayachandran, Ann E. Rundell, Robert E. Hannemann, Terry A. Vik, and Doraiswami Ramkrishna. Optimal Chemotherapy for Leukemia: A Model-Based Strategy for Individualized Treatment. *PLoS One*, 9(10):e109623, oct 2014.

[164] Michael Engelhart, Dirk Lebiedz, and Sebastian Sager. Optimal control for selected cancer chemotherapy ODE models: A view on the potential of optimal schedules and choice of objective function. *Math. Biosci.*, 229(1):123–134, jan 2011.

[165] Urszula Ledzewicz and Heinz Schättler. Application of Optimal Control to a System Describing Tumor Anti-Angiogenesis. In *17th Int. Symp. Math. Theory Networks Syst.*, pages 478–484, Kyoto, Japan, 2006.

[166] Reiko J. Tanaka, Masahiro Ono, and Heather a. Harrington. Skin Barrier Homeostasis in Atopic Dermatitis: Feedback Regulation of Kallikrein Activity. *PLoS One*, 6(5):e19895, may 2011.

[167] E. Dominguez-Huttinger, Masahiro Ono, Mauricio Barahona, and Reiko J. Tanaka. Risk factor-dependent dynamics of atopic dermatitis: modelling multi-scale regulation of epithelium homeostasis. *Interface Focus*, 3(2):20120090–20120090, feb 2013.

[168] Anaïs Briot, Céline Deraison, Matthieu Lacroix, Chrystelle Bonnart, Aurélie Robin, Céline Besson, Pierre Dubus, and Alain Hovnanian. Kallikrein 5 induces atopic dermatitislike lesions through PAR2-mediated thymic stromal lymphopoietin expression in Netherton syndrome. *J. Exp. Med.*, 206(5):1135–1147, may 2009.

[169] Jason R Picardo and Anand V P Gurumoorthy. Evaluation of MATCONT of MATLAB for Constructing Bifurcation Diagrams of Chemical Process Systems. III(3), 2011.

[170] Douglas S. Shafer. Nonlinear Dynamics and Chaos: With Applications to Physics, Biology, Chemistry, and Engineering (Steven H. Strogatz). *SIAM Rev.*, 37(2):280–281, jun 1995.

[171] Alexandra Goeke and Sebastian Walcher. Quasi-Steady State: Searching for and Utilizing Small Parameters. In Stephan Johann, Andreas and Kruse, Hans-Peter and Rupp, Florian and Schmitz, editor, *Springer Proc. Math. Stat.*, volume 35, chapter 8, pages 153–178. Springer Basel, 2013.

[172] Marianne Demerjian, Jean-Pierre Hachem, Erwin Tschachler, Geertrui Denecker, Wim Declercq, Peter Vandenabeele, Theodora Mauro, Melanie Hupe, Debra Crumrine, Truus Roelandt, Evi Houben, Peter M Elias, and Kenneth R Feingold. Acute Modulations in Permeability Barrier Function Regulate Epidermal Cornification. *Am. J. Pathol.*, 172(1):86–97, jan 2008.

[173] Piyush Koria, Daniel Brazeau, Keith Kirkwood, Patrick Hayden, Mitchell Klausner, and Stelios T. Andreadis. Gene expression profile of tissue engineered skin subjected to acute barrier disruption. *J. Invest. Dermatol.*, 121(2):368–382, aug 2003.

[174] Lennart M. Roesner, Thomas Werfel, and Annice Heratizadeh. The adaptive immune system in atopic dermatitis and implications on therapy. *Expert Rev. Clin. Immunol.*, 12(7):787–796, jul 2016.

[175] Thomas Bieber, Natalija Novak, Nadine Herrman, and Susanne Koch. Role of Dendritic Cells in Atopic Dermatitis: An Update. *Clin. Rev. Allergy Immunol.*, 41(3):254–258, dec 2011.

[176] Alan B. Arehart and William A. Wolovich. Bumpless switching in hybrid systems. In *Hybrid Syst. IV*, number 1, pages 1–17. 1997.

[177] Michael S Branicky and Sven Erik Mattsson. Simulation of hybrid systems. In *Hybrid Syst. IV*, pages 31–56. 1997.

[178] Mario di Bernardo, Chris J. Budd, Alan R. Champneys, Piotr Kowalczyk, Arne B. Nordmark, Gerard Olivar Tost, and Petri T. Piiroinen. Bifurcations in Nonsmooth Dynamical Systems. *SIAM Rev.*, 50(4):629–701, jan 2008.

[179] E. M. Izhikevich. Hybrid spiking models. *Philos. Trans. R. Soc. A Math. Phys. Eng. Sci.*, 368(1930):5061–5070, nov 2010.

[180] J.-I. Imura, Kenji Kashima, Masami Kusano, Tsukasa Ikeda, and Tomohiro Morohoshi. Piecewise affine systems approach to control of biological networks. *Philos. Trans. R. Soc. A Math. Phys. Eng. Sci.*, 368(1930):4977–4993, nov 2010.

[181] Theodore J Perkins, Roy Wilds, and Leon Glass. Robust dynamics in minimal hybrid models of genetic networks. *Philos. Trans. R. Soc. A Math. Phys. Eng. Sci.*, 368(1930):4961–4975, nov 2010.

[182] Abhyudai Singh and João P Hespanha. Stochastic hybrid systems for studying biochemical processes. *Philos. Trans. R. Soc. A Math. Phys. Eng. Sci.*, 368(1930):4995–5011, nov 2010.

[183] Luonan Chen, Ruiqi Wang, Tetsuya J. Kobayashi, and Kazuyuki Aihara. Dynamics of gene regulatory networks with cell division cycle. *Phys. Rev. E*, 70(1):011909, jul 2004.

[184] Dorjsuren Battogtokh, Kazuyuki Aihara, and John J. Tyson. Synchronization of Eukaryotic Cells by Periodic Forcing. *Phys. Rev. Lett.*, 96(14):148102, apr 2006.

[185] J. M. Osborne, A. Walter, S. K. Kershaw, G. R. Mirams, A. G. Fletcher, P. Pathmanathan, D. Gavaghan, O. E. Jensen, P. K. Maini, and H. M. Byrne. A hybrid approach to multi-scale modelling of cancer. *Philos. Trans. R. Soc. A Math. Phys. Eng. Sci.*, 368(1930):5013–5028, nov 2010.

[186] Alberto Bemporad and Manfred Morari. Control of systems integrating logic, dynamics, and constraints. *Automatica*, 35(3):407–427, mar 1999.

[187] Kazuyuki Aihara and Hideyuki Suzuki. Theory of hybrid dynamical systems and its applications to biological and medical systems. *Philos. Trans. R. Soc. A Math. Phys. Eng. Sci.*, 368(1930):4893–4914, nov 2010.

[188] P Riedinger, C. Lung, and F Kratz. An Optimal Control Approach for Hybrid Systems. *Eur. J. Control*, 9(5):449–458, jan 2003.

[189] M.S. Branicky, V.S. Borkar, and S.K. Mitter. A unified framework for hybrid control: model and optimal control theory. *IEEE Trans. Automat. Contr.*, 43(1):31–45, 1998.

[190] Elisa Domínguez-Hüttinger, Panayiotis Christodoulides, Kosuke Miyauchi, Alan D. Irvine, Mariko Okada-Hatakeyama, Masato Kubo, and Reiko J. Tanaka. Mathematical modeling of atopic dermatitis reveals "double-switch" mechanisms underlying 4 common disease phenotypes. *J. Allergy Clin. Immunol.*, 139(6):1861–1872.e7, jun 2017.

[191] Lawrence F. Eichenfield, Wynnis L. Tom, Timothy G. Berger, Alfons Krol, Amy S. Paller, Kathryn Schwarzenberger, James N. Bergman, Sarah L. Chamlin, David E. Cohen, Kevin D. Cooper, Kelly M. Cordoro, Dawn M. Davis, Steven R. Feldman, Jon M. Hanifin, David J. Margolis, Robert A. Silverman, Eric L. Simpson, Hywel C. Williams, Craig A. Elmets, Julie Block, Christopher G. Harrod, Wendy Smith Begolka, and Robert Sidbury. Guidelines of care for the management of atopic dermatitis. *J. Am. Acad. Dermatol.*, 71(1):116–132, 2014.

[192] Jonathan M. Spergel. Epidemiology of Atopic Dermatitis and Atopic March in Children. *Immunol. Allergy Clin. North Am.*, 30(3):269–280, aug 2010.

[193] T. Bieber, C. Akdis, R. Lauener, C. Traidl-Hoffmann, P. Schmid-Grendelmeier, G. Schäppi, J.-P. Allam, C. Apfelbacher, M. Augustin, L. Beck, T. Biedermann, C. Braun-Fahrländer, F. T. Chew, T. Clavel, R. Crameri, U. Darsow, M. Deleuran, D. Dittlein, H.-W. Duchna, L. Eichenfeld, K. Eyerich, R. Frei, C. Gelmetti, U. Gieler, S. Gilles, M. Glatz, K. Grando, J. Green, J. Gutermuth, E. Guttman-Yassky, J. Hanifin, D. Hijnen, W. Hoetzenecker, A. Irvine, A. Kalweit, N. Katoh, E. Knol, H. Koren, M. Möhrenschlager, D. Münch, N. Novak, L. O'Mahony, A. S. Paller, C. Rhyner, C. Roduit, K. Schiesser, J. Schröder, D. Simon, H.-U. Simon, M. Sokolowska, P. Spuls, J.-F. Stalder, D. Straub, Z. Szalai, A. Taieb, R. Takaoka, G. Todd, A. Todorova, C. Vestergaard, T. Werfel, A. Wollenberg, and J. Ring. Global Allergy Forum and 3rd Davos Declaration 2015. *Allergy*, 71(5):588–592, may 2016.

[194] Reiko J Tanaka and Masahiro Ono. Skin Disease Modeling from a Mathematical Perspective. *J. Invest. Dermatol.*, 133(6):1472–1478, jun 2013.

[195] N.J. Reynolds. One hundred and twenty-five years and counting: into an era of systems dermatology. *Br. J. Dermatol.*, 171(6):1279–1281, dec 2014.

[196] Colin N a Palmer, Alan D Irvine, Ana Terron-Kwiatkowski, Yiwei Zhao, Haihui Liao, Simon P Lee, David R Goudie, Aileen Sandilands, Linda E Campbell, Frances J D Smith, Gráinne M O'Regan, Rosemarie M Watson, Jo E Cecil, Sherri J Bale, John G Compton, John J DiGiovanna, Philip Fleckman, Sue Lewis-Jones, Gehan Arseculeratne, Ann Sergeant, Colin S Munro, Brahim El Houate, Ken McElreavey, Liselotte B Halkjaer, Hans Bisgaard, Somnath Mukhopadhyay, and W H Irwin McLean. Common loss-of-function variants of the epidermal barrier protein filaggrin are a major predisposing factor for atopic dermatitis. *Nat. Genet.*, 38(4):441–446, apr 2006.

[197] Sara J Brown, Karin Kroboth, Aileen Sandilands, Linda E Campbell, Elizabeth Pohler, Sanja Kezic, Heather J Cordell, W H Irwin McLean, and Alan D Irvine. Intragenic Copy Number Variation within Filaggrin Contributes to the Risk of Atopic Dermatitis with a Dose-Dependent Effect. *J. Invest. Dermatol.*, 132(1):98–104, jan 2012.

[198] Alan D. Irvine, W.H. Irwin McLean, and Donald Y.M. Leung. Filaggrin Mutations Associated with Skin and Allergic Diseases. *N. Engl. J. Med.*, 365(14):1315–1327, oct 2011.

[199] Ikue Nemoto-Hasebe, Masashi Akiyama, Toshifumi Nomura, Aileen Sandilands, W.H. Irwin McLean, and Hiroshi Shimizu. Clinical Severity Correlates with Impaired Barrier in Filaggrin-Related Eczema. *J. Invest. Dermatol.*, 129(3):682–689, mar 2009.

[200] Sanja Kezic, Gráinne M. O'Regan, René Lutter, Ivone Jakasa, Ellen S. Koster, Sean Saunders, Peter Caspers, Patrick M.J.H. Kemperman, Gerwin J. Puppels, Aileen Sandilands, Huijia Chen, Linda E. Campbell, Karin Kroboth, Rosemarie Watson, Padraic G. Fallon, W. H Irwin McLean, and Alan D. Irvine. Filaggrin loss-of-function mutations are associated with enhanced expression of IL-1 cytokines in the stratum corneum of patients with atopic dermatitis and in a murine model of filaggrin deficiency. *J. Allergy Clin. Immunol.*, 129(4):1031–1039.e1, apr 2012.

[201] Tiffany C. Scharschmidt, Mao-Qiang Man, Yutaka Hatano, Debra Crumrine, Roshan Gunathilake, John P. Sundberg, Kathleen a. Silva, Theodora M. Mauro, Melanie Hupe, Soyun Cho, Yan Wu, Anna Celli, Matthias Schmuth, Kenneth R. Feingold, and Peter M. Elias. Filaggrin deficiency confers a paracellular barrier abnormality that reduces inflammatory thresholds to irritants and haptens. *J. Allergy Clin. Immunol.*, 124(3):496–506.e6, sep 2009.

[202] Hiroshi Kawasaki, Keisuke Nagao, Akiharu Kubo, Tsuyoshi Hata, Atsushi Shimizu, Hideaki Mizuno, Taketo Yamada, and Masayuki Amagai. Altered stratum corneum barrier and enhanced percutaneous immune responses in filaggrin-null mice. *J. Allergy Clin. Immunol.*, 129(6):1538–1546.e6, jun 2012.

[203] Eric L. Simpson, Joanne R. Chalmers, Jon M. Hanifin, Kim S. Thomas, Michael J. Cork, W.H. Irwin McLean, Sara J. Brown, Zunqiu Chen, Yiyi Chen, and Hywel C. Williams. Emollient enhancement of the skin barrier from birth offers effective atopic dermatitis prevention. *J. Allergy Clin. Immunol.*, 134(4):818–823, oct 2014.

[204] Kenta Horimukai, Kumiko Morita, Masami Narita, Mai Kondo, Hiroshi Kitazawa, Makoto Nozaki, Yukiko Shigematsu, Kazue Yoshida, Hironori Niizeki, Ken-ichiro Motomura, Haruhiko Sago, Tetsuya Takimoto, Eisuke Inoue, Norio Kamemura, Hiroshi Kido, Junzo Hisatsune, Motoyuki Sugai, Hiroyuki Murota, Ichiro Katayama, Takashi Sasaki, Masayuki Amagai, Hideaki Morita, Akio Matsuda, Kenji Matsumoto, Hirohisa Saito, and Yukihiro Ohya. Application of moisturizer to neonates prevents development of atopic dermatitis. *J. Allergy Clin. Immunol.*, 134(4):824–830.e6, oct 2014.

[205] Henrik Dommisch, Whasun O. Chung, Maryam G. Rohani, David Williams, Minnie Rangarajan, Mike A. Curtis, and Beverly A. Dale. Protease-Activated Receptor 2 Mediates Human Beta-Defensin 2 and CC Chemokine Ligand 20 mRNA Expression in Response to Proteases Secreted by Porphyromonas gingivalis. *Infect. Immun.*, 75(9):4326–4333, sep 2007.

[206] Hidehiro Yamane, Jinfang Zhu, and William E Paul. Independent roles for IL-2 and GATA-3 in stimulating naive CD4 + T cells to generate a Th2-inducing cytokine environment. *J. Exp. Med.*, 202(6):793–804, sep 2005.

[207] Zhe Zhang, Thomas B. Clarke, and Jeffrey N. Weiser. Cellular effectors mediating Th17-dependent clearance of pneumococcal colonization in mice. *J. Clin. Invest.*, 119(7):1899–1909, jun 2009.

[208] T. Hofer, Holger Nathansen, M. Lohning, Andreas Radbruch, and Reinhart Heinrich. GATA-3 transcriptional imprinting in Th2 lymphocytes: A mathematical model. *Proc. Natl. Acad. Sci.*, 99(14):9364–9368, jul 2002.

[209] Susanna Celli, Mark Day, A. J. Muller, C. Molina-Paris, Grant Lythe, and Philippe Bousso. How many dendritic cells are required to initiate a T-cell response? *Blood*, 120(19):3945–3948, nov 2012.

[210] Min Chen, Li Huang, Zainuer Shabier, and Jin Wang. Regulation of the lifespan in dendritic cell subsets. *Mol. Immunol.*, 44(10):2558–2565, apr 2007.

[211] Shigetoshi Sano. Keratinocyte-specific ablation of Stat3 exhibits impaired skin remodeling, but does not affect skin morphogenesis. *EMBO J.*, 18(17):4657–4668, sep 1999.

[212] Stephen J Galli, Mindy Tsai, and Adrian M Piliponsky. The development of allergic inflammation. *Nature*, 454(7203):445–454, jul 2008.

[213] Karin M Aberg, Mao-Qiang Man, Richard L Gallo, Tomas Ganz, Debra Crumrine, Barbara E Brown, Eung-Ho Choi, Dong-Kun Kim, Jens M Schröder, Kenneth R Feingold, and Peter M Elias. Co-Regulation and Interdependence of the Mammalian Epidermal Permeability and Antimicrobial Barriers. *J. Invest. Dermatol.*, 128(4):917–925, apr 2008.

[214] Nicolas Cenac, Alex C Chin, Rafael Garcia-Villar, Christel Salvador-Cartier, Laurent Ferrier, Nathalie Vergnolle, André G Buret, Jean Fioramonti, and Lionel Bueno. PAR 2 activation alters colonic paracellular permeability in mice via IFN-γ-dependent and -independent pathways. *J. Physiol.*, 558(3):913–925, aug 2004.

[215] J Das, C H Chen, L Yang, L Cohn, P Ray, and A Ray. A critical role for NF-kappa B in GATA3 expression and TH2 differentiation in allergic airway inflammation. *Nat. Immunol.*, 2(1):45–50, 2001.

[216] Patrick Duckney, Heng Wong, José Serrano, Diaraf Yaradou, Thierry Oddos, and Georgios N Stamatas. The role of the skin barrier in modulating the effects of common skin microbial species on the inflammation, differentiation and proliferation status of epidermal keratinocytes. *BMC Res. Notes*, 6(1):474, 2013.

[217] Kenshi Yamasaki, Kimberly Kanada, Daniel T Macleod, Andrew W Borkowski, Shin Morizane, Teruaki Nakatsuji, Anna L Cogen, and Richard L Gallo. TLR2 Expression Is Increased in Rosacea and Stimulates Enhanced Serine Protease Production by Keratinocytes. *J. Invest. Dermatol.*, 131(3):688–697, mar 2011.

[218] Wei-ping Zheng and Richard A Flavell. The Transcription Factor GATA-3 Is Necessary and Sufficient for Th2 Cytokine Gene Expression in CD4 T Cells. *Cell*, 89(4):587–596, may 1997.

[219] Donald Y.M. Leung and Emma Guttman-Yassky. Deciphering the complexities of atopic dermatitis: Shifting paradigms in treatment approaches. *J. Allergy Clin. Immunol.*, 134(4):769–779, oct 2014.

[220] Takashi Sasaki, Aiko Shiohama, Akiharu Kubo, Hiroshi Kawasaki, Akemi Ishida-Yamamoto, Taketo Yamada, Takayuki Hachiya, Atsushi Shimizu, Hideyuki Okano, Jun Kudoh, and Masayuki Amagai. A homozygous nonsense mutation in the gene for Tmem79, a component for the lamellar granule secretory system, produces spontaneous eczema in an experimental model of atopic dermatitis. *J. Allergy Clin. Immunol.*, 132(5):1111–1120.e4, nov 2013.

[221] Sean P. Saunders, Christabelle S.M. Goh, Sara J. Brown, Colin N.A. Palmer, Rebecca M. Porter, Christian Cole, Linda E. Campbell, Marek Gierlinski, Geoffrey J. Barton, Georg Schneider, Allan Balmain, Alan R. Prescott, Stephan Weidinger, Hansjörg Baurecht, Michael Kabesch, Christian Gieger, Young-Ae Lee, Roger Tavendale, Somnath Mukhopadhyay, Stephen W. Turner, Vishnu B. Madhok, Frank M. Sullivan, Caroline Relton, John Burn, Simon Meggitt, Catherine H. Smith, Michael A. Allen, Jonathan N.W. N. Barker, Nick J. Reynolds, Heather J. Cordell, Alan D. Irvine, W.H. Irwin McLean, Aileen Sandilands, and Padraic G. Fallon. Tmem79/Matt is the matted mouse gene and is a predisposing gene for atopic dermatitis in human subjects. *J. Allergy Clin. Immunol.*, 132(5):1121–1129, nov 2013.

[222] Steven M Holland, Frank R DeLeo, Houda Z Elloumi, Amy P Hsu, Gulbu Uzel, Nina Brodsky, Alexandra F Freeman, Andrew Demidowich, Joie Davis, Maria L Turner, Victoria L Anderson, Dirk N Darnell, Pamela a Welch, Douglas B Kuhns, David M Frucht, Harry L Malech, John I Gallin, Scott D Kobayashi, Adeline R Whitney, Jovanka M Voyich, James M Musser, Cristina Woellner, Alejandro A Schäffer, Jennifer M Puck, and Bodo Grimbacher. STAT3 Mutations in the Hyper-IgE Syndrome. *N. Engl. J. Med.*, 357(16):1608–1619, oct 2007.

[223] Atsushi Okuma, Katsuaki Hoshino, Tomoyuki Ohba, Sawako Fukushi, Setsuya Aiba, Shizuo Akira, Masao Ono, Tsuneyasu Kaisho, and Tatsushi Muta. Enhanced Apoptosis by Disruption of the STAT3-IκB-ζ Signaling Pathway in Epithelial Cells Induces Sjögren's Syndrome-like Autoimmune Disease. *Immunity*, 38(3):450–460, mar 2013.

[224] Mao-Qiang Man, Yutaka Hatano, Seung H Lee, Mona Man, Sandra Chang, Kenneth R Feingold, Donald Y.M. Leung, Walter Holleran, Yoshikazu Uchida, and Peter M Elias. Characterization of a Hapten-Induced, Murine Model with Multiple Features of Atopic Dermatitis: Structural, Immunologic, and Biochemical Changes following Single Versus Multiple Oxazolone Challenges. *J. Invest. Dermatol.*, 128(1):79–86, jan 2008.

[225] Yasutomo Imai, Koubun Yasuda, Yoshiko Sakaguchi, Takashi Haneda, Hitoshi Mizutani, Tomohiro Yoshimoto, Kenji Nakanishi, and Kiyofumi Yamanishi. Skin-specific expression of IL-33 activates group 2 innate lymphoid cells and elicits atopic dermatitis-like inflammation in mice. *Proc. Natl. Acad. Sci.*, 110(34):13921–13926, aug 2013.

[226] Emily Hams, Rachel Bermingham, and Padraic G. Fallon. Macrophage and Innate Lymphoid Cell Interplay in the Genesis of Fibrosis. *Front. Immunol.*, 6:597, nov 2015.

[227] Parviz Ahmad-Nejad, Salima Mrabet-Dahbi, Kristine Breuer, Martina Klotz, Thomas Werfel, Udo Herz, Klaus Heeg, Michael Neumaier, and Harald Renz. The Toll-like receptor 2 R753Q polymorphism defines a subgroup of patients with atopic dermatitis having severe phenotype. *J. Allergy Clin. Immunol.*, 113(3):565–567, mar 2004.

[228] M Zasloff. Antimicrobial peptides of multicellular organisms. *Nature*, 415(0028-0836 (Print)):389–395, 2002.

[229] Diego a. Oyarzún, Madalena Chaves, and Marit Hoff-Hoffmeyer-Zlotnik. Multistability and oscillations in genetic control of metabolism. *J. Theor. Biol.*, 295:139–153, feb 2012.

[230] Shizuo Akira and Kiyoshi Takeda. Toll-like receptor signalling. *Nat. Rev. Immunol.*, 4(7):499–511, jul 2004.

[231] Takuwa Yasuda, Toshiyuki Fukada, Keigo Nishida, Manabu Nakayama, Masashi Matsuda, Ikuo Miura, Teruki Dainichi, Shinji Fukuda, Kenji Kabashima, Shinji Nakaoka, Bum-Ho Bin, Masato Kubo, Hiroshi Ohno, Takanori Hasegawa, Osamu Ohara, Haruhiko Koseki, Shigeharu Wakana, and Hisahiro Yoshida. Hyperactivation of JAK1 tyrosine kinase induces stepwise, progressive pruritic dermatitis. *J. Clin. Invest.*, 126(6):2064–2076, apr 2016.

[232] Yoshito Hirata, Mario di Bernardo, Nicholas Bruchovsky, and Kazuyuki Aihara. Hybrid optimal scheduling for intermittent androgen suppression of prostate cancer. *Chaos An Interdiscip. J. Nonlinear Sci.*, 20(4):045125, dec 2010.

[233] Stefanie Schoepe, Heike Schacke, Ekkehard May, and Khusru Asadullah. Glucocorticoid therapy-induced skin atrophy. *Exp. Dermatol.*, 15(6):406–420, jun 2006.

[234] S.G. Danby, J. Chittock, K. Brown, L.H. Albenali, and M.J. Cork. The effect of tacrolimus compared with betamethasone valerate on the skin barrier in volunteers with quiescent atopic dermatitis. *Br. J. Dermatol.*, 170(4):914–921, apr 2014.

[235] Luonan Chen, Rui Liu, Zhi-Ping Liu, Meiyi Li, and Kazuyuki Aihara. Detecting early-warning signals for sudden deterioration of complex diseases by dynamical network biomarkers. *Sci. Rep.*, 2(1):342, dec 2012.

[236] R Shouval, O Bondi, H Mishan, A Shimoni, R Unger, and A Nagler. Application of machine learning algorithms for clinical predictive modeling: a data-mining approach in SCT. *Bone Marrow Transplant.*, 49(3):332–337, mar 2014.

[237] Panayiotis Christodoulides, Yoshito Hirata, Elisa Domínguez-Hüttinger, Simon G. Danby, Michael J. Cork, Hywel C. Williams, Kazuyuki Aihara, and Reiko J. Tanaka. Computational design of treatment strategies for proactive therapy on atopic dermatitis using optimal control theory. *Philos. Trans. R. Soc. A Math. Phys. Eng. Sci.*, 375(2096):20160285, jun 2017.

[238] Eric L. Simpson. Atopic dermatitis: a review of topical treatment options. *Curr. Med. Res. Opin.*, 26(3):633–640, mar 2010.

[239] Thomas Bieber. Personalized Management of Atopic Dermatitis: Beyond Emollients and Topical Steroids. In Thomas Bieber and Frank Nestle, editors, *Pers. Treat. Options Dermatology*, chapter 5, pages 61–76. Springer Berlin Heidelberg, Berlin, Heidelberg, 2015.

[240] Rainer Storn and Kenneth Price. No Title. *J. Glob. Optim.*, 11(4):341–359, sep 1997.

[241] K. V. Price, R. M. Storn, and J. A. Lampinen. *Differential Evolution*. Natural Computing Series. Springer-Verlag, Berlin/Heidelberg, 2005.

[242] Jens Michael Jensen, Kerstin Ahrens, Josef Meingassner, Andreas Scherer, Matthias Bräutigam, Anton Stütz, Thomas Schwarz, Regina Fölster-Holst, Jürgen Harder, Regine Gläser, and Ehrhardt Proksch. Differential suppression of epidermal antimicrobial protein expression in atopic dermatitis and in EFAD mice by pimecrolimus compared to corticosteroids. *Exp. Dermatol.*, 20(10):783–788, 2011.

[243] Daniela Rozkova, Rudolf Horvath, Jirina Bartunkova, and Radek Spisek. Glucocorticoids severely impair differentiation and antigen presenting function of dendritic cells despite upregulation of Toll-like receptors. *Clin. Immunol.*, 120(3):260–271, 2006.

[244] James M Mason, Julie Carr, Carolyn Buckley, Steve Hewitt, Phillip Berry, Josh Taylor, and Michael J Cork. Improved emollient use reduces atopic eczema symptoms and is cost neutral in infants: before-and-after evaluation of a multifaceted educational support programme. *BMC Dermatol.*, 13(1):7, 2013.

[245] Ming Yang, Changhe Li, Zhihua Cai, and Jing Guan. Differential Evolution With Auto-Enhanced Population Diversity. *IEEE Trans. Cybern.*, 45(2):302–315, feb 2015.

[246] H. Aubert-Wastiaux, L. Moret, A. Le Rhun, A.M. Fontenoy, J.M. Nguyen, C. Leux, L. Misery, P. Young, M. Chastaing, N. Danou, P. Lombrail, F. Boralevi, J.P. Lacour, J. Mazereeuw-Hautier, J.-F. Stalder, and S. Barbarot. Topical corticosteroid phobia in atopic dermatitis: a study of its nature, origins and frequency. *Br. J. Dermatol.*, 165(4):808–814, oct 2011.

[247] Rachel M. Ellis, Laine H. Koch, Erin McGuire, and Judith V. Williams. Potential Barriers to Adherence in Pediatric Dermatology. *Pediatr. Dermatol.*, 28(3):242–244, may 2011.

[248] E. F. Camacho and C. Bordons. *Model Predictive control*. Advanced Textbooks in Control and Signal Processing. Springer London, London, 2007.

[249] William L Clarke, Stacey Anderson, Marc Breton, Stephen Patek, Laurissa Kashmer, and Boris Kovatchev. Closed-Loop Artificial Pancreas Using Subcutaneous Glucose Sensing and Insulin Delivery and a Model Predictive Control Algorithm: The Virginia Experience. *J. Diabetes Sci. Technol.*, 3(5):1031–1038, sep 2009.

[250] Roman Hovorka, Janet M. Allen, Daniela Elleri, Ludovic J. Chassin, Julie Harris, Dongyuan Xing, Craig Kollman, Tomas Hovorka, Anne Mette F Larsen, Marianna Nodale, Alessandra De Palma, Malgorzata E. Wilinska, Carlo L. Acerini, and David B. Dunger. Manual closed-loop insulin delivery in children and adolescents with type 1 diabetes: a phase 2 randomised crossover trial. *Lancet*, 375(9716):743–751, feb 2010.

[251] Yoshito Hirata, Shun ichi Azuma, and Kazuyuki Aihara. Model predictive control for optimally scheduling intermittent androgen suppression of prostate cancer. *Methods*, 67(3):278–281, 2014.

[252] Sarah L. Noble, Eric Sherer, Robert E. Hannemann, Doraiswami Ramkrishna, Terry Vik, and Ann E. Rundell. Using adaptive model predictive control to customize maintenance therapy chemotherapeutic dosing for childhood acute lymphoblastic leukemia. *J. Theor. Biol.*, 264(3):990–1002, 2010.

[253] P G van der Valk, E Snater, W Verbeek-Gijsbers, P Duller, and P C van de Kerkhof. Out-patient treatment of atopic dermatitis with crude coal tar. *Dermatology*, 193(1):41–4, 1996.

[254] Jordan B Slutsky, Richard A F Clark, Alexander A Remedios, and Peter A Klein. An evidence-based review of the efficacy of coal tar preparations in the treatment of psoriasis and atopic dermatitis. *J. Drugs Dermatol.*, 9(10):1258–64, oct 2010.

[255] Benjamin Farahnik, Kourosh Beroukhim, Melissa Danesh, Mio Nakamura, Michael Abrouk, Tian Hao Zhu, Rasnik Singh, Kristina Lee, Tina Bhutani, and John Koo. Successful use of a modified Goeckerman regimen in the treatment of chronic severe atopic dermatitis: A prospective pilot study. *J. Am. Acad. Dermatol.*, 75(5):1068–1071, nov 2016.

[256] Gurvinder P Thami and R Sarkar. Coal tar: past, present and future. *Clin. Exp. Dermatol.*, 27(2):99–103, mar 2002.

[257] W P Arnold. Tar. *Clin. Dermatol.*, 15(5):739–44, 1997.

[258] Judith H J Roelofzen, Katja K H Aben, Ursula T H Oldenhof, Pieter-Jan Coenraads, Hans A Alkemade, Peter C M van de Kerkhof, Pieter G M van der Valk, and Lambertus A L M Kiemeney. No increased risk of cancer after coal tar treatment in patients with psoriasis or eczema. *J. Invest. Dermatol.*, 130(4):953–61, apr 2010.

[259] W Z Maughan, S A Muller, H O Perry, M R Pittelkow, and P C O'Brien. Incidence of skin cancers in patients with atopic dermatitis treated with ocal tar. A 25-year follow-up study. *J. Am. Acad. Dermatol.*, 3(6):612–5, dec 1980.

[260] A M Niordson and D Stahl. Treatment of psoriasis with Clinitar Cream. A controlled clinical trial. *Br. J. Clin. Pract.*, 39(2):67–8, 72, feb 1985.

[261] P Boffetta, N Jourenkova, and P Gustavsson. Cancer risk from occupational and environmental exposure to polycyclic aromatic hydrocarbons. *Cancer Causes Control*, 8(3):444–72, may 1997.

[262] A D Burden, H Muston, and M H Beck. Intolerance and contact allergy to tar and dithranol in psoriasis. *Contact Dermatitis*, 31(3):185–6, sep 1994.

[263] Cosmetic Ingredient Review Expert Panel. Final Safety Assessment of Coal Tar as Used in Cosmetics. *Int. J. Toxicol.*, 27(2_suppl):1–24, mar 2008.

[264] Andrew N. Lin and Kathleen Moses. Tar Revisited. *Int. J. Dermatol.*, 24(4):216–218, may 2007.

[265] W.H. Irwin McLean and Alan D. Irvine. Old King Coal molecular mechanisms underlying an ancient treatment for atopic eczema. *J. Clin. Invest.*, 123(2):551–553, jan 2013.

[266] Roland Aschoff, Jochen Schmitt, Peter Knuschke, Edmund Koch, Matthias Bräutigam, and Michael Meurer. Evaluation of the atrophogenic potential of hydrocortisone 1% cream and pimecrolimus 1% cream in uninvolved forehead skin of patients with atopic dermatitis using optical coherence tomography. *Exp. Dermatol.*, 20(10):832–836, oct 2011.

[267] Elizabeth Moore, A Williams, E Manias, and G Varigos. Nurse-led clinics reduce severity of childhood atopic eczema: a review of the literature. *Br. J. Dermatol.*, 155(6):1242–1248, dec 2006.

[268] Matthew J Zirwas and Jessica L Holder. Patient education strategies in dermatology: part 2: methods. *J. Clin. Aesthet. Dermatol.*, 2(12):28–34, dec 2009.

[269] H.E. Gustavsen and P. Gjersvik. Topical corticosteroid phobia among parents of children with atopic dermatitis in a semirural area of Norway. *J. Eur. Acad. Dermatology Venereol.*, 30(1):168–168, jan 2016.

[270] Reiji Kojima, Takeo Fujiwara, Akio Matsuda, Masami Narita, Osamu Matsubara, Shigeaki Nonoyama, Yukihiro Ohya, Hirohisa Saito, and Kenji Matsumoto. Factors Associated with Steroid Phobia in Caregivers of Children with Atopic Dermatitis. *Pediatr. Dermatol.*, 30(1):29–35, jan 2013.

[271] Se-Young Park, Mi-Ra Choi, Jung-Im Na, Sang-Woong Youn, Kyoung-Chan Park, and Chang-Hun Huh. Recalcitrant Atopic Dermatitis Treated with Omalizumab. *Ann. Dermatol.*, 22(3):349, 2010.

[272] Emma Mooney, Marius Rademaker, Rebecca Dailey, Ben S. Daniel, Catherine Drummond, Gayle Fischer, Rachael Foster, Claire Grills, Anne Halbert, Sarah Hill, Emma King, Elizabeth Leins, Vanessa Morgan, Roderic J. Phillips, John Relic, Michelle Rodrigues, Laura Scardamaglia, Saxon Smith, John Su, Orli Wargon, and David Orchard. Adverse effects of topical corticosteroids in paediatric eczema: Australasian consensus statement. *Australas. J. Dermatol.*, 56(4):241–251, nov 2015.

[273] Liat Samuelov and Eli Sprecher. Peeling off the genetics of atopic dermatitislike congenital disorders. *J. Allergy Clin. Immunol.*, 134(4):808–815, oct 2014.

[274] Eleonora Candi, Rainer Schmidt, and Gerry Melino. The cornified envelope: a model of cell death in the skin. *Nat. Rev. Mol. Cell Biol.*, 6(4):328–340, apr 2005.

[275] Sandra Pankow. Regulation of epidermal homeostasis and repair by phosphoinositide 3-kinase. *J. Cell Sci.*, 119(19):4033–4046, oct 2006.

[276] Daniel D Bikle, Zhongjian Xie, and Chia-Ling Tu. Calcium regulation of keratinocyte differentiation. *Expert Rev. Endocrinol. Metab.*, 7(4):461–472, jul 2012.

[277] Cécile Caubet, Nathalie Jonca, Maria Brattsand, Marina Guerrin, Dominique Bernard, Rainer Schmidt, Torbjörn Egelrud, Michel Simon, and Guy Serre. Degradation of Corneodesmosome Proteins by Two Serine Proteases of the Kallikrein Family, SCTE/KLK5/hK5 and SCCE/KLK7/hK7. *J. Invest. Dermatol.*, 122(5):1235–1244, may 2004.

[278] Man Mao-Qiang, Theodora Mauro, Graham Bench, Raphael Warren, Peter M. Elias, and Kenneth R. Feingold. Calcium and potassium inhibit barrier recovery after disruption, independent of the type of insult in hairless mice. *Exp. Dermatol.*, 6(1):36–40, feb 1997.

[279] D.G. Koopman, S. Kezic, and M.M. Verberk. Skin reaction and recovery: a repeated sodium lauryl sulphate patch test vs. a 24-h patch test and tape stripping. *Br. J. Dermatol.*, 150(3):493–499, mar 2004.

[280] Danuta Gutowska-Owsiak, Anna L. Schaupp, Maryam Salimi, Tharini A. Selvakumar, Tess McPherson, Stephen Taylor, and Graham S. Ogg. IL-17 downregulates filaggrin and affects keratinocyte expression of genes associated with cellular adhesion. *Exp. Dermatol.*, 21(2):104–110, feb 2012.

[281] Xiao-Jun Tian, Xiao-Peng Zhang, Feng Liu, and Wei Wang. Interlinking positive and negative feedback loops creates a tunable motif in gene regulatory networks. *Phys. Rev. E. Stat. Nonlin. Soft Matter Phys.*, 80(1 Pt 1):011926, jul 2009.

[282] R Maithreye and Somdatta Sinha. Propagation of extrinsic perturbation in a negatively auto-regulated pathway. *Phys. Biol.*, 4(1):48–59, apr 2007.

[283] Tony Yu-Chen Tsai, Yoon Sup Choi, Wenzhe Ma, Joseph R. Pomerening, Chao Tang, and James E. Ferrell. Robust, tunable biological oscillations from interlinked positive and negative feedback loops. *Science*, 321(5885):126–9, jul 2008.

[284] David Angeli, James E Ferrell, and Eduardo D Sontag. Detection of multistability, bifurcations, and hysteresis in a large class of biological positive-feedback systems. *Proc. Natl. Acad. Sci. U. S. A.*, 101(7):1822–7, feb 2004.

[285] Eduardo D. Sontag. Some new directions in control theory inspired by systems biology. *Syst. Biol. (Stevenage).*, 1(1):149–158, 2004.

[286] N Blüthgen and H Herzel. MAP-Kinase-Cascade: Switch, Amplifier or Feedback Controller? In *2nd Work. Comput. Biochem. Pathways Genet. Networks*, volume Logos-Verl, pages 55–62, Berlin, 2001. Logos-Verlag.

[287] Onn Brandman and Tobias Meyer. Feedback loops shape cellular signals in space and time. *Science*, 322(5900):390–395, oct 2008.

[288] Jörg Schaber, Anastasiya Lapytsko, and Dietrich Flockerzi. Nested autoinhibitory feedbacks alter the resistance of homeostatic adaptive biochemical networks. *J. R. Soc. Interface*, 11:20130971, 2014.

[289] Mustafa Khammash. An engineering viewpoint on biological robustness. *BMC Biol.*, 14(1):22, 2016.

[290] T M Yi, Y Huang, M I Simon, and J Doyle. Robust perfect adaptation in bacterial chemotaxis through integral feedback control. *Proc. Natl. Acad. Sci. U. S. A.*, 97(9):4649–4653, apr 2000.

[291] Olivier Cinquin and Jacques Demongeot. Roles of positive and negative feedback in biological systems. *C. R. Biol.*, 325(11):1085–1095, nov 2002.

[292] Kim Sneppen, Sandeep Krishna, and Szabolcs Semsey. Simplified models of biological networks. *Annu. Rev. Biophys.*, 39:43–59, 2010.

[293] Nick I. Markevich, Jan B. Hoek, and Boris N. Kholodenko. Signaling switches and bistability arising from multisite phosphorylation in protein kinase cascades. *J. Cell Biol.*, 164(3):353–359, feb 2004.

[294] Hao Song, Paul Smolen, Evyatar Av-Ron, Douglas a Baxter, and John H Byrne. Dynamics of a minimal model of interlocked positive and negative feedback loops of transcriptional regulation by cAMP-response element binding proteins. *Biophys. J.*, 92(10):3407–24, may 2007.

[295] Julia a. Segre. Epidermal barrier formation and recovery in skin disorders. *J. Clin. Invest.*, 116(5):1150–1158, may 2006.

[296] Chrystelle Bonnart, Céline Deraison, Matthieu Lacroix, Yoshikazu Uchida, Céline Besson, Aurélie Robin, Anaïs Briot, Marie Gonthier, Laurence Lamant, Pierre Dubus, Bernard Monsarrat, and Alain Hovnanian. Elastase 2 is expressed in human and mouse epidermis and impairs skin barrier function in Netherton syndrome through filaggrin and lipid misprocessing. *J. Clin. Invest.*, 120(3):871–882, mar 2010.

[297] Peter M. Elias. Epidermal barrier function: intercellular lamellar lipid structures, origin, composition and metabolism. *J. Control. Release*, 15(3):199–208, jun 1991.

[298] Michelle Janssens, Jeroen van Smeden, Gert S. Gooris, Wim Bras, Guiseppe Portale, Peter J. Caspers, Rob J. Vreeken, Thomas Hankemeier, Sanja Kezic, Ron Wolterbeek, Adriana P. Lavrijsen, and Joke a. Bouwstra. Increase in short-chain ceramides correlates with an altered lipid organization and decreased barrier function in atopic eczema patients. *J. Lipid Res.*, 53(12):2755–2766, dec 2012.

[299] Akemi Ishida-Yamamoto, Satomi Igawa, and Mari Kishibe. Order and disorder in corneocyte adhesion. *J. Dermatol.*, 38(7):645–54, jul 2011.

[300] Melanie K. Kuechle, Craig D. Thulin, Richard B. Presland, and Beverly A. Dale. Profilaggrin Requires both Linker and Filaggrin Peptide Sequences to Form Granules: Implications for Profilaggrin Processing In Vivo11This work was presented in part at the Society of Investigative Dermatology meeting in 1997. *J. Invest. Dermatol.*, 112(6):843–852, jun 1999.

[301] Geertrui Denecker, Petra Ovaere, Peter Vandenabeele, and Wim Declercq. Caspase-14 reveals its secrets. *J. Cell Biol.*, 180(3):451–458, feb 2008.

[302] Takeshi Matsui, Kenichi Miyamoto, Akiharu Kubo, Hiroshi Kawasaki, Tamotsu Ebihara, Kazuya Hata, Shinya Tanahashi, Shizuko Ichinose, Issei Imoto, Johji Inazawa, Jun Kudoh, and Masayuki Amagai. SASPase regulates stratum corneum hydration through profilaggrin-to-filaggrin processing. *EMBO Mol. Med.*, 3(6):320–333, jun 2011.

[303] Jun-ichi Sakabe, Mami Yamamoto, Satoshi Hirakawa, Akira Motoyama, Isao Ohta, Kazuki Tatsuno, Taisuke Ito, Kenji Kabashima, Toshihiko Hibino, and Yoshiki Tokura. Kallikrein-related Peptidase 5 Functions in Proteolytic Processing of Profilaggrin in Cultured Human Keratinocytes. *J. Biol. Chem.*, 288(24):17179–17189, jun 2013.

[304] Assar Bäckman, Annelii Ny, Michael Edlund, Elisabeth Ekholm, Barbro Ekstrand Hammarström, Jan Törnell, Pia Wallbrandt, Torbjörn Egelrud, Lennart Hansson, and Håkan Wennbo. Epidermal Overexpression of Stratum Corneum Chymotryptic Enzyme in Mice: A Model for Chronic Itchy Dermatitis. *J. Invest. Dermatol.*, 118(3):444–449, mar 2002.

[305] R. Voegeli, A. V. Rawlings, S. Doppler, and T. Schreier. Increased basal transepidermal water loss leads to elevation of some but not all stratum corneum serine proteases. *Int. J. Cosmet. Sci.*, 30(6):435–42, dec 2008.

[306] C. A. Borgono, Iacovos P. Michael, Nahoko Komatsu, Arumugam Jayakumar, Ravi Kapadia, Gary L. Clayman, Georgia Sotiropoulou, and Eleftherios P. Diamandis. A Potential Role for Multiple Tissue Kallikrein Serine Proteases in Epidermal Desquamation. *J. Biol. Chem.*, 282(6):3640–3652, nov 2006.

[307] Peter M. Elias, Sung K. Ahn, Mitsuhiro Denda, Barbara E. Brown, Debra Crumrine, Llewellyn K. Kimutai, Laszlo Kömüves, Seung H. Lee, and Kenneth R. Feingold. Modulations in epidermal calcium regulate the expression of differentiation-specific markers. *J. Invest. Dermatol.*, 119(5):1128–1136, nov 2002.

[308] Hans Törmä, Magnus Lindberg, and Berit Berne. Skin Barrier Disruption by Sodium Lauryl Sulfate-Exposure Alters the Expressions of Involucrin, Transglutaminase 1, Profilaggrin, and Kallikreins during the Repair Phase in Human Skin In Vivo. *J. Invest. Dermatol.*, 128(5):1212–1219, may 2008.

[309] Chia-Ling Tu, Debra a Crumrine, Mao-Qiang Man, Wenhan Chang, Hashem Elalieh, Michael You, Peter M Elias, and Daniel D Bikle. Ablation of the Calcium-Sensing Receptor in Keratinocytes Impairs Epidermal Differentiation and Barrier Function. *J. Invest. Dermatol.*, 132(10):2350–2359, oct 2012.

[310] H.D. de Koning, E.H. van den Bogaard, J.G.M. Bergboer, M. Kamsteeg, I.M.J.J. van Vlijmen-Willems, K. Hitomi, J. Henry, M. Simon, N. Takashita, A. Ishida-Yamamoto, J. Schalkwijk, and P.L.J.M. Zeeuwen. Expression profile of cornified envelope structural proteins and keratinocyte differentiation-regulating proteins during skin barrier repair. *Br. J. Dermatol.*, 166(6):1245–1254, jun 2012.

[311] Chung Tin and Chi-Sang Poon. Integrative and Reductionist Approaches to Modeling of Control of Breathing. In Jerry J. Batzel, , Mostafa Bachar, , and Franz Kappel, editors, *Math. Model. Valid. Physiol. Appl. to Cardiovasc. Respir. Syst.*, pages 89–103. Springer Berlin Heidelber, 2013.

[312] Dan Siegal-Gaskins, Elisa Franco, Tiffany Zhou, and Richard M Murray. An analytical approach to bistable biological circuit discrimination using real algebraic geometry. *J. R. Soc. Interface*, 12(108):20150288, jul 2015.

[313] S. Barnett and D. D. Šiljak. Routh's Algorithm: A Centennial Survey. *SIAM Rev.*, 19(3):472–489, jul 1977.

[314] Hal Smith. *An Introduction to Delay Differential Equations with Applications to the Life Sciences*, volume 57 of *Texts in Applied Mathematics*. Springer New York, New York, NY, 1 edition, 2011.

[315] K Engelborghs, T Luzyanina, and G Samaey. DDE-BIFTOOL v. 2.00: a Matlab package for bifurcation analysis of delay differential equations. Technical Report October, K.U.Leuven, Leuven, Belgium, 2001.

[316] K. Engelborghs, T. Luzyanina, and D. Roose. Numerical bifurcation analysis of delay differential equations using DDE-BIFTOOL. *ACM Trans. Math. Softw.*, 28(1):1–21, mar 2002.

[317] B. Eberlein-König, T. Schäfer, J. Huss. Skin Surface pH, Stratum Corneum Hydration, Trans-epidermal Water Loss and Skin Roughness Related to Atopic Eczema and Skin Dryness in a Population of Primary School Children: Clinical Report. *Acta Derm. Venereol.*, 80(3):188–191, aug 2000.

[318] Amy B. Truong and Paul A. Khavari. Control of Keratinocyte Proliferation and Differentiation by p63. *Cell Cycle*, 6(3):295–299, feb 2007.

[319] Nahoko Komatsu, Kiyofumi Saijoh, Cynthia Kuk, Amber C. Liu, Saba Khan, Fumiaki Shirasaki, Kazuhiko Takehara, and Eleftherios P. Diamandis. Human tissue kallikrein expression in the stratum corneum and serum of atopic dermatitis patients. *Exp. Dermatol.*, 16(6):513–519, jun 2007.

[320] Ružica Jurakić Tončić and Branka Marinović. The Role of Impaired Epidermal Barrier Function in Atopic Dermatitis. *Acta Dermatovenerol. Croat.*, 24(2):95–109, jun 2016.

[321] Vanessa Petry, Giancarlo Resende Bessa, Claudia Schermann Poziomczyck, Caio Fernando de Oliveira, Magda Blessmann Weber, Renan Rangel Bonamigo, and Pedro Alves D'Azevedo. Bacterial skin colonization and infections in patients with atopic dermatitis. *An. Bras. Dermatol.*, 87(5):729–734, oct 2012.

[322] Ernest Fontich and Josep Sardanyés. General scaling law in the saddlenode bifurcation: a complex phase space study. *J. Phys. A Math. Theor.*, 41(1):015102, jan 2008.

[323] I. a. van de Leemput, M. Wichers, a. O. J. Cramer, D. Borsboom, F. Tuerlinckx, P. Kuppens, E. H. van Nes, W. Viechtbauer, E. J. Giltay, S. H. Aggen, C. Derom, N. Jacobs, K. S. Kendler, H. L. J. van der Maas, M. C. Neale, F. Peeters, E. Thiery, P. Zachar, and M. Scheffer. Critical slowing down as early warning for the onset and termination of depression. *Proc. Natl. Acad. Sci.*, 111(1):87–92, 2014.

[324] Marten Scheffer, Jordi Bascompte, William A. Brock, Victor Brovkin, Stephen R. Carpenter, Vasilis Dakos, Hermann Held, Egbert H. van Nes, Max Rietkerk, and George Sugihara. Early-warning signals for critical transitions. *Nature*, 461(7260):53–59, sep 2009.

[325] Hyosun Jang, Akira Matsuda, Kyungsook Jung, Kaoru Karasawa, Kenshiro Matsuda, Kumiko Oida, Saori Ishizaka, Ginnae Ahn, Yosuke Amagai, Changjong Moon, Sung-Ho Kim, Peter D Arkwright, Kenji Takamori, Hiroshi Matsuda, and Akane Tanaka. Skin pH Is the Master Switch of Kallikrein 5-Mediated Skin Barrier Destruction in a Murine Atopic Dermatitis Model. *J. Invest. Dermatol.*, 136(1):127–135, jan 2016.

[326] Francesca Mascia, Mitchell Denning, Raphael Kopan, and Stuart H. Yuspa. The Black Box Illuminated: Signals and Signaling. *J. Invest. Dermatol.*, 132(3):811–819, mar 2012.

[327] Enikö Sonkoly, Tianling Wei, Elizabeth Pavez Loriè, Hiroyuki Suzuki, Mitsuyasu Kato, Hans Törmä, Mona Ståhle, and Andor Pivarcsi. Protein kinase C-dependent upregulation of miR-203 induces the differentiation of human keratinocytes. *J. Invest. Dermatol.*, 130(1):124–34, 2010.

[328] Andrzej A. Dlugosz. Coordinate changes in gene expression which mark the spinous to granular cell transition in epidermis are regulated by protein kinase C. *J. Cell Biol.*, 120(1):217–225, jan 1993.

[329] Andrew Kovalenko, Jin-Chul Kim, Tae-Bong Kang, Akhil Rajput, Konstantin Bogdanov, Oliver Dittrich-Breiholz, Michael Kracht, Ori Brenner, and David Wallach. Caspase-8 deficiency in epidermal keratinocytes triggers an inflammatory skin disease. *J. Exp. Med.*, 206(10):2161–2177, sep 2009.

[330] T. Cartner, N. Brand, K. Tian, A. Saud, T. Carr, P. Stapleton, M. E. Lane, and A. V. Rawlings. Effect of different alcohols on stratum corneum kallikrein 5 and phospholipase A 2 together with epidermal keratinocytes and skin irritation. *Int. J. Cosmet. Sci.*, 39(2):188–196, apr 2017.

[331] Chika Katagiri, Junko Sato, Junko Nomura, and Mitsuhiro Denda. Changes in environmental humidity affect the water-holding property of the stratum corneum and its free amino acid content, and the expression of filaggrin in the epidermis of hairless mice. *J. Dermatol. Sci.*, 31(1):29–35, feb 2003.

[332] Elisa Domínguez Hüttinger. *Mathematical modelling of epithelium homeostasis*. PhD thesis, 2015.

[333] Ioana Agache and Cezmi A. Akdis. Endotypes of allergic diseases and asthma: An important step in building blocks for the future of precision medicine. *Allergol. Int.*, 65(3):243–252, jul 2016.

[334] Jennifer Krejci-Manwaring, Mark G. Tusa, Christie Carroll, Fabian Camacho, Mandeep Kaur, David Carr, Alan B. Fleischer, Rajesh Balkrishnan, and Steven R. Feldman. Stealth monitoring of adherence to topical medication: Adherence is very poor in children with atopic dermatitis. *J. Am. Acad. Dermatol.*, 56(2):211–216, feb 2007.

[335] Alexandria Bass, Kathryn Anderson, and Steven Feldman. Interventions to Increase Treatment Adherence in Pediatric Atopic Dermatitis: A Systematic Review. *J. Clin. Med.*, 4(2):231–242, jan 2015.

[336] Patrick Poulin and Frank-Peter Theil. Prediction of Pharmacokinetics Prior to In Vivo Studies. II. Generic Physiologically Based Pharmacokinetic Models of Drug Disposition. *J. Pharm. Sci.*, 91(5):1358–1370, may 2002.

[337] Arijit Coondoo, Meghana Phiske, Shyam Verma, and Koushik Lahiri. Side-effects of topical steroids: A long overdue revisit. *Indian Dermatol. Online J.*, 5(4):416, 2014.

[338] Arijit Coondoo and Chandan Chattopadhyay. Use and abuse of topical corticosteroids in children. *Indian J. Paediatr. Dermatology*, 15(1):1, 2014.

[339] D.Q. Mayne, J.B. Rawlings, C.V. Rao, and P.O.M. Scokaert. Constrained model predictive control: Stability and optimality. *Automatica*, 36(6):789–814, jun 2000.

[340] E Tkaczyk. Innovations and Developments in Dermatologic Non-invasive Optical Imaging and Potential Clinical Applications. *Acta Derm. Venereol.*, 97:5–13, 2017.

[341] Jyh-Hong Lee, Szu-Yu Chen, Che-Hang Yu, Shih-Wei Chu, Li-Fang Wang, Chi-Kuang Sun, and Bor-Luen Chiang. Noninvasive in vitro and in vivo assessment of epidermal hyperkeratosis and dermal fibrosis in atopic dermatitis. *J. Biomed. Opt.*, 14(1):014008, 2009.

[342] Asuman Gürkan, Ayegül Atak Yücel, Cemile Sönmez, ennur Kele, and lknur Bostanc. Serum Cytokine Profiles in Infants with Atopic Dermatitis. *Acta Dermatovenerol. Croat.*, 24(4):268–273, dec 2016.

[343] James Q. Del Rosso. Repair and maintenance of the epidermal barrier in patients diagnosed with atopic dermatitis: an evaluation of the components of a body wash-moisturizer skin care regimen directed at management of atopic skin. *J. Clin. Aesthet. Dermatol.*, 4(6):45–55, jun 2011.

[344] J M Jungersted, H Scheer, M Mempel, H Baurecht, L Cifuentes, J K Høgh, L I Hellgren, G B E Jemec, T Agner, and S Weidinger. Stratum corneum lipids, skin barrier function and filaggrin mutations in patients with atopic eczema. *Allergy*, 65(7):911–918, jul 2010.

[345] Shu-Mei Guo and Chin-Chang Yang. Enhancing Differential Evolution Utilizing Eigenvector-Based Crossover Operator. *IEEE Trans. Evol. Comput.*, 19(1):31–49, feb 2015.

[346] Rammohan Mallipeddi and Ponnuthurai Nagaratnam Suganthan. Differential Evolution Algorithm with Ensemble of Parameters and Mutation and Crossover Strategies. In *Lect. Notes Comput. Sci. (including Subser. Lect. Notes Artif. Intell. Lect. Notes Bioinformatics)*, volume 6466 LNCS, pages 71–78. 2010.

[347] Rainer Storn. On the usage of differential evolution for function optimization. In *Proc. North Am. Fuzzy Inf. Process.*, pages 519–523. IEEE, 1996.

[348] Chuan Lin, Anyong Qing, and Quanyuan Feng. A comparative study of crossover in differential evolution. *J. Heuristics*, 17(6):675–703, dec 2011.

[349] Jacques Bélair and Sue Ann Campbell. Stability and Bifurcations of Equilibria in a Multiple-Delayed Differential Equation. *SIAM J. Appl. Math.*, 54(5):1402–1424, 1994.

[350] D. V. Senthilkumar M. Lakshmanan. *Dynamics of Nonlinear Time-Delay Systems*. Springer-Verlag, New York, 1 edition, 2010.

[351] J M Mahaffy and C V Pao. Models of genetic control by repression with time delays and spatial effects. *J. Math. Biol.*, 20:39–57, 1984.

[352] B C Goodwin. Oscillatory behavior in enzymatic control processes. *Adv. Enzyme Regul.*, 3:425–438, 1965.

[353] Basak Karpuz. Existence and uniqueness of solutions to systems of delay dynamic equations on time scales. page 15, jan 2010.

[354] Je Forde. *Delay differential equation models in mathematical biology*. PhD thesis, The University of Michigan, 2005.

[355] Thomas Erneux. *Applied Delay Differential Equations*, volume 3. Springer New York, New York, NY, 1 edition, 2009.

[356] Farshid Maghami Asl and Galip A. Ulsoy. Analysis of a System of Linear Delay Differential Equations. *J. Dyn. Syst. Meas. Control*, 125(2):215, 2003.

[357] R. M. Corless, G. H. Gonnet, D. E. G. Hare, D. J. Jeffrey, and D. E. Knuth. On the LambertW function. *Adv. Comput. Math.*, 5:329–359, 1996.

[358] Sun Yi, A. Galip Ulsoy, and Patrick W. Nelson. Solution of Systems of Linear Delay Differential Equations via Laplace Transformation. In *Proc. 45th IEEE Conf. Decis. Control*, number 3, pages 2535–2540. IEEE, 2006.

[359] Nejat Olgac and Rifat Sipahi. An exact method for the stability analysis of time-delayed linear time-invariant (LTI) systems. *IEEE Trans. Automat. Contr.*, 47(5):793–797, may 2002.

[360] Y N Kyrychko and S J Hogan. On the Use of Delay Equations in Engineering Applications. *J. Vib. Control*, 16(7-8):943–960, feb 2010.

[361] J. M. Carnicer and J. M. Peña. Characterizations of the Optimal Descartes' Rules of Signs. *Math. Nachrichten*, 189(1):33–48, 1998.

[362] Thomas Eissing, Holger Conzelmann, Ernst D. Gilles, Frank Allgöwer, Eric Bullinger, and Peter Scheurich. Bistability Analyses of a Caspase Activation Model for Receptor-induced Apoptosis. *J. Biol. Chem.*, 279(35):36892–36897, aug 2004.

[363] K. Parmar, K. B. Blyuss, Y. N. Kyrychko, and S. J. Hogan. Time-Delayed Models of Gene Regulatory Networks. *Comput. Math. Methods Med.*, 2015:1–16, 2015.

Appendix A

Supplementary Methods for Chapter 2

A.1 LPS challenges and histological evaluation of epidermis-specific *Stat3* knockout mice

We backcrossed the keratinocyte-specific $Stat3-ko$ ($Stat3^{f/f}$) mice with B6X129 mixed background with a B6 background. We applied three intra-dermal injections, with an interval of a week of sterile PBS with 0.1% DMSO, with and without LPS (10 μg), to their ears of asymptomatic keratinocyte-specific $Stat3^{f/f}$ mice with a B6 background (8-9 weeks). Two days after the last injection, ears were fixed with paraformaldehyde (4%) and frozen in OCT compound (Sakura Finetek Japan Co, Tokyo, Japan). 5μm sections were taken using a cryostat (Leica, Wtzlar, Germany) and fixed onto slide glasses. After the retrieval by Target Retrieval Solution (Agilent Technologies, Santa Clara, CA) and permeabilisation (0.1% Trironx-100), the sections were stained with Hematoxylin and Eosin (HE staining).

A.2 Minimum flare time and minimum relaxation time to trigger systemic T_H2 sensitization

The solution of Eq. (3.1c),

$$\frac{dD(t)}{dt} = \kappa_{\rm D} R(t) - \delta_D D(t),$$

is described by

$$D(t) = e^{-\delta_D (t-t_0)} D(t_0) + \int_{t_0}^{t} e^{-\delta_D (t-\tau)} \kappa_{\rm D} R(\tau) d\tau, \tag{A.1}$$

where the integral is defined over each time segment, on which $R(t)$ is continuously defined, either by $R(t) = R_{\rm on}$ for the duration of a flare time, $t_{\rm on}$, or by $R(t) = R_{\rm off} = 0$ for the duration of a relaxation time, $t_{\rm off}$. Note that the steady-state value, $D_{\rm ss}$, of $D(t)$ while $R(t) = R_{\rm on}$ is obtained by $D_{\rm ss} = \dfrac{\kappa_{\rm D}\, R_{\rm on}}{\delta_D}$. The period of the R-spike is denoted by $T = t_{\rm on} + t_{\rm off}$.

To determine the dynamics of $D(t)$, we derive $D(t_k)$ and $D(T_k)$ $(k = 1, 2, \ldots)$, where t_k and T_k denote the time when the k-th spike of $R(t) = R_{\rm on}$ starts and the time when the k-th spike ends, respectively. We define $t_1 = 0$ and $D(t_1) = 0$. $D(t)$ decreases during $T_k \le t \le t_{k+1}$ when $R(t) = R_{\rm off} = 0$ and reaches $D(t_{k+1}) = e^{-\delta_D t_{\rm off}} D(T_k)$, whereas it increases during $t_k \le t \le T_k$ with $R(t) = R_{\rm on}$ and achieves

$$\begin{aligned} D(T_k) &= e^{-\delta_D t_{\rm on}} D(t_k) + \kappa_{\rm D}\, R_{\rm on} \int_{t_k}^{T_k} e^{-\delta_D (T_k - \tau)} d\tau \\ &= e^{-\delta_D t_{\rm on}} D(t_k) + \kappa_{\rm D}\, R_{\rm on}\, e^{-\delta_D T_k} \int_{t_k}^{T_k} e^{\delta_D \tau} d\tau \\ &= e^{-\delta_D t_{\rm on}} D(t_k) + D_{\rm ss}\, (1 - e^{-\delta_D t_{\rm on}}). \end{aligned} \tag{A.2}$$

Since $D(t_1) = 0$ for $t_1 = 0$, we have $D(T_1) = D_{\rm ss}\, (1 - e^{-\delta_D t_{\rm on}})$ and

$$\begin{aligned} D(T_k) &= e^{-\delta_D t_{\rm on}} e^{-\delta_D t_{\rm off}} D(T_{k-1}) + D_{\rm ss}\, (1 - e^{-\delta_D t_{\rm on}}) \\ &= e^{-\delta_D T} D(T_{k-1}) + D_{\rm ss}\, (1 - e^{-\delta_D t_{\rm on}}), \quad k = 2, 3, \ldots. \end{aligned} \tag{A.3}$$

Therefore, $D(T_k)$ is described as

$$D(T_k) = D_{\rm ss}\left(1 - e^{-\delta_D t_{\rm on}}\right)\sum_{i=0}^{k-1} e^{-i\delta_D T}, \tag{A.4}$$

which converges to

$$D(T_\infty) = \lim_{k\to\infty} D(T_k) = D_{\rm ss}(1 - e^{-\delta_D t_{\rm on}})\frac{1}{1 - e^{-\delta_D T}}. \tag{A.5}$$

The minimum flare time, $t^*_{\rm on}$, for a single-pulse of $R(t) = R_{\rm on}$ to trigger systemic T_H2 sensitization is analytically obtained from the corresponding solution

$$D(t) = \int_0^t e^{-\delta_D(t-\tau)}\kappa_{\rm D} R(\tau)d\tau = D_{\rm ss}(1 - e^{-\delta_D t})$$

of Eq. (A.1). Solving $D(t^*_{\rm on}) = D^+$ leads to

$$t^*_{\rm on} = -\frac{\ln\left(1 - \frac{D^+}{D_{\rm ss}}\right)}{\delta_D}. \tag{A.6}$$

The minimum relaxation time, $t^*_{\rm off}$, for a periodic R-spike with a fixed $t_{\rm on}$ to trigger systemic T_H2 sensitization is analytically obtained by solving $D(T_\infty) = D^+$ as

$$t^*_{\rm off} = -\left[t_{\rm on} + \frac{1}{\delta_D}\ln\left\{1 - \frac{D_{\rm ss}}{D^+}(1 - e^{-\delta_D t_{\rm on}})\right\}\right]. \tag{A.7}$$

Note that the solution in Eq. (A.7) exists if $1 - \dfrac{D_{\rm ss}}{D^+}(1 - e^{-\delta_D t_{\rm on}}) > 0$ and $t_{\rm on} + \dfrac{1}{\delta_D}\ln\left\{1 - \dfrac{D_{\rm ss}}{D^+}(1 - e^{-\delta_D t_{\rm on}})\right\} < 0$. These conditions are equivalent to

$$t_{\rm on} < -\frac{1}{\delta_D}\ln\left(1 - \frac{D^+}{D_{\rm ss}}\right) = t^*_{\rm on} \quad \text{and} \quad D^+ < D_{\rm ss}.$$

A.3 OVA patch challenges and measurement of IgE levels in *Stat3* knockout mice

We applied an OVA soaked patch (1mg/ml in 100μl) on shaven back skin of the 8-9 weeks old mice (3 WT and 4 epidermis-specific *Stat3* knockout mice), 4 times at a week interval between individual applications. We measured the level of OVA-specific IgE titer in the serum by sandwich ELISA, a week after the last OVA challenge. Briefly, the serum was applied on the plastic plate coated with captured antibody for IgE. After washing, the plate was probed with the biotinilated specific OVA antibody for the cytokines and HRP-conjugated streptavidin (Zymed, San Francisco, CA) and developed with 2,2'-azino-bis (3-ethylbenzthiazoline-6-sulfonic acid) (Kirkegard & Perry Laboratories, Gaithersburg, MD). The 405 *nm* absorbance was measured by spectrophotometer (Bio-Rad Laboratories, Hercules, CA).

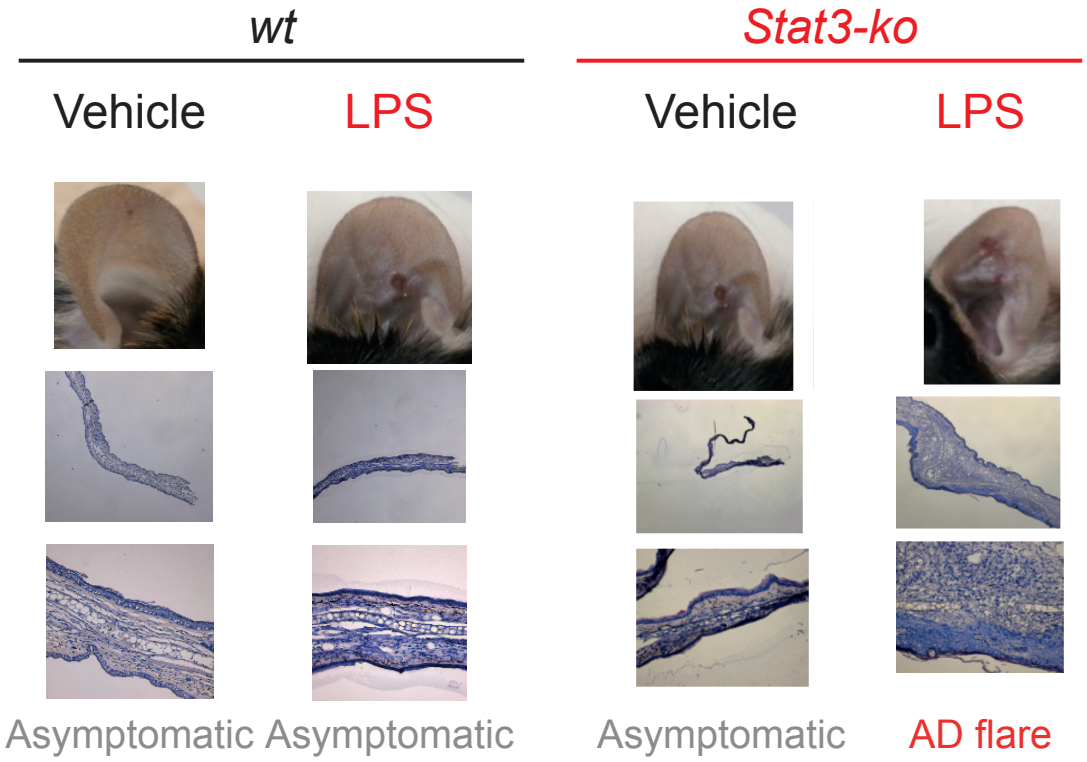


Figure A.1: Induction of AD symptoms by environmental triggers (LPS) in *Stat3* knockout mouse model of AD.

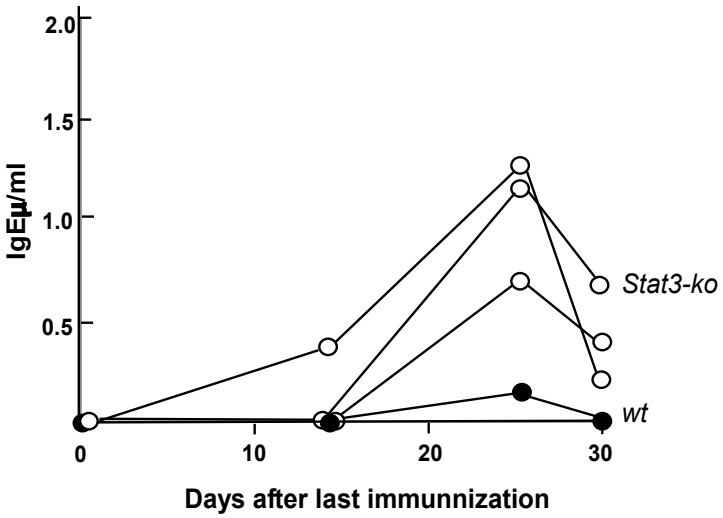


Figure A.2: Constitutive environmental challenges with OVA result in an increase in IgE levels in *Stat3* knockout mice ($n = 3$) but not in WT ($n = 1$) mice.

Appendix B

Supplementary Methods for Chapter 3

We conducted sensitivity analysis to confirm that the optimal strategies calculated for the nominal parameter set (Tables 3.1 and 4.1) are robust to changes in the model parameters and the weighting coefficients for the objective function. The robustness was evaluated by whether,

- the duration of the optimal induction phase (T_{r}) corresponds to the clinically accepted range of less than 4 weeks,
- the optimal treatment duration in each maintenance cycle (T_{C}^{i}) corresponds to 2-3 days (weekend therapy), and
- the potency of corticosteroid required during the maintenance phase is lower than that required during the remission phase ($\bar{C} > \bar{C}^{\mathrm{i}}$).

Sensitivity analysis for the weights of the objective function and the model parameters was performed by varying each weight and parameter by ±50%. An illustration of the method is depicted in Fig. B.1.

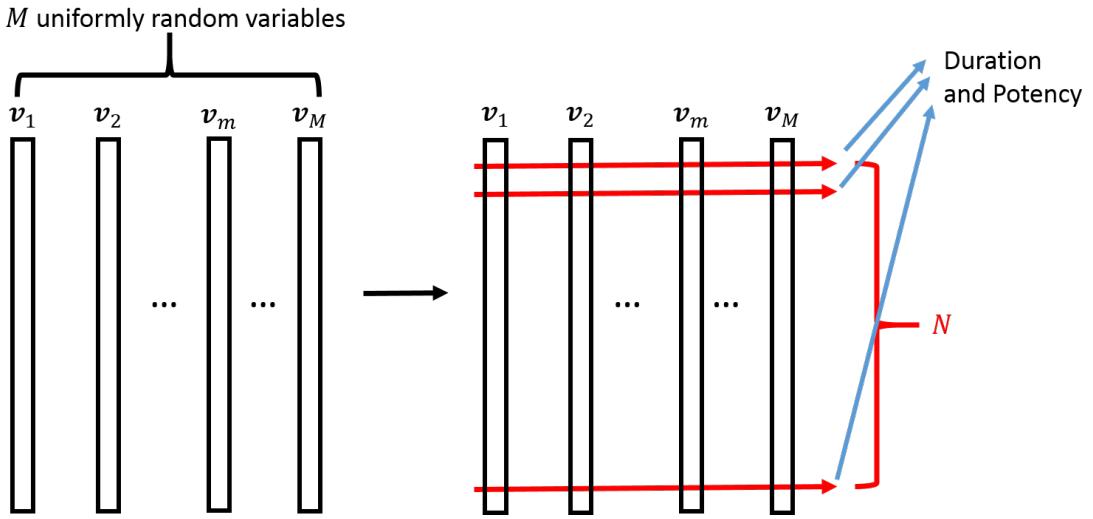


Figure B.1: Schematic for the procedure used to complete the sensitivity analysis. Each variable $\boldsymbol{v}_{\mathrm{m}}$ is a uniformly random vector of size N corresponding to the m^{th} weight of the objective function ($M = 8$) or model parameter ($M = 9$). Then a selection of all the weights or parameters in the n^{th} index of each vector produces a single duration and potency pair for both the induction of remission and maintenance phases. The variables where varied by $\pm 50\%$, i.e $Range = \frac{\boldsymbol{v}_{\mathrm{m}}}{2} + (2\boldsymbol{v}_{\mathrm{m}} - \frac{\boldsymbol{v}_{\mathrm{m}}}{2}) * rand(N, 1)$.

B.1 Sensitivity to risk factors $(\kappa_{\mathrm{P}}, \alpha_{\mathrm{I}})$

We calculated the optimal treatment strategies with a uniform grid within the ranges $0.83 \leq \kappa_{\mathrm{P}} \leq 1$ and $0.03 \leq \alpha_{\mathrm{I}} \leq 0.06$ (Fig. B.2), corresponding to moderate to severe AD patients with chronically damaged phenotype, for $N = 1600$ combinations of $(\kappa_{\mathrm{P}}, \alpha_{\mathrm{I}})$. Among the 1600 combinations, 683 combinations successfully achieved the induction of remission (Fig. B.2 (a)), with the optimally calculated potency and duration given in Fig. B.2(b) and Fig. B.2(c), respectively. Their calculated optimal treatment strategies for both the induction and maintenance phases are robust to the changes in the values of $(\kappa_{\mathrm{P}}, \alpha_{\mathrm{I}})$ (Fig. B.3).

B.2 Sensitivity to weights of objective functions $(k_{\mathrm{r}}^1,\ k_{\mathrm{r}}^2,\ k_{\mathrm{r}}^3,\ k_{\mathrm{r}}^4,\ k_{\mathrm{m}}^1,\ k_{\mathrm{m}}^3,\ k_{\mathrm{m}}^4)$

To investigate the sensitivity of the optimal treatment strategies to the weights of the objective function terms, we varied (uniformly random) eight weights simultaneously

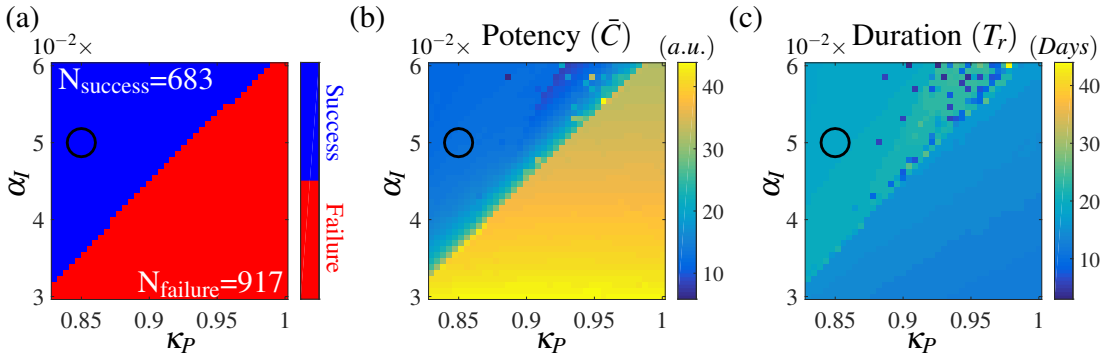


Figure B.2: The calculated optimal treatment strategies for the induction phase for 1600 different combinations of (κ_P, α_I). (a) Binary heatmap indicating success (blue) or failure (red) to induce remission, by the calculated optimal treatment strategies; (b) The potency of corticosteroids; (c) The duration of the induction phase. The black circles represent the nominal parameter pair $(\kappa_P, \alpha_I) = (0.85, 0.05)$.

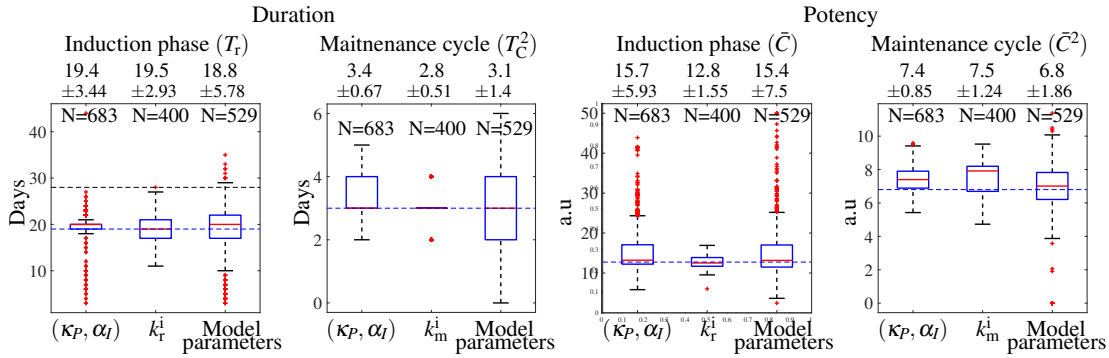


Figure B.3: Sensitivity of the calculated optimal treatment strategies with respect to the changes in (κ_P, α_I), weights for the objective function terms (k_r^i and k_m^i), and model parameters. The blue dashed line is the result of the optimization for the nominal conditions (Fig. 4.3(a)). The black dashes line is the maximum acceptable induction of remission duration. The values shown are mean ± std.

by ±50% from their nominal values ($N = 400$); four for the induction phase (k_r^1, k_r^2, k_r^3, k_r^4) and four for the maintenance phase (k_m^1, k_m^2, k_m^3, k_m^4). We assumed $k_r^2 = k_m^2$ since the efficacy of the corticosteroid treatment is the same in both remission and maintenance phases. Our analysis (Fig. B.3) confirmed that the calculated optimal treatment strategies were robust to the changes of the weighting parameters.

B.3 Sensitivity to model parameters (γ_B, δ_P, κ_B, γ_R, γ_G, δ_B, β_1, β_2, β_3)

To investigate the sensitivity of the optimal treatment strategies to the model parameters, we varied (uniformly random) the parameters simultaneously by $\pm 50\%$ from their nominal values ($N = 529$). Our analysis (Fig. B.3) confirmed that the calculated optimal treatment strategies were robust to the changes in the model parameters.

Appendix C

Differential evolution

C.1 Introduction

Differential Evolution (DE), introduced by Storn and Price [240], is a subclass of Evolutionary Algorithms (EA) reputed to tackle global optimisation problems [241]. Its use has been popularised due to its good convergence properties [240], its simplicity [245] and a plethora of successful examples in diverse domains [345].

C.2 DE description

DE is a population-based stochastic numerical optimisation algorithm, that uses NP, D-dimensional parameter vectors as a population for each generation G. We next consider the stages of DE. The schematic in Fig. C.1 shows the operational flowchart for DE.

(A) Initialisation: In the initialisation stage, NP real-valued target vectors ($\boldsymbol{x}_{i,0} \in \mathbb{R}^D$) populate uniformly ($\Omega \sim U[0,1]$) the user-defined parameter space, $x_j^{min} \leq x_{ji,0} \leq x_j^{max}$. Each vector, represents a candidate solution for the optimisation problem.

(B) Mutation: Mutation is the process of perturbing the population randomly to find better solutions. The three indices r_1, r_2 and r_3 are random events taken from a discrete uniform distribution ($\Upsilon \sim U\{1, NP\}$) that identify three vectors $\boldsymbol{x}_{r_1}$, $\boldsymbol{x}_{r_2}$ and $\boldsymbol{x}_{r_3}$ from

the population. A mutant vector ($\boldsymbol{v}_{i,G}$) is generated using a specific mutation strategy. There are several frequently used mutation strategies [346], however we will be using DE/rand-to-best/1 [245] or DE/rand/1 [347], where the mutant vector is calculated as:

$$\boldsymbol{v}_{i,G+1} = \boldsymbol{x}_{i,G} + F_1(\boldsymbol{x}_{r_2,G} - \boldsymbol{x}_{r_3,G}) + F_2(\boldsymbol{x}_{best,G} - \boldsymbol{x}_{i,G}), \tag{C.1}$$

and

$$\boldsymbol{v}_{i,G+1} = \boldsymbol{x}_{r_1,G} + F(\boldsymbol{x}_{r_2,G} - \boldsymbol{x}_{r_3,G}), \tag{C.2}$$

respectively, where F_1, F_2, and F are the differential weights ($F_1 = F_2$).

Perturbation of the vectors can give solutions with parameters that lie outside the user-defined bounds. To prevent this we constrain the pertubation and define the bounds as hard constraints. Any solution outside the bounds will then take the maximum/minimum bound if it was above/below the maximum/minimum.

(C) Recombination/Crossover: A crossover operation is employed to increase the diversity of the perturbed vectors. A trial vector ($\boldsymbol{u}_{i,G}$) is generated based on binomial crossover as follows:

$$u_{ji,G+1} = \begin{cases} v_{ji,G+1}, & \text{if } \Phi_{j,i} \leq \text{CR or } j = \Psi \\ x_{ji,G}, & \text{if } \Phi_{j,i} > \text{CR and } j \neq \Psi, \end{cases} \tag{C.3}$$

where $CR \in [0, 1]$ is the crossover rate and is user-defined. The distributions $\Phi_{j,i}$ and Ψ define uniform continuous and discrete distributions, respectively. Exponential crossover is an another widely used crossover method in DE [348].

(D) Selection: In the selection process the target vector is compared with the trial vector according to a user-defined objective function and the one which admits the lowest cost survives to the next generation.

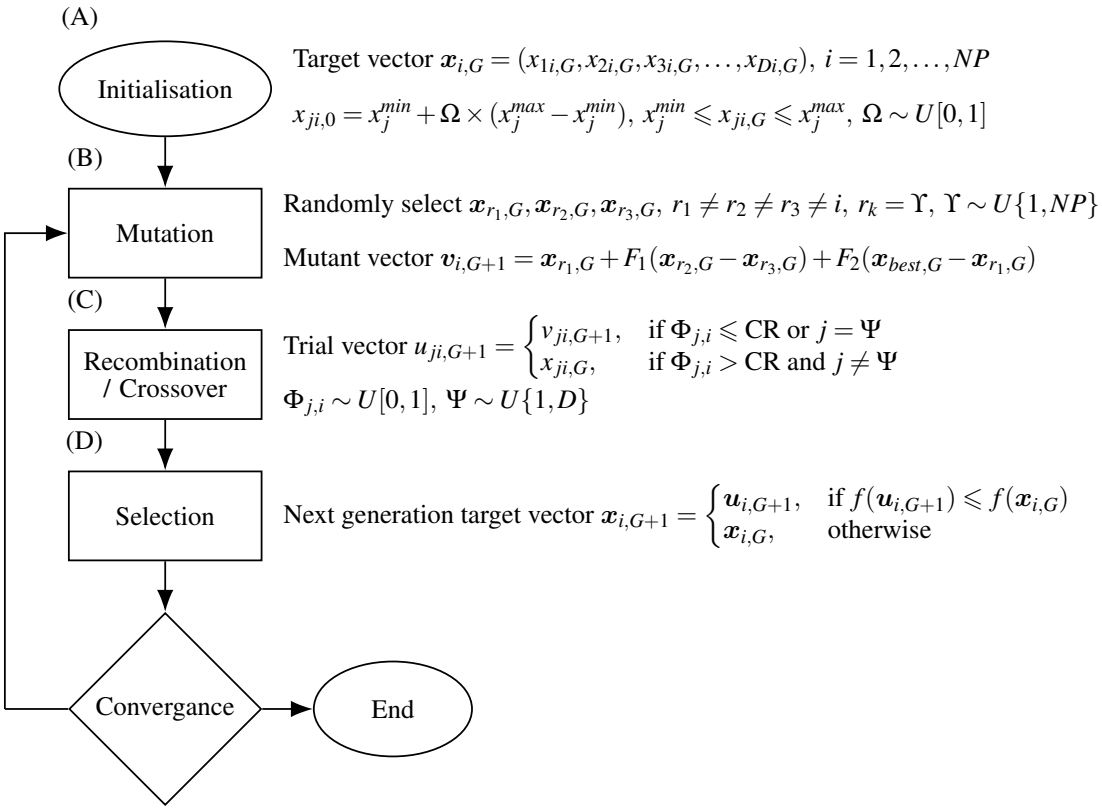


Figure C.1: Differential Evolution flowchart with mutation strategy DE/rand-to-best and binomial crossover rate.

Appendix D

Delay-Differential Equations

D.1 Introduction

In this section we begin by defining the general representation of the systems of interest; namely Delay Differential Equations (DDE). We then proceed by documenting some standard techniques used in the analysis of DDE, in particular calculation of steady-states and linearisation to obtain local stability information. Finally, some additional information on DDE is discussed with the purpose of presenting a brief literature review.

D.2 System definition

DDE constitute an important class of dynamical systems that arise naturally in many biological and physical systems. DDE are differential equations in which the time evolution of the state-variables can depend not only on the current state of the state-variables, but also on past values at some discrete time. Given this definition it is easy to see how DDE may arise in biological systems: time required for a cell to mature [349]; the delay occurring during the travel of action potentials along the axon [349, 350]; and the process of gene expression in protein-gene networks [351, 352].

There are different kinds of DDE and here we will focus on DDE with constant discrete

and positive time-delays that admit the following initial value problem (IVP),

$$\dot{\mathbf{x}}(t) = \mathbf{f}(\mathbf{x}(t), \mathbf{x}(t-\tau_1), \mathbf{x}(t-\tau_2), \ldots, \mathbf{x}(t-\tau_m); \boldsymbol{\eta}), \quad t \geq 0 \tag{D.1}$$

$$\mathbf{x}(t) = \phi(t), \quad t \in [-\tau_m, 0] \tag{D.2}$$

where $\mathbf{x}(t) \in \mathbb{R}^n$ is the vector of state-variables, $\mathbf{f} : \mathbb{R}^{n(m+1)} \times \mathbb{R}^p \longrightarrow \mathbb{R}^n$ is a non-linear function, and $\phi(t)$ is an initial history function that corresponds to the shape of $\mathbf{x}(t)$ on the interval $t \in [-\tau_m, 0]$. The vector $\boldsymbol{\eta} \in \mathbb{R}^p$ is the vector of parameters and we also define $\max\limits_{1 \leq i \leq m} \{\tau_i\} = \tau_m$.

Although DDE are similar to ODEs their solution is much more involved. Due to the dependence of the derivatives on past values of the state-variables, an IVP requires more information. To solve a delay differential system one needs to specify information on the value of $\mathbf{x}(t)$ on the interval $t \in [t_0 - \tau_m, t_0]$ where t_0 is the initial time and τ_m is the maximal discrete delay in the system. Thus the solution of DDE requires the specification of an initial function or initial history, $\phi(t)$, and each initial function determines a unique solution under certain regulatory conditions [314,353]. These initial functions are usually defined on the space of continuous functions that map the line segment $[t_0 - \tau_m, t_0]$ to $\mathbb{R}^n$, $\phi \in \mathcal{C}([t_0 - \tau_m, t_0], \mathbb{R}^n)$, which defines a function space with an infinite basis set[1] and thus is infinite dimensional [350]. As a consequence the solution space of a delay differential system is infinite dimensional [354]. In other words we need to define a set with an infinite number of initial conditions, that are continuous on $[t_0 - \tau_m, t_0]$, which leads to the infinite dimensional character [350]. This is a crucial concept that will be revisited later when we study the stability of DDE.

D.3 Stability considerations

To acquire insights on the nature of the solutions of DDE, we perform linear stability analysis on the equilibrium solutions in a similar way as for ODEs. An *equilibrium point* of a DDE of the form given in Eq. (D.1) is defined as,

$$\mathbf{x}(t) = \mathbf{x}(t - \tau_i) \coloneqq \mathbf{x}^* \qquad \forall i \in \{x \in \mathbb{N} : 1 \leq x \leq m\}, \tag{D.3}$$

[1] We cannot represent a function using a finite superposition of other functions.

such that Eq. (D.1) satisfies,

$$\dot{\mathbf{x}}(t) = \mathbf{f}(\mathbf{x}^*, \mathbf{x}^*, \ldots, \mathbf{x}^*; \boldsymbol{\eta}) = \mathbf{0}, \tag{D.4}$$

Linear stability analysis is more involved in DDE in that we must also consider the delayed dependent state-variables. Below we first present some notational conventions and then show the procedure of linearisation.

The derivative of a vector function is a row vector given by:

$$\frac{\partial g}{\partial \mathbf{x}} := \begin{bmatrix} \dfrac{\partial g}{\partial x_1} & \dfrac{\partial g}{\partial x_2} & \cdots & \dfrac{\partial g}{\partial x_n} \end{bmatrix} \tag{D.5}$$

By considering Eq. (D.1) in vector form we have:

$$\dot{\mathbf{x}}(t) = \begin{bmatrix} \dot{x}_1(t) \\ \dot{x}_2(t) \\ \vdots \\ \dot{x}_n(t) \end{bmatrix} = \begin{bmatrix} f_1(\mathbf{x}(t), \mathbf{x}(t-\tau_1), \mathbf{x}(t-\tau_2), \ldots, \mathbf{x}(t-\tau_m); \boldsymbol{\eta}) \\ f_2(\mathbf{x}(t), \mathbf{x}(t-\tau_1), \mathbf{x}(t-\tau_2), \ldots, \mathbf{x}(t-\tau_m); \boldsymbol{\eta}) \\ \vdots \\ f_n(\mathbf{x}(t), \mathbf{x}(t-\tau_1), \mathbf{x}(t-\tau_2), \ldots, \mathbf{x}(t-\tau_m); \boldsymbol{\eta}) \end{bmatrix} \tag{D.6}$$

To check the nature of the stability of an equilibrium point we apply infinitesimal time dependent perturbations, $\delta\mathbf{x}(t)$ or $\delta\mathbf{x}(t-\tau_i)$, around the equilibrium, $\mathbf{x}^*$, that last at least as long as the largest delay, i.e persisting for an interval $t \in [t_0 - \tau_m, t_0]$ [350] and have the following form,

$$\mathbf{x}(t) = \mathbf{x}^* + \delta\mathbf{x}(t) \tag{D.7}$$

$$\mathbf{x}(t-\tau_i) = \mathbf{x}^* + \delta\mathbf{x}(t-\tau_i), \tag{D.8}$$

Hence, by differentiating Eq. (D.7) wrt to time and substituting in Eq. (D.1) we have:

$$\dot{\mathbf{x}} = \delta\dot{\mathbf{x}} = \mathbf{f}(\mathbf{x}^* + \delta\mathbf{x}(t), \mathbf{x}^* + \delta\mathbf{x}(t-\tau_1), \mathbf{x}^* + \delta\mathbf{x}(t-\tau_2), \ldots, \mathbf{x}^* + \delta\mathbf{x}(t-\tau_m); \boldsymbol{\eta}) \tag{D.9}$$

If the perturbations are small we can linearise the differential equations around the equilibrium point using the Taylor expansion. For the k^{th} element, the scalar Taylor

expansion up to first order terms is given by:

$$f_k(\mathbf{x}^* + \delta\mathbf{x}(t), \mathbf{x}^* + \delta\mathbf{x}(t-\tau_1), \mathbf{x}^* + \delta\mathbf{x}(t-\tau_2), \ldots, \mathbf{x}^* + \delta\mathbf{x}(t-\tau_m); \boldsymbol{\eta}) \approx$$
$$\cancelto{0}{f_k(\mathbf{x}^*, \mathbf{x}^*, \ldots, \mathbf{x}^*; \boldsymbol{\eta})} + \left.\frac{\partial f_k}{\partial \mathbf{x}(t)}\right|_{(\mathbf{x}^*,\mathbf{x}^*,\ldots,\mathbf{x}^*;\boldsymbol{\eta})} \delta\mathbf{x}(t) + \left.\frac{\partial f_k}{\partial \mathbf{x}(t-\tau_1)}\right|_{(\mathbf{x}^*,\mathbf{x}^*,\ldots,\mathbf{x}^*;\boldsymbol{\eta})} \delta\mathbf{x}(t-\tau_1)$$
$$+ \cdots + \left.\frac{\partial f_k}{\partial \mathbf{x}(t-\tau_m)}\right|_{(\mathbf{x}^*,\mathbf{x}^*,\ldots,\mathbf{x}^*;\boldsymbol{\eta})} \delta\mathbf{x}(t-\tau_m). \tag{D.10}$$

Note that the first term on the right hand side is by definition equal to zero. By writing the expressions for all elements in matrix form and collecting the appropriate terms we have:

$$\begin{bmatrix} \delta\dot{x}_1(t) \\ \vdots \\ \delta\dot{x}_n(t) \end{bmatrix} = \overbrace{\begin{bmatrix} \frac{\partial f_1}{\partial x_1(t)} & \cdots & \frac{\partial f_1}{\partial x_n(t)} \\ \vdots & & \vdots \\ \frac{\partial f_n}{\partial x_1(t)} & \cdots & \frac{\partial f_n}{\partial x_n(t)} \end{bmatrix}}^{J_0} \overbrace{\begin{bmatrix} \delta x_1(t) \\ \vdots \\ \delta x_n(t) \end{bmatrix}}^{\delta\mathbf{x}(t)} + \sum_{i=1}^{m} \overbrace{\begin{bmatrix} \frac{\partial f_1}{\partial x_1(t-\tau_i)} & \cdots & \frac{\partial f_1}{\partial x_n(t-\tau_i)} \\ \vdots & & \vdots \\ \frac{\partial f_n}{\partial x_1(t-\tau_i)} & \cdots & \frac{\partial f_n}{\partial x_n(t-\tau_i)} \end{bmatrix}}^{J_{\tau_i}} \overbrace{\begin{bmatrix} \delta x_1(t-\tau_i) \\ \vdots \\ \delta x_n(t-\tau_i) \end{bmatrix}}^{\delta\mathbf{x}_{\tau_i}}$$
$$\delta\dot{\mathbf{x}}(t) = J_0\delta\mathbf{x}(t) + \sum_{i=1}^{m} J_{\tau_i}\delta\mathbf{x}_{\tau_i}, \tag{D.11}$$

where $\delta\mathbf{x}_{\tau_i} \coloneqq \delta\mathbf{x}(t-\tau_i)$, J_0 is the Jacobian with respect to $\delta\mathbf{x}(t)$ evaluated at the equilibrium point, $\mathbf{x}^*$, and the matrices J_{τ_i} correspond to Jacobian matrices with respect to $\delta\mathbf{x}(t-\tau_i)$, respectively, evaluated at the equilibrium point.

It is known (and can also be shown) that the general solutions to a set of linear ODEs are exponential functions which have either real or complex exponent values that correspond to the eigenvalues of the Jacobian matrix. Similarly, lets assume that the solutions to the linear DDE (Eq. (D.11)) are exponential functions of time. By substituting the ansatz $\delta\mathbf{x}(t) = \mathbf{x}(0)e^{\lambda t}$, where $\mathbf{x}(0) \in \mathbb{R}^n$ in Eq. (D.11) we obtain,

$$\lambda\mathbf{x}(0)e^{\lambda t} = J_0\mathbf{x}(0)e^{\lambda t} + \sum_{i=1}^{m} J_{\tau_i}\mathbf{x}(0)e^{\lambda(t-\tau_i)}$$
$$\Rightarrow \mathbf{x}(0)e^{\lambda t}(\lambda I - J_0 - \sum_{i=1}^{m} J_{\tau_i}e^{-\lambda\tau_i}) = \mathbf{0}. \tag{D.12}$$

Linear systems theory tells us that Eq. (D.12) has a unique solution if and only if the

determinant is equal to zero i.e,

$$det(\lambda I - J_0 - \sum_{i=1}^{m} J_{\tau_i} e^{-\lambda \tau_i}) = 0. \tag{D.13}$$

Eq. (D.13) is known as the characteristic equation of the equilibrium point and the set of $\lambda \in \mathbb{C}$, $\lambda = \alpha + \beta i$, are called the characteristic roots. The steady-state solution is *locally asymptotically stable* provided all characteristic roots have negative real part and is *unstable* if at least a root has a positive real part [314,316]. Here the difference between ODEs and DDE becomes more apparent. Expanding the left-hand side of Eq. (D.13) we get a polynomial that includes the exponential terms $e^{-\lambda \tau_i}$, whereas in ODEs we do not. Such polynomials are called *quasi-polynomials* and are *transcendental*, i.e they cannot be solved for the unknown term explicitly and they usually possess an infinite number of solutions [354,355]. This comes back to the discussion in Section D.2 where the infinite-dimensionality of DDE was mentioned. The transcendental nature of the characteristic equation presents the main difficulty in studying DDE [356] and there is no universal strategy to tackle the calculation of the characteristic roots (although some special forms do admit exact solutions [357–359]), as such numerical methods, perturbation methods to find asymptotic solutions, and graphical tools (geometric approaches) are employed [356].

Another important result is a theorem which states that there are at most finitely many eigenvalues with positive real part [314]. This ensures that stability is governed by a finite number of dominant eigenvalues.

The linearised form given by Eq. (D.11) can also be examined using the Laplace transform as has been done in [358]. By applying the transform on Eq. (D.11), solving for the transformed state-variables and setting to zero the denominator of the final equation will give us Eq. (D.13) thus showing the equivalence of these two methods. The *Laplace transform* of a function $f(t)$ is defined as,

$$F(s) = \mathcal{L}[f(t)]|_s \coloneqq \int_{t=0}^{t=+\infty} e^{-st} f(t) dt. \tag{D.14}$$

Using Eq. (D.14) on Eq. (D.11) we have,

$$s\mathbf{X}(s) - \mathbf{x}(0) = J_0\mathbf{X}(s) + \sum_{j=1}^{m} J_{\tau_i} e^{-s\tau_i}\mathbf{X}(s)$$
$$\Rightarrow \mathbf{X}(s) = \frac{\mathbf{x}(0)}{(sI - J_0 - \sum_{j=1}^{m} J_{\tau_i} e^{-s\tau_i})}. \tag{D.15}$$

The denominator of Eq. (D.15) is equal to the vector zero if and only if the determinant is zero. Noting that $s = \sigma + \omega i$ we obtain Eq. (D.13).

Another standard technique to find solutions of the transcendental equation given by Eq. (D.13) is the use of the Lambert W function [355, 358] which is defined as every function $W(z)$ such that,

$$W(z)e^{W(z)} = z, \tag{D.16}$$

where $z \in \mathbb{C}$ and $W : \mathbb{C} \longrightarrow \mathbb{C}$ and has infinite branches $W_k(z)$, $k = -\infty, \ldots, -1, 0, 1, \ldots, +\infty$. Specifically, the Lambert W function has been used to find solutions to the DDE $\dot{x}(t) = ax(t-1)$ which are given by [357],

$$x(t) = \sum_{k=-\infty}^{+\infty} c_k e^{(W_k(a)t)}. \tag{D.17}$$

In general the Lambert W function can be used to find solutions to the class of scalar DDE $\dot{x}(t) = ax(t-1) + bx(t)$ [357]. In [358] there is an extensive reference list dedicated to the historical development and use of DDE as well as important results on stability, analytical results, and uniqueness and existence of solutions.

Finally, to assess global stability behaviour of the equilibrium points of the system, one can use an extension of the Lyapunov stability theory, where the Lyapunov function depends on the delayed variable [360]. The main theorem is know as the Lyapunov-Krasovskii stability theorem which proves asymptotic stability for the system [350, 360]. This material is beyond the scope of this Thesis but is mentioned here for completion.

Appendix E

Linear stability analysis of the self-recovery model

E.1 Positivity of solutions

Since the state-variables in Eq. (6.1a) and Eq. (6.1b) represent concentration of molecular species, we need to show that their solutions are positive. To show that the solutions, $(x(t), y(t))$, are positive for all positive time, $t > a \in \mathbb{R}^+$, we first impose the assumption that the initial history function, $\phi(t)$, is positive on the interval $t \in [a - \tau_d, a]$, i.e both $x(t)$,$y(t) > 0$ for $t \in [a - \tau_d, a]$. From Eq. (6.1a) it is trivial that on $t \in [a, a + \tau_d]$,

$$\begin{aligned} \dot{x}(t) &= k_x \frac{y(t)}{1 + f_x x(t)} - \delta_x x(t) \\ \Rightarrow \dot{x}(t) &> -\delta_x x(t). \end{aligned}$$

Given this, it can be shown that $x(t)$ on the arbitrary interval $t \in [a, a + \tau_d]$ remains positive. To see this suppose $x(t) < 0$ on $t \in [a, a+\tau_d]$. Since $\delta_x > 0$, then the inequality is not true for every δ_x and therefore we have a contradiction. Another way of thinking about it is that $\dot{x}(t)$ is "more positive" than the function $\dot{\tilde{x}}(t) = -\delta_x \tilde{x}(t)$, which has general solution a negative exponential function, and is therefore always positive for positive initial conditions[1]. Since the solution of $\dot{x}(t)$ is bounded by the solution of $\dot{\tilde{x}}(t)$,

[1] Note that in this case we discuss about initial conditions since the equation is a linear, single-variable, first-order ODE.

$x(t)$ will remain positive. This is in fact an example of a comparison principle with a differential inequality and a formal proof is given by Theorem 3.6 in [314].

Moreover, we can show that the solution on that interval is finite. Re-arranging Eq. (6.1a) and multiplying by $e^{\delta_x t}$ we have,

$$\begin{aligned}
& e^{\delta_x t}\dot{x} + e^{\delta_x t}\delta_x x(t) = e^{\delta_x t} k_x \frac{y(t)}{1 + f_x x(t)} \\
\Rightarrow & \frac{d}{dt}(e^{\delta_x t} x(t)) = e^{\delta_x t} k_x \frac{y(t)}{1 + f_x x(t)} \\
\Rightarrow & \int_{v=a}^{v=a+\tau_d} \frac{d}{dv}(e^{\delta_x v} x(v))dv = \int_{v=a}^{v=a+\tau_d} e^{\delta_x v} k_x \frac{y(v)}{1 + f_x x(v)} dv \\
\Rightarrow & e^{\delta_x (a+\tau_d)} x(a+\tau_d) - e^{\delta_x a} x(a) = \int_{v=a}^{v=a+\tau_d} e^{\delta_x v} k_x \frac{y(v)}{1 + f_x x(v)} dv \\
\Rightarrow & x(a+\tau_d) = e^{-\delta_x \tau_d} x(a) + \int_{v=a}^{v=a+\tau_d} e^{\delta_x (s-a-\tau_d)} k_x \frac{y(v)}{1 + f_x x(v)} dv.
\end{aligned}$$

In the last expression, the first term on the right-hand side is a negative exponential, which is bounded above for positive delay values. The second term, involving the integral is also bounded, since it is multiplied by an exponential function having a negative exponent on the interval $[a, a+\tau_d]$. Therefore $x(t)$ is finite on the said interval.

Similar arguments can be made for Eq. (6.1b), considering that,

$$\dot{y}(t) > -k_x \frac{y(t)}{1 + f_x x(t)} - \delta_x y(t),$$

and that $x(t)$ is bounded and positive on $t \in [a, a+\tau_d]$. Hence, both state-variables are positive on the specified interval. Finally, the argument can be iterated for any interval $t \in [a, a+\tau_d]$ since it was arbitrarily chosen thus proving positivity of solutions $(x(t), y(t))$ for any $t > a \in \mathbb{R}^+$.

E.2 Linear stability analysis

Although, linear stability analysis for 2-dimensional ODE systems might be trivial, in the case of DDE systems it is necessary to establish stability with respect to the delay as a parameter. Here, local linear stability analysis is conducted on both the non-delayed ($\tau_d = 0$) and delayed ($\tau_d \neq 0$) system of equations. Analytical conditions proving that

the equilibrium points of both systems are locally asymptotically stable are derived.

E.2.1 Non-delayed system

Studying the stability with $\tau_d = 0$ reduces the system of differential equations to a set of non-linear ODEs.

With $\tau_d = 0$, Eq. (6.1a) and (6.1b) become:

$$\dot{x}(t) = k_x \frac{y(t)}{1 + f_x x(t)} - \delta_x x(t) \tag{E.1}$$

$$\dot{y}(t) = k_y(1 + f_y x(t)) - k_x \frac{y(t)}{1 + f_x x(t)} - \delta_y y(t). \tag{E.2}$$

The Jacobian matrix of this system is given by:

$$J\big|_{(x^*,y*)} = \begin{bmatrix} \frac{d\dot{x}}{dx} & \frac{d\dot{y}}{dx} \\ \frac{d\dot{x}}{dy} & \frac{d\dot{y}}{dy} \end{bmatrix} = \begin{bmatrix} -k_x f_x \frac{y^*}{(1 + f_x x^*)^2} - \delta_x & \frac{k_x}{1 + f_x x^*} \\ k_y f_y + k_x f_x \frac{y^*}{(1 + f_x x^*)^2} & -\frac{k_x}{1 + f_x x^*} - \delta_y \end{bmatrix}, \tag{E.3}$$

with characteristic equation

$$det(\lambda I - J\big|_{(x^*,y*)}) = 0.$$

This leads to the polynomial expression

$$\lambda^2 + (a + d)\lambda + (ad - bc) = 0, \tag{E.4}$$

where

$$a = k_x f_x \frac{y^*}{(1 + f_x x^*)^2} + \delta_x,$$

$$b = \frac{k_x}{1 + f_x x^*},$$

$$c = k_y f_y + k_x f_x \frac{y^*}{(1 + f_x x^*)^2},$$

$$d = \frac{k_x}{1 + f_x x^*} + \delta_y.$$

The parameters and the steady-states are positive real numbers, therefore, by inspection $a + d > 0$. With some basic algebra it can be shown that $ad - bc > 0$ for any set of parameters. Using Descartes' Rule of Signs [361] it is then obvious that there are no positive real roots to Eq. (E.4) since there are no sign changes. Looking at $f(-\lambda) = (-\lambda)^2(a+d)(-\lambda)+(ad-bc) = \lambda^2-(a+d)\lambda+(ad-bc)$ we can determine that there are either two negative real roots (two sign changes) or a pair of complex conjugate roots.

By applying the Routh-Hurwitz criterion [313, 362] we can find necessary and sufficient conditions under which the roots of Eq. (E.4) are located in the left-half of the complex plane, i.e to have negative real part. These conditions are $a + d > 0$ and $ad - bc > 0$, which hold for any selection of parameters, thus showing that the equilibrium point is locally asymptotically stable. Moreover, inspection of the discriminant of Eq. (E.4) we can establish whether the equilibrium point is a locally asymptotically stable node or a locally asymptotically stable spiral. Since $b > 0$ and $c > 0$, then $(a+d)^2-4(ad-bc) > 0$, thus the eigenvalues are purely real which establishes the fact that the equilibrium point (x^*, y^*) is a locally asymptotically stable node.

E.2.2 Delayed system

To proceed with the results of linear stability analysis in the case of non-zero delay, the system of equations (Eq. (E.1) and Eq. (E.2)) are non-dimensionalised, which makes the analysis simpler because of fewer parameters. The following change of variables are made: $y = y_c\psi$, $x = x_c\chi$, $t = t_c\tau$ and $\tau_d = t_c\xi$ where y_c, x_c are the characteristic units of measure of the state-variables, and t_c the characteristic unit for time. The variables χ, ψ , τ, and ξ represent the dimensionless state-variables (x and y), time, and delay, respectively. Setting $x_c = \frac{1}{f_x}$, $t_c = \frac{1}{k_x}$ and $\frac{t_c y_c k_x}{x_c} = 1$, Eq. (6.1a) and Eq. (6.1b) can be put in the dimensionless form,

$$\frac{d\chi(\tau)}{d\tau} = \frac{\psi(\tau)}{1+\chi(\tau)} - \delta_\chi\chi(\tau) \tag{E.5}$$

$$\frac{d\psi(\tau)}{d\tau} = \kappa_\psi(1 + r_f\chi(\tau-\xi)) - \frac{\psi(\tau)}{1+\chi(\tau)} - \delta_\psi\psi(\tau), \tag{E.6}$$

with lumped parameters $\kappa_\psi = \frac{k_y f_x}{k_x}$, $r_f = \frac{f_y}{f_x}$, $\delta_\chi = \frac{\delta_x}{k_x}$ and $\delta_\psi = \frac{\delta_y}{k_x}$. Parameter κ_ψ is the effective production of ψ, r_f is the ratio feedback strength, and the parameters δ_χ and δ_ψ are the normalised degradations of each species. Re-working the steady-state

solution with these substitutions we have,

$$\boldsymbol{\chi}^* = (\chi^*, \psi^*) = \left(\frac{(\kappa_\psi r_f - \delta_\chi - \delta_\psi \delta_\chi) + \sqrt{(\kappa_\psi r_f - \delta_\chi - \delta_\psi \delta_\chi)^2 + 4\delta_\chi \delta_\psi \kappa_\psi}}{2\delta_\psi \delta_\chi}, \delta_\chi \chi^* (1+\chi^*) \right). \tag{E.7}$$

Linearising the system of equations given by Eq. (E.5) and Eq. (E.6) we have the following linear system of DDEs,

$$\begin{bmatrix} \delta\dot{\chi}(\tau) \\ \delta\dot{\psi}(\tau) \end{bmatrix} = \overbrace{\begin{bmatrix} -\dfrac{\psi^*}{(1+\chi^*)^2} - \delta_\chi & \dfrac{1}{1+\chi^*} \\ \dfrac{\psi^*}{(1+\chi^*)^2} & -\dfrac{1}{1+\chi^*} - \delta_\psi \end{bmatrix}}^{J_0} \overbrace{\begin{bmatrix} \delta\chi(\tau) \\ \delta\psi(\tau) \end{bmatrix}}^{\delta\boldsymbol{\chi}(\tau)} + \overbrace{\begin{bmatrix} 0 & 0 \\ \kappa_\psi r_f & 0 \end{bmatrix}}^{J_\xi} \overbrace{\begin{bmatrix} \delta\chi(\tau-\xi) \\ \delta\psi(\tau-\xi) \end{bmatrix}}^{\delta\boldsymbol{\chi}_\xi}. \tag{E.8}$$

The system of Eq. (E.8) admits the following characteristic equation,

$$det(\lambda I - J_0 - J_\xi e^{-\lambda\xi}) = 0 \tag{E.9}$$

$$\Rightarrow det \begin{bmatrix} \lambda + \dfrac{\psi^*}{(1+\chi^*)^2} + \delta_\chi & -\dfrac{1}{1+\chi^*} \\ -\dfrac{\psi^*}{(1+\chi^*)^2} - \kappa_\psi r_f e^{-\lambda\xi} & \lambda + \dfrac{1}{1+\chi^*} + \delta_\psi \end{bmatrix} = 0. \tag{E.10}$$

Expanding the characteristic equation we get the following polynomial expression,

$$\lambda^2 + (a+d)\lambda + ad - bc - b\kappa_\psi r_f e^{-\lambda\xi} = 0, \tag{E.11}$$

where

$$a = \frac{\psi^*}{(1+\chi^*)^2} + \delta_\chi,$$

$$b = \frac{1}{1+\chi^*},$$

$$c = \frac{\psi^*}{(1+\chi^*)^2},$$

$$d = \frac{1}{1+\chi^*} + \delta_\psi.$$

In the simplest of cases what one can do is substitute $\lambda = \alpha + \beta i$ in the characteristic equation, equate the real and imaginary parts and try to find an argument contradicting the fact that $\alpha > 0$ by finding bounds on β. In the case of coupled, two-dimensional systems most of the times there is no straight forward argument to show this.

The analysis that follows is considered a general approach to determine linear stability of the equilibrium points of a system of DDEs and examples can be found in [350,363]. Let $\lambda = \alpha + \beta i$ be the eigenvalue associated with the equilibrium point (χ^*, ψ^*). The *critical stability curve* is the curve/surface defined by the dimensionless time-delay parameter, ξ, which is a function of the equilibrium point and the system's parameters, and has the form,

$$\xi = f(\boldsymbol{\chi}^*, \hat{\boldsymbol{\eta}}), \tag{E.12}$$

on which $\alpha = 0$ and where $\hat{\boldsymbol{\eta}} = [\kappa_\psi, r_f, \delta_\chi, \delta_\psi]^T$ is the vector of parameters for the dimensionless system. Since on this curve $\alpha = 0$, the eigenvalues are purely imaginary, while away from this curve, α is either positive or negative, which is determined by the gradient with respect to the delay, i.e $\frac{d\alpha}{d\xi}$. With this information we can identify stable and unstable regions, called *stability islands*, in the parameter space $(\xi, \hat{\boldsymbol{\eta}})$. The stability of the equilibrium changes as α crosses the imaginary axis, at $\lambda = \beta i$, with $\alpha > 0$ rendering the equilibrium point unstable and $\alpha < 0$ admitting a locally asymptotically stable equilibrium.

Substituting $\lambda = \alpha + \beta i$ in Eq. (E.11) and equating the real and imaginary parts we have,

$$\alpha^2 - \beta^2 + \alpha A + B = b\kappa_\psi r_f e^{-\alpha\xi}\cos(\beta\xi) \tag{E.13}$$

$$2\alpha\beta + \beta A = -b\kappa_\psi r_f e^{-\alpha\xi}\sin(\beta\xi), \tag{E.14}$$

where $A = a + d$ and $B = ad - bc$. By inspection it can be seen that both $A > 0$ and $B > 0$ for any set of parameters.

Setting $\alpha = 0$, squaring and adding together Eq. (E.13) and Eq. (E.14), we get a 4^{th} degree polynomial with respect to β, given by,

$$\beta^4 + (A^2 - 2B)\beta^2 + B^2 - b^2{\kappa_\psi}^2{r_f}^2 = 0. \tag{E.15}$$

Before proceeding with the analysis we should confirm whether β is real or imaginary. Suppose $\beta = \omega i$ then $\lambda = \beta i = (\omega i)i = -\omega$ which implies that the real part of λ is neg-

ative and hence the equilibrium point is locally asymptotically stable. More explicitly, by setting $\alpha = 0$ in Eq. (E.13) and Eq. (E.14) we have,

$$-\beta^2 + B = b\kappa_\psi r_f \cos(\beta\xi) \tag{E.16}$$

$$\beta A = -b\kappa_\psi r_f \sin(\beta\xi) \tag{E.17}$$

and if β is imaginary then there is no β that simultaneously solves Eq. (E.16) and Eq. (E.17).

Let $\mu = \beta^2$ which turns Eq. (E.15) into,

$$\mu^2 + (A^2 - 2B)\mu + B^2 - b^2{\kappa_\psi}^2{r_f}^2 = 0 \tag{E.18}$$

The roots of Eq. (E.18) are given by the quadratic formula:

$$\mu_{1,2} = \frac{-(A^2 - 2B) \pm \sqrt{(A^2 - 2B)^2 - 4(B^2 - b^2{\kappa_\psi}^2{r_f}^2)}}{2} \tag{E.19}$$

With some algebra the coefficients of Eq. (E.18) can be shown to be positive. For the case of $A^2 - 2B$, one needs to expand the square and after a few manipulations it is clear that $A^2 - 2B > 0$. For the second coefficient, we can express $B^2 - b^2{\kappa_\psi}^2{r_f}^2$ as a difference of squares i.e. $(B - b\kappa_\psi r_f)(B + b\kappa_\psi r_f)$, thus requiring to show $B > b\kappa_\psi r_f$. The positivity of this term in fact holds. Using Descartes' Rule of Sings it is clear that Eq. (E.18) has no positive roots and it either has exactly two negative roots or one complex conjugate pair. To ensure that the roots are real we must show that $(A^2 - 2B)^2 - 4(B^2 - b^2{\kappa_\psi}^2{r_f}^2) > 0$. Expanding the square again, the problem reduces to showing that $A^2 - 4B > 0$, which holds true, thus the roots are not complex and are both negative. Since the roots $\mu_{1,2}$ are negative then β is imaginary and this result indicates that the real part of the eigenvalues on the critical stability curves is negative thus ensuring, by the discussion in the previous paragraph, that the equilibrium point is locally asymptotically stable for all $\xi > 0$. It should be highlighted that the conditions for stability of the equilibrium, $A^2 - 2B > 0$ and $B^2 - b\kappa_\psi r_f > 0$, coincide with general conditions given in Proposition 2.3 in [354].

Based on the aforementioned analysis there was no need to derive the critical stability curves and then check the sign of $\frac{d\alpha}{d\xi}$ since β was shown to be imaginary. With the result proved for the non-delayed and delayed systems, we deduced that the system given by Eq. (6.1a) and Eq. (6.1b) admits a locally asymptotically stable equilibrium point for

any value of delay, $\xi \geq 0$.

Appendix F

Computational investigation of the stability of the self-recovery and skin barrier homeostasis models

F.1 Introduction

We complement our analysis of Appendix E by exploring model stability using a MATLAB compatible DDE continuation software (DDE-BIFTOOL). This performs branch continuation of steady-states and corresponding stability analyses [316]. It is worth mentioning that the software DDE-BIFTOOL uses Linear Multi-Step (LMS) methods to approximate the roots of Eq. (D.11) at the steady-state solution, while corrections to the roots are obtained using the typical Newton-Raphson method[316]. Periodic solutions can also be computed using orthogonal collocation methods. For more details see the manual [315] or the reference list in [316].

F.2 Stability considerations

F.2.1 Self-recovery model

To perform stability analysis with DDE-BIFTOOL we use the arbitrary parameters presented in Table 6.1 to plot the eigenvalues of the steady-state in the complex plane (Fig. F.1). For the specific set of parameters all the eigenvalues, $\lambda = \alpha + \beta i$, are plotted with a minimal real part of $\alpha = -5$.

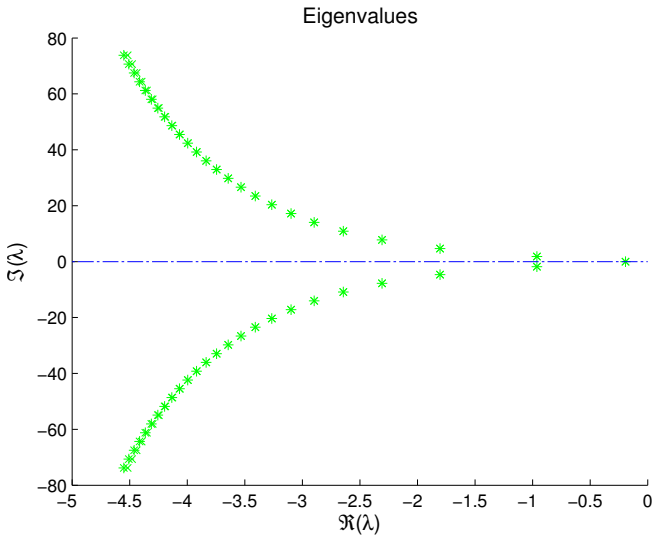
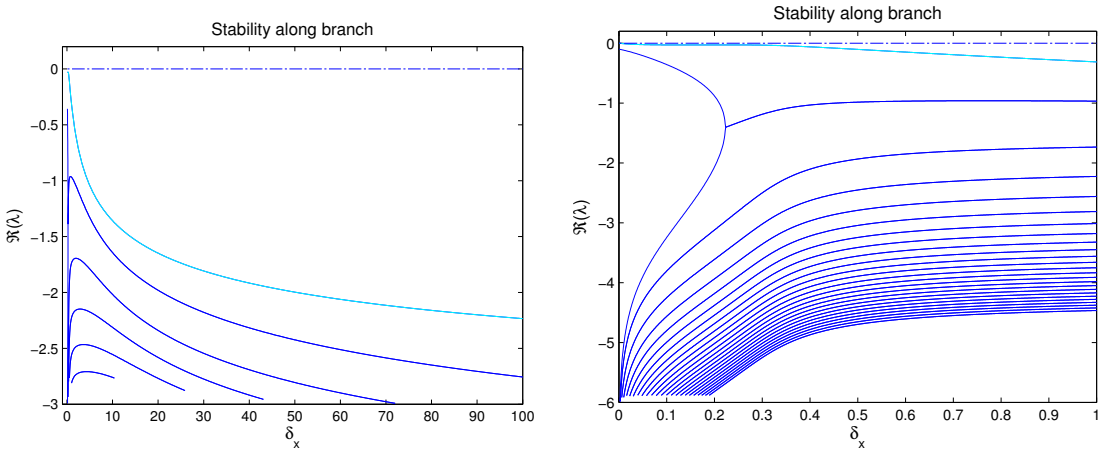


Figure F.1: Eigenvalues with minimal real part $\alpha = -5$ in the complex plane for the system of Eq. (6.1a) and (6.1b). Simulation parameters are shown in Table 6.1.

There is an infinite number of eigenvalues because the characteristic equation is transcendental. As stated in Section D.1, the stability of DDE systems is governed by a finite number of eigenvalues, therefore setting a lower bound on α does not affect the overall stability discussion, as long as, there is no upper bound on the real part and the dominant eigenvalues are plotted. Notice that none of the eigenvalues are on the right-half of the complex plane signifying that the equilibrium is locally asymptotically stable (Fig. F.1).

To assess the stability of the equilibrium point, a parameter of the model is varied and the real part of the eigenvalues is ploted against that parameter; we define such figures as *stability diagrams*. Fig. F.2 depicts such a diagram with respect to the parameter δ_x,

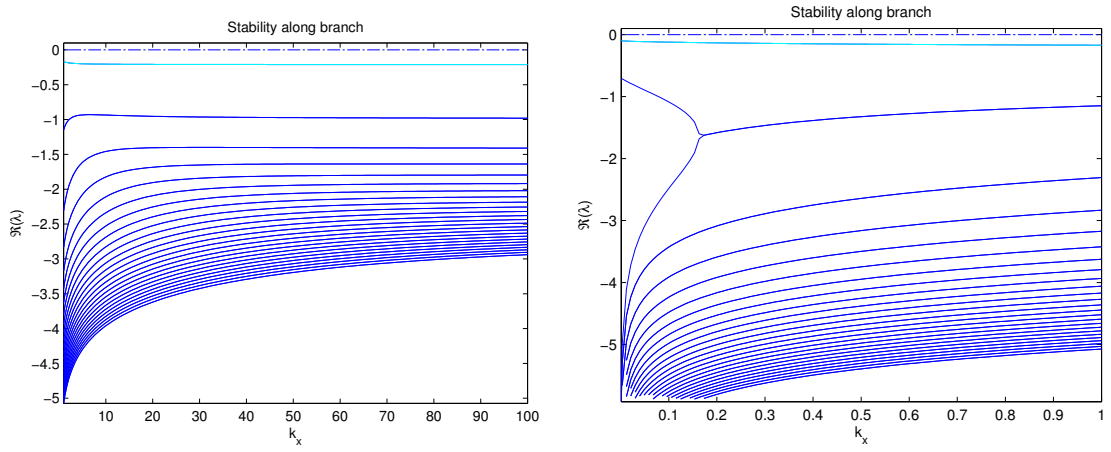
with Fig. F.2a and Fig. F.2b plotted for the range $\delta_x \in [0.1, 100]$ and $\delta_x \in [0.001, 1]$, respectively. Each blue line in the figures corresponds to the trajectory of the real part of the eigenvalue as the parameter is varied and the cyan line corresponds to the dominant eigenvalue i.e the eigenvalue that is closest to the imaginary axis. The results of Fig. F.2 indicate that in the range $\delta_x \in [0.001, 100]$ the real part of the eigenvalues does not cross the imaginary axis, hence showing that no change in stability occurs and that the equilibrium is locally asymptotically stable, as predicted by theoretical results.



(a) $\delta_x \in [0.1, 100]$ **(b)** $\delta_x \in [0.001, 1]$

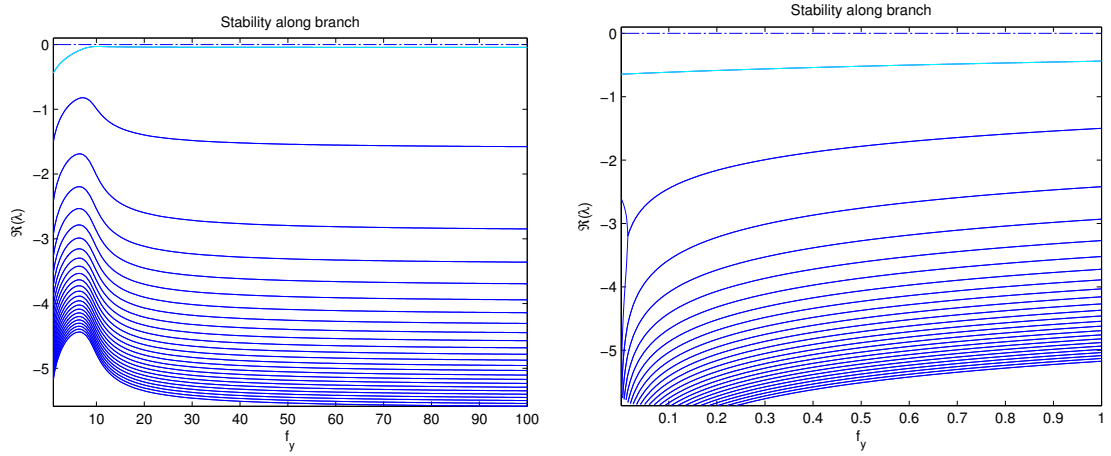
Figure F.2: Stability diagram: Trajectory of the real part of the eigenvalues as the parameter δ_x is varied (blue lines). Cyan line is the trajectory of the dominant eigenvalue. Dashed line is the imaginary axis.

This analysis was also carried out for the other parameters of the model (k_x and f_y) and the results (Fig. F.3 and Fig. F.4) show that for the specific range of parameter variation $[0.001, 100]$, the equilibrium point remains locally asymptotically stable. Simulations for the rest of the parameters (f_x, k_y and δ_y) were also carried out but are not shown in this document due to the redundancy in the results. Similarly, for those parameters the equilibrium point was shown to be locally asymptotically stable. This is in agreement with the analytical results of Section E.2.2.



(a) $k_x \in [1, 100]$ **(b)** $k_x \in [0.001, 1]$

Figure F.3: Stability diagram: Trajectory of the real part of the eigenvalues as the parameter k_x is varied (blue lines). Cyan line is the trajectory of the dominant eigenvalue. Dashed line is the imaginary.

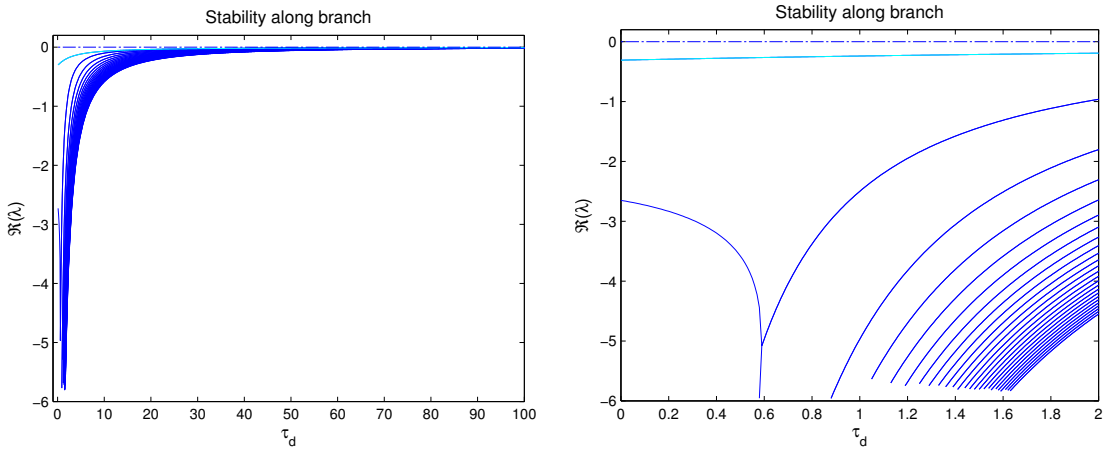


(a) $f_y \in [1, 100]$ **(b)** $f_y \in [0.001, 1]$

Figure F.4: Stability diagram: Trajectory of the real part of the eigenvalues as the parameter f_y is varied (blue lines). Cyan line is the trajectory of the dominant eigenvalue. Dashed line is the imaginary axis.

Of particular interest in delay differential systems is to examine the nature of the stability with respect to changes in the delay parameter. Fig. F.5 represent stability diagrams with respect to the delay. From the figures it can be seen that the real parts of the eigenvalues remain positive for the given range of delay, between $\tau_d \in [0.001, 2]$ (Fig.

F.5a) and $\tau_d \in [0.1, 100]$ (Fig. F.5b), and therefore the computional results confirm that the equilibrium point is locally asymptotically stable. We performed the same computational experiments fo longer delay values ($100 < \tau_d < 1000$), which revealed that the eigenvalues do not cross the imaginary axis.



(a) $\tau_d \in [0.1, 100]$ **(b)** $\tau_d \in [0.001, 2]$

Figure F.5: Stability diagram: Trajectory of the real part of the eigenvalues as the parameter τ_d is varied (blue lines). Cyan line is the trajectory of the dominant eigenvalue. Dashed line is the imaginary axis.

The computational results presented in this section are not rigorous, due to the simulations being prone to round-up errors of the numerical algorithms, nor extensive, since not all parameter combinations are checked. Nevertheless, these kind of analyses could drive better selection of nominal parameters.

F.2.2 Skin barrier homeostasis model

To explore the stability of the equilibria admitted by the *skin barrier homeostasis model* we plot the trajectory of the eigenvalues as we vary one parameter. We vary the parameter f_x across five orders of magnitude $[0.001, 1000]$. In the range $f_x \in [1, 1000]$ the system admits only one equilibrium point, while in the range $f_x \in [0.001, 1]$ the system admits three equilibrium points.

Fig. F.6 is the stability diagram in terms of f_x in the range $[1, 1000]$. In this range of f_x their is only one equilibrium point, given the fixed parameters in Table 6.1, and since the

real part of the dominant eigenvalue does not cross the imaginary axis, the equilibrium point is locally stable. On the other hand, Figs. F.7a-F.7d are the stability diagrams in terms of f_x in the range $[0.001, 1]$ where the system admits three equilibrium points. It is clearly seen here that the equilibrium points 1 and 2 are unstable, while equilibrium point 3 is locally stable for the range of f_x.

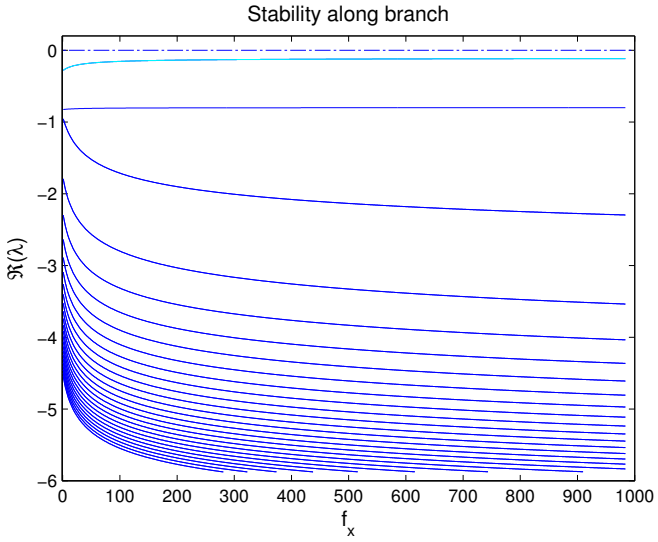
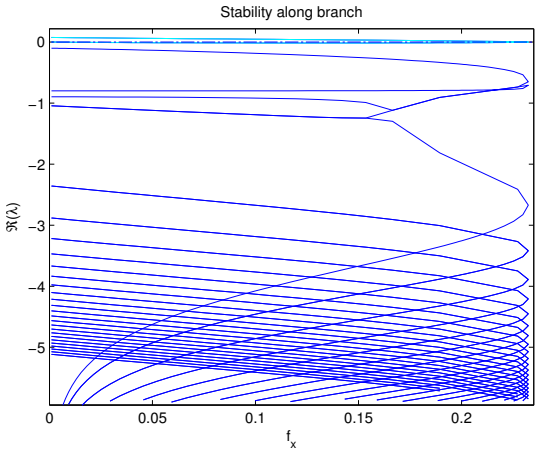
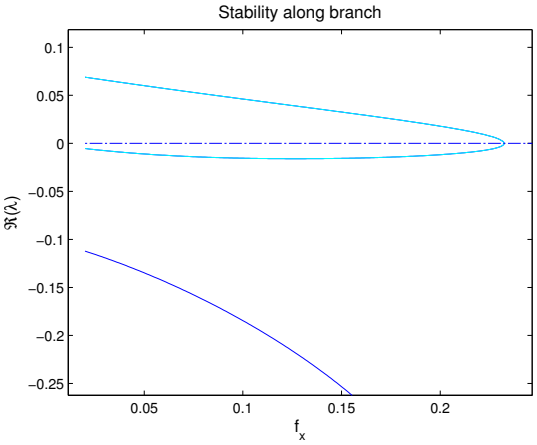


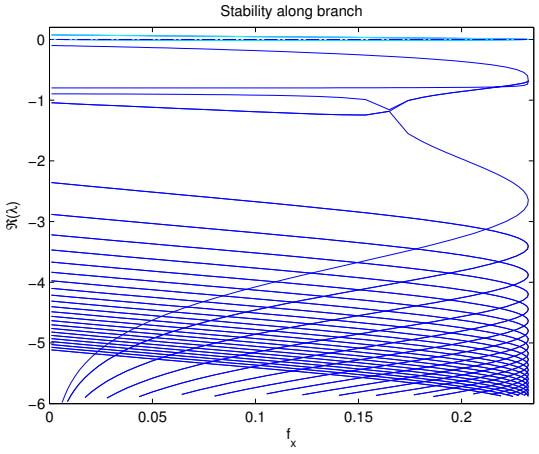
Figure F.6: Stability diagram: Trajectory of the real part of the eigenvalues as the parameter f_x is varied in $[1, 1000]$ (blue lines). Cyan line is the trajectory of the dominant eigenvalue. Dashed line is the imaginary axis.



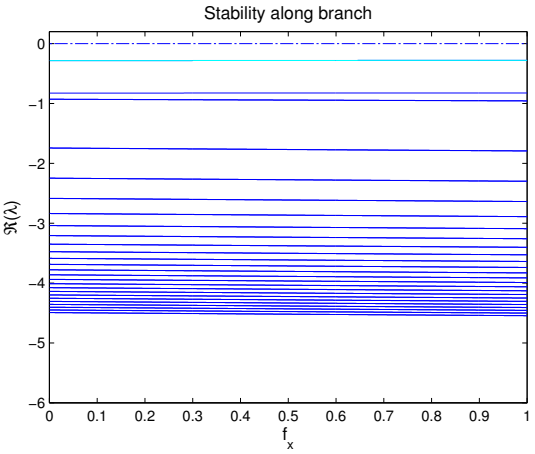
(a) Equilibrium point 1, $f_x \in [0.001, 1]$



(b) Equilibrium point 1, zoom-in where the dominant eigenvalue crosses the imaginary axis.



(c) Equilibrium point 2, $f_x \in [0.001, 1]$



(d) Equilibrium point 3, $f_x \in [0.001, 1]$

Figure F.7: Stability diagram: Trajectory of the real part of the eigenvalues for all equilibria as the parameter f_x is varied in $[0.001, 1]$ (blue lines). Cyan line is the trajectory of the dominant eigenvalue. Dashes lines are the imaginary axes.